SIMULATION OF GEOTHERMAL RESERVOIRS WITH HIGH AMOUNT OF CARBON DIOXIDE

A THESIS SUBMITTED TO
THE GRADUATE SCHOOL OF NATURAL AND APPLIED SCIENCES
OF
MIDDLE EAST TECHNICAL UNIVERSITY

BY

SERHAT KÜÇÜK

IN PARTIAL FULFILLMENT OF THE REQUIREMENTS
FOR
THE DEGREE OF MASTER OF SCIENCE
IN
PETROLEUM AND NATURAL GAS ENGINEERING

SEPTEMBER 2018

Approval of the Thesis:

SIMULATION OF GEOTHERMAL RESERVOIRS WITH HIGH AMOUNT OF CARBON DIOXIDE

submitted by **SERHAT KÜÇÜK** in partial fulfillment of the requirements for the degree of **Master of Science in Petroleum and Natural Gas Engineering Department, Middle East Technical University** by,

Prof. Dr. Halil Kalıpçılar
Dean, Graduate School of **Natural and Applied Sciences** _____

Prof. Dr. Serhat Akın
Head of Department, **Petroleum and Natural Gas Engineering** _____

Prof. Dr. Serhat Akın
Supervisor, **Petroleum and Natural Gas Eng. Dept., METU** _____

Examining Committee Members:

Assoc. Prof. Ali Bülbül
Geological Engineering Dept., Pamukkale University _____

Prof. Dr. Serhat Akın
Petroleum and Natural Gas Engineering Dept., METU _____

Asst. Prof. İsmail Durgut
Petroleum and Natural Gas Engineering Dept., METU _____

Date: 07.09.2018

I hereby declare that all information in this document has been obtained and presented in accordance with academic rules and ethical conduct. I also declare that, as required by these rules and conduct, I have fully cited and referenced all material and results that are not original to this work.

Name, Last name: SERHAT KÜÇÜK

Signature:

ABSTRACT

SIMULATION OF GEOTHERMAL RESERVOIRS WITH HIGH AMOUNT OF CARBON DIOXIDE

Küçük, Serhat

M.S., Department of Petroleum and Natural Gas Engineering

Supervisor: Prof. Dr. Serhat Akın

September 2018, 186 pages

Geothermal energy is always attributed as a sustainable and environmentally friendly source of energy. But in some cases, amount of the greenhouse gas emissions from geothermal fields become a big issue. Kızıldere Geothermal Field, one of the most important and large scale geothermal fields of the world, is a subject of these issues, experiencing excess amount of CO_2 production rates and a rapid decline in the reservoir pressures. This study aims to construct a numerical model of the Kızıldere Geothermal Field and predict the consequences of potential/possible future operations. Petrasim interface is used for the creation and the visualization of the model, as well as preparation of the simulation input files. EOS2 fluid property module of TOUGH2 simulation codes is used for the numerical simulation of the geothermal model. The natural state model of the field is obtained by running the simulation for a long time until the reservoir parameters are reached to stabilized conditions. In order to test the model, static pressure and temperature data of 53 wells, as well as dynamic pressure data of 15 observation wells are matched with the simulation results, within an error range of 10%, and the model is validated with a great accuracy. Based on the validated model, different reinjection scenarios under two different strategies are carried out. In the first strategy, production rates are kept constant in exchange for the wellhead pressures, while wellhead pressures

are kept constant by adjusting the production rates in the second strategy. The results of different scenarios show that the current reinjection plan of the field restricts to have higher impacts on the reservoir pressures by higher reinjection rates. Results also show that Kızıldere Geothermal Field can be used as a sink for greenhouse gases (especially CO2), which have positive effects on the reservoir management purposes beside the environmental benefits.

Keywords: Kızıldere, geothermal, numerical simulation, TOUGH2, Petrasim, carbon dioxide

ÖZ

YÜKSEK MİKTARLARDA KARBON DİOKSİT İÇEREN JEOTERMAL SAHALARIN SİMÜLASYONU

Küçük, Serhat
Yüksek Lisans, Petrol ve Doğal Gaz Mühendisliği Bölümü
Tez Yöneticisi: Prof. Dr. Serhat Akın

Eylül 2018, 186 sayfa

Jeotermal enerji genel olarak sürdürülebilir ve temiz bir enerji kaynağı olarak bilinmektedir. Ancak bazı jeotermal sahalardan salınan sera gazları büyük bir problem oluşturabilmektedir. Dünyanın en büyük ve en önemli jeotermal sahalarından birisi olan Kızıldere Jeotermal Sahası'nda da yüksek miktarlardaki karbon dioksit salımı ve rezervuar basınçlarındaki hızlı düşüş başlıca sıkıntı kaynaklarıdır. Bu çalışmanın amacı Kızıldere Sahası'nın sayısal bir modelini oluşturarak bu model üzerinde performans tahminleri ve rezervuar yönetim çalışmaları yürütmektir. Sayısal simülasyonlar TOUGH2 simülasyon kodlarının EOS2 akışkan modülü yürütülmüştür. Modelin oluşturulması, ve simülasyon giriş dosyalarının oluşturulması Petrasim arayüzü kullanılarak yapılmıştır. Doğal durum modelinin elde edilebilmesi adına, oluşturulan model uzun bir süre çalıştırılarak rezervuar değişkenlerinin dengeli bir hale gelmesi sağlanmıştır. 53 kuyudan alınan statik basınç ve sıcaklık verileri ile 15 kuyudan elde edilen dinamik basınç okumaları kullanılarak modelin doğruluğu sınanmıştır. Simülasyondan elde edilen sonuçlar ile gerçek verilerin arasındaki farkın 10%'dan daha küçük olması ile, oluşturulan modelin geçerliliği kabul edilmiştir. Daha sonra performans tahmini çalışmalarına geçilmiştir. Bu amaçla birçok reenjeksiyon senaryosu iki farklı strateji altında incelenmiştir. İlk stratejide, kuyubaşı basınçları karşılığında üretim

miktarları sabit tutulmuştur. İkinci stratejide ise üretim miktarları rezervuar basıncına göre değiştirilerek kuyubaşı basınçlarının sabit tutulması simüle edilmiştir. Bu senaryolar neticesinde elde edilen veriler göstermiştir ki sahanın şu andaki reenjeksiyon planında yüksek miktarlarda reenjeksiyon yapılmasının rezervuar basınçları üzerinde büyük etkileri olması ihtimali çok kısıtlıdır. Aynı zamanda Kızıldere Jeotermal Sahası'nda uygulanacak muhtemel karbon dioksit reenjeksiyonu operasyonlarının hem rezervuar basınçları açısından hem de çevreye olan katkıları açısından faydalı olacağı saptanmıştır.

Anahtar Kelimeler: Kızıldere, jeotermal, sayısal simülasyon, TOUGH2, Petrasim, karbon dioksit

To My Beloved Family

ACKNOWLEDGEMENT

Foremost, I would like to express my sincere gratitude to my advisor Prof. Dr. Serhat Akın for his continuous guidance, support, patience and valuable advices.

I owe special thanks to my colleague Ali Başer. I gratefully acknowledge his contributions and appreciate his devotion to this work and his encouragement. He always kept me motivated.

I also would like to include special note of thanks to my roommates Berk Bal, Selin Güven Erge, Tuğçe Özdemir, and Gökhan Mamak who provided me with unfailing support through the process of researching and writing the thesis.

I am also grateful to Zorlu Energy Group for the opportunity they have given to me to complete this thesis. This study would not have been possible without their continuous and valuable support.

Finally, my deep and sincere gratitude to my family for their continuous and unparalleled love, help and support. I am grateful to my father Ragıp Küçük, my mother Ganime Küçük, and my brother Aykut Küçük, for their patience and warm support during my studies. I must express my very profound gratitude to Gülsüm İriş for providing me with continuous encouragement throughout my years of study and her continuous patience through the process of researching and writing this thesis.

TABLE OF CONTENTS

CHAPTERS

LIST OF TABLES

TABLES

LIST OF FIGURES

FIGURES

CHAPTER 1

INTRODUCTION

The rapid growth in human population and the advancements in the technology, result in a considerable increase in the global energy demand. Although fossil fuels such as coal, petroleum, and natural gas have been the most dominant energy sources for a long time, in 21st century the new trend is to meet the energy needs from cleaner and more sustainable resources, like renewable energy sources.

Geothermal energy is one of the renewable energy sources. It can simply be defined as the energy of heat that is coming from the Earth's mantle, and stored in the Earth crust. Simply, a hole is drilled to deeper parts of the Earth's crust, where the temperatures are higher, and a heat carrier fluid brings this heat to the surface, and the heat is utilized. Geothermal energy is accepted as renewable, because Earth's interior keeps heating the geothermal systems.

Utilization of this natural, geological heat has a long history. For centuries, people used hot springs for cooking, bathing, and heating purposes. Today, direct use of geothermal energy has a wide range of applications such as space heating (buildings and greenhouses), food drying, industrial process heating, aquaculture water heating, snow melting, chemical and mineral production, and more (Chatenay and Jóhannesson, 2014). Generally, low to medium temperature geothermal resources (<150 °C) are utilized for such direct use applications. On the other hand, high temperature geothermal resources

(>150 °C) are considered as the most suitable for electricity generation, since generating electricity from the energy of Earth itself is attributed as the most important and economically the most attractive form of geothermal energy utilization. Among other renewable resources, the load factor of geothermal energy is much higher (i.e. electricity generation is continuous rather than intermittent, unlike solar and wind) which makes it a more reliable source of energy.

1.1 History of Geothermal Energy

The first successful electricity production from a geothermal energy source was accomplished in 1904 by Prince Piero Ginori Conti in Larderello Field, northwestern Italy. He installed the first geothermal power plant with a capacity of 10 kW, enough to light 5 bulbs (Lund, 2005) . After that time, lots of experiments have been carried out and inventions have been made to increase the electricity production from geothermal resources. As of 2016, the total installed geothermal electricity capacity of the world is more than 13.4 GW, where USA is the leading country with more than 3.5 GW installed capacity (BP, 2017). Turkey, one of the most promising countries in terms of geothermal energy resources, is rapidly developing its geothermal power capacity. In 2015, Turkey contributed 50% of the total geothermal power increase in the world (REN21, 2016), and as of the end of 2017, total capacity reached 1,064 MW with 40 operating geothermal power plants (Directorate of Mineral Research & Exploration, 2017) . There are many other plants under construction all over the world, and more power plants are planned to be constructed in the future. At the same time, researchers and scientist are working on new methods and new technologies to enable more effective utilization of that natural energy of Earth. So, it can be foreseen that geothermal energy will be one of the most efficient and most widely used energy sources of the world in the near future.

1.2 Geothermal System Types

Temperature is the most important parameter in geothermal systems, but low-medium-high temperature geothermal reservoir classification can further be detailed based on the controlling mechanism of the movement and concentration of heat; convective systems and conductive systems (World Energy Council, 2016).

In convective geothermal systems, heat is distributed along the reservoir by the flow of a hot, buoyant, naturally occurring liquid or steam. Fluid is heated up by a deeper heat source, generally in tectonically active regions, and circulates through the reservoir, moving along mostly vertical fractures. If the mobile phase is liquid, it is classified as liquid-dominated, if vapor is the mobile phase, then it is classified as a vapor dominated geothermal system. In liquid dominated systems, fractures are occupied by water and the matrix is water saturated. On the other hand, in vapor-dominated systems, fractures are occupied by steam, with a thin layer of water in the fracture walls, and the matrix is partially or fully saturated with water (Grant & Bixley, 2011). Almost all of the geothermal power stations operate on convective hydrothermal systems, and majority of such systems are liquid-dominated. A simplified schematic of a convective heat flow in a geothermal system is shown in Figure 1 (Saemundsson, 2015)

In conductive geothermal systems, in contrast to convective systems where the heat is circulated by a geothermal fluid, the main heating mechanism is the natural thermal gradient. Some deep sedimentary aquifers can be an example to conductive geothermal systems. These aquifers are not a part of an active heat circulation, but their temperature is higher due to the thermal gradient. Since they are generally low-to-medium temperature reservoirs (depending on the depth), they are more suitable for direct use applications of geothermal energy, such as district or greenhouse heating. In some cases, the pressure of reservoir fluids in deep sedimentary formations may reach abnormally high levels. Also, the temperature of fluids in these formations may be raised due to conductive heat transfer mechanisms. Such aquifers are called geopressured-geothermal aquifers. In addition to high pressure and temperature features, the water in geopressured-geothermal reservoirs generally contains significant amount of methane. Depending on the amount of methane

content, geopressured geothermal reservoirs are often considered as an unconventional source of natural gas (Griggs, 2005). Since the three forms of energy; mechanical energy (high pressure), thermal energy and significant amount of methane dissolved in water are co-exist in geopressured geothermal reservoirs, both geothermal energy utilization and natural gas extraction can be achieved with a hybrid-production approach. Another example to conductive systems is hot dry rock reservoirs. In some locations, reasonably high temperature, but low permeability formations can be encountered at drillable levels of the crust. Such a formation can be considered as a source of geothermal energy, but absence of heat carrier fluid and low permeability of the rock require new development approaches. For example, injecting a fluid with a high pressure, fracturing the rock, circulating the fluid through these artificial openings in the hot-rock, and then producing the heated fluid from another well was experimented as a successful application in Fenton Hill, Los Alamos, USA (Brown, 1995). In literature, some other approaches to develop hot dry rock systems can be found like using CO_2 as a working fluid to extract the heat from a hot-rock with a great efficiency (Brown, 2000). This novel approach also aims to sequester greenhouse gases (especially CO_2) to deep formations which also makes it an environmentally friendly way of energy production.

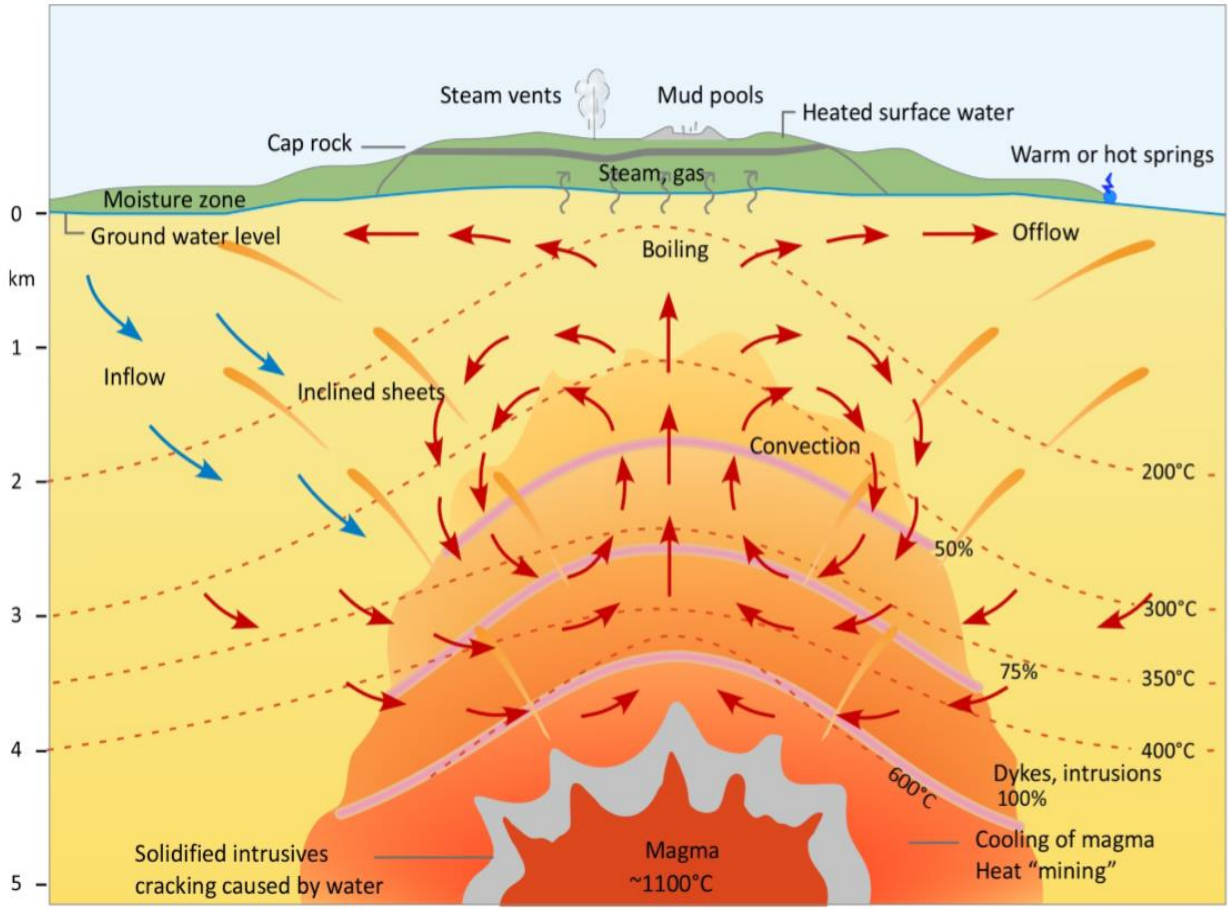

Figure 1.1 Convective heat circulation in a geothermal system (Saemundsson, 2015)

Although, it is not always technologically and economically feasible, high temperature geothermal energy can be reached at any point on Earth, theoretically, if a hole is drilled deep enough into the crust. According to Grant & Bixley (2011), temperature gradient in shallowest depths of Earth crust is 30 °C/km, but in the thick crust the gradient can be as low as 16 °C/km (Lund & Zoback, 1999). In some regions, especially volcanically active tectonic plate boundaries, thermal gradients can be really high. For example, in The Phlegrean Fields area, located west of Naples, southern Italy, thermal gradients as high as 168 °C/km was observed (Corrado et al., 1998)

1.3 Geothermal Power Plant Types

Geothermal energy resources are widely used to produce electricity all over the world. Geothermal power plants convert thermal energy to mechanical energy, and eventually to electrical energy. In its simplest form, geothermal hot fluids are brought to the surface, where they are used to spin the blades of a turbine, which drives a generator to produce electricity. There are 3 main types of geothermal power plants:

1.3.1 Dry-Steam Power Plants

They are the first type of geothermal power plants. In 1904, Prince Piero Ginori Conti used a small scale dry-steam power plant with a capacity of 10 kW, in Larderello Field (Lund, 2005). Geothermal fluid, primarily steam, is directly used to drive a turbine, which runs an electricity generator. Generally, dry-steam (vapor dominated) fields are high temperature resources, and dry-steam power plants work at high temperatures.

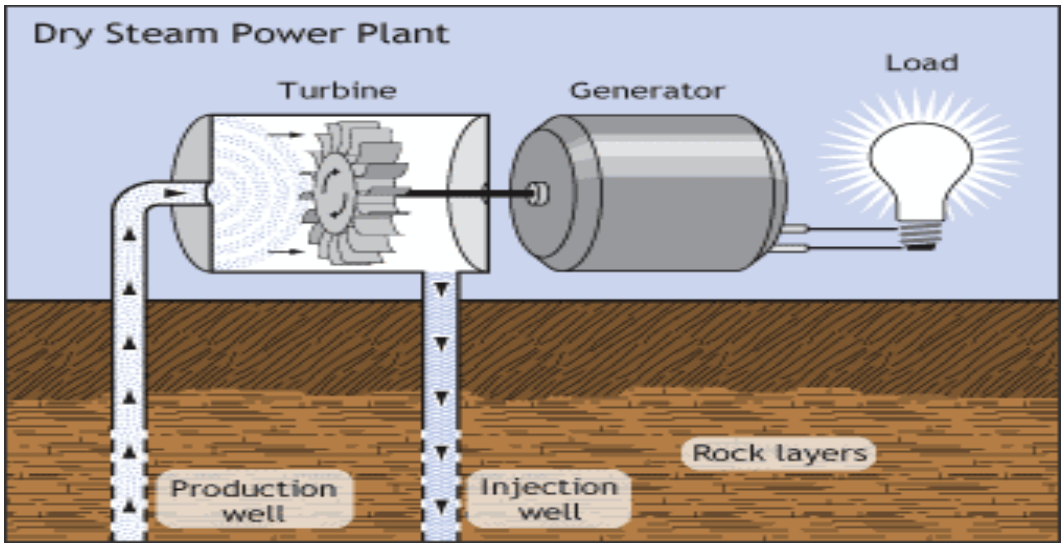

Figure 1.2 Schematic of a Dry Steam Power Plant

(U.S. Department of Energy's Office of Energy Efficiency & Renewable Energy, 2016)

1.3.2 Flash Steam Power Plant

In these systems, high temperature geothermal fluids brought to the surface and pumped into a flash tank, where the pressure is much lower. Since the high pressure hot water enters a low pressure environment, it rapidly vaporizes, or “flashes”. Then, the produced steam turns a turbine, which runs a generator. The remaining liquid can even undergo a secondary flash (double-flash systems), to produce more energy. After the heat extraction, the steam condenses, and it is reinjected back to the reservoir through reinjection wells, to maintain the reservoir pressure, as well as to dispose the reservoir liquids.

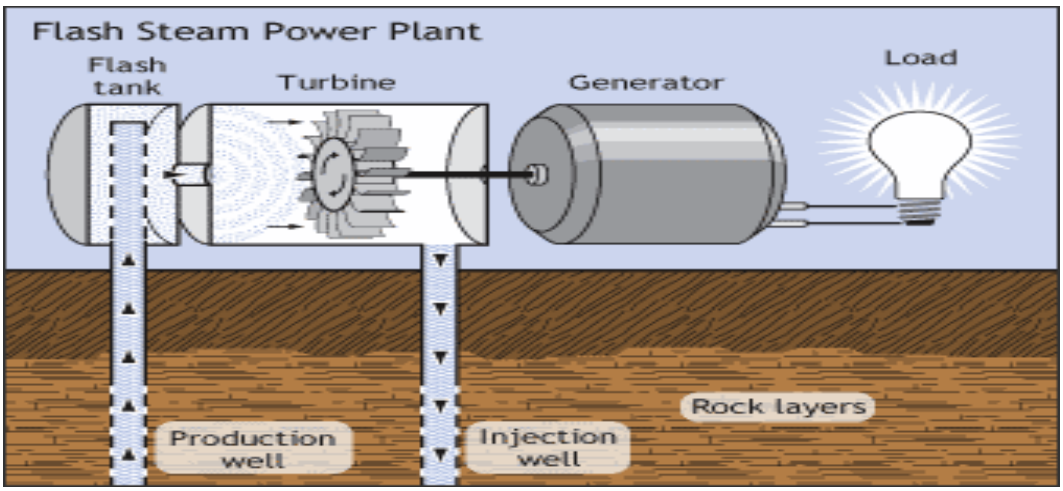

Figure 1.3 Schematic of a Flash Steam Power Plant

(U.S. Department of Energy’s Office of Energy Efficiency & Renewable Energy, 2016)

1.3.3 Binary Cycle Power Plants

The main difference between the binary systems and dry or flash steam systems is that the geothermal fluid is circulated in a closed loop and never comes in contact with the turbine. Instead, it is used to heat another fluid (generally an organic fluid, such as isopentane) which has a much lower boiling point and high vapor pressure at low temperatures, hence these systems are called “binary”. Such systems are operated through a conventional

Organic Rankine Cycle (ORC), where geothermal fluid gives its thermal energy to a secondary fluid (binary fluid, working fluid) in a heat exchanger. As the temperature of the secondary fluid increases, it flashes to vapor, and then drives a turbine which turns a generator to produce electricity. Since the secondary fluid vaporizes at lower temperatures, binary cycle power plants are generally preferred in low-to-intermediate temperature resources. While the lower temperature limit is generally determined by economic analyses, the upper temperature limit of binary cycle systems is restricted by the type of the working fluid, since molecular stability issues may arise at high temperatures.

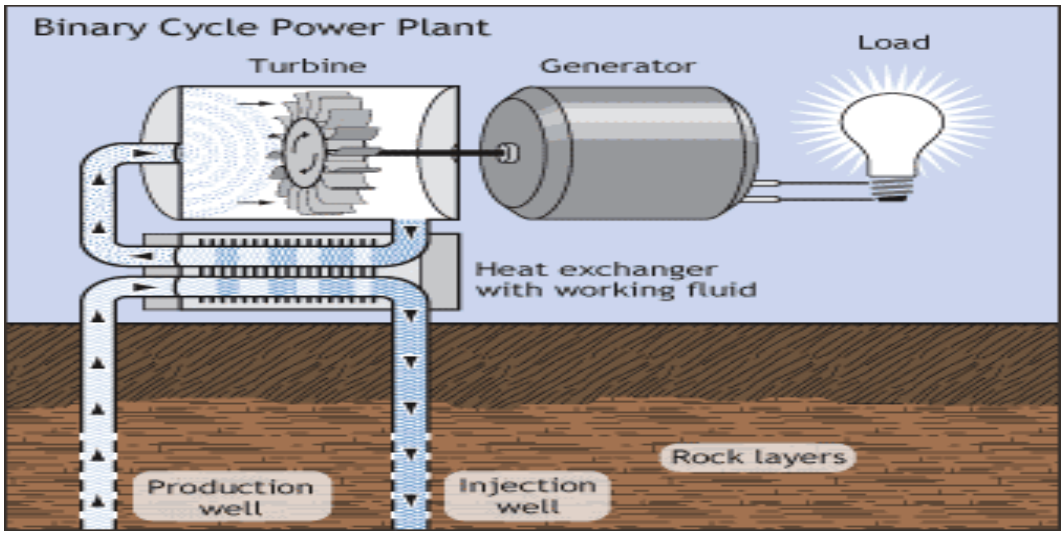

Figure 1.4 Schematic of a Binary Cycle Power Plant

(U.S. Department of Energy's Office of Energy Efficiency & Renewable Energy, 2016)

Since, the output water of flash steam power plants has intermediate temperature levels, they can further be used to feed a binary cycle power plant, to extract more heat and produce more electricity (flash-binary combined cycle). Double and Triple Flash Steam Power plants are also widely used.

1.4 Geothermal Energy in Turkey

Turkey is located in eastern part of Alpine-Himalayan orogenic belt. As a result of tectonic activities, the region has many young grabens, great amount of faults and extensive volcanism, which are some of the most important parameters for existence of a geothermal field. The geothermal potential of the region is manifested by many hot springs, fumaroles, and hydrothermal alterations.

When uplifting occurs in tectonically active regions, grabens may form as a result of tensional forces. Since the earth's crust is thinner under grabens, with an existing heat source (e.g. rising of magma), geothermal fields may occur along these grabens, just like the east-west trending Büyük Menderes and Gediz Grabens in the Western Anatolia (Şimşek, 1985b). These grabens host the most important high and low enthalpy geothermal fields of Turkey. Some examples are: Kızıldere - Denizli (242 °C), Germencik – Aydın (232 °C), Balçova – İzmir (142 °C), Salihli – Manisa (150 °C), Salavatlı – Aydın (171 °C), Seferihisar – İzmir (158 °C), Yılmazköy – Aydın (142 °C), Tekkehamam – Denizli (116 °C) (Ş. Şimşek, 2002), and Alaşehir – Manisa (251 °C) (Akin, 2017)

Turkey has a huge geothermal energy potential. The theoretical geothermal capacity of Turkey is 31,500 MW (Directorate of Mineral Research & Exploration, 2017). 78% of this potential is situated in the Western Anatolia, 9% in Central Anatolia, 7% in Marmara Region, 5% in Eastern Anatolia, and 1% in the other regions. 90% of the potential geothermal fields have low-to-moderate temperatures which are more suitable for direct use. And the remaining 10% high temperature fields can be utilized electricity generation. But, advancements in science and technology may increase the electricity utilization temperature range (e.g. binary cycle power plants, which can use intermediate temperature fluids to produce electricity). As of the end of 2017, total geothermal energy capacity of Turkey reached 1,064 MW with 40 operating geothermal power plants.

1.5 Kızıldere Geothermal Field

Kızıldere geothermal field is the first geothermal energy field of Turkey. It was discovered by Directorate of Mineral Research & Exploration (MTA) after a broad range of geological, geophysical, hydrogeological, and geochemical studies. KD-1 well was completed in 1968 with a depth of 540 m, resulting in the first geothermal discovery of Turkey with a temperature of 198 °C. 16 more wells were drilled until 1973 at varying depths, between 370m – 1240m. In 1974, a 500 kW pilot turbine was installed on KD-13 to produce electricity. The produced electricity was given to the neighboring villages for 6 years, free of charge. After the initial evaluations, the first commercial scale geothermal power plant of Turkey was constructed in Kızıldere by government's electricity authority Electricity Generation Co. Inc. (EÜAŞ) in 1984, with a capacity of 17.8 MW. Only 6 wells (KD-6, KD-7, KD-13, KD-14, KD-15, and KD-16) were found to have appropriate characteristics to generate electricity. As the amount of the produced steam became insufficient in time, three new wells were drilled (KD-20, KD-21, and KD-22) in 1985-1986, to support the power plant. Later, KD-7 was converted to an observation well because of its poor production performance. The R-1 well was drilled to the depth of 2261 m, in 1998, for the purpose of reinjection, but it is found to be very productive with a bottom hole temperature of 242 °C and steam ratio of 18% (Şimşek et al., 2009) . The geothermal potential of deep formations was also investigated by the drilling of R-1. Until the R-2 well starts to injection in 2002, there were no any permanent reinjection operations in Kızıldere, resulting in a reduction in the reservoir pressure and power plant's electricity output.

After being operated for 24 years by Turkish Electricity Generation Co. Inc. (EÜAŞ), Kızıldere Geothermal Field had undergone privatization in September 1, 2008. Zorlu Energy had acquired the operational rights of the license area (64.375 km^2), including the power plant, for 30 years. The output of the plant was almost as low as 6 MW when Zorlu Energy started to operate the field. This reduction was mainly due to the calcite scaling problem, which is very common in geothermal fields of Turkey. Firstly, Zorlu Energy implemented inhibitor injection operations to the wells, to clean the calcite scaling. As a result, power plant's output was increased to 15 MW. As a second step, new production

and reinjection wells were drilled as a part of Kızıldere II development plan. In 2013, the 80 MW Kızıldere II Geothermal Power Plant became operational. The output fluid of Kızıldere II power plant is also utilized in direct geothermal applications such as heating greenhouses and households, and heating the waters at thermal hotels. Since the CO_2 content of Kızıldere geothermal fluid is high (1.5 – 3 % by weight), it is used in dry ice production. Drilling activities, together with geophysical and geochemical studies, have shown that a deeper and hotter reservoir is exist in the field. So, Kızıldere III development plan was prepared, aiming to exploit the deeper resources. Kızıldere III Geothermal Power Plant is the biggest geothermal power plant of Turkey and one of the biggest in the world, with a total capacity of 165 MW. The total capacity of the Kızıldere Geothermal Field has reached 260 MW, making the field one of the most important geothermal energy places of the world.

1.5.1 Geographical Setting of the Kızıldere Field

Kızıldere geothermal field is located between Denizli and Aydın provinces, at the eastern part of the Büyük Menderes Graben, between the Buldan and Babadağ Horsts. The field is at the southern part of the Menderes Massifs, which is one of the largest (300x200 km) metamorphic massifs in Turkey (Bozkurt & Oberhänsli, 2001). The meandering Büyük Menderes River is in the vicinity of the Kızıldere Geothermal Field.

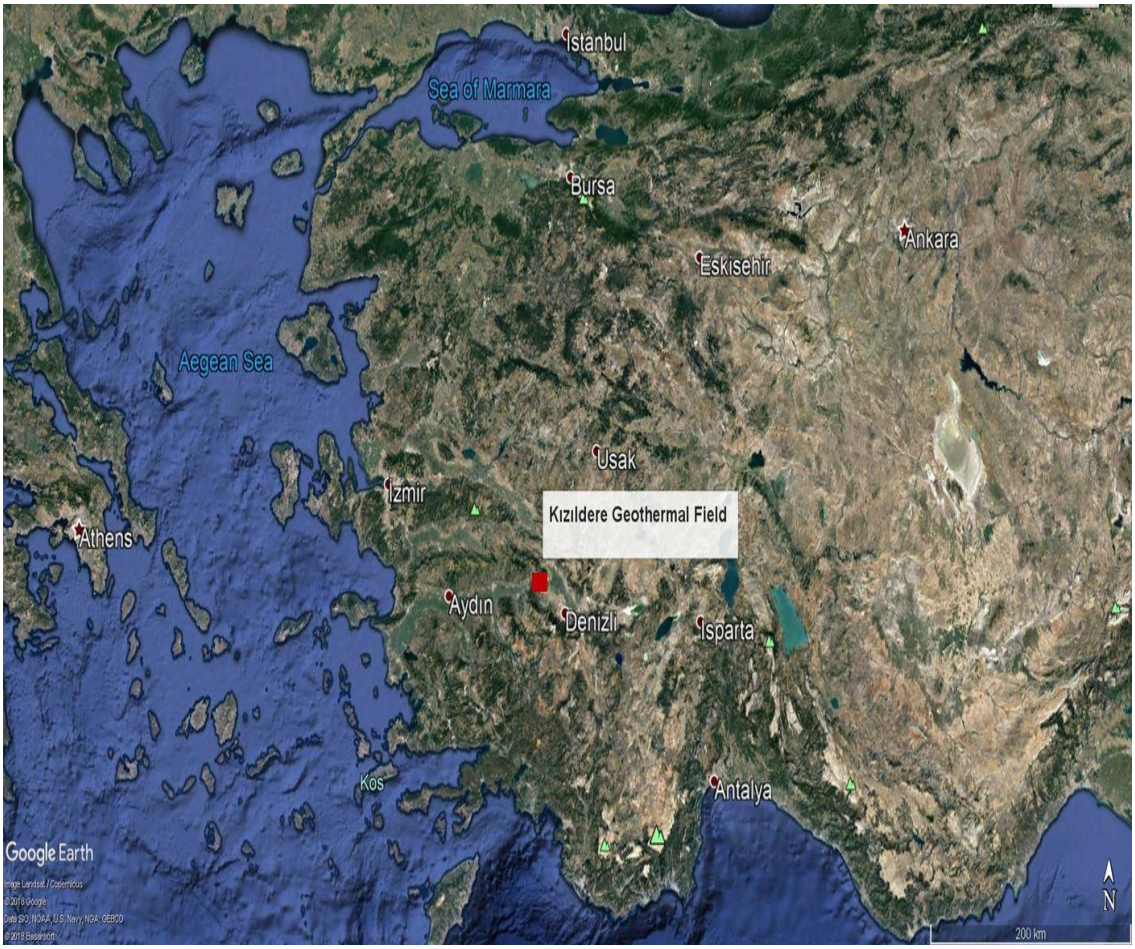

Figure 1.5 Location of the Kızıldere Geothermal Field

1.5.2 Geology of the Kızıldere Geothermal Field

Kızıldere Geothermal Field is in the eastern part of the Büyük Menderes Graben. Paleozoic metamorphics of Menderes Massifs and Pliocene and Quaternary sedimentary rocks form the general stratigraphy of the field (Şimşek et al., 2009). Menderes metamorphics form the basement rocks, which mainly consist of augen gneisses, schists, quartzite, micaschists and marbles (Karamanderesi, 2013). The upper Pliocene and Quaternary sedimentary rocks have been divided into four lithological units(Şimşek, 1985a). These units, from bottom to top, are Kızılburun Formation, Sazak Formation, Kolankaya Formation, and Tosunlar Formation. The Kızılburun Formation consists of

well-consolidated 200 m thick red-brownish conglomerates, sandstones, and claystones. It behaves as a caprock due to its impermeability and forms the boundary between the Paleozoic metamorphics and Pliocene sediments. Sazak Formation is the shallow reservoir section of the field and mainly consist of 100 - 250 m thick limestones, but gradations into marls and sandstones were observed, laterally and vertically, which makes a restriction for a continuous reservoir aspect. Most of the first wells of the Kızıldere Field (KD-1, KD-1A, KD-2, KD-3, KD-4, KD-8, KD-12) were producing from the Pliocene limestones of the Sazak Formation. The 350 – 500 m thick intercalated yellowish green marls, siltstones, and sandstones which overlie the Sazak Formation is named as Kolankaya Formation. This impermeable formation forms the caprock of the shallow reservoir section. The Tosunlar Formation forms the upper unit of the Pliocene and Quaternary sedimentary rocks. It consists of poorly consolidated conglomerates, mudstones, and sandstones and have a thickness of about 500 m.

The interbedded marble-quartzite-schist section of the upper unit of the Menderes metamorphics are called İğdecik Formation, and forms the intermediate level reservoir of the Kızıldere geothermal field, with a varying thickness of 100 - 300 m. This formation is reached for the first time with the drilling of KD-111 well, in 1969, and followed by the drilling of KD-6, KD-7, KD-9, KD-13, KD-14, KD-15 and KD-16 wells. Temperature values as high as 212 °C were observed (KD-16) (Şimşek, 1985b) . İğdecik Formation has better reservoir characteristics compared to the Sazak Formation. Secondary porosity and permeability values are higher than that of the Sazak Formation. The water of the first power plant of the Kızıldere geothermal field were coming from the KD-6, KD-7, KD-13, KD-14, KD-15, KD-16, KD-20, KD-21, and KD-22 wells, all penetrates to the İğdecik Formation. Although they show different reservoir characteristics, Sazak and İğdecik Formations are thought to be connected by faulting.

A deeper, third reservoir section, which mainly consists of metamorphic schist and marble, was discovered with the drilling of R-1 well in 1998, with a depth of 2261 m. This schist-marble formation is found to be a good production zone, but is not suitable for reinjection purposes (Karamanderesi, 2013). The wells which penetrates through the third reservoir can supply the water to the power plants, while the second reservoir (İğdecik

Formation) can be used as reinjection purposes, since it has enough permeability for reinjection.

The general stratigraphy of the Kızıldere Geothermal Field is shown below (Şimşek et al., 2009).

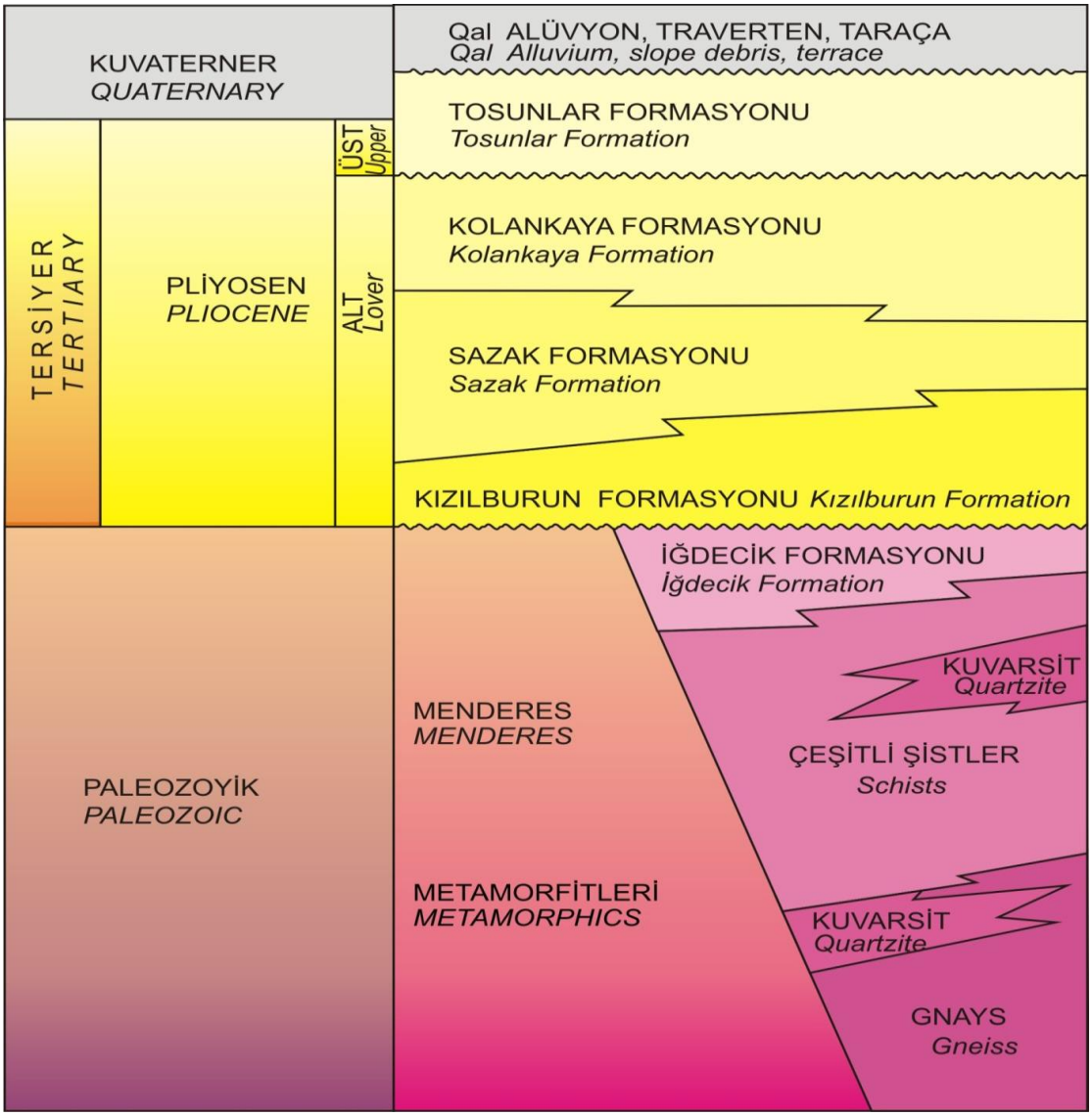

Figure 1.6 General Stratigraphy of the Kızıldere Geothermal Field (Şimşek et al., 2009)

1.5.3 Previous Modeling Studies of Kızıldere Geothermal Field

Many modeling studies of the Kızıldere Geothermal Field can be found in the literature. (Özkaya, 2007) used the SUTRA (Saturated-Unsaturated TRAnsport) numerical simulator which uses a hybrid finite element method and integrated finite difference method with two-dimensional (2D) quadrilateral finite elements for the discretization of the continuous space. In that time, there were only 8 production wells and the areal extent of the model was only limited compared to the current operational area. Since the model was two-dimensional, producing zone was fixed to a level equal to a representative depth of İğdecik Formation. Therefore, two deep wells of that time (R-1 and R-2) were considered as shallow wells with high productions by modifying their actual pressures with the subtraction of the hydrostatic pressures below the İğdecik Formation. Additionally, it was considered in the study that, both pressure responses and temperature declines of the reservoir would be modeled separately throughout the modeling studies. Similarly, the areal extent of the Kızıldere model by (Yeltekin, 2001) was only limited with Phase-I wells, and the area was divided into only 480 grid blocks (8x12x5). Production history of the field for the period of 1984 – 2000 was used for history matching. In that time, there were only 8 production wells. A three-phase multi-component thermal and steam additive simulator, STARS of GMC (Computer Modeling Group) was used throughout the study. Although, the software is capable of handling non-isothermal flow, in most cases the reservoir was assumed as isothermal because of the numerical instabilities occurred during the simulations. The reservoir temperature was taken as 200 °C throughout the study. The main explanation for assuming an isothermal reservoir was that the temperature decline was small enough within the production period, 1984 – 2000. The most important deficiency of both of the above-mentioned studies is that CO_2 was not considered in their simulations. A recently published numerical model of the Kızıldere Geothermal Field (Garg et al., 2015), reaches a bigger areal extent and uses the available production and injection data for the period January 1984 – March 2013, including both the Phase-I and Phase-II wells in that time. Leidos's STAR geothermal reservoir simulator was used to construct a 3D numerical model of the field. In their study, CO_2 and NaCl were included in the simulation as 3% and 0.5%, respectively. The computed pressure and

temperature data were compared with the available actual data at several computational times. It was decided to use the computed state at 100,000 years for history matching. However, it can be observed in the pressure vs. time plots that the simulation pressures were still increasing at the beginning of the history matching, indicating that the natural state conditions had not been reached, yet. So, it can be deduced that although good matches were obtained, 100,000 years were not enough for the model to reach the stabilized conditions (natural state conditions). Or, another possible explanation for this situation can be related with the amount of the water flux entering to the model from the bottom heat source. High amount of water flux into a limited area model might be increasing the pressures even at the natural state conditions.

CHAPTER 2

STATEMENT OF THE PROBLEM

In geothermal reservoirs, varying quantities of CO_2, H_2S, NH_3, H_2, N_2, and CH_4 may present in the geothermal fluid. These gases are called non-condensable gases (NCG), since they are at gaseous state at reservoir conditions and generally dissolved in the geothermal water. Among others, carbon dioxide (CO_2) is the most dominant NCG. It may constitute as much as 99% of the all non-condensable gases.

Geothermal fields of Turkey contain high amount of CO_2. Geothermal fluids of Büyük Menderes and Gediz grabens were reported to have 900 – 1300 grams of CO_2 per kWh of electricity production, while the global average, in 2001, was 122 gCO_2/kWh (Callos et al., 2015) . Although binary cycle power plants work in a closed loop, flash steam plants release the CO_2 into the atmosphere, which arises environmental concerns, and also negatively effects the reservoir management targets in terms of the reservoir pressures.

In Kızıldere Geothermal Field, the amount of CO_2-dissolved in the water is around 1.5 wt.% in shallow reservoirs, and around 3 wt.% in deep reservoirs. As high as 6 wt.% of dissolved CO_2 values were observed. As of May 2018, 34 wells are producing approximately 6900 tonnes of geothermal fluid per hour to feed the power plants of the Kızıldere field. Considering 3 wt.% CO_2, approximately 200 tonnes of carbon dioxide is produced per hour in Kızıldere Geothermal Field. Although, geothermal energy is always considered as a clean and renewable source of energy, the high CO_2 emission rates of

geothermal fields such as the Kızıldere field, are against the general opinion.

To develop solutions to the reservoir management problems of the Kızıldere Geothermal Field, and predict the consequences of potential/possible future operations, a computer-based model of the entire geothermal field needs to be created. Deficiencies of the previous studies arises the need of an accurate and more realistic numerical model of the Kızıldere Geothermal Field. This model

- should include the effects of non-condensable gases, especially the carbon dioxide,
- should has a larger areal extent, covering all the current and potential future operation areas,
- should be three-dimensional (3D), covering productive deep metamorphic rocks.

Beside these,

- Simulation should be carried out non-isothermally, and
- History matches should be based on a natural state model where no instabilities are observed.

This study aims to create a model where the above-mentioned conditions are satisfied, and to carry out future predicting studies to develop solutions to the excess amount of CO_2 production rates and also the rapid decline in the reservoir pressures.

CHAPTER 3

GENERAL OVERVIEW OF GEOTHERMAL RESERVOIR SIMULATION

Simulating a geothermal reservoir in a digital environment (e.g. computers) is a strong technique to visualize and better understand the real world situation of the reservoir, which also enables to carry out any desired operation and observe its consequences instantly without even doing it in real world, which in turn saves time and money.

A geothermal system is composed of four main elements: a heat source, a carrier fluid, a fracture system which provides the required flow paths for the carrier fluid, and a reservoir which hosts the geothermal fluid. A successful simulation of a geothermal system should include as accurate and reliable information as possible about these elements.

The first step in reservoir simulation is to construct the conceptual model of the field. Then, the conceptual model should be represented by mathematical equations which describe all the processes and interactions given in the conceptual model. Thirdly, these mathematical equations should be solved with a numerical solution technique, which also requires the discretization of the model domain both in space and time. After obtaining the numerical model of the field, simulations can be carried out. As a last step, results of the numerical solution should be calibrated and validated by comparing the available field data. In this step, model parameters and assumptions are reevaluated. After successfully going through all these steps, the numerical simulation will be a good representation of the geothermal system, and it can be used for implementation of scenarios of interest.

3.1 Data Acquisition

Before constructing the conceptual model of a geothermal system, as many data as possible should be collected by means of field (or wellbore) surveys. These surveys provide information about the geological, geophysical, and geochemical properties of the field, as well as fluid and rock interactions, and physical and chemical processes occurring in the geothermal system. Their accuracy and reliability is often a question mark for scientist and engineers, but collected data is a good starting point for constructing the conceptual model. They can be reevaluated as the simulation proceeds.

Data acquisition methods in geothermal exploitation can be regarded as field surveys (geophysical and geochemical surveys), measurements performed through a wellbore (tracer tests, pressure transient tests, well logs, injectivity tests) and laboratory experiments.

3.1.1 Geophysical Surveys

Geophysical surveying methods can be used for exploring potential geothermal energy fields, as well as monitoring geothermal reservoirs under exploitation (Mariita, 2011). Geophysical surveying methods either use the natural energy of the earth or artificial energy induced into the ground. Gravity, magnetics, and Magnetotelluric (MT) methods make use of the natural energy of the earth, while direct current, electro-magnetic, and seismic methods make use of artificially created energy to get information from the subsurface. Using these methods in combination with another is much more practical than trusting only one source of information. By doing so, if there is ambiguities or anomalies arising from one of the geophysical surveying methods, the other method can be considered for the corresponding zone.

Geophysical surveys can be grouped into four, according to the physical properties they utilize while investigating the subsurface geothermal structures:

- Gravity surveys (rock density)

- Magnetic surveys (magnetic susceptibility)
- Seismic surveys (propagation velocity of elastic waves)
- Electrical surveys - MT and TEM (electrical conductivity)

3.1.1.1 Gravity Surveys

In gravity surveying, the variations in the earth's gravitational field are measured to investigate geothermal activity and subsurface geology. Gravitational variations are generated by lateral density differences between subsurface rocks. Rock with a different density than the surroundings may be related to the magmatic history of the area. Rock densities are generally in between 2-3 g/cm^3, and crystalline rocks generally have higher densities than sedimentary rocks. Gravity surveys detects subsurface density variations in forms of gravity anomalies, which may be related to a deep magmatic body, or a heat source. Another important application of gravity surveys is to monitor the fluid removal rate in the reservoir, which in turn, determines the reinjection rates. By repeating gravity surveys, differences between mass extraction and replacement by natural inflow can be estimated, since fluid removal effects the density of the reservoir rock (Manzella, 1973).

The device which measures the variations in the earth's gravitational field is called gravimeter. The acceleration unit is taken as mGal, where 1 Gal is equal to 1 cm/sec^2. Information about subsurface density can be obtained after making some correlations to the measured gravity values. After the correction of gravity anomalies, the Bouguer anomaly is obtained, which is given by Santos & Rivas (2009):

$$g(corrected) = g(observed) - gf + 0.3086h - 0.04193\rho h + TC \ (in\ mGal)$$

where g(observed); the gravity readings of each gravimeter after the corrections for instrument drift and earth tides, gf; normal reference gravity, 0.3086h; gravity variations due to elevation differences between the locations of gravimeters, 0.04193ρh; correction for mass material between the gravimeter location and sea level, TC; Terrain correction accounts for differences between observed gravitational values, h; thickness in meters,

and ρ; density in g/cm^3.

Gravity surveying is an economic method since gravimeters are portable and easy to use, and also there is no need to use energy to create pulses on the ground. It also provides results within a short term. Using with other means of geophysical surveys, gravity technique is very useful to investigate geothermal activities beneath the surface.

3.1.1.2 Magnetic Surveys

Magnetic surveying is another widely used technique in geothermal exploration studies, generally together with other surveying methods (such as gravity and seismic), to map geological structures. Anomalies in the earth's magnetic field are measured in magnetic surveys. These anomalies are depending on the magnetic properties of subsurface rocks and the surrounding environment. Generally, dykes, faults, and lava flows are the main causes for magnetic anomalies (Mariita, 2011).

Magnetic surveys are carried out by magnetometers. The two types of magnetization of rocks; induced magnetization and permanent magnetization are measured. The strength of the magnetic field is commonly presented in gamma (γ) or nanotesla (nT). In high temperature environments, magnetization is reduced, which is a good indication of geothermal activity.

3.1.1.3 Seismic Surveying

Seismic surveying relies on the fact that propagation velocity of elastic waves changes when travelling through different rock types. The refracted or reflected signals are corresponding to discontinuities in or between formations. The elastic body waves are two types:

- P-waves (primary waves), the propagation of the elastic wave is in the travel direction. They can travel through solids, liquids, and gases.

- S-waves (secondary waves), they move perpendicular (up and down, or side-to-side) to the propagation direction. They can only travel through solids, but not fluids. S-waves are slower than P-waves.

Seismic surveys are divided into two: active seismic methods and passive seismic methods. In active methods, an external source (such as hammer devices or explosions) is used to create seismic waves penetrating through the earth. In passive methods, the source of seismicity is the earth itself, where the seismic activities are detected and analyzed. Propagation times of seismic waves are converted into depth values, and the distribution of subsurface interfaces is acquired.

It should be noted that geothermal activity is generally found within volcanic areas (or at least area with a volcanic history), which are generally associated with crystalline rock bodies. Thus, penetration depth is not high and data interpretation is quite complicated, which makes seismic surveys not cost effective.

3.1.1.4 Electrical Methods

Resistivity is a very important measure in geothermal exploration and monitoring operations. There is a good correlation between resistivity and subsurface material properties such as temperature, pressure lithology, permeability, porosity of rocks, and salinity, phases, and saturations of pore fluids. This correlation can provide valuable information about the geothermal activity of the area of interest. Two most widely used electrical methods in the geothermal exploration and monitoring studies are Transient Electromagnetic method and Magnetotelluric method.

TEM method is an electromagnetic surveying method which uses artificially created signals to be measured as the reflection of the resistivity structure of the subsurface. A strong current is passed through a big ungrounded loop, and a constant magnetic field is generated. Then, the current is turned off. A secondary field is formed as a result of the induced current, decaying with time. The decay rate is then monitored by a receiver located at the center of the loop on the surface. Decay rate and current distribution as a

function of time gives information about the subsurface resistivity structure.

TEM equipment is relatively expensive. To create a strong magnetic field, heavy currents should be induced, which requires heavy generators and measuring coil and wires being able to carry heavy currents. With TEM surveys, subsurface resistivity structure down to 1 – 1.5 km can be studied (Georgsson, 2009).

Magnetotelluric is one of the most powerful and widely used geophysical surveying methods. It uses earth's natural electromagnetic field as its power source to probe the earth without drilling any well. Magnetotellurics is simply measuring the time variations of naturally induced electric currents (telluric currents), E(t), on the earth's surface, and resultant magnetic fields, B(t). As a result, information about electrical conductivity (or resistivity) of the subsurface material is obtained. A region with a low resistivity can be an indication of high temperature geothermal reservoir, since as the temperature increases resistivity decreases (conductivity increases).

In geothermal exploration, the amount of depth of penetration depends on the frequency of the signal. Low frequency signals (0.00001 – 10 Hz) penetrate deeper than high frequency signals (10 – 1000 Hz) (Georgsson, 2009). The measurement equipment is quite simple and portable. But measuring magnetic field, **B**, and naturally induced electrical field, **E**, both as function of time, requires several hours at each measurement location. Details about the analysis of MT data (including 3-D inversion using Bayesian statistics) can be found in Spichak et al. (1999).

This method can be used in combination with TEM method, where TEM measurement are used to map the uppermost levels. By that way, interpretation of MT measurements is enhanced, providing better understanding of deeper levels. A good resistivity distribution information can be obtained from deeper parts of a geothermal system (5 – 10 km).

3.1.2 Tracer Tests

A geothermal tracer test simply involves injecting a compound (tracer) into a geothermal system and monitoring its recovery through time from predetermined observation points. The most common utilization of tracer tests in conventional geothermal development is to investigate flow paths between injection and production wells. The main purpose is to predict the cooling effects of the reinjected fluid on the production wells (since reinjected fluid is much cooler than the reservoir fluid). The selected tracer should meet some important criteria:

a. Its concentration should not be higher than the expected tracer concentration so that the tracer can easily be distinguished
b. It should be stable under the reservoir conditions
c. It should be relatively inexpensive, since high amount of tracers may need to be used
d. Its analysis should be fast and inexpensive
e. It should be environmentally benign.

Tracers can be liquid-phase, gaseous-phase, or two-phase (Axelsson, 2013b). The most widely used liquid tracers are halides (iodide, bromide), radioactive tracers (iodide-125, iodide-131), fluorescent dyes (fluorescein, rhodamine), aromatic acids (benzoic acid), naphthalene sulfonates. Sulphur hexafluoride and fluorinated hydrocarbons are examples of gaseous tracers. Examples of two-phase tracers can be tritiated-water (HTO) and alcohols (methanol, ethanol, n-propanol).

Geothermal tracer tests can be conducted by injecting the selected tracer (i) from a single injection well, and then produced back from the same well, (ii) one injection and one production well, (iii) more than one injection and production wells. If single well technique is used, only the peripheral of the well is investigated. The duration of the tracer test is specific for each geothermal system, and difficult to determine beforehand.

3.1.3 Pressure Transient Analysis (PTA)

Pressure Transient Analysis (PTA) is one of the main tools of geothermal subsurface characterization. Some key parameters such as formation permeability-thickness value, formation storage coefficient, skin factor of the well, wellbore storage capacity, and reservoir boundary conditions (if the test is long enough) can be obtained through a pressure transient test. Such parameters form the basis of conceptual model of a geothermal system.

Pressure transient analysis is generally performed based on the basic reservoir model, Theis model, and its variants. Theis model describes a reservoir as a laterally permeable, homogeneous, constant thickness layer which is bounded at the top and bottom. A two-dimensional horizontal flow occurs towards a production well. A basic Theis model and different reservoir and wellbore-reservoir models are given by Bödvarsson and Whiterspoon (1989), (as cited in Axelsson, 2013a).

Different reservoir models (or boundaries), as well as reservoir-wellbore interactions will yield different responses in pressure transient testing. A good representation of such responses can be seen on a semi log plot of pressure change vs. time.

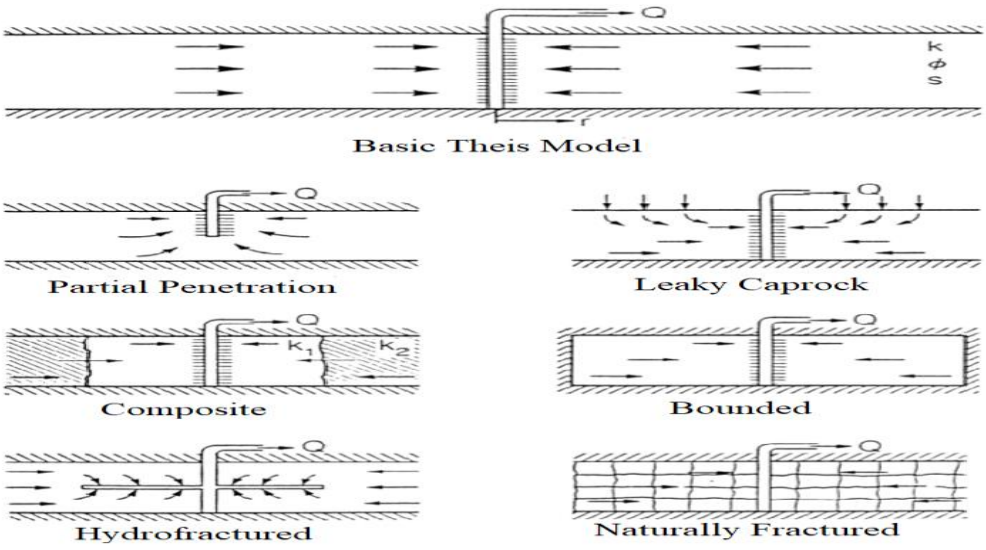

Figure 3.1 Sketches of basic Theis model and other variants

(by Bödvarsson and Whiterspoon (1989), (as cited in Axelsson, 2013a)

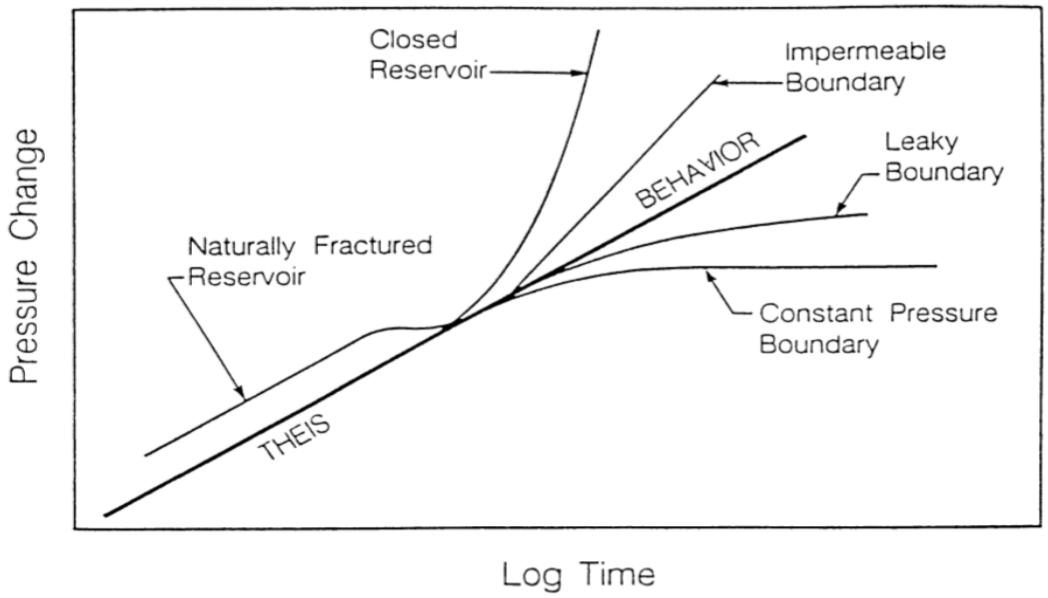

Figure 3.2 Behavior of different reservoir and boundary models on a Semi-log plot

(by Bödvarsson and Whiterspoon (1989), (as cited in Axelsson, 2013a)

There are different types of pressure transient test implementations. The most widely used methods are build-up tests, drawdown tests, injection tests, fall-off tests, and interference tests.

- In a build-up test, the production should be kept approximately constant for several days, before closing the well. The pressure will start to increase (pressure build-up) with the shut-in of the well. The rate of pressure build-up with respect to time reflects the formation properties.
- In drawdown tests, a well is flowed at a constant rate, and bottom-hole pressure as a function of time is measured. Then, the measured values are analyzed to estimate the reservoir properties. The biggest issue in a drawdown test is the inability to ensure a constant flow rate.
- In injection tests, the procedure is just reverse of the drawdown test. Instead of producing, fluid is injected into to reservoir and the pressure responses vs. time is measured. The injectivity index, among others, is a good parameter which is

obtained through injection tests. It reflects the performance of the well, meaning that higher the injectivity index higher the reservoir permeability. It is simply defined as the ratio of the change in the injection rate and the change in the measured pressure.

$$Injectivity\ Index = \frac{\Delta Q}{\Delta P}$$

- In fall-off tests, instead of measuring the pressure build-up after the shut-in of a producing well, pressure fall-off is measured after the shut-in of an injection well.
- In interference tests, a production well and observation wells are selected so that the reservoir properties and connectivity between these wells are determined. Interference tests simply based on production from a well, and observing pressure responses with respect to time from offset wells.

Generally, injection and fall-off tests are implemented alternately, because of the harmony in the nature of their methodology. But in the injection part of the test, reservoir fracturing may occur. In this case, conventional pressure transient test analysis will fail, since they do not account for fracture (rock) mechanics (Bakar & Zarrouk, 2016). Build-up tests are generally more practical and preferable compared to constant-flow rate tests (drawdown), since maintaining a no-flow condition is much easier than maintaining a constant flow rate condition.

There are different ways to analyze the pressure transient data, coming from any of the above mentioned testing methods. These are: semi logarithmic analysis, dimensionless variables and type curve analysis, pressure derivative method, and deconvolution method. The details of pressure transient analysis methods, as well as general overview of pressure transient analysis in geothermal resource assessment are given in (Rutagarama, 2012).

3.1.4 Well Logging

Well logging is a strong tool in geothermal reservoir investigations, which is conducted through a drilled well. Measurement electronics and sensors are lowered into a well, on a

wireline, to conduct intended measurements through the intended intervals. Objectives of well logging (or wireline logging) can be (i) studying the borehole geometry and determining the variations in the completed interval diameter, (ii) investigating the rock properties and fractures intersected by the wellbore, (iii) measuring reservoir pressure and temperature values, (iv) locating the feed zones. The most widely used geothermal loggings are (Axelsson & Steingrimsson, 2012):

- Caliper and cement bond logging (CBL), which measure variations in wellbore diameter and integrity of casing-cement bond, respectively. Wellbore diameter is generally needed to determine wash-out intervals through the wellbore. Information about casing-cement bonding is very important for measuring the success of cementing operations, which directly determines the life of the wellbore.
- Geophysical wireline logging (often includes resistivity logs, neutron-neutron porosity logs, and natural gamma-ray logs) measures different physical properties of the formation, intersected by the wellbore. Resistivity logging is an electrical method which measures formation resistivity, a valuable parameter for reservoir engineering studies. It can either be used for qualitative description of the measured interval, or can be used quantitative analysis such as porosity calculations through Archie's equation (Archie, 1942). Results of resistivity logs are generally evaluated with the results of TEM and MT surface geophysical surveys. Neutron-neutron porosity logging provides information about formation porosity by measuring the total hydrogen content, correlated as the amount of water by formation volume, which depends on the formation porosity. Detailed procedure can be found in Steingrímsson (2011). Natural gamma-ray logging makes use of the natural decaying properties of natural radioactive isotopes (Potassium, Thorium, Uranium) to distinguish certain formation types.
- Televiewer logging is an acoustic method, which is used to get images of the wellbore, where fractures can easily be observed, with their dip angle and strike direction. Steingrímsson (2011) gives details of the application of the televiewer logging, as well as other uses of the method. The following figure is taken from

his study, where output of a televiewer log, showing an open permeable fracture (traced with a green line on the log), is given.

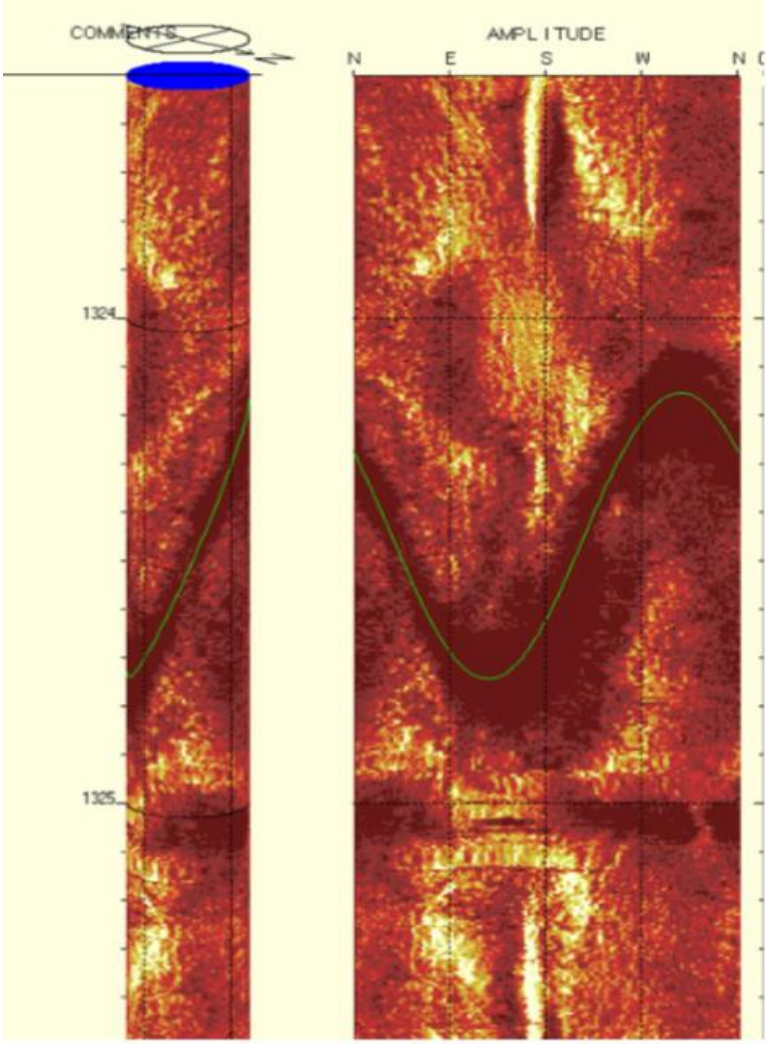

Figure 3.3 Illustration of an open permeable fracture on a televiewer log

- PTS logging, which stands for pressure-temperature-spinner measurements, provides main physical properties of a geothermal reservoir. Spinner logging is often conducted to measure flow rates in a wellbore, as well as inflow and outflow through feed zones.

The instrument used in geothermal wellbore (wireline) logging operations are generally adapted from the oil&gas industry. But, the main feature of a geothermal reservoir, high temperature, limits the usage of conventional logging tools. It requires specifically built devices and electrical cables to conduct logging operations in a high temperature geothermal well (see Massiot et al., 2010).

3.1.5 Laboratory Experiments

Wide variety of rock and fluid properties can be determined in laboratory using different methods. But it should be taken into consideration that parameters measured in the laboratories may not fit the actual field parameters, since there can be huge differences between the laboratory conditions and the field conditions. However, determining thermal properties, compressibility, viscosity and density as function of time, solute concentration, hydraulic conductivity, storage coefficient, and effective porosity properties provide vital information in a simulation study.

3.2 Conceptual Model

A conceptual, theoretical model should be developed before setting up a simulation model of a geothermal field. In geothermal reservoir simulations, the conceptual model is an idealized, descriptive and qualitative representation of the geothermal system. Many of the required data may not be available prior to modeling and simulation studies, or may contain high amount of inaccuracy. So, appropriate assumptions, corrections, and modifications should be made before, during, or after the construction of the conceptual model. Most of the time, working with more than one conceptual model is more sufficient and more practical.

Among other elements of a geothermal system, understanding and describing the flow in porous and fractured media is especially of a great importance in reservoir simulation studies, since most of the geothermal reservoirs are situated in fractured rocks. The main

issue for flow in fractured reservoirs is describing the fracture-matrix interaction, under various conditions (e.g. multiphase flow). There are many different approaches to describe the flow in fractured media, generally depending on the geometry, amount and properties of the fractures and properties of the reservoir medium. The three main types of conceptual models of fracture flow are: effective continuum method (ECM), dual continuum approach, and discrete fracture network (DFN) approach. Each approach has its own advantages and disadvantages depending on the purpose of the model and field properties.

3.2.1 Equivalent Continuum Method (ECM)

The equivalent continuum method can be attributed as the simplest approach for modeling flow in fractured and porous media. This approach describes the model area as a single porous medium. The properties of the model are chosen in a way that this single porous medium approximately represent the properties of the fractured reservoir. According to Long et al. (1992, as cited in Bundschuh & Suarez, 2010) four criteria must be satisfied for using equivalent porous medium approach for fractured rocks:

1. The density of the fractures must be high enough
2. Fracture orientations must be randomly distributed
3. The apertures of fractures are assumed to have a constant width, rather than randomly distributed widths
4. The extension of the model area must be large enough

The ECM approach is widely used due to its simplicity, but becomes unsuitable as the fracture, rock, and flow characteristics become so complex that they cannot be represented by a single porous medium.

3.2.2 Dual Continuum Approach

Dual continuum concept (where the matrix and the fractures are modeled as different but interconnected continua) is the most widely used approach for the fractured rock flow

models (Wu & Pruess, 2005). This concept includes dual porosity model (Barenblatt et al., 1960; Warren & Root, 1963), multiple porosity model, dual permeability model (which permits vertical flow between matrix blocks), and more general multiple interacting continua (MINC) models (Pruess & Narasimhan, 1982, 1985).

Dual porosity approach is based on two concepts: (1) Fractured reservoirs have two types of porosities: matrix porosity and fracture porosity. The fracture porosity is so small that almost all the fluid is stored in the matrix porosity. (2) Fractures have much higher permeability than the matrix. So, the fractures are the main flow paths, and when the fluid in the fractures have been drained, the stored fluid begins to flow from matrix to the fractures.

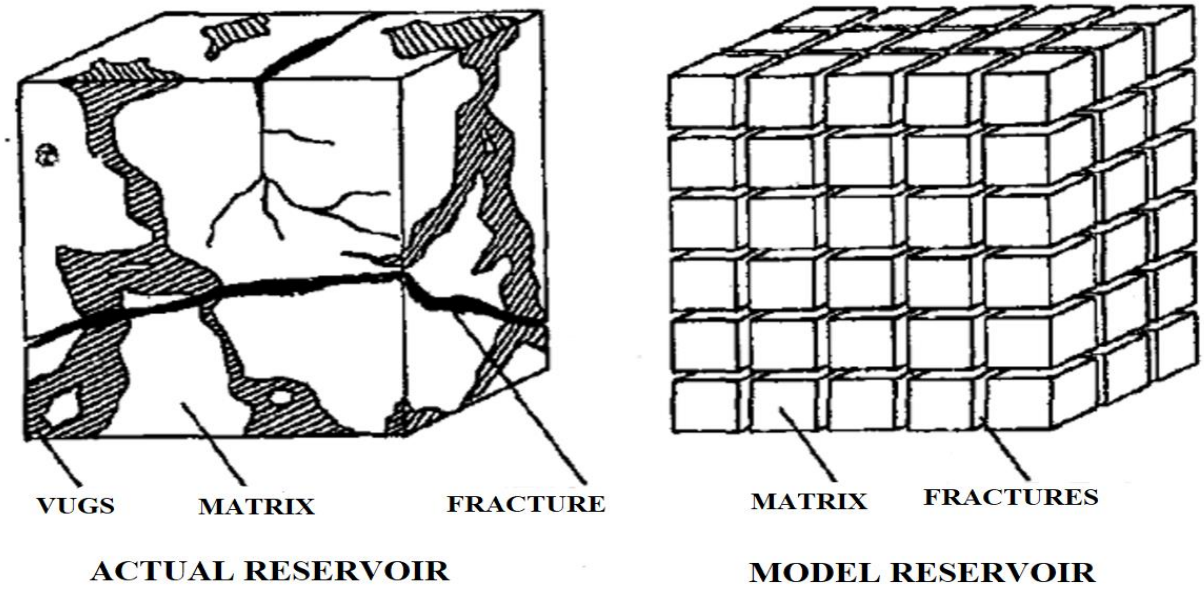

Figure 3.4 The actual reservoir and its representation in dual continuum approach (Warren & Root, 1963)

In the dual porosity approach, low permeability matrix blocks are interconnected by a network of high permeability fractures. Local fluid and heat exchange may occur between the rock matrix and fractures by means of interporosity flow, where the driving force is

the pressure (or temperature) differences between them. Global flow occurs only through the fracture system, which can be described as an effective porous continuum (Pruess, 2002). Double porosity approach does not account for matrix-to-matrix flow, and treats matrix blocks as sinks and sources of fractures.

The main issue in double porosity model is that the pressure or heat changes in fractures quickly penetrates into the matrix blocks. However, transition from fractures to matrix occurs only slowly, especially for multiphase or coupled fluid and heat flows. So, an interporosity approach is needed, which accounts for the mass, pressure, and temperature transitions at the fracture-matrix interface. Multiple interacting continua (MINC) method describes the interporosity flow accurately by subgridding the matrix blocks (as shown in Figure 3.5), and resolves the pressure, temperature, and mass gradients at the fracture-matrix interface. In this concept, the changes caused by production and injection wells (sources/sinks) will be perceived rapidly in the fracture system, while penetrating the matrix blocks slowly. The MINC method cannot be used in the systems where the fractures are so sparse that they cannot be approximated as a continuum.

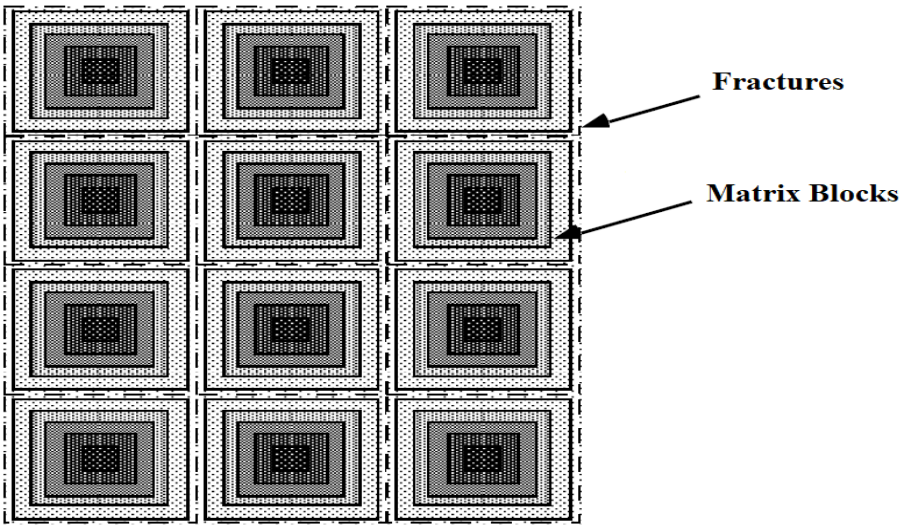

Figure 3.5 Matrix subgridding in the MINC approach (Pruess, 2002)

3.2.3 Discrete Fracture Network (DFN) Approach

In discrete fracture network approach, fractures are treated as the central features of flow and transport, and the rock matrix is considered as impermeable. The main motivation of DFN method is the fact that the flow in fractured rocks tends to be dominated by discrete conduits created by faults, fractures, and fissures, unlike the continuum models where heterogeneities and discrete properties are averaged and represented by a representative elementary volume (REV).

Although it is very advantageous to describe every single fracture, the main issue of this approach is the requirement of lots of information on every single fracture (orientation, size, aperture, shape, location, hydraulic properties) in the model area, which is very difficult and time consuming especially if the number of fractures is high and fractures have irregular surfaces (Bundschuh & Suarez, 2010), which makes the application of this method in field scale simulation studies highly computationally demanding.

3.3 Mathematical Model

After the conceptual model is created, the governing physical and chemical relations in a geothermal system should be expressed mathematically. The flow equations in porous media are based on conservation of mass, momentum, and energy equations, and some other constitutive fluid and porous material properties (compressibility, density, viscosity, porosity etc.) (Kleppe, 2018).

3.3.1 Mass Balance

Conservation of mass or mass balance equation is of fundamental importance to fluid flow studies in porous media. It simply states that, the difference between the mass flow into and out of some reservoir volume represents the change in fluid mass in that volume.

Rate of mass into the reservoir volume	−	Rate of mass out from the reservoir	=	Rate of change of mass in the reservoir

3.3.2 Momentum Balance

The governing equations for conservation of momentum are the Navier-Stokes equations, but generally Darcy's Equation is used to describe the low velocity, laminar flows in porous medium (Kleppe, 2018). The Darcy's Equation for single phase, horizontal flow is:

$$q = A\frac{k}{\mu}\frac{\Delta P}{L}$$

Where q is the flow rate, A is the cross sectional area of the given reservoir volume, k is the permeability of the rock, μ is the viscosity of the fluid, L is the length of the fluid flow, and ΔP is the pressure difference between two ends of the corresponding reservoir volume.

There are alternative equations to Darcy's Equation such as Forchheimer Equation (which describes high velocity flow) and Brinkman Equation (which describes both porous and non-porous flow).

3.3.3 Energy Balance

Unlike hydrocarbon reservoirs, geothermal systems are highly temperature dependent and cannot be attributed as isothermal systems. Temperature must be included in governing mathematical equations and conservation of energy must be satisfied in geothermal reservoir studies. The first law of the thermodynamic, or energy balance,

$$\Delta U = Q - W$$

where ΔU is the change in the internal energy of the system due to the heat added Q to the system, and mechanical work W done by the system. This law states that the heat added to the system does not fully contribute to the internal energy of the system, but some portion of the heat is converted to mechanical work. In a finite reservoir volume, fluid exchange with surroundings must be considered together with heat and work exchanges. So, the general energy balance can be written as follows (Pruess, 2002).

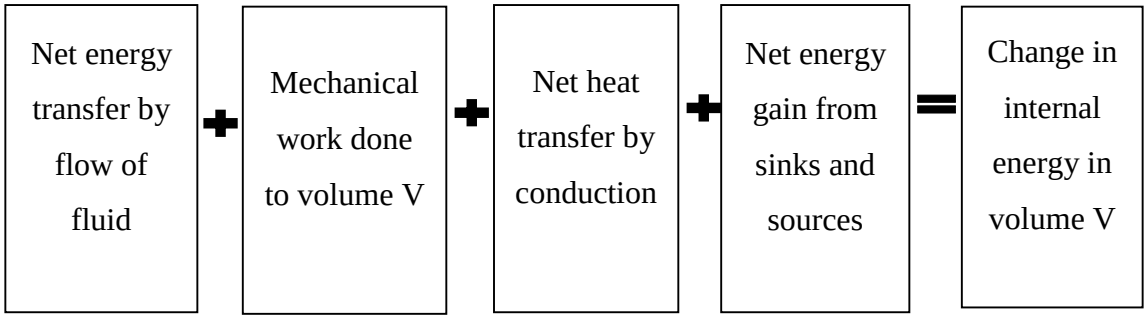

3.3.4 Fluid and Rock Properties

Geothermal fluids are generally a mixture of water and steam, with dissolved non-condensable gases (NCG) such as carbon dioxide (CO_2), and dissolved solids such as sodium chloride (NaCl). The physical and chemical properties of the geothermal fluid, properties of the porous material (rock), and their interactions must be expressed in mathematical equations.

3.4 Numerical Solution

The mathematical model forms the basis of the geothermal reservoir simulation. Space and time dependent problems are usually defined as partial differential equation (PDEs). For simplified systems, analytical solution to these partial differential equations is possible. However, geothermal reservoir systems contain high amount of complexity due

to the irregularities in thermodynamic conditions and fluid and formation properties. So, the conservation of mass, momentum, and energy equations in geothermal conditions must be solved numerically (Pruess, 2002). There are three main discretization techniques (other methods are also available such as boundary element method or meshless methods) to solve the mathematical model (partial differential equations) of a geothermal system:

1. Finite Difference Method
2. Finite Element Method
3. Finite Volume Method (Integral Finite Difference Method)

It should be noted that before implementing any of the mesh-based numerical solution techniques, the space and time variables must be discretized. By that way, the partial differential equations can be approximated by algebraic equations for each grid block.

3.4.1 Discretization of the Space and Time

Geologically, space discretization is simply breaking down the entire volume of the reservoir into smaller sub-volumes. The idea behind the discretization is that the variations and heterogeneities within the geothermal system can be averaged locally in sub-volumes, or "grid blocks", which provides a better representation of the system, and also provides easier and faster solutions to the mathematical equations. But as the grid size gets smaller, more computational power and time will be required to solve the equations by numerical methods.

Although there are many different grid shapes, the regular hexahedral Cartesian grids (Figure 4.3.1.a) are the most common and practical type of model grids. The three widely used grid types; structured regular grid, structured irregular (stratigraphic) grid, and unstructured irregular (fully unstructured) grid are shown below (taken from Souche, 2003, as cited in Moog, 2013).

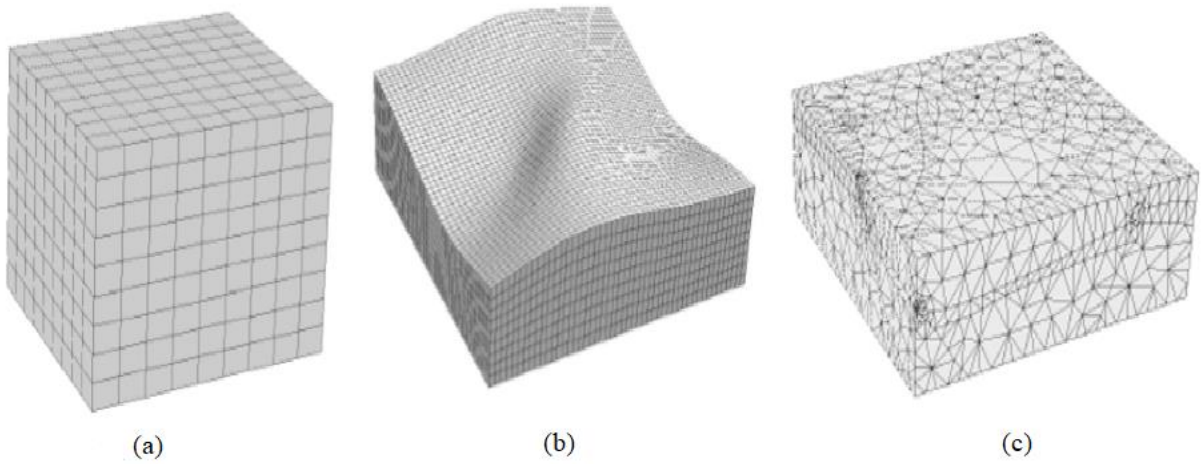

Figure 3.6 (a) Structured regular grid (b) Structured irregular (stratigraphic) grid (c) Unstructured irregular (Fully unstructured) grid

(taken from Souche (2003), as cited in Moog, (2013))

After the space discretization, if the numerical simulation is performed (i.e. solving the discretized mathematical equations for the each of the grid blocks) for a long period of time, it would yield an erroneous simulation of the geothermal system. So, dividing the period of time into smaller increments Δt, or "time steps", and performing the numerical solution at each of these times steps, the amount of error would be greatly reduced. In other words, knowing the thermodynamic conditions in each grid blocks in a given time t, the mass and energy interactions between the cells can be obtained at the time $t + \Delta t$. Performing this process repeatedly, the thermodynamic condition of the geothermal system corresponding to any time period of interest can be obtained. And if the incremental time Δt is reasonably small, the amount of error at the end of the simulation will be relatively smaller.

It should be noted that, numerical solutions may need to be carried out several times at a given time step in order to check the convergence problems, if exist, because thermodynamic conditions are not constant during a time step (Pruess, 2002).

The workflow of a numerical simulation (e.g. TOUGH2 numerical simulator) includes evaluation of thermophysical properties for all grid blocks, assembly of the vector of

residuals and the Jacobian matrix, and solution of the linear equation system for each Newton-Raphson iteration step. The most computational intensive part is the solution of the linear equation system. Direct and iterative linear equation solvers are available. Direct solvers are generally more robust than the iterative solution, but comes at the expense of large computational power and time requirements. In contrast, iterative solvers need less memory requirements. For large problems and especially 3-D problems with several thousand grid blocks or more, iterative conjugate gradient (CG) type solvers are therefore the method of choice (Pruess, Oldenburg, & Moridis, 1999). The technical details of the linear equation solvers can be found (George J. Moridis & Pruess, 1998).

3.4.2 Initial and Boundary Conditions

Solving partial differential equations by numerical techniques can yield infinite number of solutions, if boundary and initial conditions are not specified (Artun, 2016) . As stated before, at the beginning of a numerical simulation, a proper distribution of parameters (pressure, temperature, CO_2, porosity, permeability, etc. distribution) must be set (initial conditions). The numerical solution is started upon these values, so it is important to determine the most realistic initial conditions.

Setting the boundary conditions are also of a great importance before starting a numerical reservoir simulation. The limits of the modeled area represent the outer boundaries, and the faults, lithological change zones, production-injection wells are the internal boundaries. There are two main types of boundary conditions: first order (Dirichlet) and second order (Neumann). If the magnitude of an independent variable is known at a boundary, then this boundary is said to be Dirichlet type boundary. Constant pressure external boundaries or constant operating sandface pressures fall into Dirichlet boundary category. On the other hand, Neumann boundary conditions refer to the borders of known fluxes. In other words, the magnitude of the gradient of an independent variable is known at a boundary, this boundary is named as Neumann boundary. No flow boundaries and sources/sinks (e.g. production/injection wells) are examples of Neumann boundaries. Dirichlet and Neumann boundary conditions in a two-dimensional (2D) representative

field is shown below.

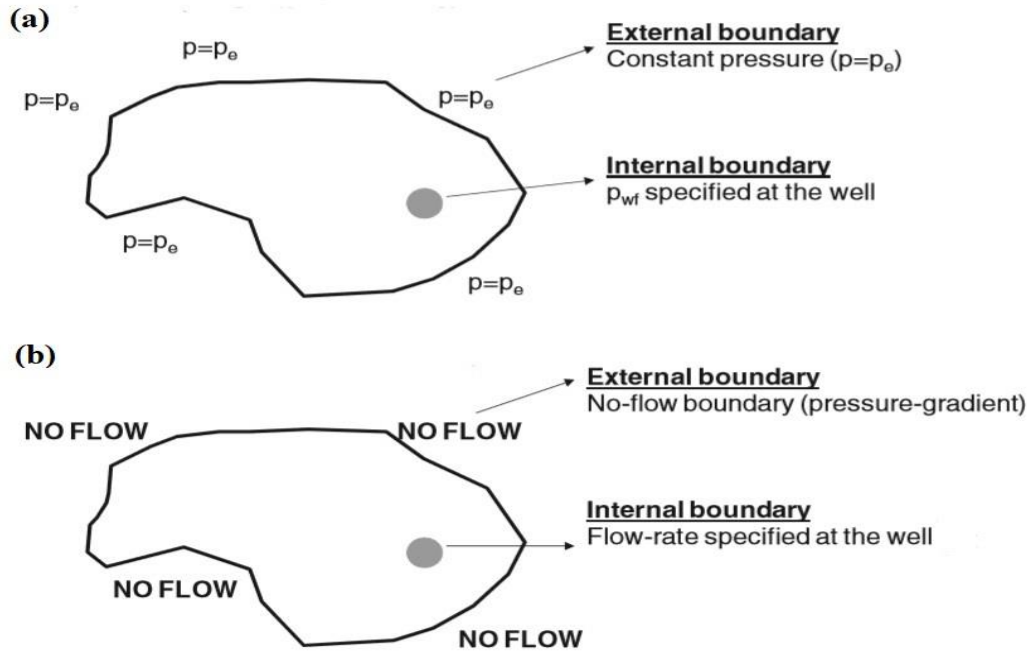

Figure 3.7 (a) Dirichlet Boundary C. (b) Neumann Boundary C. (Artun, 2016)

3.5 Model Calibration and Validation (History Matching)

The constructed model needs to be verified to determine whether it is a good representation of the actual geothermal system or not, before it is used for reservoir management purposes and future prediction scenarios. This verification is done usually through a process called history matching, where variations between the data obtained by the simulator and the actual field data are compared. If these variations are smaller than a predetermined level, the model is said to be a good representation of the actual geothermal field. On the other hand, if the differences between the actual field data and the simulation data are not small enough, the model input parameters needs to be adjusted.

The process of adjusting the model input parameters according to the simulation results is called calibration. This is required to improve the simulation results and to obtain a better

representation of the actual field. Calibration is carried out until the simulation results show a good match with the actual field data. The assumptions, made during the construction of the model, need to be revised first. Then, the least accurately known input parameters are calibrated according to the significance of their impact on the simulation results, in a predetermined confidence interval.

3.6 Performance Predictions

Once a validated model is obtained, future prediction scenarios can be carried out just by simulating the model according to the desired scenario. Most of the time, effects of different production/injection operations on the reservoir pressure and the flowing enthalpy are investigated. The successfulness of the future predictions directly related with the successfulness of the constructed natural state model.

CHAPTER 4

NUMERICAL SIMULATION OF KIZILDERE GEOTHERMAL FIELD

Kızıldere geothermal field is located in the eastern part of the Büyük Menderes Graben, and one of the most important geothermal fields of Turkey. Initial studies conducted by Directorate of Mineral Research & Exploration during 1960s showed the geothermal potential of the area. First wells were drilled during 1970s and the first commercial scale power plant was installed in 1984 by government's electricity authority Electricity Generation Co. Inc. (EÜAŞ), with a capacity of 17.8 MW. But acquisition of the Kızıldere geothermal field by Zorlu Energy in 2009 was the real breakthrough for the development of the field. The company conducted many data gathering and reassessment studies after the acquisition. Phase-II power plant (80 MW) and Phase-III power plant (99.5 MW) became operational in 2013 and 2017, respectively.

Numerical simulation of the field is another important area of study for the development of the field. Construction of the conceptual model is the first step in such a study. To do so, gathering all the accurate and reliable information about the Kızıldere field must be carried out. Many geological, hydrogeological, geochemical, and geophysical studies on the Büyük Menderes Graben and Kızıldere geothermal field can be found in the literature (Bozkurt & Oberhänsli, 2001; Gökgöz, 1998; Karamanderesi, 2013; Özgüler et al., 1983; Serpen & Uğur, 1998; Şimşek, 1985a, 1985b; Şimşek et al., 2009).

4.1 Numerical Simulation Codes: TOUGH2 V2.0

The TOUGH family codes allow the numerical simulation of non-isothermal flows of multiphase, multi-component fluids in one, two, and three dimensional porous and fractured media (Pruess, 1991; Pruess et al., 1999). The acronym TOUGH stands for "Transport Of Unsaturated Groundwater and Heat". The ancestor to the current TOUGH codes is a simulation program known as MULKOM. The codes were initially developed at the Earth Sciences Division of the Lawrence Berkeley National Laboratory in Berkeley, in the early 1980s. Since then, the codes are continually updated to address a vast range of subsurface problems. For example, ECO2N (Pruess, 2005) and ECO2M (Pruess, 2011) modules were developed in specifically for the applications of geological sequestration of CO2 into saline aquifers. iTOUGH2 (inverse TOUGH2) provides inverse modeling capabilities for the TOUGH2 codes, and performs sensitivity, uncertainty, and optimization analysis (Finsterle, 2007). TOUGHREACT couples TOUGH2 codes with transport and reactive geochemistry packages (Xu et al., 2012). In order to enhance the computational performance of large scale numerical simulations TOUGH2-MP (Zhang et al., 2008) was developed. TOUGH+ (Moridis et al., 2008) focuses on advance applications, such as gas hydrate simulations. Many different issues and developments have been addressed in the new base version of TOUGH - which is named as TOUGH3 (Jung en al., 2017).

In the numerical simulation of Kızıldere Geothermal Field, TOUGH2 version 2.0 codes have been used. There are many fluid property modules contained in the TOUGH2 codes. They are represented as different equation-of-state (EOS) modules and extensions. The following table summarizes the fluid property modules contained in the TOUGH2 v2.0 numerical simulation codes.

MODULE	PURPOSE
EOS 1	basic fluid property module for water (liquid, vapor, two-phase), including “two waters" for tracing fluid movement
EOS 2	water-CO_2 mixtures; originally developed by O’Sullivan et al., (1985)
EOS 3	water-air mixtures; an adaptation of the EOS module of the TOUGH simulator (Pruess, 1987)
EOS 4	water-air mixtures, including vapor pressure lowering according to Kelvin's equation (Edlefsen & Anderson, 1943)
EOS 5	water-hydrogen mixtures
EOS 7	mixtures of water-brine-air
EOS 7R	water-brine-air, plus two volatile and water-soluble radionuclides
EOS 8	fluid property module for three-phase flow of water, non-condensable gas, and black oil
EOS 9	fluid property module for saturated/unsaturated flow according to Richards' equation (gas phase a passive bystander)
EWASG	fluid property module for three-component two-phase mixtures of water, water-soluble salt, and non-condensable gas; includes salt dissolution and precipitation, and associated porosity and permeability change
T2VOC	Three phase flow of water, air, and a volatile organic chemical, adapted from Falta et al. (1995)
TMVOC	fluid property module for three-phase flow of water, non-condensable gas, and non-aqueous phase liquid (NAPL), where the NAPL may consist of a multicomponent mixture of volatile organic chemicals

Table 4.1 Fluid property modules of TOUGH2 v2.0 (Pruess, 2003)

TOUGH2 codes solves mass and energy balance equations that describe the fluid and heat flow in the porous and fractured media. Fluid advection and diffusive mass transport in all phases, as well as convective and conductive heat flows are all included in the codes. The local equilibrium of all phases is assumed to describe the thermodynamic conditions.

To discretize the continuous space and time variables “Integral Finite Difference Method” (also known as Finite Volume Method) is used (Edwards, 1972; Narasimhan & Witherspoon, 1976). Space discretization is made directly from the integral form of the basic conservation equations, without converting them into partial differential equations. By that way, it is avoided to reference any global system of coordinates, which offers the advantage of being applicable to regular or irregular discretization in one, two, and three dimensions. It also provides the flexibility to implement double/multi porosity methods for fractured media, by means of a simple processing of geometric data. Time is discretized fully implicitly using first order backward finite difference method. The discretization results in a set of strongly coupled nonlinear algebraic equations, with the time-dependent primary thermodynamic variables of all grid blocks as unknowns. These equations are solved simultaneously by Newton-Raphson iteration method. Different methods are available to solve the linear equations arising at each iteration step, including preconditioned conjugate gradient solvers, as well as sparse direct matrix methods (see While direct methods are more predictable and less problem-dependent in their performance, it is only through the application of iterative conjugate gradient methods that solutions for large grid systems (10,000 blocks or more) and three-dimensional problems can be accomplished (George J. Moridis & Pruess, 1998). For more detailed description, the TOUGH2 version 2.0 User Guide is referred (Pruess et al., 1999).

For the numerical simulation of Kızıldere Geothermal Field, EOS2 module of TOUGH2 is used, since the field contains significant amount of CO_2 which has considerable effects on the reservoir performance.

4.2 Graphical Interface: Petrasim

Petrasim is a graphical interface of TOUGH2 numerical simulator, for pre- and post-processing developed by Thunderhead Engineering. The software enables to select the appropriate EOS module and solver properties. Creating meshes, defining different material properties, setting up initial and boundary conditions, and adjusting output options are made simpler with the visualization of the model. But it has found that other

means of data analysis tools are required for the post-processing of the numerical simulation. For further information, the Petrasim User Manual is referred (Thunderhead Engineering, 2016).

4.3 Conceptual Model of the Kizildere Geothermal Field

Surface manifestations such as fumaroles and hot springs encouraged people to investigate the geothermal potential of the Kızıldere region. Initial studies carried out by the Directorate of Mineral Research & Exploration during 1960s, including gravity and resistivity surveys and drilling of more than hundred temperature gradient wells (Demirörer, 1969). A previously constructed conceptual model of the Kızıldere Geothermal Field (Şimşek et al., 2009) shows the main features of the geothermal system.

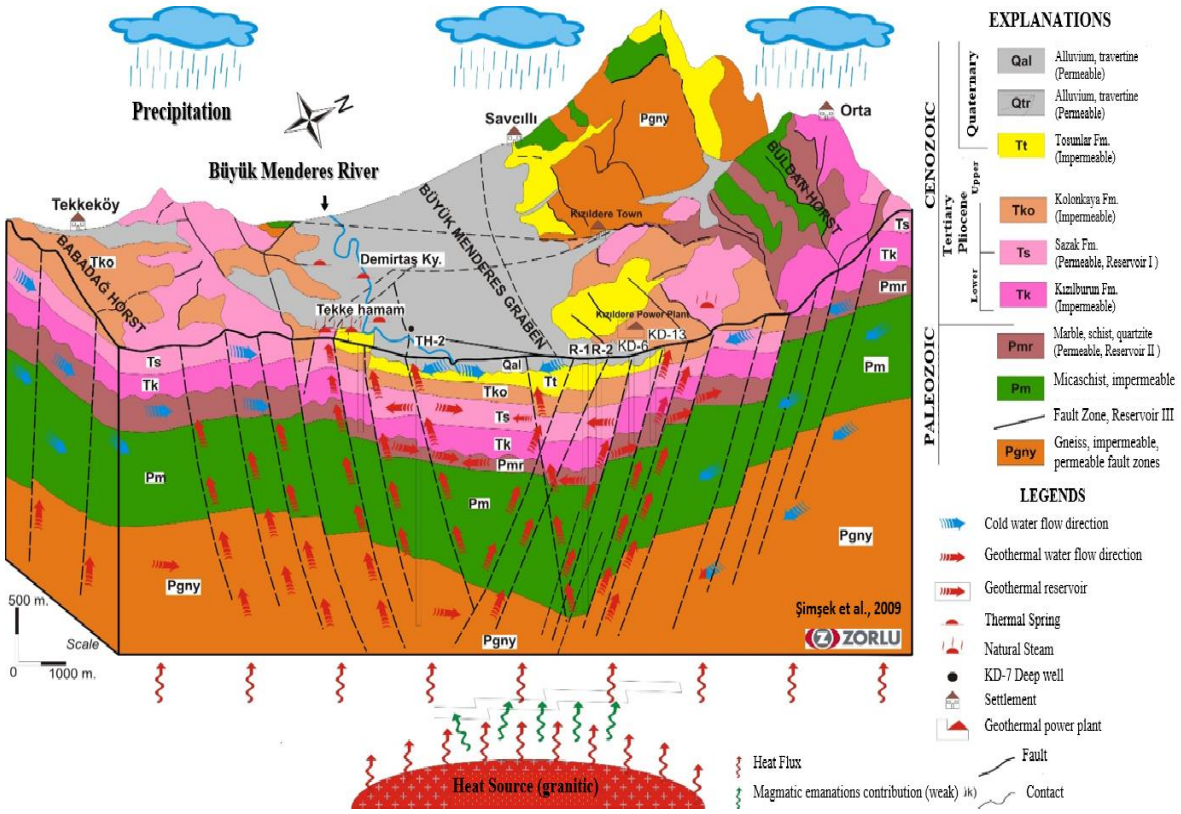

Figure 4.1 Conceptual Model of the Kızıldere Geothermal Field (Şimşek et al., 2009)

The model states that rain water is collected at the highs of the Buldan and Babadağ Horsts, then recharged into the deeper sections of the field through the flow conduits provided by faults and fractures. Since the temperature is high at these depths, water is heated up and rises toward upper sections due to buoyancy through these faults and fractures, until its flow is restricted by an impermeable section - caprock. A conceptual heat source is placed at the bottom of the field which provides the heat into the geothermal system.

After the acquisition of the field by Zorlu Energy, previous studies were reassessed and repeated, including geophysical, geochemical, and seismic surveys. Approximately hundred new wells were drilled in the Kızıldere geothermal field between 2009 and 2018. These studies and drilled wells (including tests conducted through wells such as well logs and pressure transient tests) provided valuable information about the geological structure and thermal situation of the field, as well as hydrogeological conditions and caprock properties. In the light of these information, a more detailed conceptual model of the Kızıldere Geothermal Field has been constructed, and visualized by using the graphical interface Petrasim, which is also a pre- and post- processor of the TOUGH2 reservoir simulation codes.

4.3.1 Formation and Fault Distributions

Kızıldere Geothermal Field is simply comprised of Paleozoic metamorphics of Menderes Massifs, overlain by Pliocene and Quaternary sedimentary rocks. Sedimentary rocks can be divided into four: Tosunlar, Kolankaya, Sazak, and Kızılburun (Şakir Şimşek, 1985a). Tosunlar Formation, just below the surface alluviums, forms the upper part of the field. Relatively impermeable rocks of the Kolankaya Formation overlie the first reservoir section of the field: Sazak Formation. The underlying Kızılburun Formation acts as a caprock and separates the Paleozoic metamorphics and the Pliocene sedimentary rocks. The upper part of the metamorphics is called İğdecik Formation, and forms the second reservoir. The underlying metamorphics are the third reservoir section and the main target for the recent and deeper production wells. Impermeable rocks between İğdecik and

basement metamorphics forms the caprock for the third reservoir section. Properties of these formations were estimated mainly from resistivity surveys, magnetic surveys, well logs and pressure transient analysis, and re-evaluated over the course of the simulation studies.

Seismic showed that metamorphics (second and third reservoir sections) are getting shallower in the western and north-western sections of the field. Gathering all the information from geophysical surveys and correlating them with the data obtained from drilled wells, a basic representation of the formation distribution of the Kızıldere geothermal field has been constructed in the Petrasim interface.

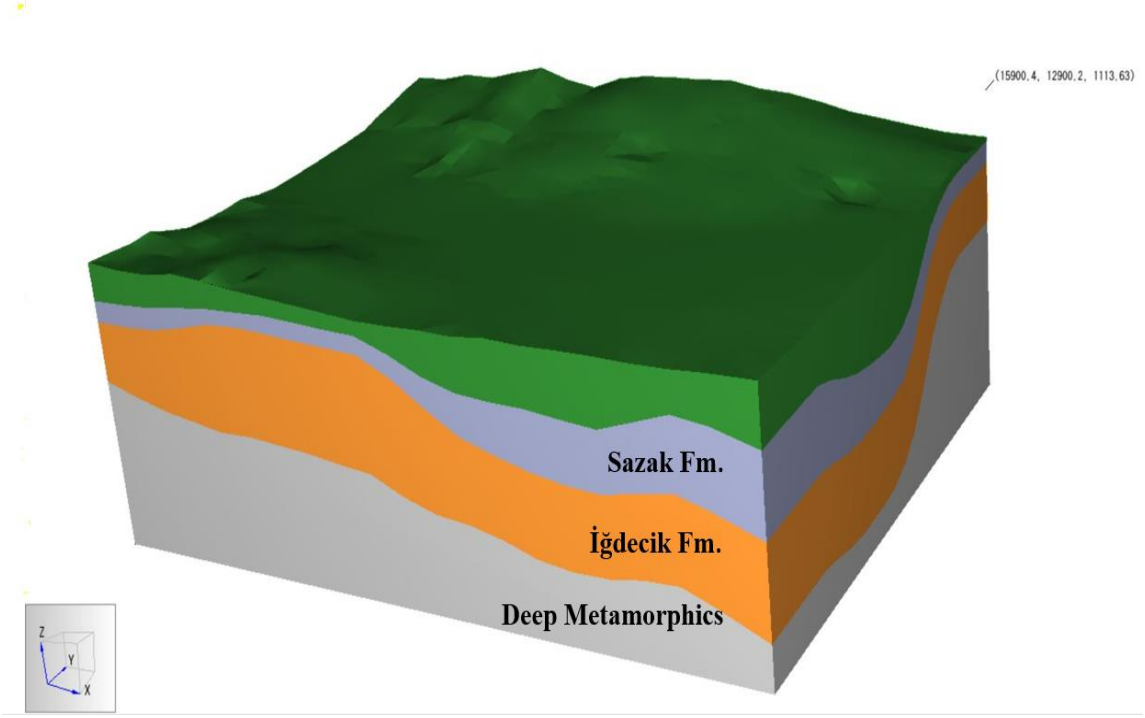

Figure 4.2 Formation Distribution of Kızıldere Geothermal Field

Note that below the surface rocks (green), only the reservoir formations are displayed on the model (Sazak, İğdecik, and deep metamorphics, from top to bottom, respectively), and caprocks are incorporated into the corresponding reservoir formation. The caprock features of the Kolankaya Formation (above the Sazak Formation), the Kızılburun

Formation (above the İğdecik Formation), and impermeable Paleozoic rocks (above the deep metamorphic rocks) are controlled by the "permeability factor" option of the simulator, and adjusted locally according to data obtained from drilled wells.

Faults, fractures, and rock fissures provide the necessary conduits for the flow of the geothermal fluid. Fluid is heated up at the deeper parts of the field, and rises towards upper sections through these conduits, as a result of buoyancy. The fluid circulation is dominated by NE-SW trending faults, especially the strike-slip Gebeler Fault. There are also some E-W trending normal faults, correlated with the drilled wells. Depth, direction, angle, and hydraulic properties (permeability) of these faults have been reevaluated and tested during the calibration-validation studies (history matching) of the model. It should be noted that the faults, fractures, and fissures have not been represented as discrete, individual formations in the simulation. So, properties of these formations should be approximated until a verified fluid circulation network is obtained (matching static and dynamic pressure, temperature, and production/injection histories of wells, with an acceptable accuracy). The figure below shows the distribution of the main faults and formation borders.

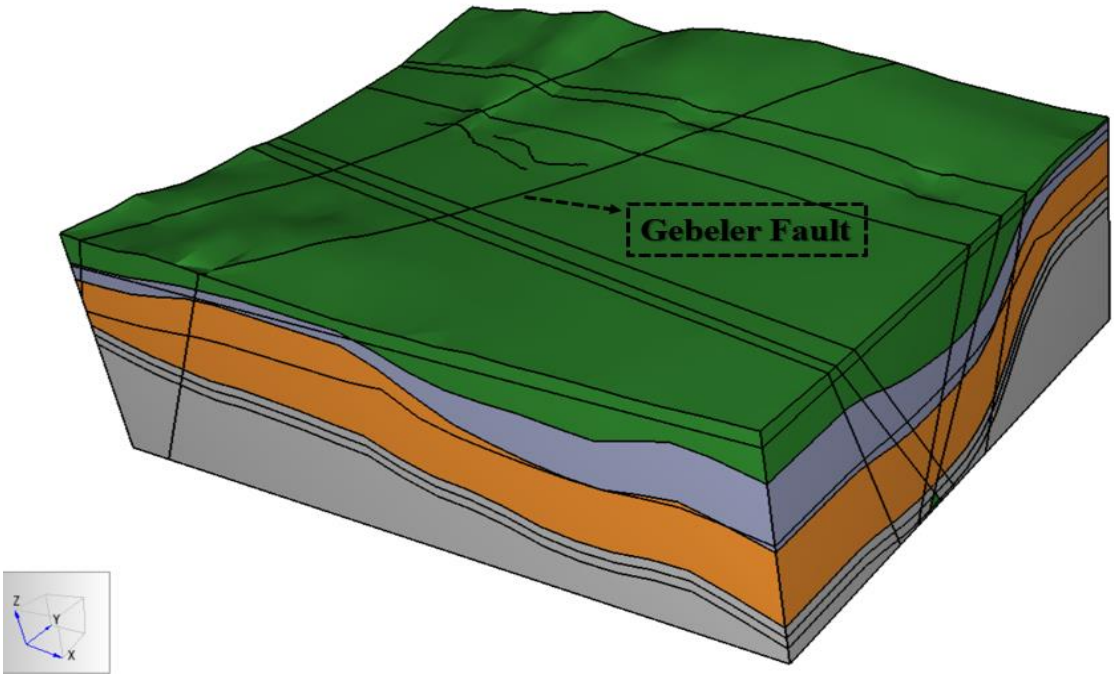

Figure 4.3 Faults and Formation Borders

4.3.2 Dimensions of the Model

The areal extent of the model is 15.9 km in E-W direction, and 12.9 km in N-S direction, approximately 200 km^2. The highest point on the surface is 1,114 meters above the sea level, and the total depth is taken to be 5,000 meters below the sea level. The coverage of the model is much bigger than the areal extent of the drilled wells, since there are other geothermal power plants run by some other energy companies in the vicinity of the Zorlu Energy's license area, and it is intended to include their possible effects into the Kızıldere model. Having a bigger model area than the drilling area also enables to predict the consequences of potential future operations on the undrilled regions of the field. Additionally, setting the boundaries of the model away from the study area is a good choice for the sake of the success of the simulation results, which would otherwise be required to deal with the complicated effects of the outer boundaries.

4.3.3 Gridding of the Model

Before proceeding further and assigning formation and fault properties, the model should be divided into smaller representative elementary volumes (grid blocks), so that variations and heterogeneities within the geothermal system can be averaged locally in sub-volumes, or "grid blocks", which provides a better representation of the system, and also provides easier, faster, and more meaningful solutions to the mathematical equations. But, the required computational power and the time issues are the limiting factors in the grid size selection. As the grids get finer, more computational power and time is required to perform the numerical simulation.

The Kızıldere model was divided into simple, three-dimensional rectangular grids, with varying sizes. The outer boundary grids kept relatively bigger compared to inner sections, since these cells are actually away from the main study area, and it was desired to minimize the interactions between outer boundary cells and the cells in the main study area. Conversely, the grid sizes kept as small as possible in the main study area (around the wells and faults), in order to be able to better represent the variations and

heterogeneities, and also to make necessary changes more elaborately, according to the results of the simulation, throughout the study.

During the early times of the study, 11,000 grid blocks were used in the model, where the computational time was short enough that performing many runs and evaluating their results in a shorter period of time was possible. But in this case, there were more than one well in a single grid block, which prevents the individual evaluation of each single well. Since the average distance between adjacent wells in Kızıldere geothermal field is around 500 meters, the grid sizes should be less than that to represent each well individually. As a result, the grid sizes was downscaled and the model was divided into approximately 24,000 grid blocks. The following table shows the dimensions and distributions of the grid blocks in x-y directions (x is in the E-W direction; y is in the N-S direction).

X, East to West		Y, North to South	
Number of Grids	**Grid Size, m**	**Number of Grids**	**Grid Size, m**
2	750	2	970
30	354.7	30	265
2	750	1	1000
1	2250	1	2000
Total: 15890m		**Total: 12890m**	

Table 4.2 Grid size distribution along the model area

In the z-direction, the model was divided into two major layers: The first layer covers the area between surface and -100 meters (according to the sea level), and the second layer extents from -100 meters to the bottom of the model (-5,000 meters). The reason behind this is to set an upper reference depth below the sea level, and avoid from any plus (+) or minus (-) sign related complications. The lower major layer was further divided into 18 more layers, where the first 16 layers (to the depth of -3000 meters) are relatively thinner and the bottom 2 layers are relatively thicker. Since most of the production wells reach out to the depth of -3000 meters, this section (-100 meters to -3000 meters) has been

divided into more and thinner layers to get more detailed information from the simulation. The figure below shows Kızıldere geothermal field after the implementation of above-mentioned grid system.

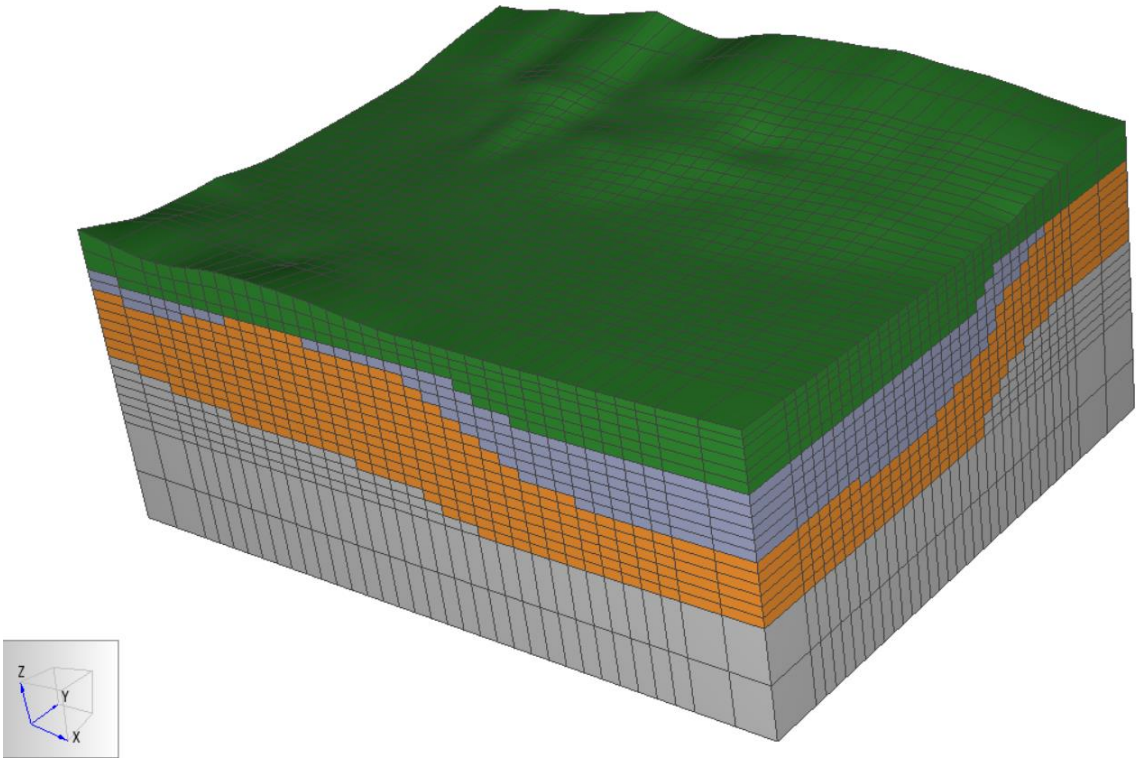

Figure 4.4 Grid system of the model

4.3.4 Formation and Fault Properties

Well tests provide good information about the permeability-thickness values of the formations, at the vicinity of the wells (investigation distance depends on the test duration). Pressure build-up data of 21 wells were analyzed, by using the PTA software Saphir (Kappa Workstation, version 5.12.03, 2017). Distribution of permeabilities along the formations both qualitatively and quantitatively were obtained from these analyses.

For most of the wells, PTA results showed that dual porosity reservoir model describes the flow system of the Kızıldere geothermal field better than any other reservoir model. In the figure below, log-log plot of "Pressure Difference (barg) vs Time (hours)" of a production well is shown.

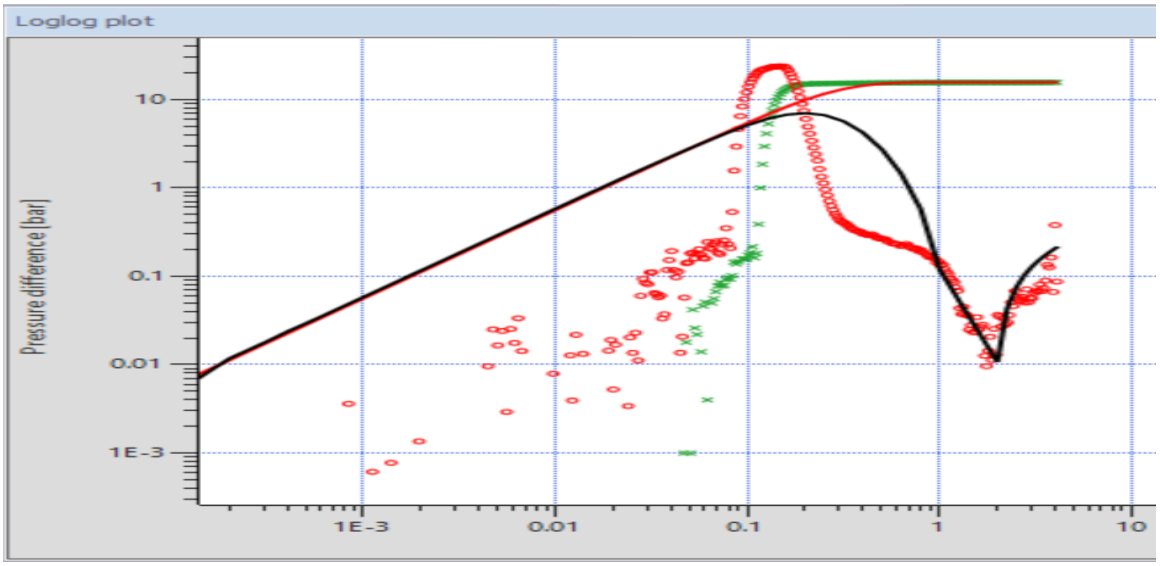

Figure 4.5 Pressure Transient Analysis of a representative production well

No boundary effects have been observed, since the measurement time is only around 6 hours. High temperature is the main factor for the short measurement duration, which restricts the usage of measurement devices for a long time. The early time measurement data reflects the wellbore storage effects. It was concluded that the irregular pressure values during the early time are due to the presence of CO_2, and not much attention have been paid to match the early time effects. Table 4.3 shows the porosity and permeability values which were assigned to the formations initially, but adjusted locally and globally during the calibration of the model. Also, Table 4.4 shows some other rock properties which were used throughout the simulation of the model.

Formation Name	Porosity	Permeability in x-direction (milli Darcy)	Permeability in y-direction (milli Darcy)	Permeability in z-direction (milli Darcy)
Sazak	0.10	50	50	5
İğdecik	0.05	50	50	5
Deep Metamorphics	0.02	60	60	6

Table 4.3 Porosity and permeability values of the formations

Formation Name	Rock Density (kg/m3)	Rock Specific Heat (J/kg °C)	Wet Heat Conductivity (W/m °C)
Sazak	2600	1000	1.0
İğdecik	2600	1000	1.0
Deep Metamorphics	2600	1000	1.0

Table 4.4 Rock properties of the model

Figure 4.6 and 4.7 show the initially assigned porosity and permeability distributions along the formations (permeability in x-direction (E-W), same as y-direction (N-S)).

As mentioned before, permeability factor option has been used in order to assign the fault, fracture, and caprock properties to the grid blocks, which are also adjusted during the calibration of the model. As high as 10 times and as low as 1/1000 of the initial permeability values were used in the model. Permeability factor of the faults were generally assigned as 2, meaning that grid blocks which represent the fractured region along the faults have permeabilities twice the initially assigned formation permeability. On the other hand, caprocks have been represented with a permeability factor of 1/1000. For example, the caprock which overlies the İğdecik Formation has a lateral permeability of 0.05 mD (50 mD x 1/1000) and vertical permeability of 0.005 mD. Figure 4.8 shows the distribution of the permeability factor values along the outer boundaries, but it should be noted that locally assigned permeability factor values are widely present in the model.

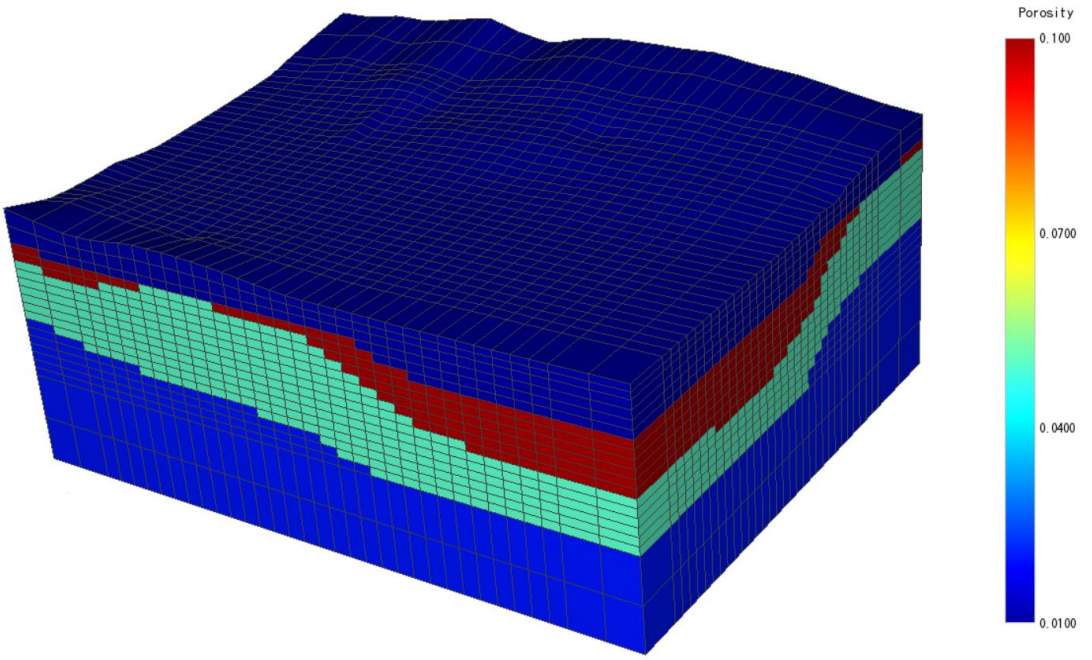

Figure 4.6 Porosity Distribution of the model

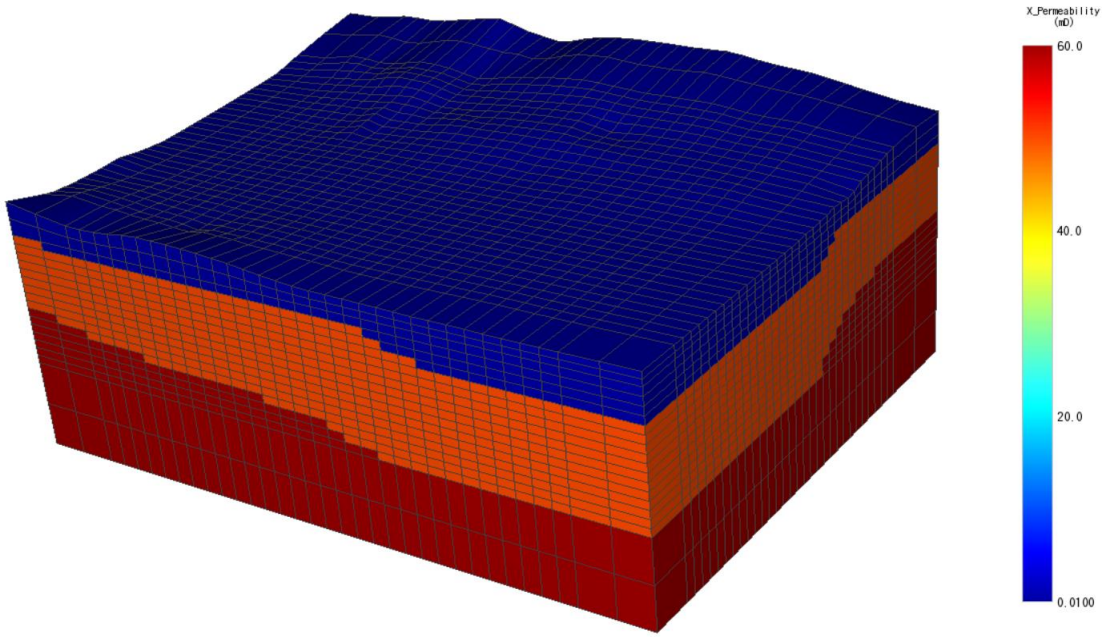

Figure 4.7 Permeability distribution of the model

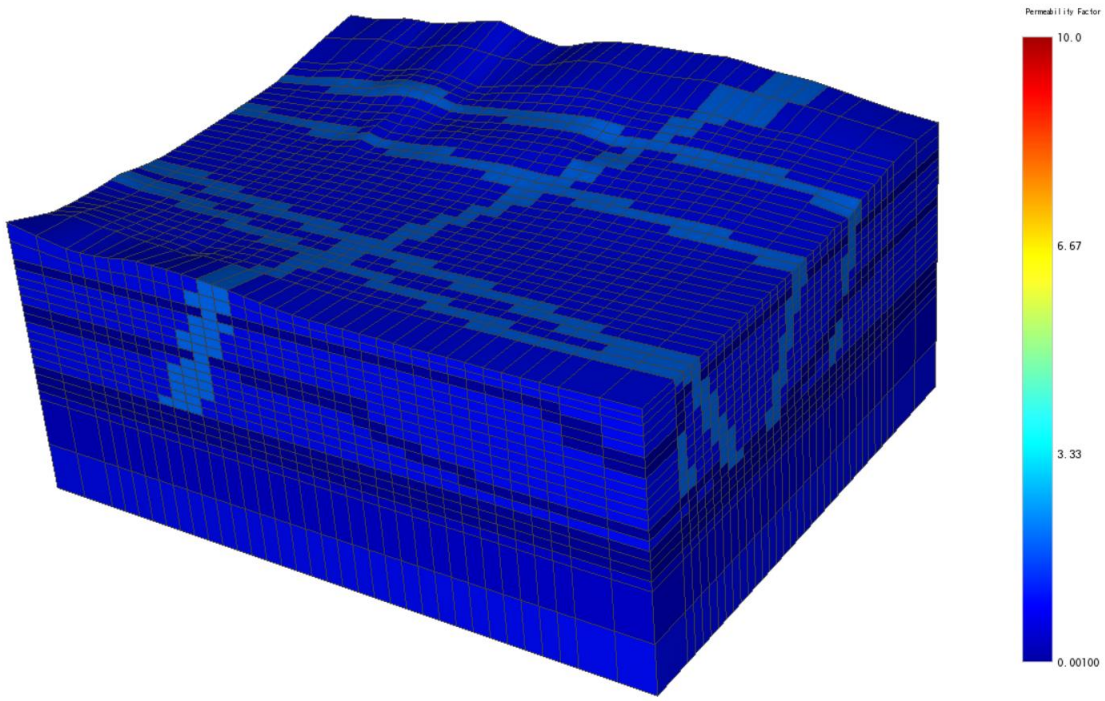

Figure 4.8 Distribution of the permeability factor values

4.3.5 Heat Sources and CO_2 Content

In order to simulate the conductive and convective heat circulation, two heat sources have been placed into the model. Geochemical analysis indicated that Kızıldere geothermal fluid shares a common parent fluid, means that there is only one upflow zone in the system. Taking this information into account, a single heat source has been placed into the bottom of the model. Water with a high CO_2 content, and conductive heat flux have been introduced to the system through this bottom-source. On the other hand, a shallow source has been placed into the İğdecik Formation at the northern part of the field, where metamorphic rocks get shallower below the Buldan Horst. This shallow source simulates the cooling effects of the rain water, which recharges to the system mainly from the highs of the Buldan Horst. The rate of mass fluxes (water and CO_2), their enthalpies, rate of conductive heat fluxes, size, shape, and locations of these deep and shallow sources are all found by trial-and-error (calibration of the model during the history matching) over the

course of the simulation studies.

Salinity and non-condensable gas (NCG) contents of geothermal fluids are important parameters, and their presence must be taken into account in a reservoir simulation. For Kızıldere geothermal fluids, especially the carbon dioxide (CO_2) content is of a great importance, since it has considerable effects on the reservoir parameters, and surface and subsurface operations. Although there is not a continuous CO_2 measurement well by well, studies showed that 1.5wt% dissolved CO_2 comprises the water produced from İğdecik Formation, and this value increases to 3 – 3.5wt% for the water coming from the deeper metamorphics. CO_2 is introduced into the model as dissolved in the water, through the source at the bottom. Since CO_2 is introduced only from the bottom source and its distribution depends only on the natural flow pattern, satisfying the above-mentioned CO_2 levels in corresponding formations would also be a good measure of the flow network of the model.

4.4 Numerical Simulation

After the construction of the conceptual model in Petrasim interface by using the available data, the next step is to define the initial conditions and properties of outer and inner boundaries of the model. After achieving these, the model was run for a long period of time, until the natural state conditions were reached. The results were compared with the measured static and dynamic pressure/temperature values. Required adjustments were made through the calibration of the model.

4.4.1 Boundary Conditions

The first layer of the model has been excluded and the upper boundary has been set to -100 meters. In this case, the center of the uppermost cell is -192 m, which is considered as quite convenient, since the very shallow depths are not the focus of this study. The uppermost layer of the model has been set as fixed-state, meaning that no changes occur

in the properties of this layer, and pressure/temperature values stays constant throughout the simulation. In other words, the top layer of the model acts as a constant pressure and constant temperature boundary. The outer side layers are no flow boundaries. The bottom layer is also a no flow boundary, except the heat source.

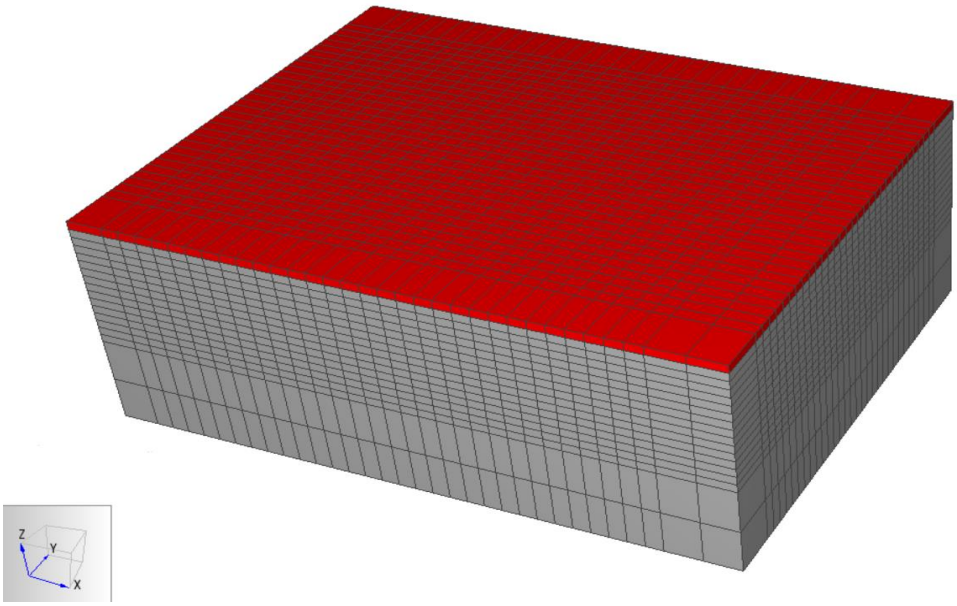

Figure 4.9 The fixed-state top layer

Pressure and temperature values at the fixed top layer are 40 bar and 82 °C, respectively. Since the temperature of the top layer is always constant, cooling effects of the rain water intrusion to the system are provided by this layer together with the low enthalpy shallow heat source. It should be recall that the center of the grid blocks of the top layer is at -192 m, and also there is an average overburden of 150 – 200 meters at the well locations. So, 40 bar and 82 °C are suitable pressure and temperature values for this layer.

There are two heat sources in the model, both of them provide meteoric water to the system. The first source is at the bottom, covering an area of approximately 13 km^2, at a depth of -5,000 meters. The water flux through this source is 27.5 kg/s, with an enthalpy of 1000 kj/kg, and with 4 wt.% dissolved CO_2. It means that approximately 1.1 kilogram

of CO_2 is entering to the system per second. The conductive heat flux is 0.7 Joule/s/m^2 through an area of 9 km^2 inside the same source.

Another source was placed into the northern, shallower İğdecik Formation (below the Buldan Horst), to simulate the cooling effects of the rain waters entering to the system from the highs of the horst. It covers an area of 4.2 km^2, at a depth of -740 meters. The amount of water flux is 7.4 kg/s. The enthalpy of the rain water is 400 kj/kg. No CO_2 is associated with the water from the source.

The production and injection wells are the inner sources and sinks. As of May 2018, there are 34 production wells (10 of Phase-II and 24 of Phase-III) with a total production rate of 6900 tonnes per hour, and 27 injection wells with a total reinjection rate of only 5200 tonnes per hour. 6 production wells of Phase-I power plant ceased operating at the beginning of 2018. Most of the production wells penetrate into deeper sections of the metamorphics, while majority of the injection wells were completed in the İğdecik Formation. The injection wells are mainly located at the eastern and north-western regions of the field. Production wells have been drilled mostly along NE-SW direction, targeting the fractured sections around the strike-slip Gebeler Fault.

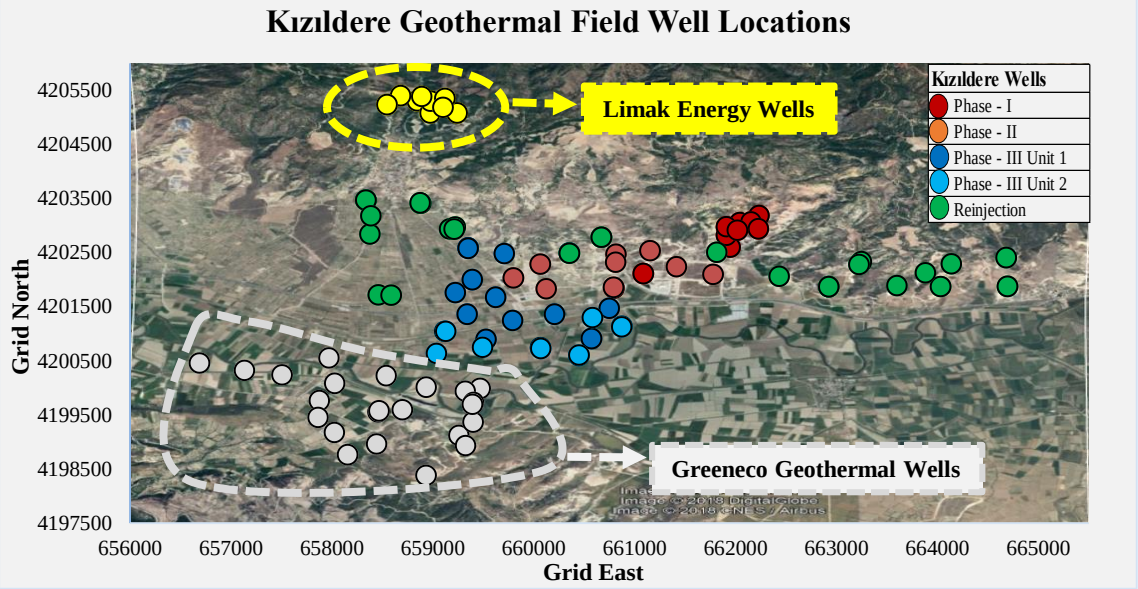

Figure 4.10 Well locations of Kızıldere and neighboring geothermal fields

4.4.2 Initial Conditions (Natural State Modeling)

The first commercial utilization of geothermal power in Kızıldere Field has been started in 1984, and this date has been used as the starting point for the simulation in this study. The field is accepted as untouched before starting to the heat extraction through the wells (natural state conditions). So, the natural state conditions (pre-production conditions, conditions before 1984) must be obtained, and must be used as the initial conditions before the field is put on production. It means that the distributions of temperature, pressure, CO_2, and fluid flow prior to human intervention should be determined. in order to create a realistic representation of the field

During the initial studies conducted by Directorate of Mineral Research & Exploration, more than 20 shallow and intermediate-depth wells (Phase-I) were completed in the Kızıldere field. It can be said that, the measured parameters (temperature, pressure, CO_2, etc.) were reflecting the natural state conditions, since there was no any fluid removal from the system. But compared to the areal extent of the model, those wells were covering only a small area in the field, and these wells were not reaching deep metamorphic rocks.

After the acquisition, Zorlu Energy drilled many wells for the Phase-II (2013) and Phase-III (2017) power plants, many of them were reaching as deep as 3500 meters (below the sea level). Although these new wells provide more information from a larger area, parameters obtained from these wells could not be used directly as the initial state conditions for the simulation, since the field was under exploitation, and perturbations caused by production and injection wells were affecting the pressure-temperature-CO_2 distributions and natural flow pattern. However, information coming from the recent wells, together with the previous wells, could be combined and be considered as a good starting point to obtain the natural state conditions.

In order to reach the natural state conditions, the model should be run for a long period of time, until the stabilization of the reservoir parameters is achieved. For our simulation, 700,000 years were long enough to reach to the stabilized conditions.

Initial pressures and temperatures are by far the most important parameters in a geothermal reservoir simulation, and determining their distribution is of a great importance. For the Kızıldere geothermal simulation, static pressure and temperature profiles of nearly 70 wells were analyzed, and their distribution throughout the field was determined. The following initial condition equations were used.

- $Temperature = 70°C \quad + \quad (Depth) * (-0.0638)\ °C$
- $Pressure = 19\ bar \quad + \quad (Depth) * (-0.0906)\ bar$

The depth here is taken according to the sea level.

Local initial pressure and initial temperature changes have been made during the calibration of the model, according to the comparison of the simulation results and the measured pressure and temperature values. The initial (pre-simulation) temperature and pressure distributions are given in the figures.

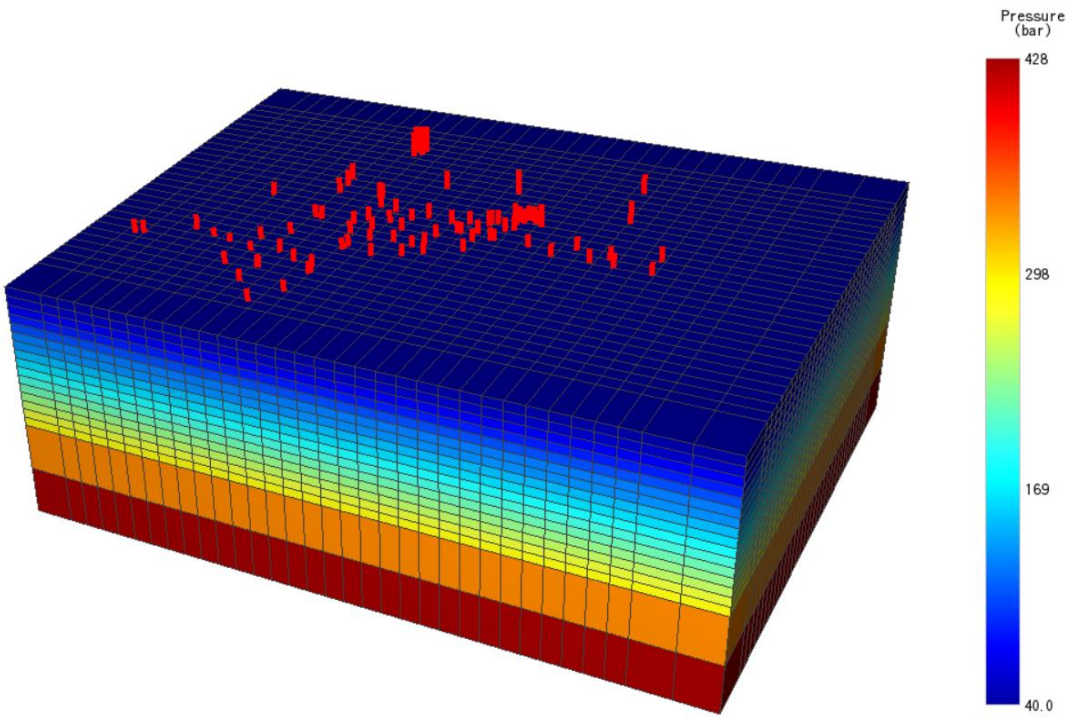

Figure 4.11 Initial pressure distribution and well locations in the region

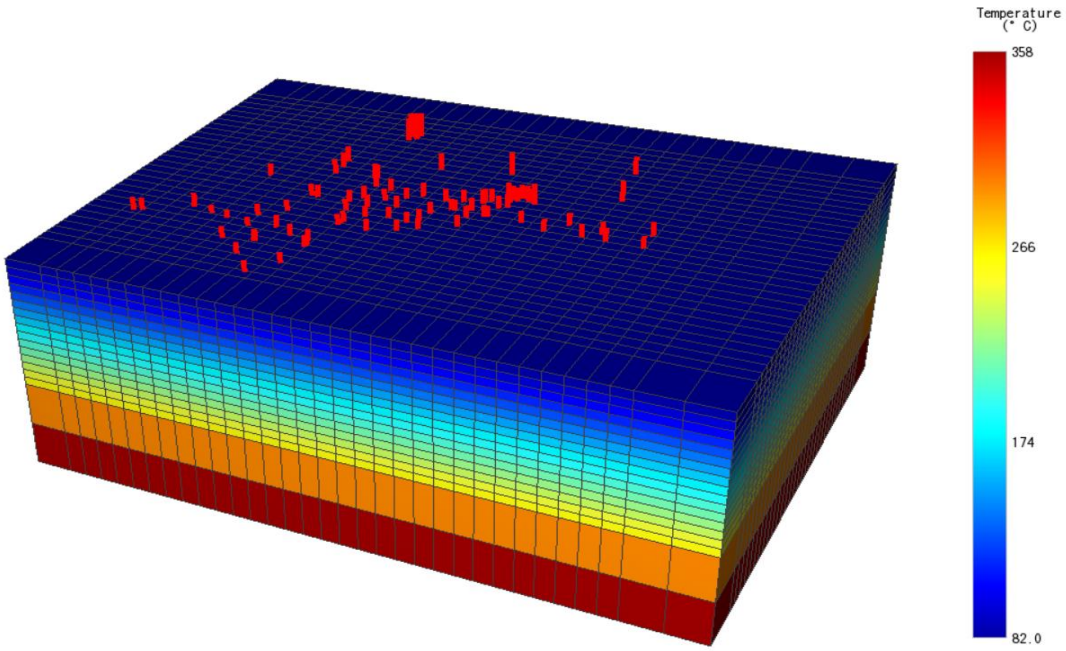

Figure 4.12 Initial temperature distribution and well locations in the region

The temperature distribution can also be shown by isosurfaces, Figure 4.13. The homogeneous distribution of the initial temperatures can be clearly seen.

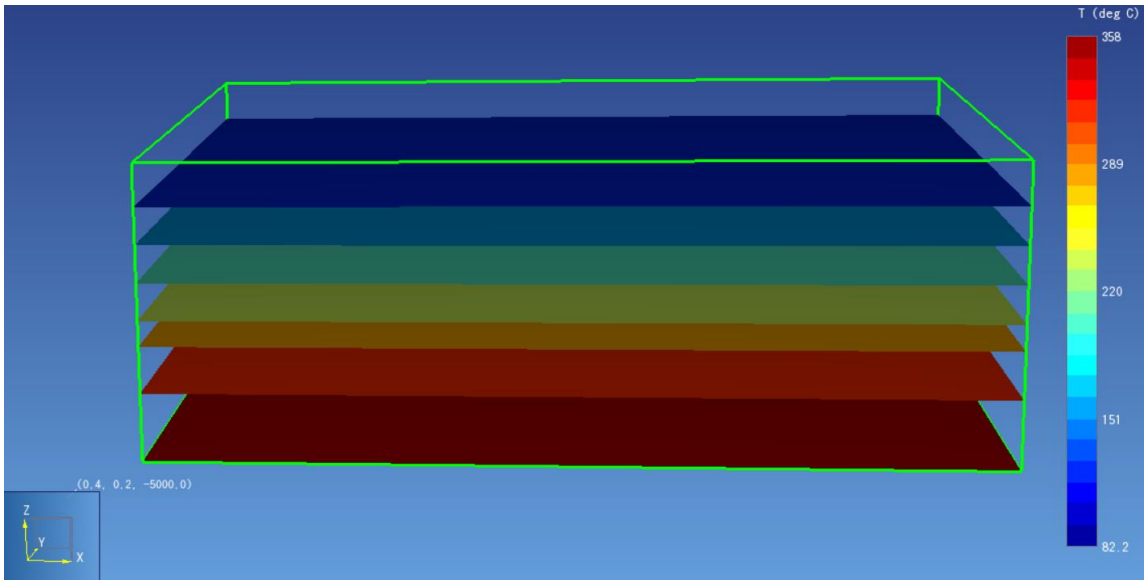

Figure 4.13 Temperature isosurfaces at the beginning of the simulation

As mentioned before, there is only a trace amount of CO_2 (0.1%) present in the model initially. CO_2 is introduced into the model as dissolved in the water, through the source at the bottom. Since CO_2 is introduced only from the bottom source and its distribution depends only on the natural flow pattern, satisfying actual CO_2 distributions would be a good measure of the flow network of the model.

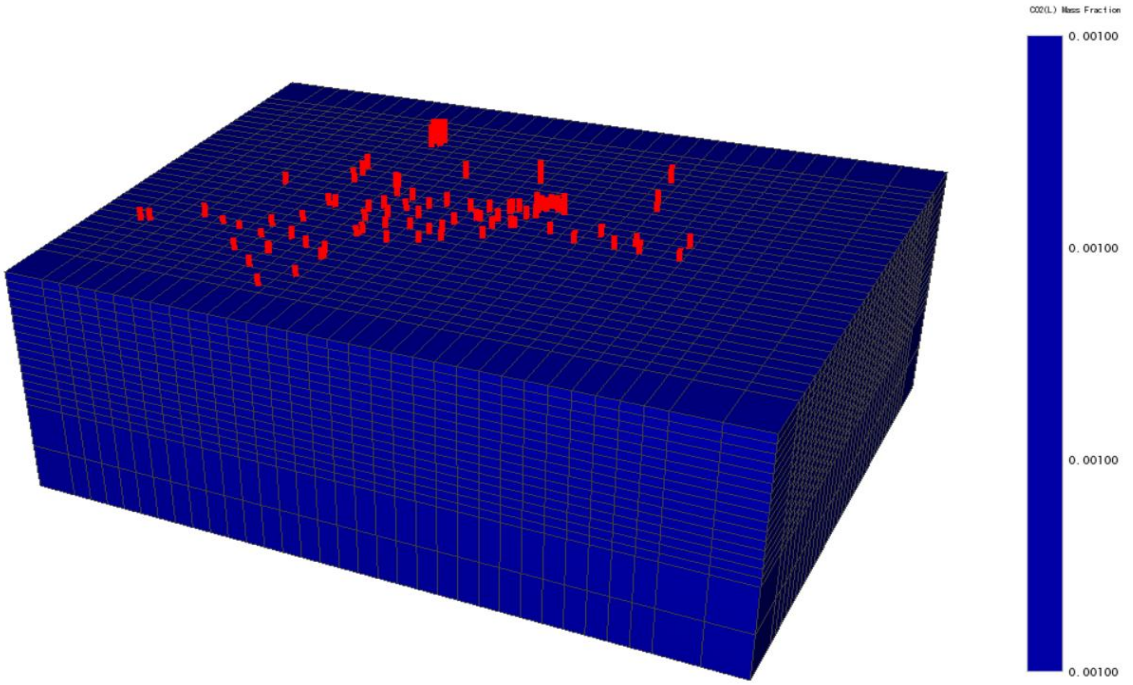

Figure 4.14 Initial CO_2 distribution

4.5 Calibration and Validation (History Matching) of the Kızıldere Model

The constructed model needs to be verified to determine whether it is a good representation of the actual geothermal system or not, before it can be used for reservoir management studies and future prediction scenarios. This verification is done usually through a process called history matching, where variations between the data obtained by the simulator and the actual field data are compared. Depending on these comparisons, input parameters are revised and adjusted accordingly, the process called calibration of the model.

The model is calibrated so that the simulation results show a great consistence with the values measured at the wells. But it should be noted that, most of the wells have been drilled after 2010, where the field were under exploitation for around 30 years, and this duration is higher for the most recent wells. So, making a comparison between the natural state model and the measured static values would be erroneous, since the measurements were performed after the perturbation of the natural state conditions for about 30 years.

In order to avoid making such erroneous comparisons, the natural state model has been tested with the actual field data at the measurement date while the field is under operation. Calibrations and adjustments have been made according to the differences between the actual and the measured data.

The following four steps are applied:

1. Run the model for 700,000 years (until it reaches stabilized conditions).
2. Insert the production/injection histories of the wells between 1984 and 2018.
3. Compare the measured and simulation parameters at the measurement date.
4. If the differences between the simulation and measured parameters are higher than a predetermined level, make necessary changes and adjustments and rerun the model. If the differences are small enough, this model is a good representation of the natural state conditions of the field.

The main history matching parameters which were used to validate the numerical simulation of the Kızıldere geothermal field were the static/dynamic pressure and temperature profiles of the wells, as well as CO_2 distributions. The confidence interval for the validation of the natural state model was taken as 10%. It means that the model was calibrated until the pressure and temperature values obtained from the simulation are in the range of 10% (or less) of the actual pressure and temperature measurements.

The most effortful studies have been made to determine the temperature profiles, both vertically and laterally. Mostly, permeability and fault properties (especially the angle and extension) were calibrated, since the heat distribution is achieved by the water circulation. Amount, enthalpy, and CO_2 content of the water flux, as well as location and size of the

sources were other important calibration parameters during the history matching studies.

The natural state model of the Kızıldere geothermal field has been validated by comparing the pressure/temperature/CO_2 output of the simulator, with the static pressure and static temperature measurements of 53 wells, as well as above-mentioned CO_2 distributions, at the corresponding measurement dates. Effects of the production and injection operations on the pressure behavior of the rest of the field have been observed from 15 observation wells and compared with the simulation output.

4.6 Results of the Natural State Modeling and History Matching

The numerical model had been run 700,000 years, long enough to reach the natural state conditions. Therefore, the obtained model was assumed to be representing the situation of the Kızıldere geothermal field before the exploitation in 1984. Based on the natural state model, production and injection operations between 1984 – 2018 have been simulated. Pressure and temperature data and CO_2 levels obtained from the numerical simulation, and compared with the actual data at the corresponding measurement date. The 10% difference target between the actual and measured parameters have been satisfied.

Pressure and temperature matches of Phase-II production well KD-25B, Phase-III production well KD-63, and injection wells KD-38A and KD-41 are shown below. These wells are selected in a way that their locations widely cover the main study area of the model. The date of static pressure/temperature measurements of these wells vary in between 2010 and 2018 (field has been developed mainly in this time period, after the acquisition by Zorlu Energy). Thus, obtaining good matches of different wells, whose static pressure and temperature profiles have been measured at different times throughout the production history of the field, would show the successfulness of the model.

Note that pressure matches are given only along the completion interval (where the slotted liner has been set), instead of from top to bottom of the wellbore. The main reason is that only the completion interval has the access to the reservoir pressure of the vicinity of the

wellbore. Above that level is due to the hydrostatic pressure of the geothermal fluid inside the wellbore, since the wellbore is protected by casings which prevents the sandface pressure measurements. On the other hand, temperature profiles are given along the wellbore, since reservoir temperature is measurable through the casing wall (assuming that temperature stabilization has occurred between the wellbore fluid and the reservoir, before the measurement).

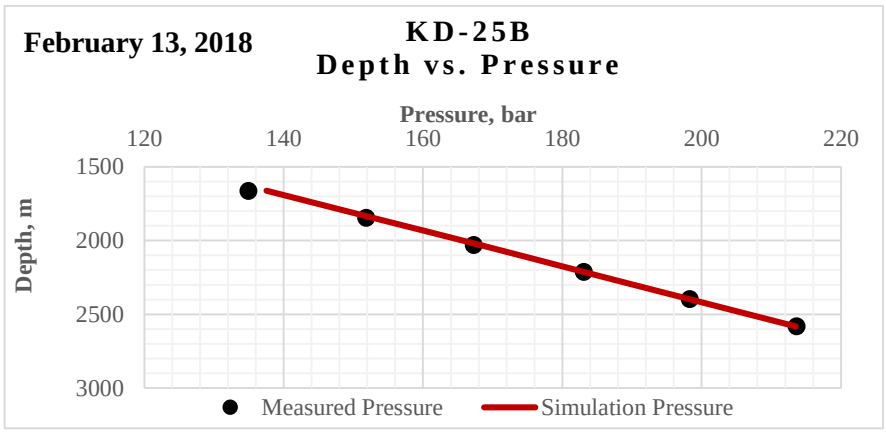

Figure 4.15 Depth vs. Pressure profile of KD-25B

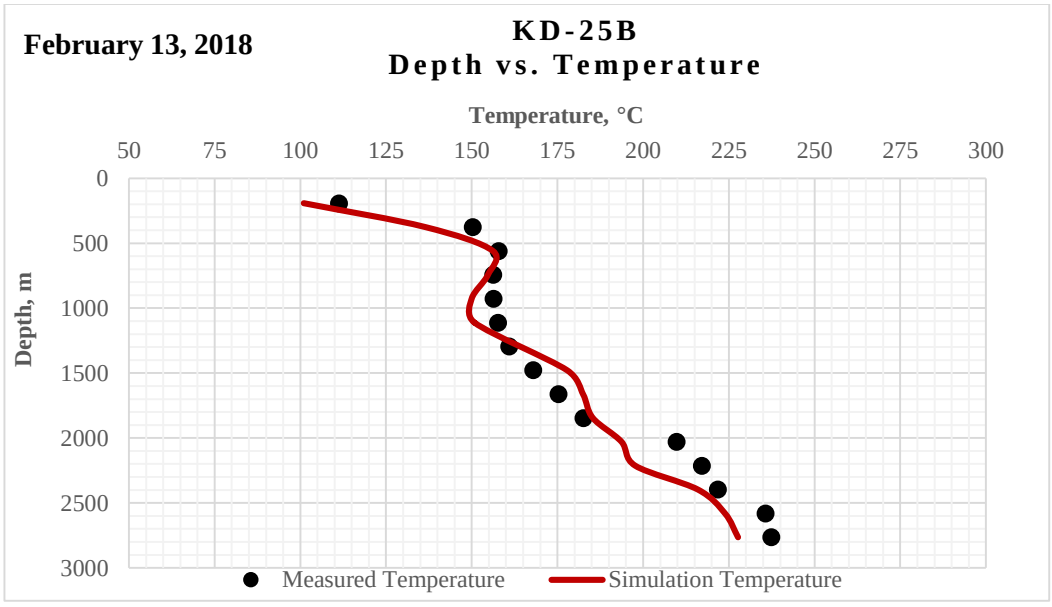

Figure 4.16 Depth vs. Temperature profile of KD-25B

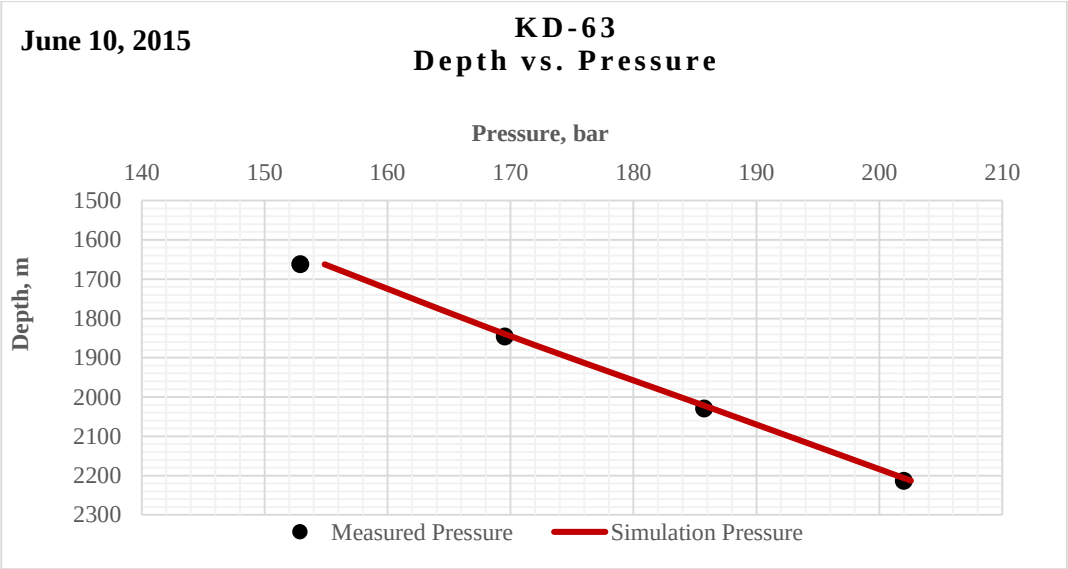

Figure 4.17 Depth vs. Pressure profile of KD-63

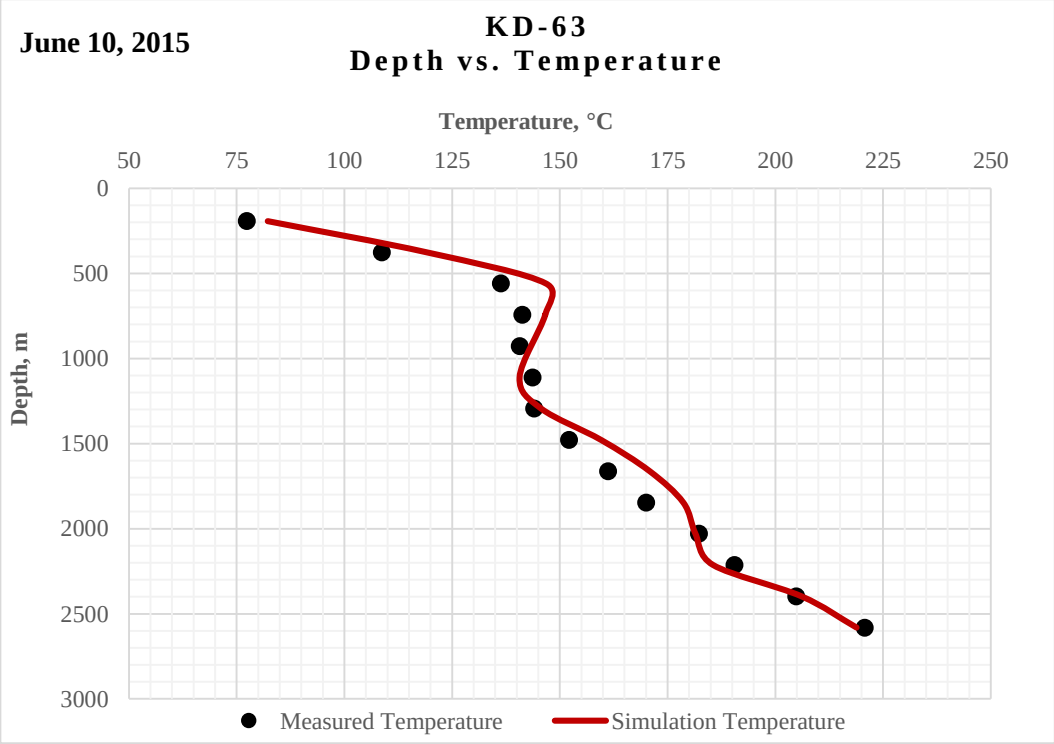

Figure 4.18 Depth vs. Temperature profile of KD-63

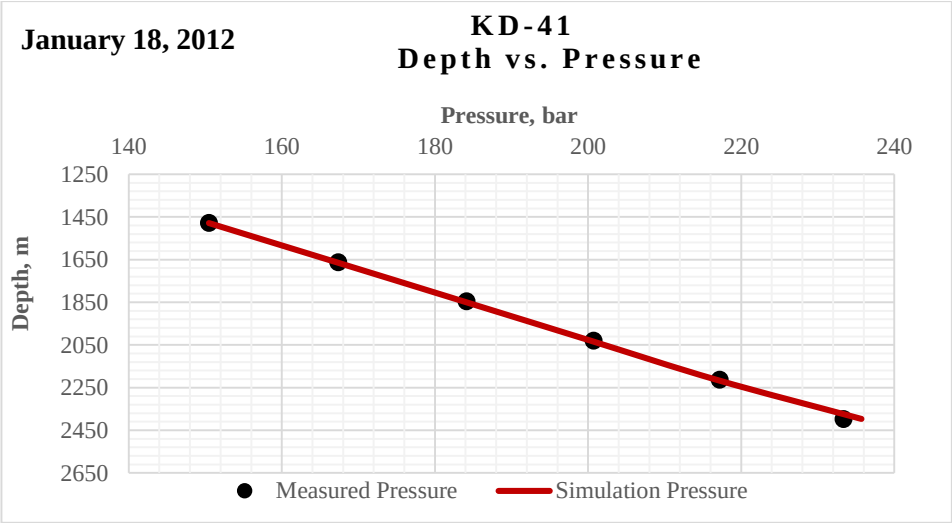

Figure 4.19 Depth vs. Pressure profile of KD-41

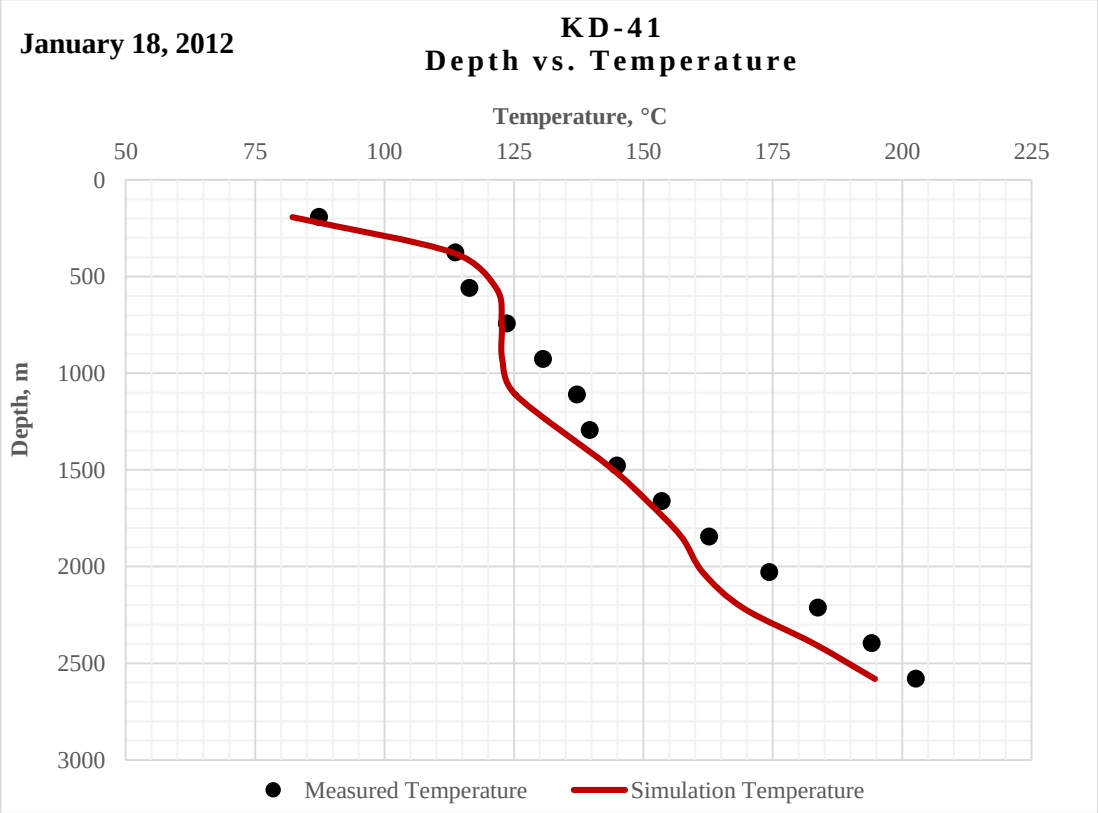

Figure 4.20 Depth vs. Temperature profile of KD-41

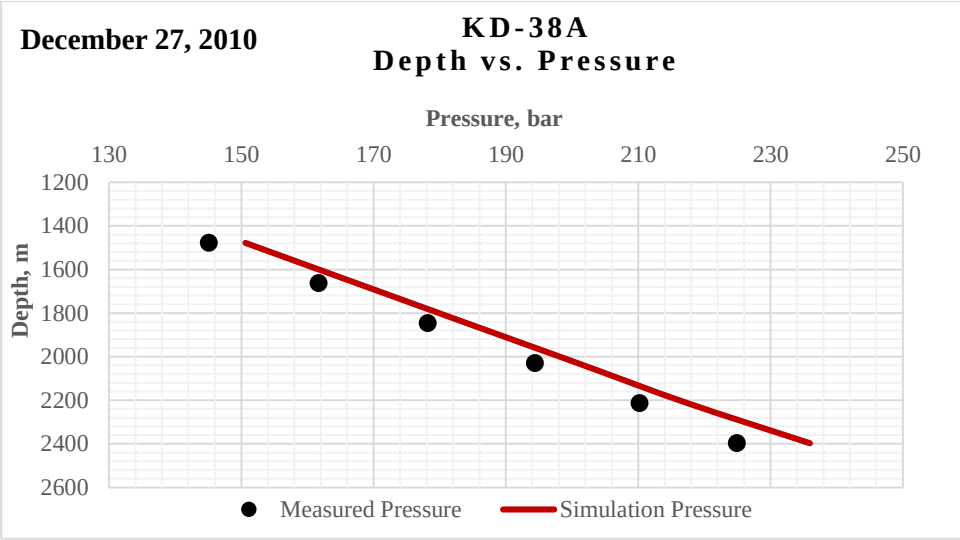

Figure 4.21 Depth vs. Pressure profile of KD-38A

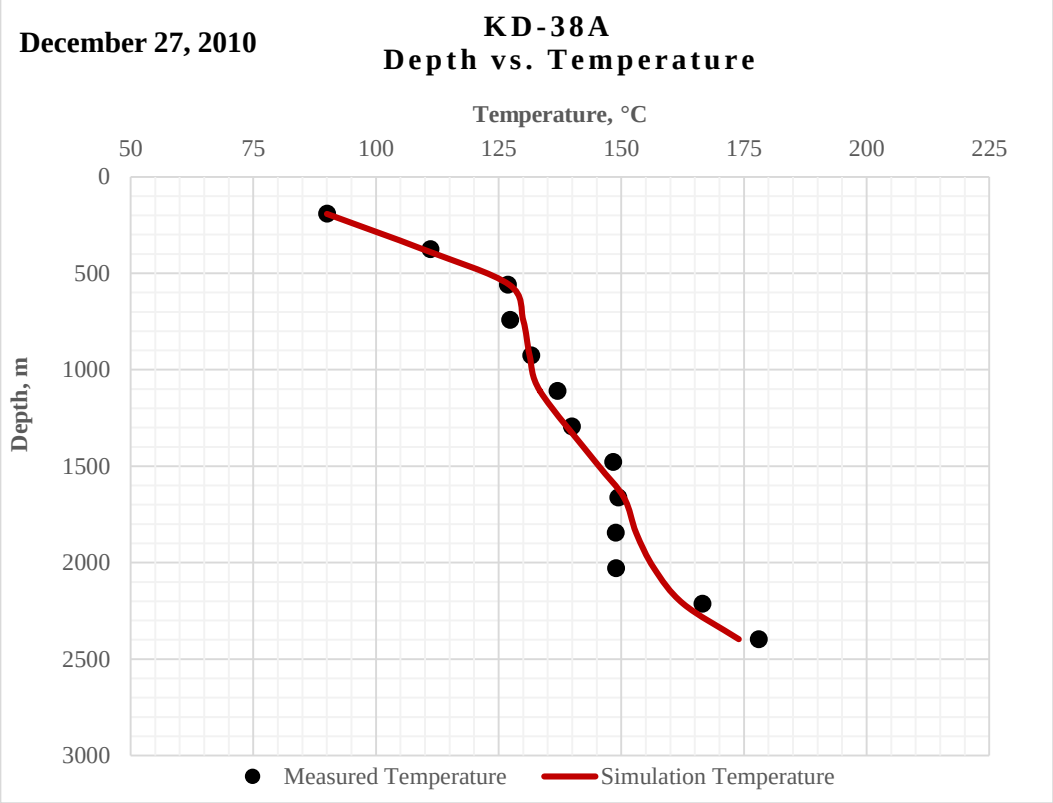

Figure 4.22 Depth vs. Temperature profile of KD-38A

At the natural state conditions, the NE-SW trending distribution of the reservoir temperatures show a consistency with the measured temperature data.

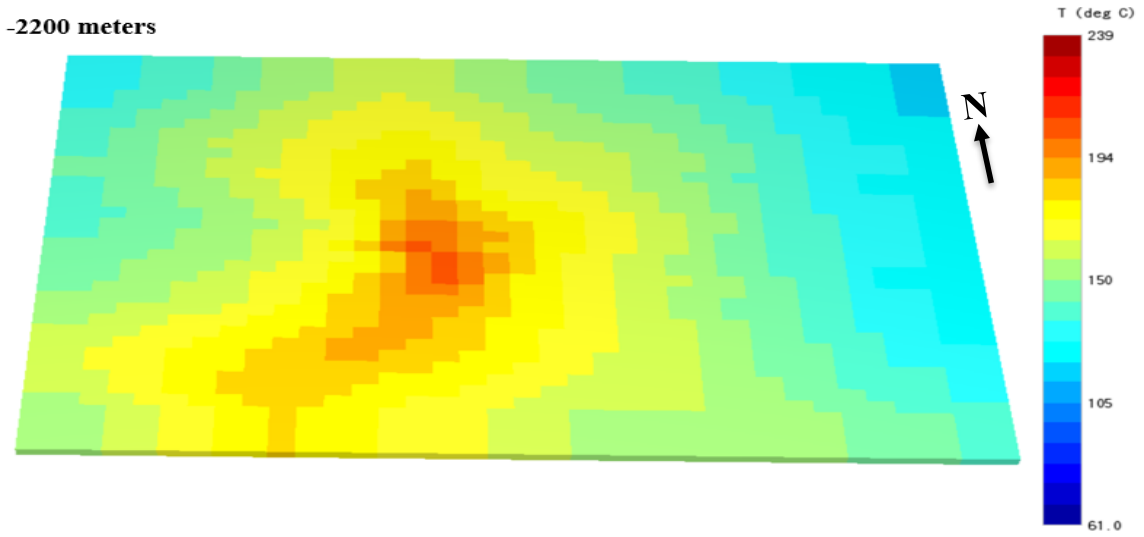

Figure 4.23 Temperature distribution at natural state conditions

The following isosurfaces show the distribution of the reservoir temperatures at the natural state conditions.

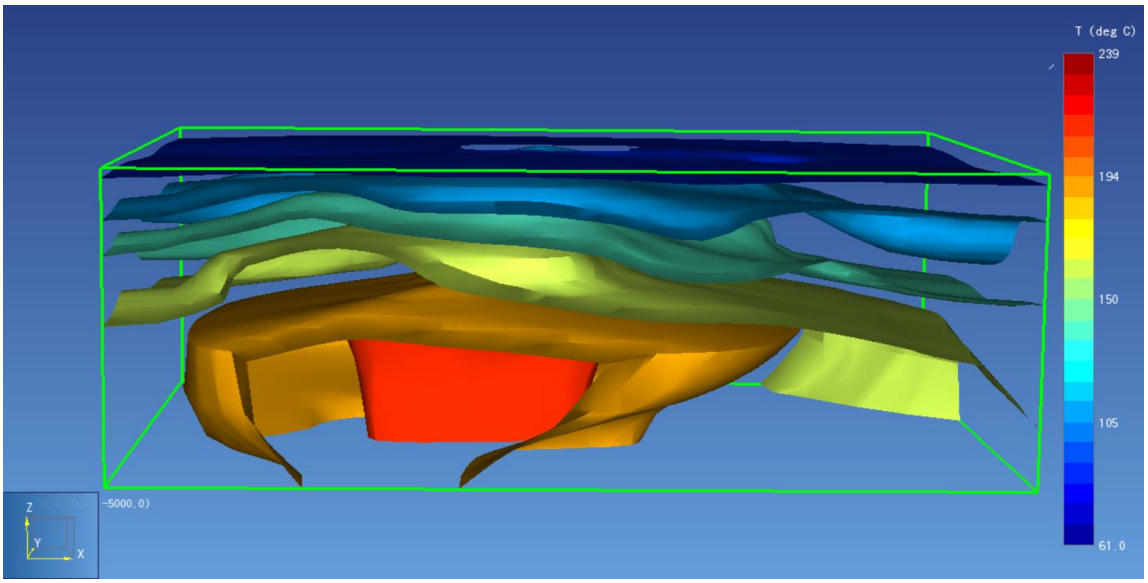

Figure 4.24 Temperature isosurfaces at natural state conditions

As the temperature isosurfaces implies, there is a high temperature zone approximately at the center of the field. A sudden temperature decrease at the flanks of this zone indicates the cold water recharge from the highs of the horsts.

For the -600m – -3000m depth interval, the simulation pressure results are in the 7% range of the measured pressure data of 53 wells, averagely. At the same interval, the average of the temperature differences is 6.8%.

Considering only the -1850m – -3000m depth interval, where most of the production wells have been completed, the average of the pressure differences between the simulator output and the actual pressure data of 53 wells is 3.8%, and average of the temperature differences is 5.6%.

Grid Block Depth, meter (bsl)	Average of Pressure Errors, %
1846 m	2.2
2029 m	2.3
2213 m	2.2
2397 m	3.6
2581 m	4.5
2764 m	6.4
2948 m	5.3
TOTAL AVERAGE	**3.8**

Table 4.5 Average of the pressure differences between measured and simulation data

Grid Block Depth, meter (bsl)	Average of Temperature Errors, %
1846 m	7.5
2029 m	7.1
2213 m	7.1
2397 m	5.1
2581 m	4.9
2764 m	4.8
2948 m	2.9
TOTAL AVERAGE:	**5.6**

Table 4.6 Average of the temperature differences between measured and simulation data

Errors have been calculated by the following formula, for each well, at each corresponding grid block. Tables above are showing averages of these errors with respect to depth.

$$Error, \% = \frac{|(Actual\ Value - Simulation\ Value)|}{Actual\ Value} * 100$$

Considering, for example, 2948 meter below the sea level, the highest pressure difference is of the KD-61 production well, with 7.9%. The measured pressure at that depth is nearly 260 bar, and the simulation pressure is nearly 280 bar. 20 bar difference is the worst case at that depth, and majority of wells are in the pressure difference range of 5 – 15 bar. Plotting "actual pressure vs. simulation pressure" graph for the top of the completion interval of the corresponding well, clearly shows the accuracy between the simulation pressures and the measured pressures.

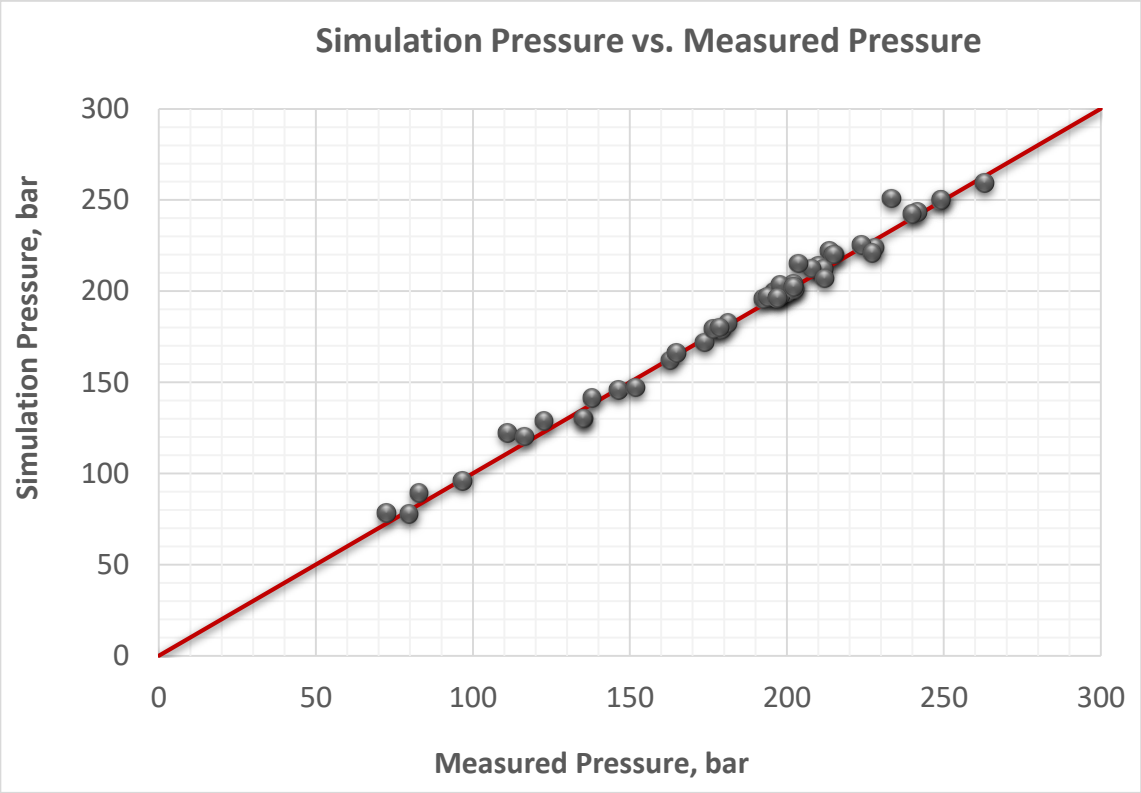

Figure 4.25 Single point comparison of simulation and measured pressures

The distribution of the dissolved CO_2 in the geothermal fluids of the Kızıldere Geothermal Field is shown in the Figure 4.26. The dominant effects of the NE-SW trending Gebeler Fault on the fluid circulation can be clearly seen. Around 3% dissolved CO_2 is present at the deep metamorphics at the natural state conditions.

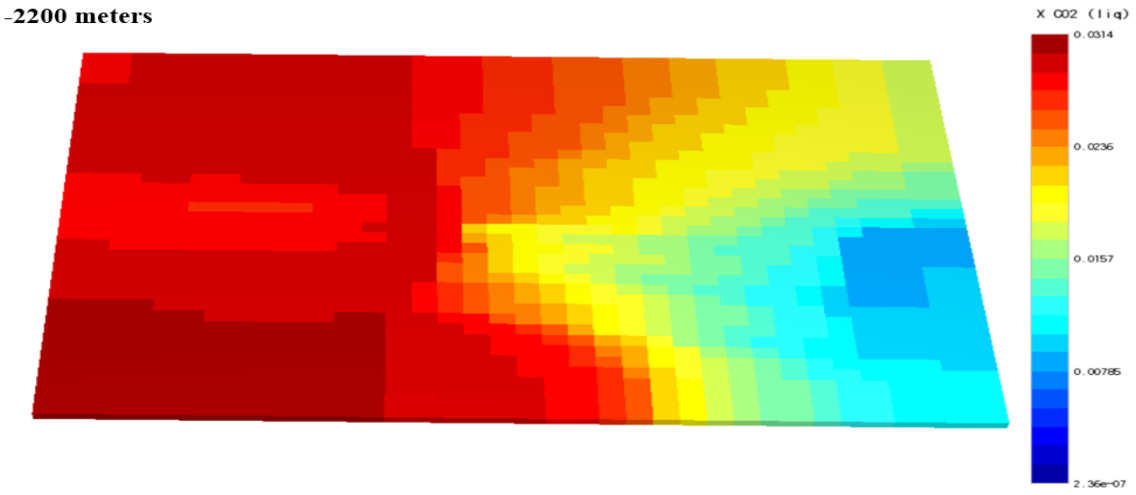

Figure 4.26 CO_2 distribution at the natural state conditions

The CO_2 isosurfaces implies that amount of the dissolved CO_2 is higher at the western and south-western sections of the field at the same depth.

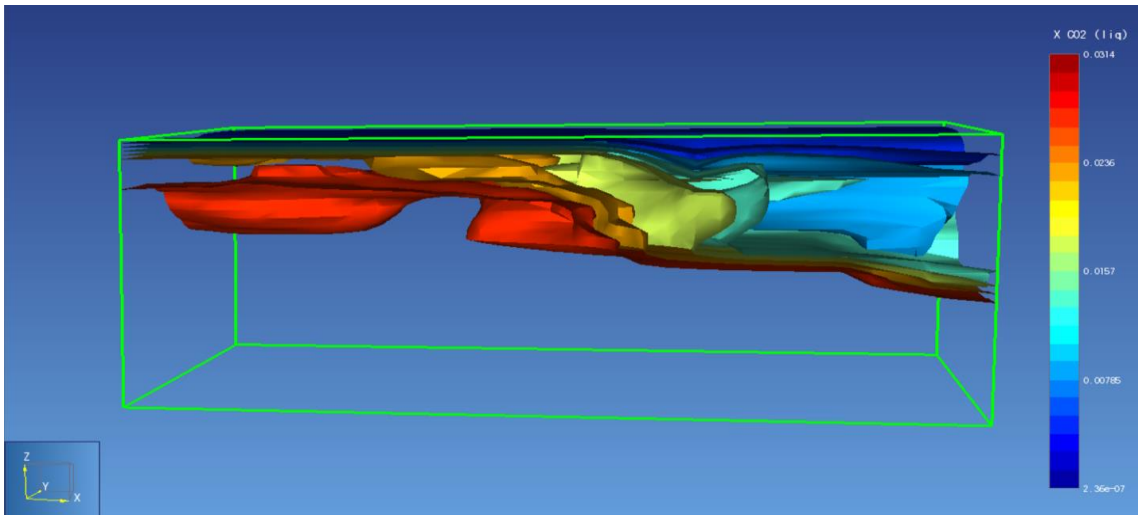

Figure 4.27 CO_2 isosurfaces at the natural state conditions

Above-mentioned results verified that the model successfully represents the natural state conditions of the Kızıldere Geothermal Field. But in addition to making single-time (measurement date) static pressure/temperature comparisons between the actual data and simulation data, behavior of the dynamic reservoir pressures should also be compared with the simulation data in order to validate the model. For that purpose, simulation pressures and the pressure history of 15 observation wells have been compared. The following table summarizes the results, and shows the error margin between the actual and simulation pressures. Note that some of the observation wells have been converted into production/injection wells, and their observation duration is only limited.

Observation Well	Observation Depth, bsl	Observation Period (dd/mm/yy)	|Error|
KD-7	304 m	17.02.2012 - 20.04.2018	≤4 bar
KD-9	535 m	22.11.1988 - 31.12.1998	≤1 bar
KD-23A	1678 m	17.05.2014 - 20.04.2018	3 - 10 bar
KD-23C	889 m	23.10.2013 - 09.02.2015	3 - 7 bar
KD-27A	1980 m	07.11.2013 - 28.02.2015	≤4 bar
KD-41	1000 m	04.11.2015 - 17.03.2017	≤1 bar
KD-42	2000 m	21.05.2014 - 04.01.2015	≤1 bar
KD-44	1294 m	17.06.2015 - 12.01.2016	2 - 4 bar
KD-46	1362 m	17.06.2015 - 16.03.2017	6 - 8 bar
KD-50A	1635 m	09.08.2015 - 02.08.2016	≤2 bar
KD-55	2203 m	17.06.2015 - 13.03.2017	≤2.5 bar
KD-56B	1713 m	09.05.2017 - 20.04.2018	≤1 bar
KD-89	2187 m	09.06.2017 - 29.09.2017	≤1 bar
KDE-8	1714 m	01.04.2017 - 20.04.2018	≤10 bar
KDE-12	1739 m	27.04.2017 - 20.04.2018	≤5 bar

Table 4.7 Observation wells and pressure error margins

For most of the observation wells, the difference between the observation depth and the center of the grid block depth is not negligibly small, and can be as high as 80 meters. To overcome making any erroneous comparison, the simulation pressures have been correlated to the corresponding observation depth by simply adding (or subtracting) the hydrostatic pressure of the geothermal fluid to the grid block pressure. To make this correlation as accurate as possible, density of the fluid has been calculated over time, and taken into account.

After making above-mentioned correlation, observation pressures and simulation pressures of 15 wells have been compared. Measured static pressures have also been included in the comparison. Following table shows the date of the static pressure measurements taken in the observation wells, and also the accuracy of the simulation pressures.

Observation Well	Static Pressure Measurement Date	Measured Static Pressure	Simulation Pressure	|Error|
KD-7	-	-	-	-
KD-9	-	-	-	-
KD-23A	16.05.2013	163.0	167.0	2.5%
KD-23C	03.01.2011	93.1	96.0	3.1%
KD-27A	28.10.2010	190.0	196.4	3.4%
KD-41	18.01.2012	106.4	106.2	0.2%
KD-42	20.01.2015	184.7	184.9	0.1%
KD-44	27.08.2014	125.4	129.4	3.2%
KD-46	07.03.2014	133.0	139.8	5.1%
KD-50A	15.05.2014	152.8	152.5	0.2%
KD-55	01.09.2014	201.9	204.2	1.2%
KD-56B	02.02.2017	151.4	152.3	0.6%
KD-89	03.02.2017	195.2	194.3	0.5%
KDE-8	15.10.2016	154.4	155.7	0.8%
KDE-12	20.12.2016	155.5	157.3	1.2%

Table 4.8 Measured static pressures of observation wells

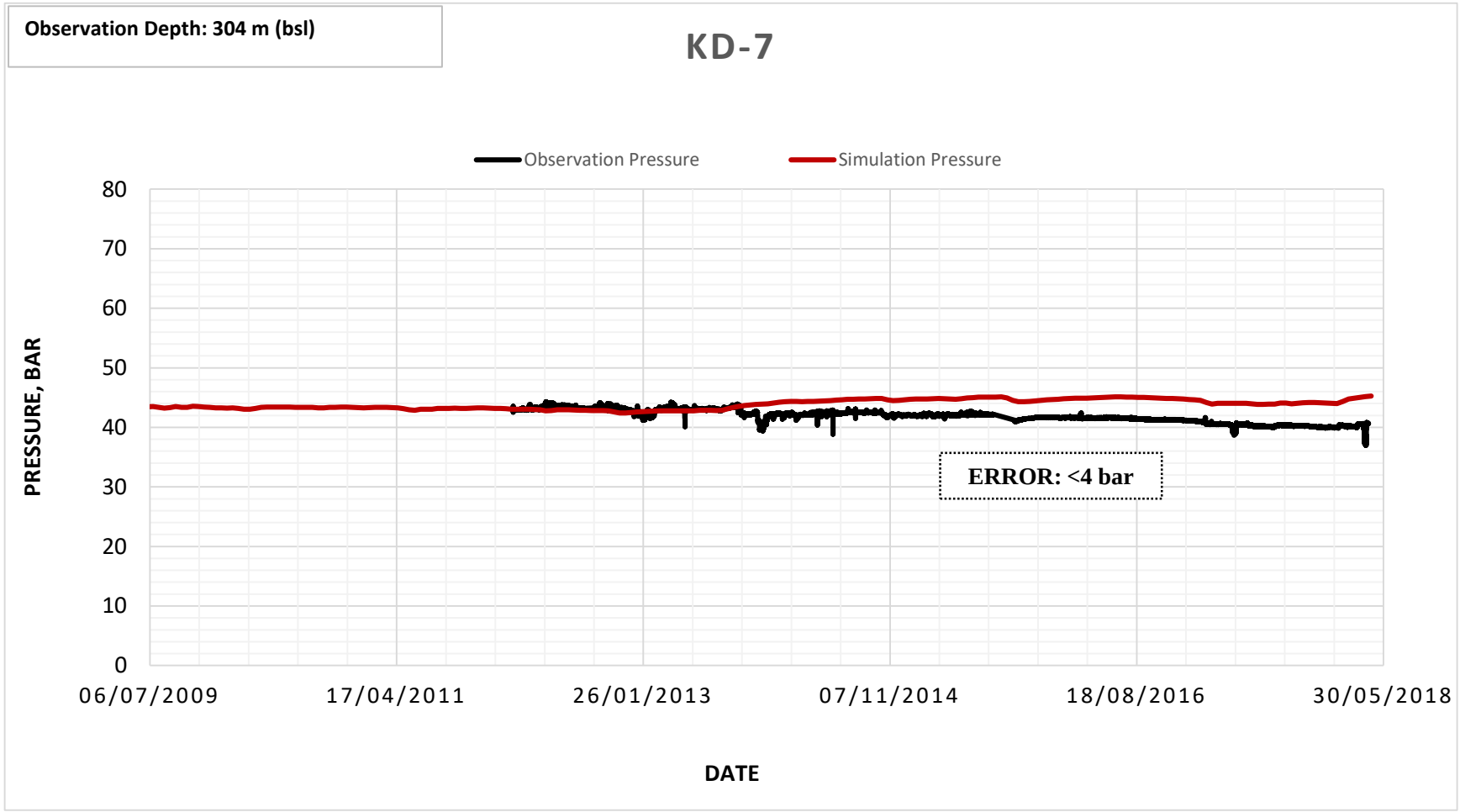

Figure 4.28 Simulated and Observed Pressure Profiles of KD-7

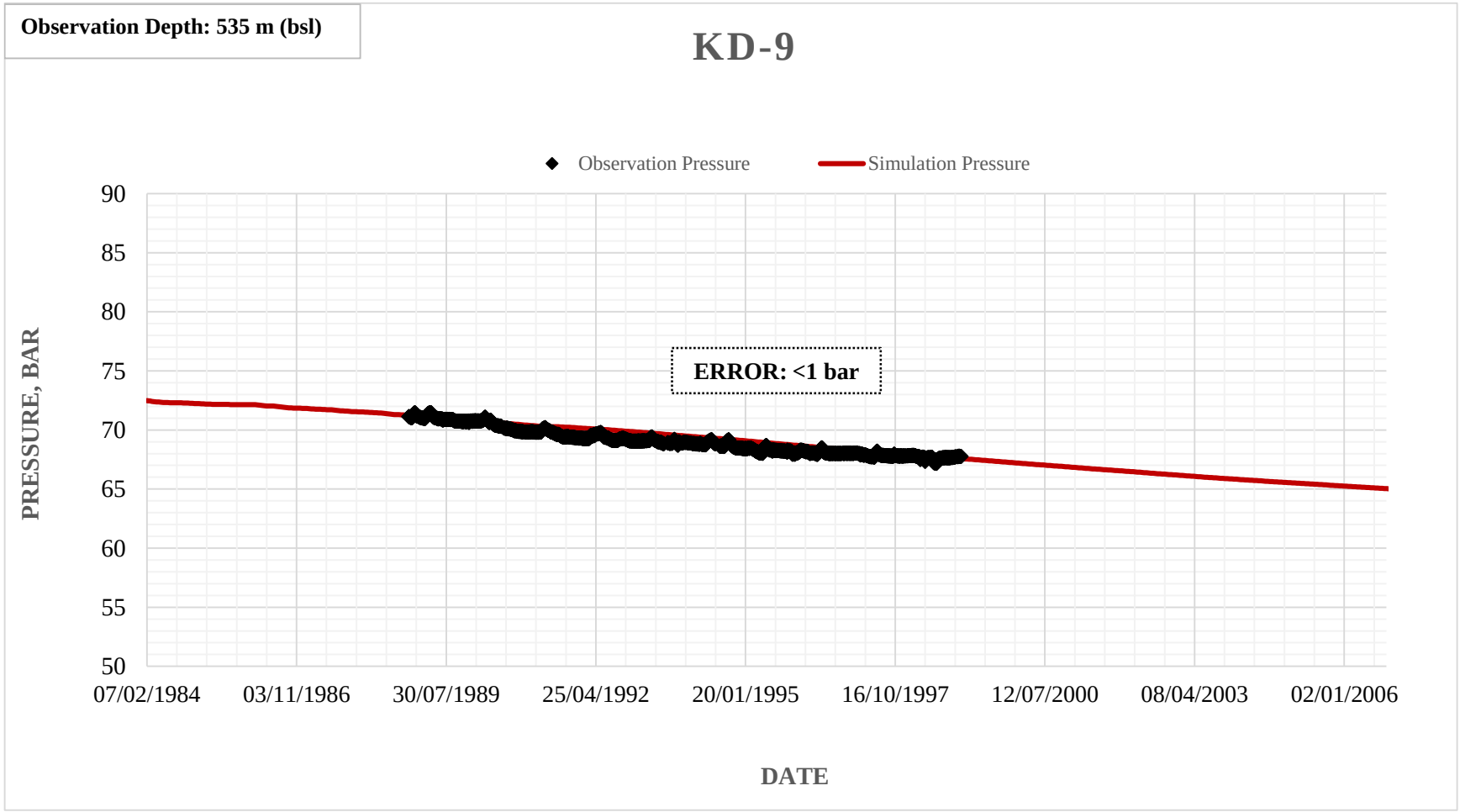

Figure 4.29 Simulated and Observed Pressure Profiles of KD-9

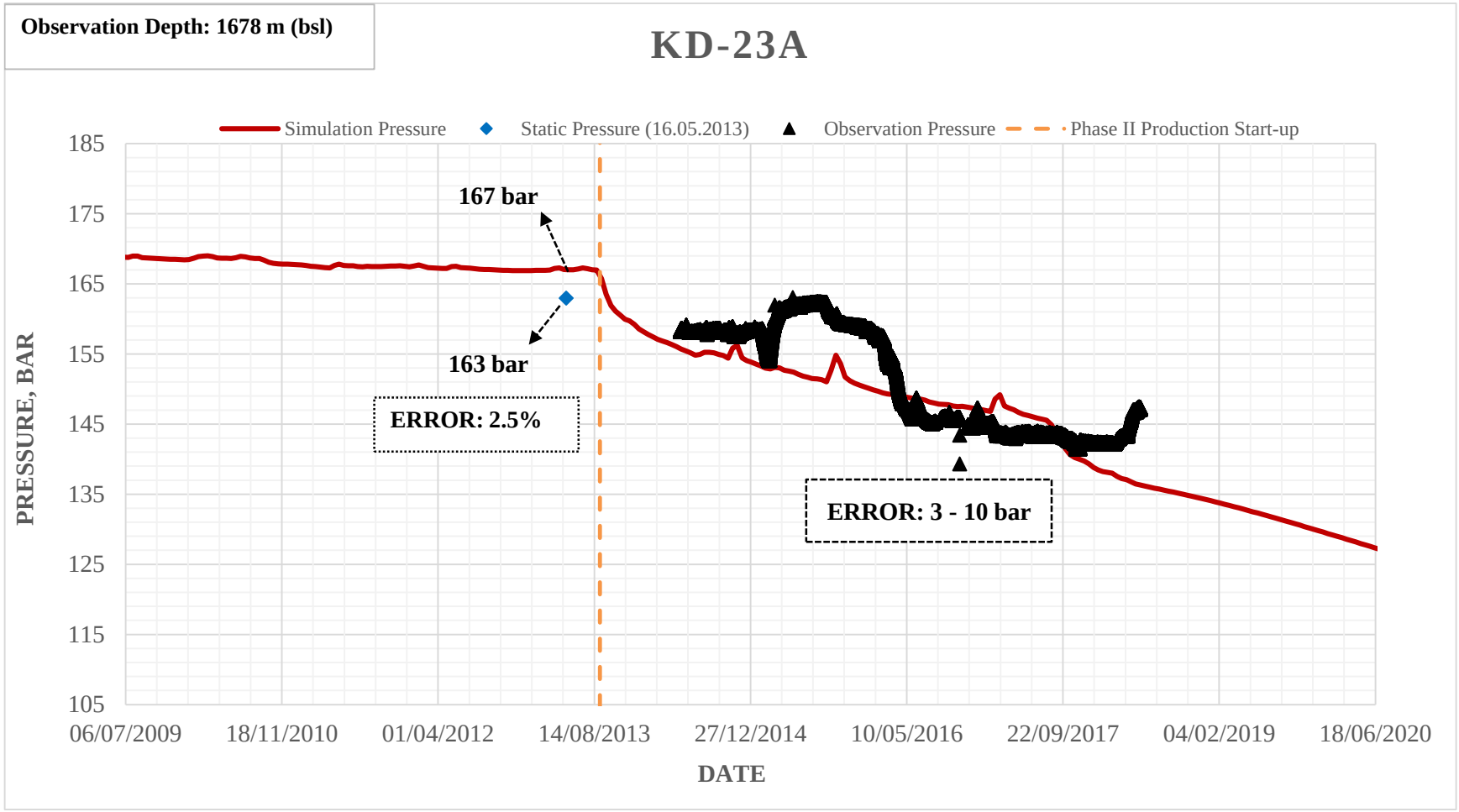

Figure 4.30 Simulated and Observed Pressure Profiles of KD-23A

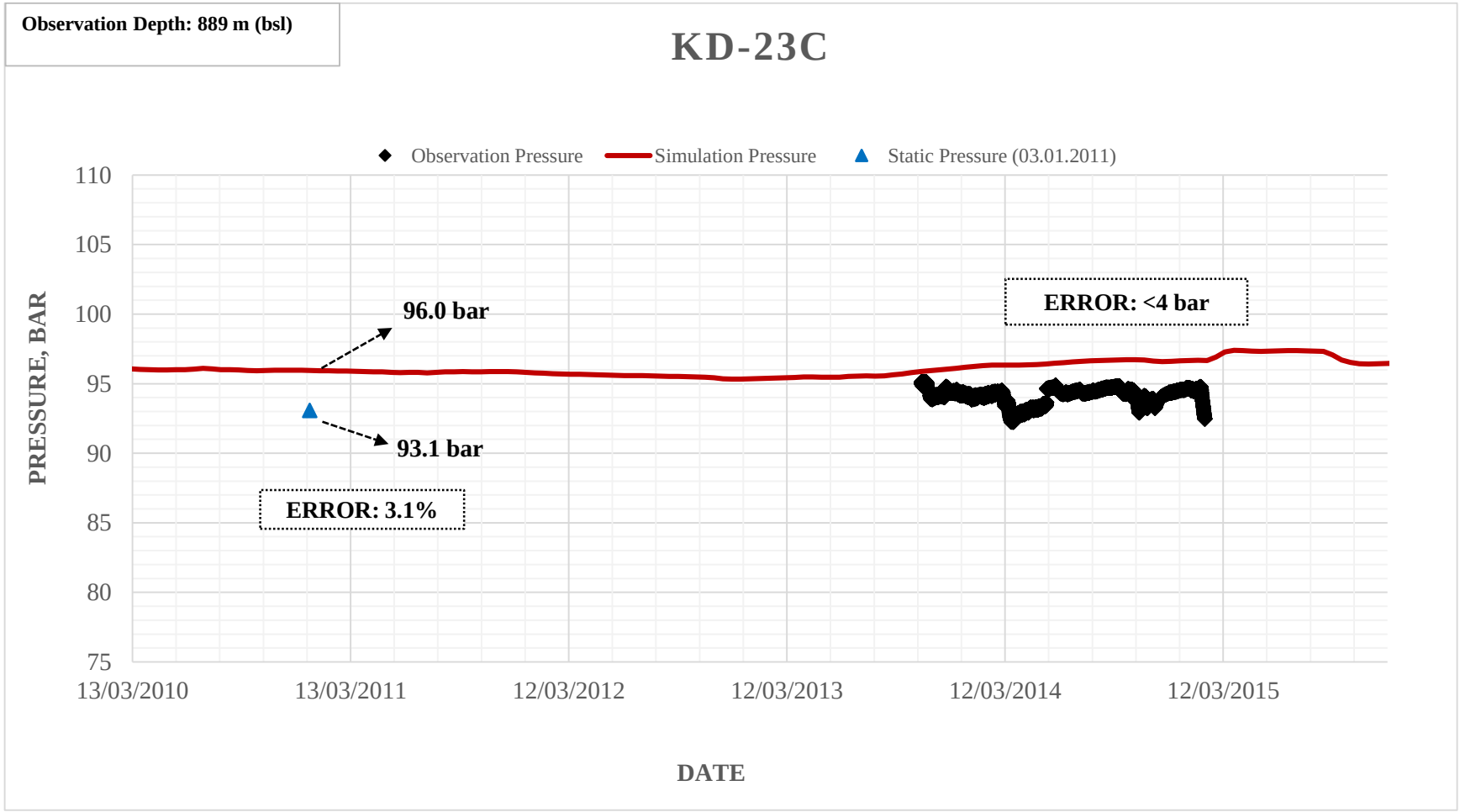

Figure 4.31 Simulated and Observed Pressure Profiles of KD-23C

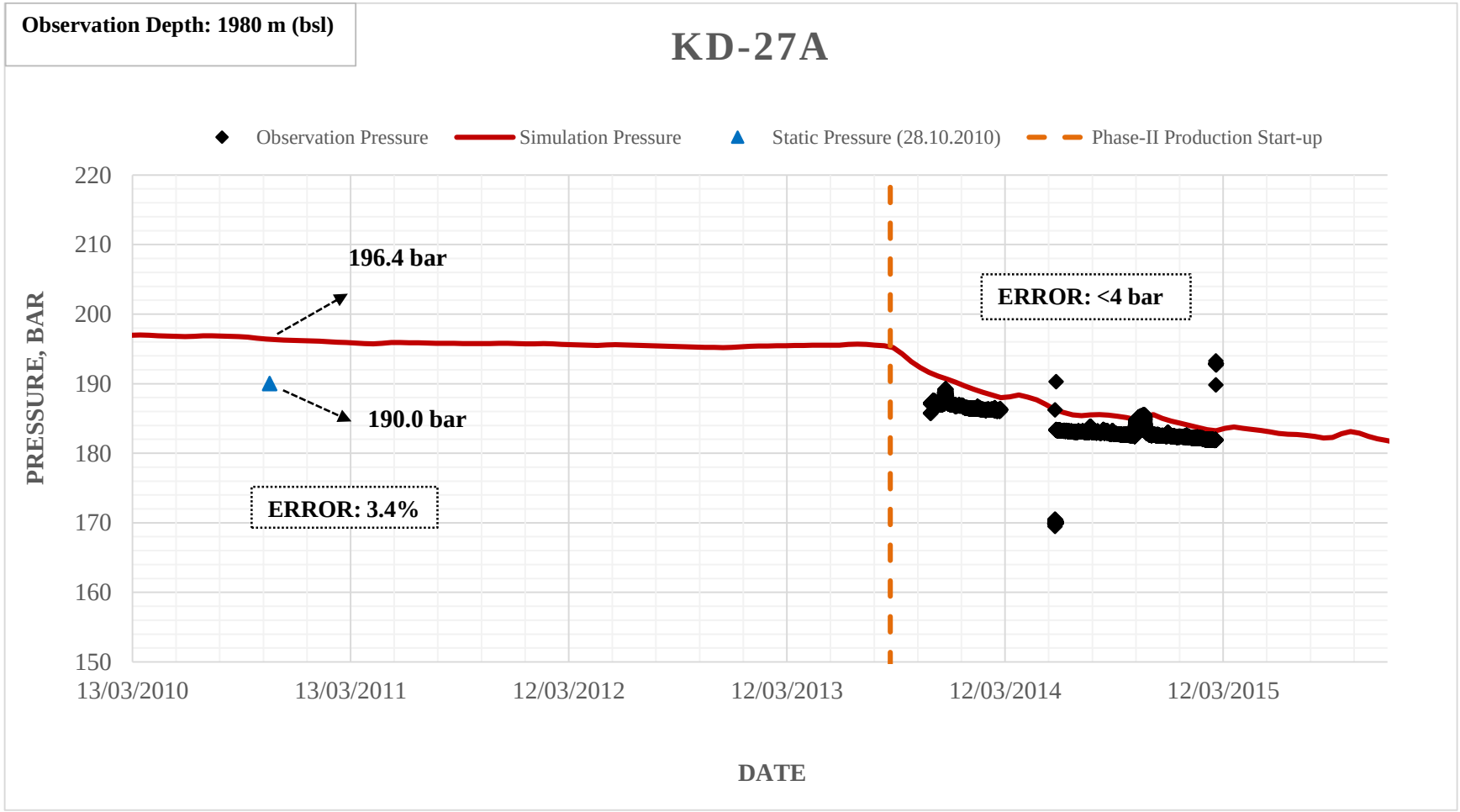

Figure 4.32 Simulated and Observed Pressure Profiles of KD-27A

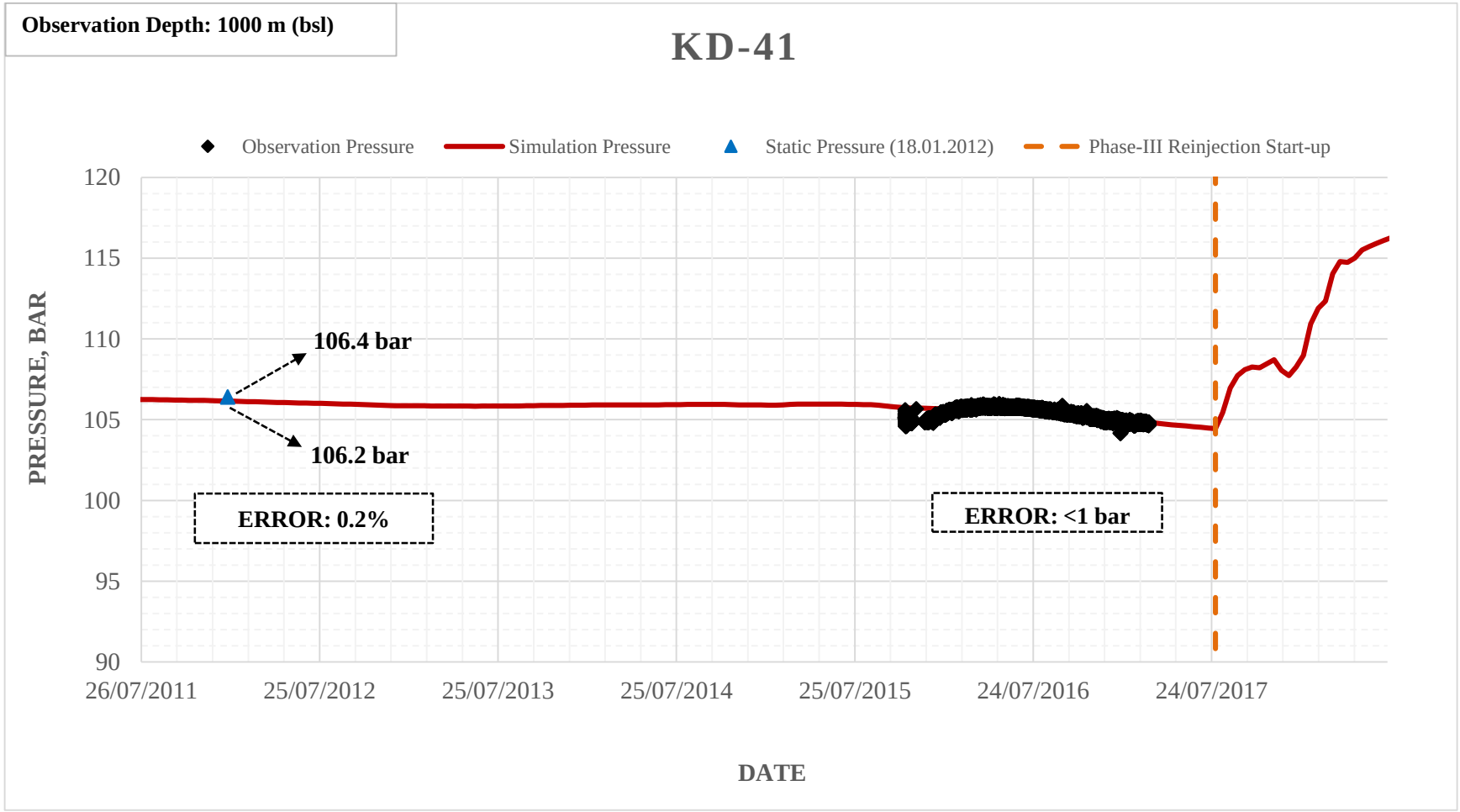

Figure 4.33 Simulated and Observed Pressure Profiles of KD-41

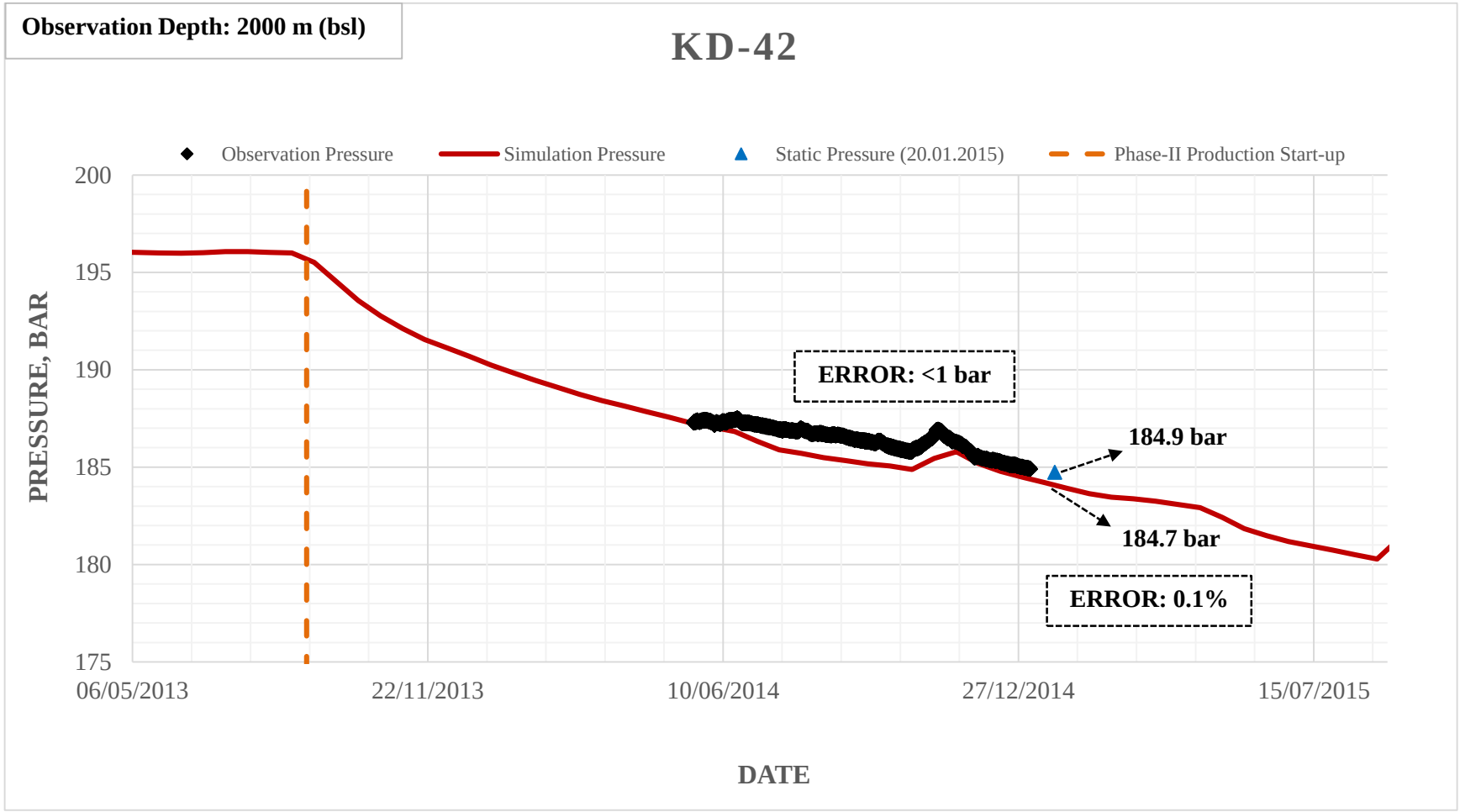

Figure 4.34 Simulated and Observed Pressure Profiles of KD-42

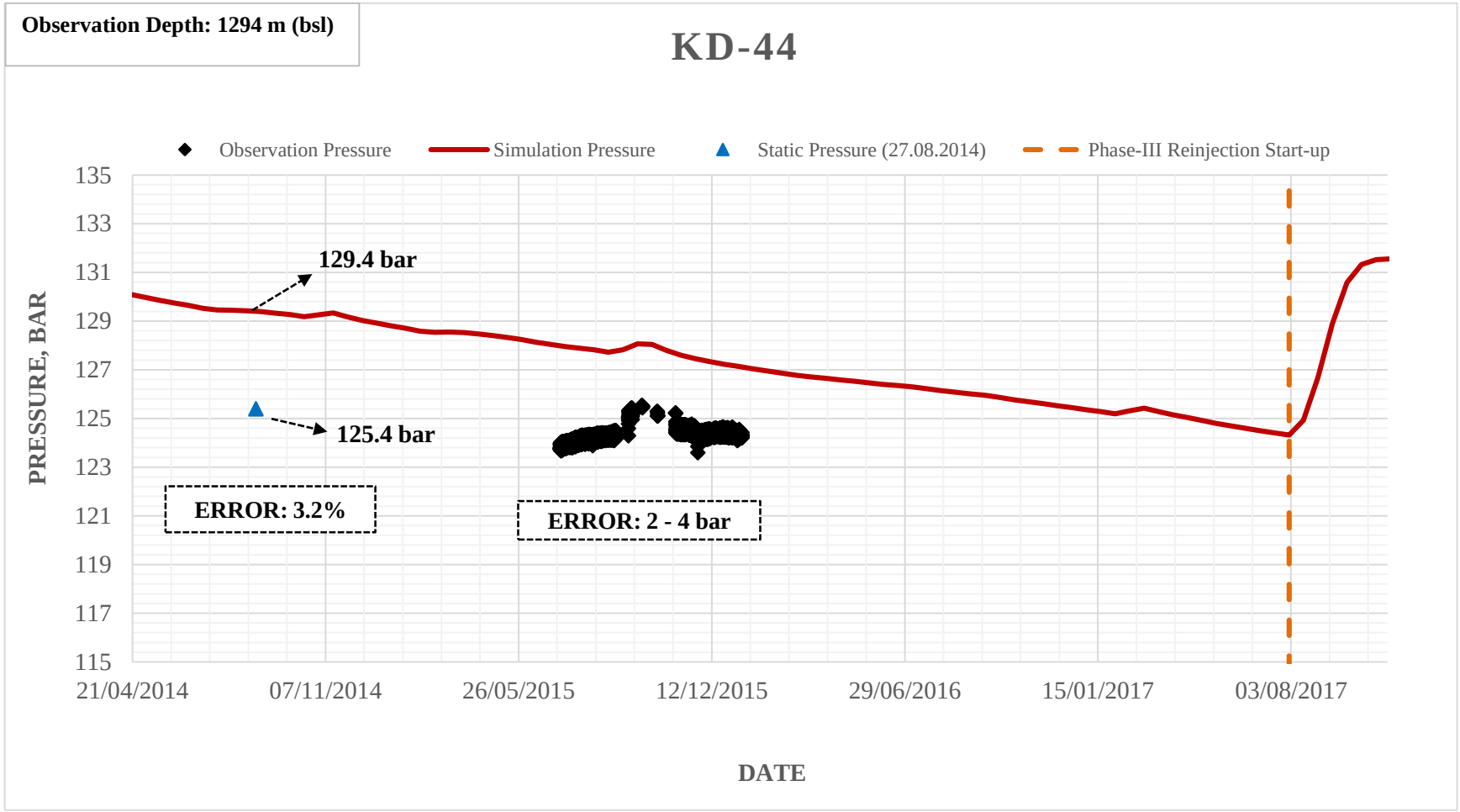

Figure 4.35 Simulated and Observed Pressure Profiles of KD-44

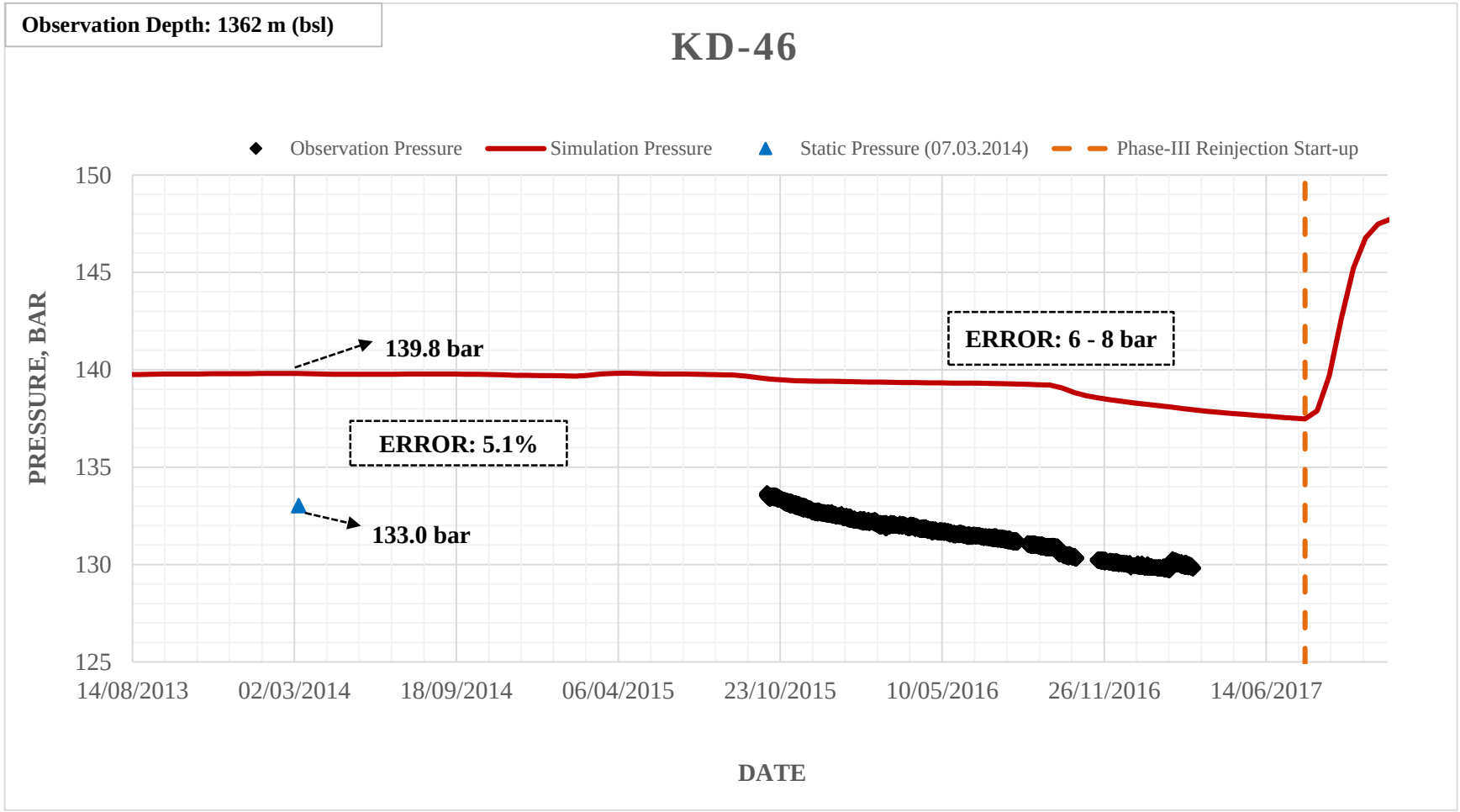

Figure 4.36 Simulated and Observed Pressure Profiles of KD-46

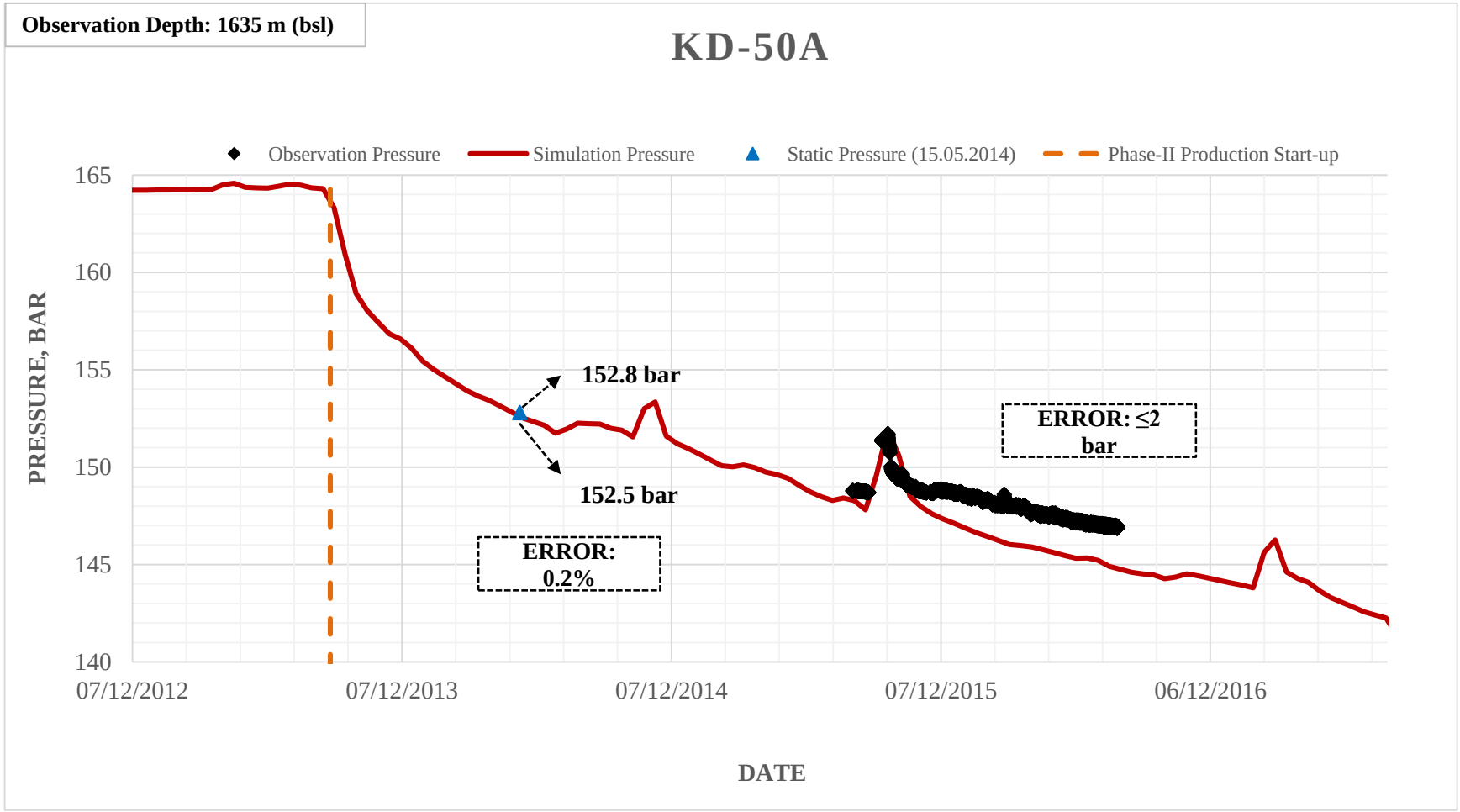

Figure 4.37 Simulated and Observed Pressure Profiles of KD-50A

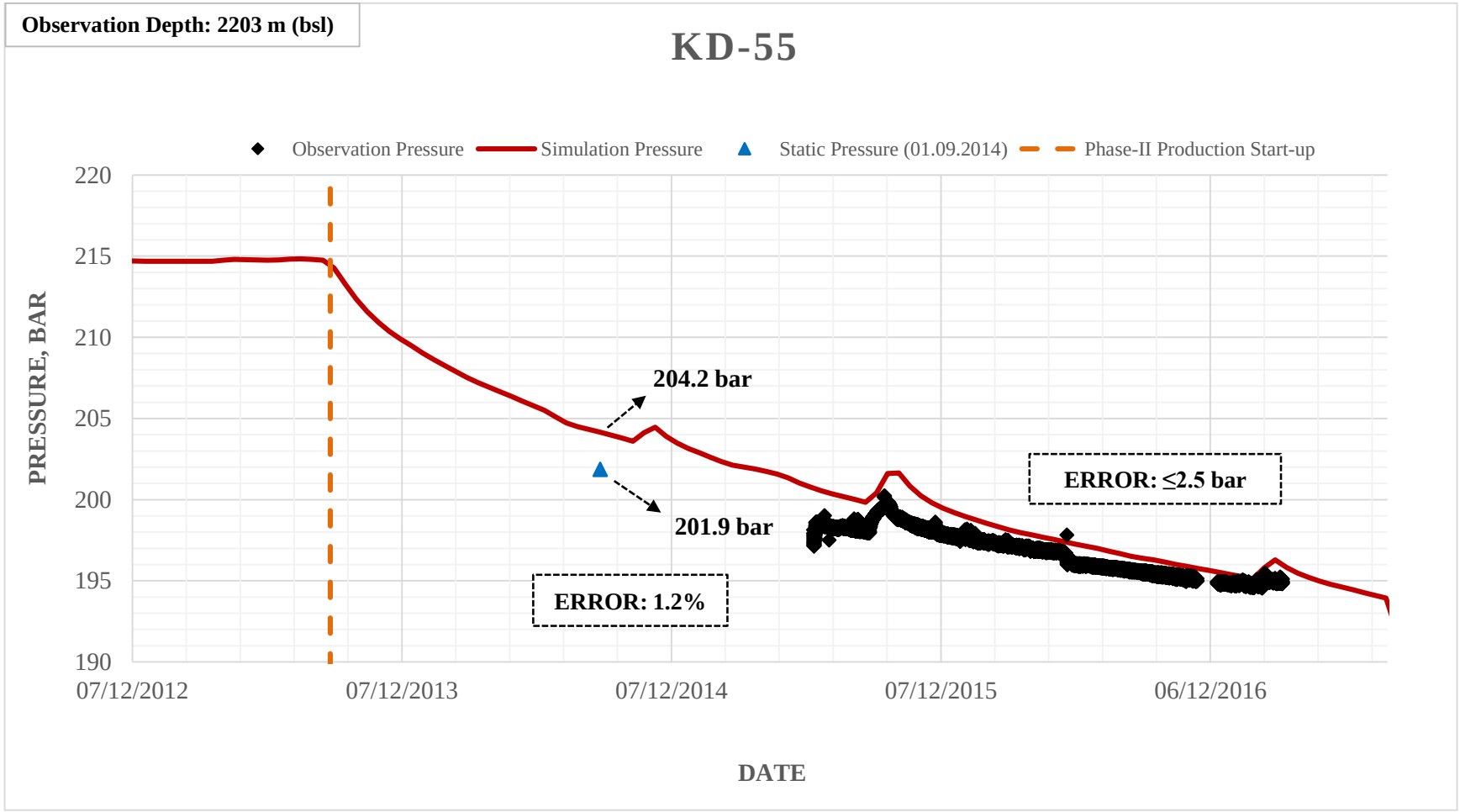

Figure 4.38 Simulated and Observed Pressure Profiles of KD-55

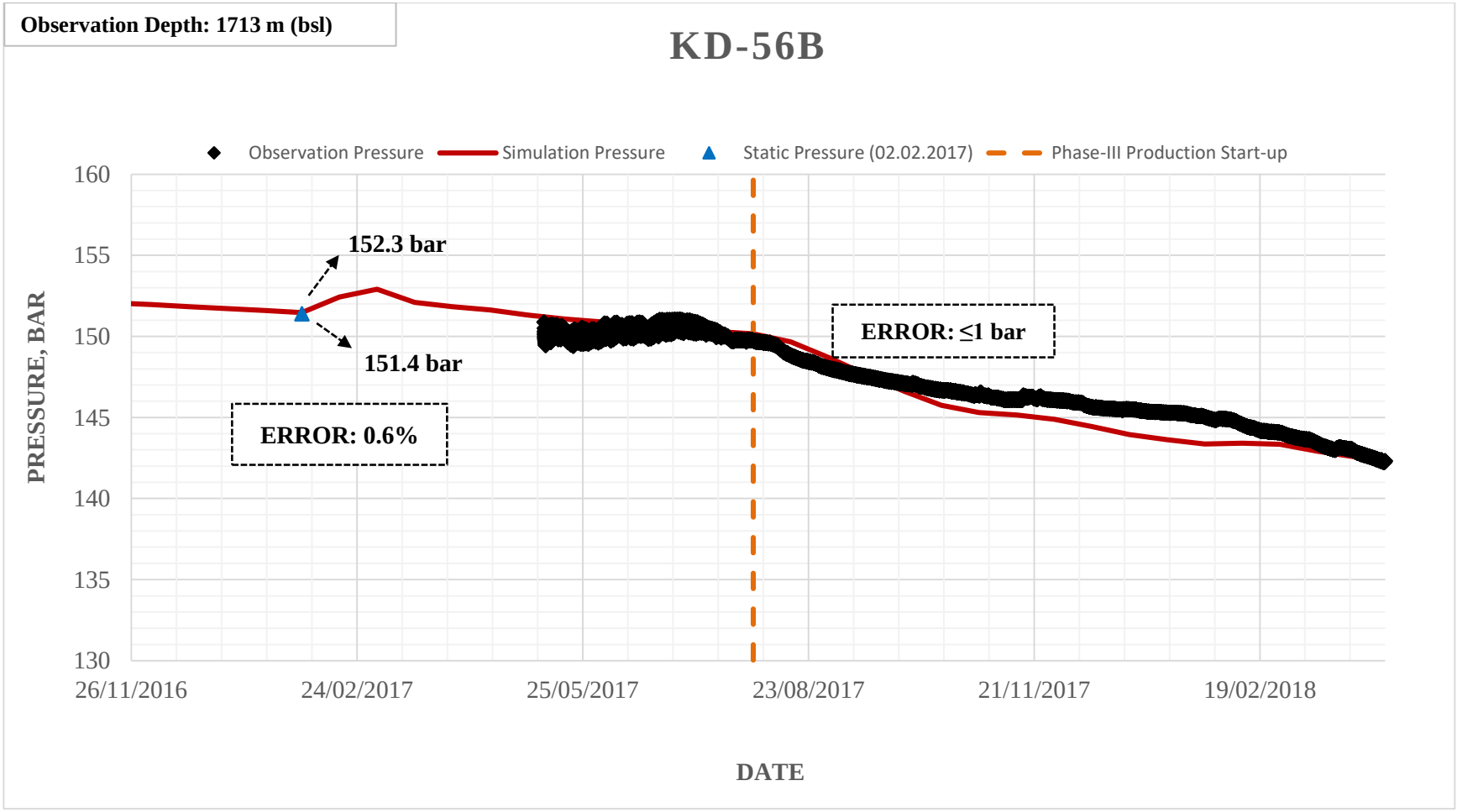

Figure 4.39 Simulated and Observed Pressure Profiles of KD-56B

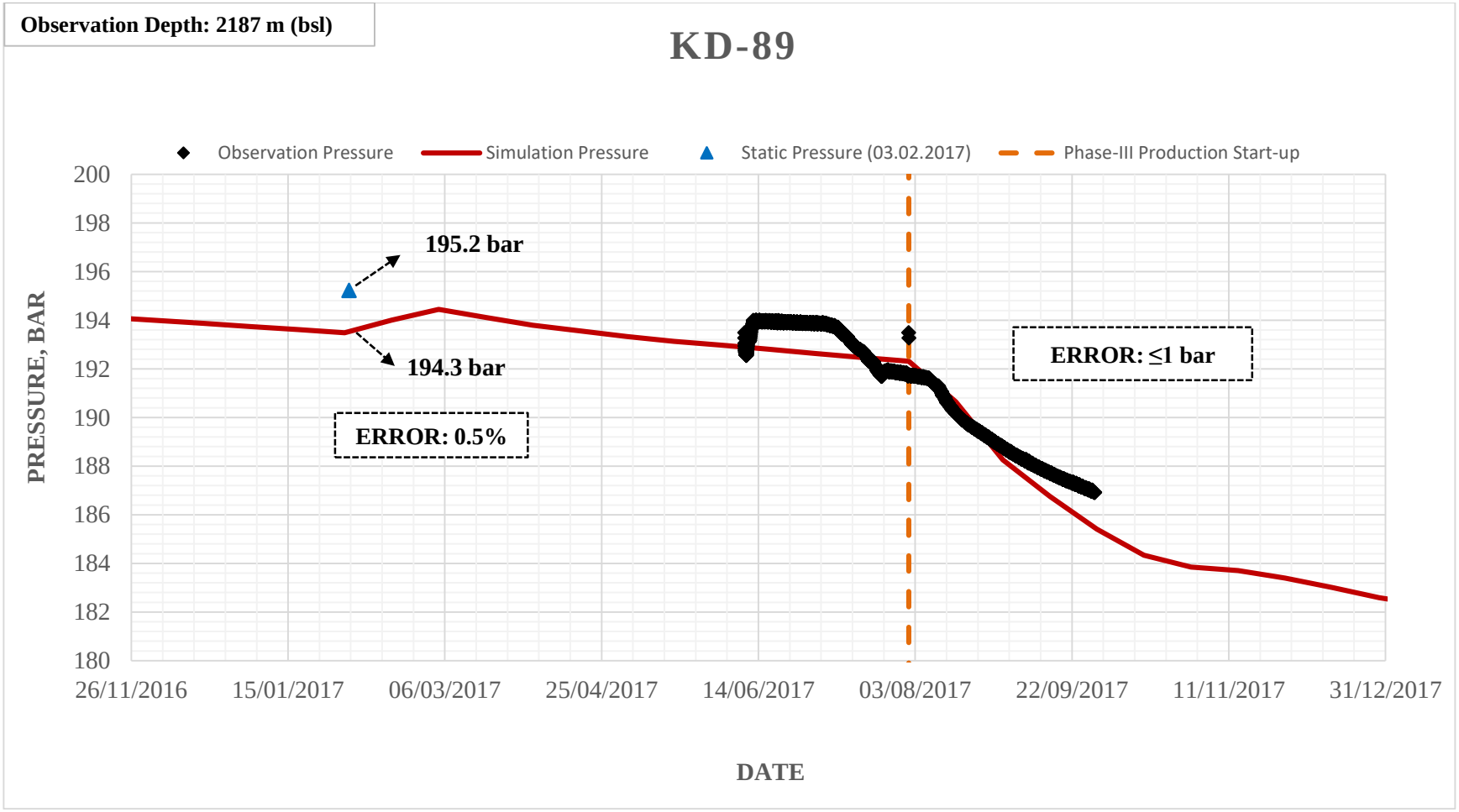

Figure 4.40 Simulated and Observed Pressure Profiles of KD-89

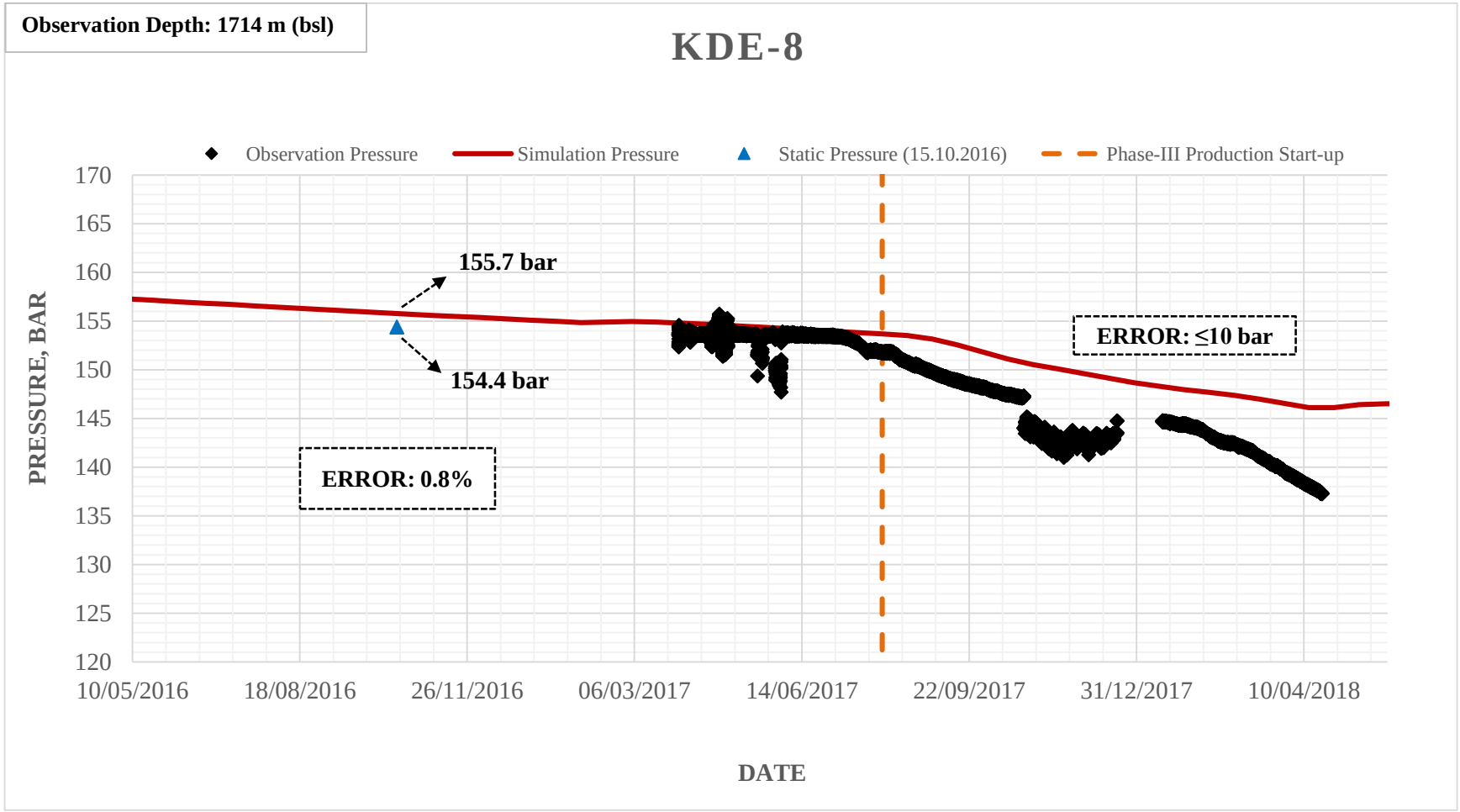

Figure 4.41 Simulated and Observed Pressure Profiles of KDE-8

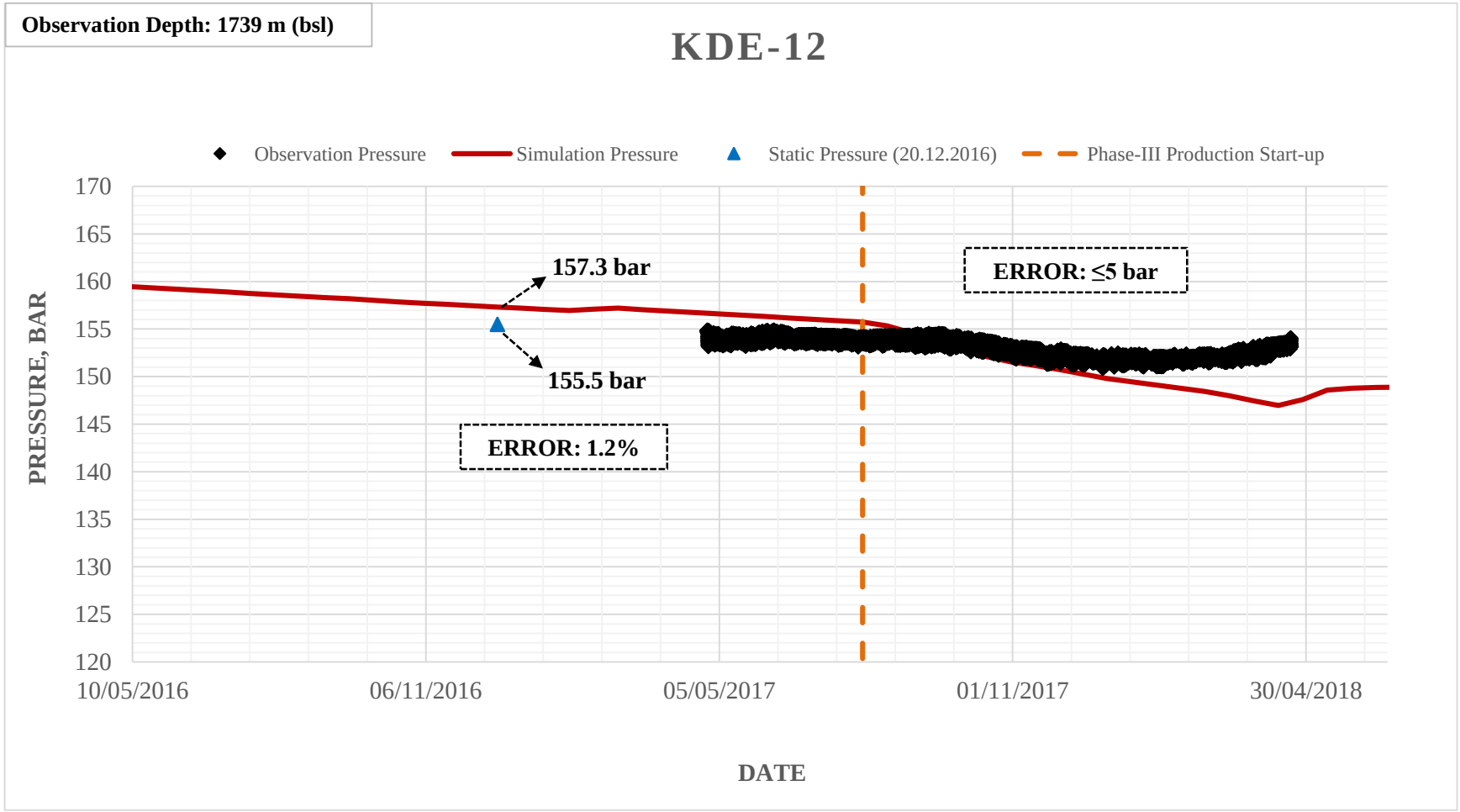

Figure 4.42 Simulated and Observed Pressure Profiles of KDE-12

The pressure output of the numerical simulation has shown a great consistency with the behavior of the observed pressures. Errors are much smaller than 10% for all of the 15 observation wells. Measured static pressures have also been compared with the simulation output, and highly satisfied results have been obtained. Even though the shallower sections of the field were not the main target of the model initially, simulation results almost perfectly matched the pressure histories of KD-7 and KD-9. Since these wells have been drilled before 1984 (starting date of the simulation), static pressures couldn't be compared. For some of the wells, such as KD-44 and KD-46, the difference between the observed pressures and the simulation pressures may seem higher than the rest of the wells. However, the error is still acceptably small, and the pattern of the pressure decline is very identical for both of the wells. On the other hand, pressure behavior of KDE-8 and KDE-12 differ from the simulation pressures at the beginning of 2018. KDE-12 is at the south-western edge of the study area, which is very close to the injection and production wells of a neighboring geothermal power plant. The increase in the observed pressure of KDE-12 may be due to an injection operation, started at a neighboring injection well. The inconsistency between the KDE-8 observed pressures and the simulation pressures is reasonable, since KDE-8 is at the western-most edge of the model and there is not enough information about this area (only a few wells have been drilled in this area).

All in all, static pressure/temperature profiles of the 53 wells and dynamic pressure histories of 15 observation wells have been compared with the simulation output and identical results have been obtained. The Kızıldere geothermal model has been validated that it is a good representation of the actual field and it can be used for future predicting studies.

CHAPTER 5

SCENARIOS

Predicting the future performance of the Kızıldere Geothermal Field and evaluating the consequences of potential field operations long before their implementations are of a great importance, and these are the main purposes to have a realistic computer model of the actual field. Pressure and temperature profiles, and CO_2 levels of production wells with respect to time at different production/reinjection scenarios have been simulated. Consequences of varying carbon dioxide injection scenarios have been investigated.

Two main strategies can be implemented in terms of the management of the field:

1. Keeping the production rates as constant as possible in exchange for the wellhead pressures.

2. Keeping the wellhead pressures as constant as possible by arranging the production rates.

Both of these strategies have their own advantages and disadvantages. For example, in the first strategy, energy extraction is maximized in the short term, but the reduction of the reservoir pressures may reach critical levels in the mid and long term of the operations due to high amount of withdrawal from the reservoir. On the other hand, the second strategy provides moderate extraction rates compared to the first strategy, but it provides a much more balanced reservoir management and surface operations.

In this chapter, 3 different performance prediction scenarios are carried out considering both of the strategies. These scenarios are mainly investigating the effects of different reinjection operations, as well as the consequences of different CO_2 injection operations.

Simulated scenarios are:

Scenario 1: No-change in the current reinjection rates

Scenario 2: Reinjecting what is produced

Part-I: Only water is reinjected, and CO_2 is released into the atmosphere,

Part-II: All of the produced CO_2 and water are reinjected

Scenario 3: Carbon Dioxide Injection

Part-I: 10% CO_2 injection with current reinjection rates

Part-II: Reinjecting the produced CO_2 in supercritical state

5.1 STRATEGY 1: Keeping Production Rates Constant

In this section, the above mentioned scenarios are applied, and the production and reinjection rates are kept constant throughout the simulations. Changes in the pressure and temperature profiles, and CO_2 levels are investigated for the next 20 years.

5.1.1 Scenario 1: No-Change in the production/reinjection rates

In the first scenario, production and injection rates, as of May 2018, have been repeated for 20 years in exchange of the well head pressures. Although it is not logical to have the same values for the next 20 years, the main purpose of this scenario is to see the pressure and temperature changes in the production wells, and make necessary actions accordingly.

Production rates of 34 production wells (Table 5.1.) and injection rates of 27 wells (Table

5.2.) have been repeated for 20 years. The difference between the production and reinjection rates is considerably high (around 1700 tph), which causes rapid decline in the reservoir pressure.

Well	Production Rate, tph	Well	Production Rate, tph
KD-47	300	**R-5**	202
R-3A	295	**KD-25B**	200
KD-64	281	**KD-61**	190
KD-42	280	**KD-90B**	190
KD-2A	273	**KD-43**	185
KD-83	250	**KD-66**	180
KD-55	240	**KD-23D**	178
KD-68B	240	**KD-29**	175
KD-60	230	**KD-45**	175
KD-61A	228	**KD-90A**	170
KD-62	220	**KD-54**	163
KD-68A	220	**KD-62A**	150
KD-63	216	**KD-89**	150
KD-49	215	**KD-59**	140
KD-58	215	**KD-58A**	120
KD-9A	208	**KD-54A**	119
KD-23B	202	**KD-50A**	100
TOTAL PRODUCTION: 6900 tph			

Table 5.1 Production rates of 34 production wells

Well	Injection Rate, tph	Well	Injection Rate, tph
KDE-11	527	**KD-46**	86
KD-38C	506	**KD-33**	86
KD-20B	489	**KD-28B**	80
KD-20A	431	**KD-38B**	74
KD-44A	376	**KD-32**	59
KD-93B	368	**KD-35**	50
KD-50	363	**KT-1**	50
KD-44B	304	**KD-28A**	50
R-2	271	**KD-41**	44
KDE-2	269	**KD-46A**	36
KD-93A	248	**KD-34**	32
KD-36A	190	**KD-38A**	14
KD-27A	104	**KDE-11A**	10
KD-44	86	**KD-25A**	0
TOTAL INJECTION: 5204 tph			

Table 5.2 Injection rates of 27 reinjection wells

Pressure changes of 3 wells (KD-42, KD-47, and KD-50A) between 1984 – 2038 have been plotted for the grid blocks at the top of the completion intervals. KD-47 has the highest production rate, while KD-50A has the lowest. KD-42 is at the edge of the production and north-western reinjection wells. The effects of Phase-II and Phase-III production/reinjection operations can easily be observed by these wells.

For most of the production wells, pressure decline reaches critical levels 3 – 4 years after the beginning of the no-change scenario. The critical level is assumed to be reached when 10% pressure reduction occurs according to the beginning of the scenario (May 2018), which is approximately 15 – 20 bar reduction in the reservoir pressures.

The following table shows the dates when 10% reservoir pressure reduction occurs in the production wells. It should be noted that effects of production well shut downs due to low reservoir pressures have not been included in the scenario. Productions assumed to continue even the critical pressure level has been reached. So, the dates should only be considered as an indication of the rapidity of the pressure declines.

Well	10% Pressure Reduction Date	Well	10% Pressure Reduction Date
KD-2A	12-01-2021	**KD-90A**	06-02-2022
KD-23B	12-04-2021	**KD-54A**	06-02-2022
R-3A	12-04-2021	**KD-89**	06-02-2022
KD-50A	12-05-2021	**KD-90B**	08-03-2022
KD-29	11-06-2021	**KD-43**	23-03-2022
KD-42	11-06-2021	**KD-25B**	07-04-2022
KD-23D	11-07-2021	**R-5**	07-04-2022
KD-83	11-07-2021	**KD-58**	07-04-2022
KD-55	25-08-2021	**KD-61A**	22-05-2022
KD-60	24-09-2021	**KD-61**	22-05-2022
KD-63	08-11-2021	**KD-62**	04-09-2022
KD-59	08-11-2021	**KD-58A**	19-09-2022
KD-54	08-11-2021	**KD-66A**	03-11-2022
KD-47	23-11-2021	**KD-62A**	02-01-2023
KD-49	08-12-2021	**KD-68B**	02-01-2023
KD-45	07-01-2022	**KD-68A**	01-02-2023
KD-64	22-01-2022	**KD-9A**	08-10-2024

Table 5.3 Dates when 10% pressure reduction occur

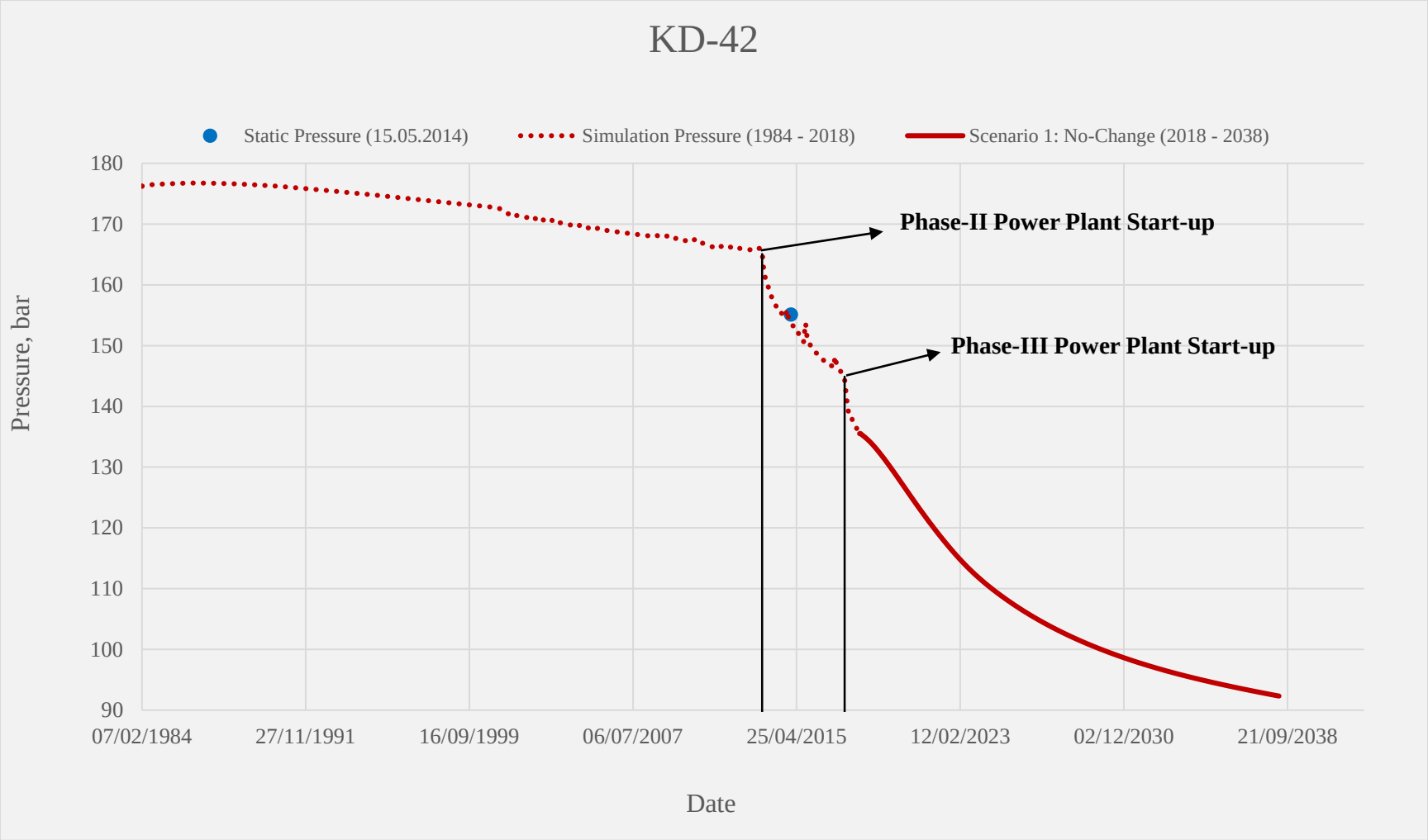

Figure 5.1 Pressure profile of KD-42 between 1984 – 2038 (Scenario 1 – Strategy 1)

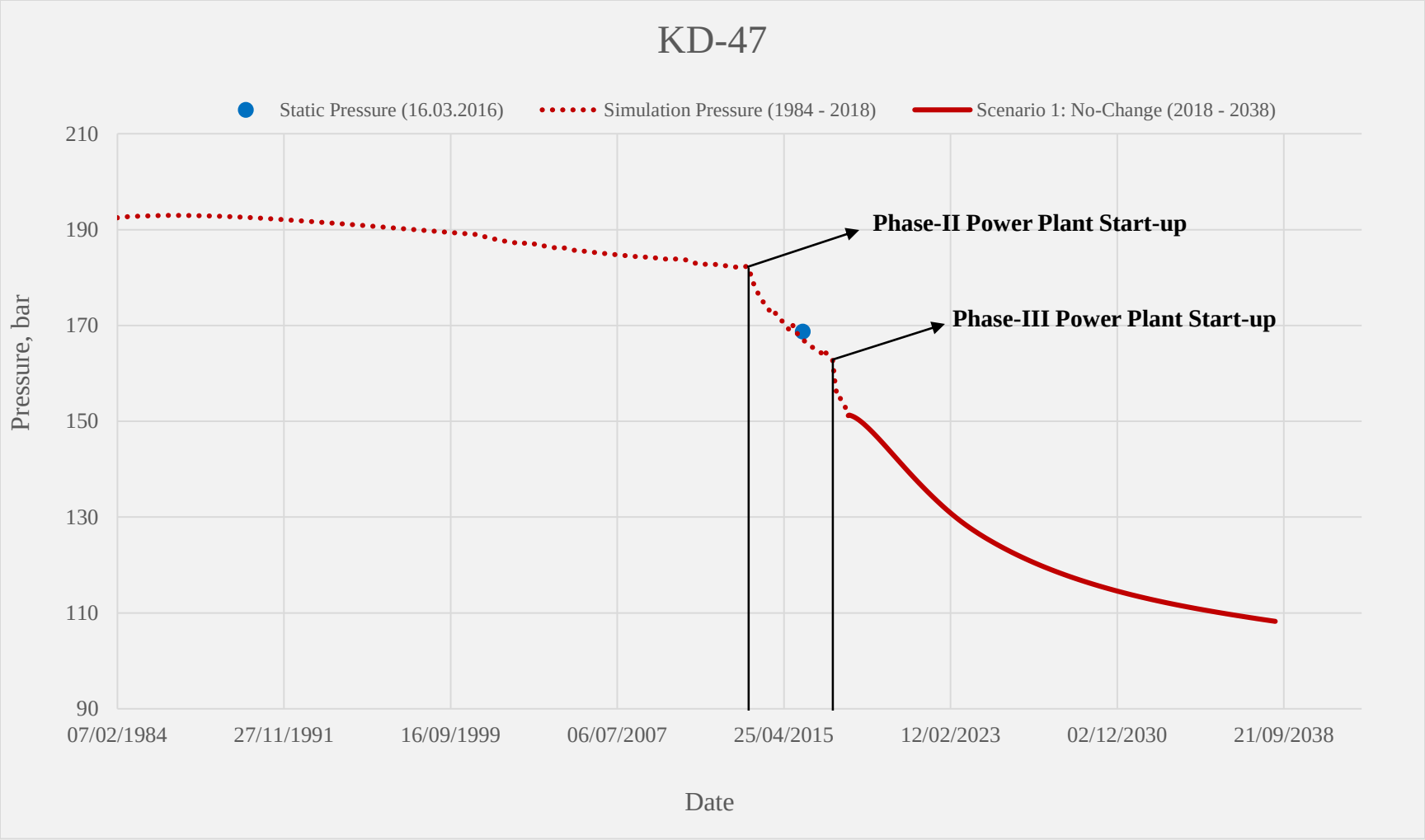

Figure 5.2 Pressure profile of KD-47 between 1984 – 2038 (Scenario 1 – Strategy 1)

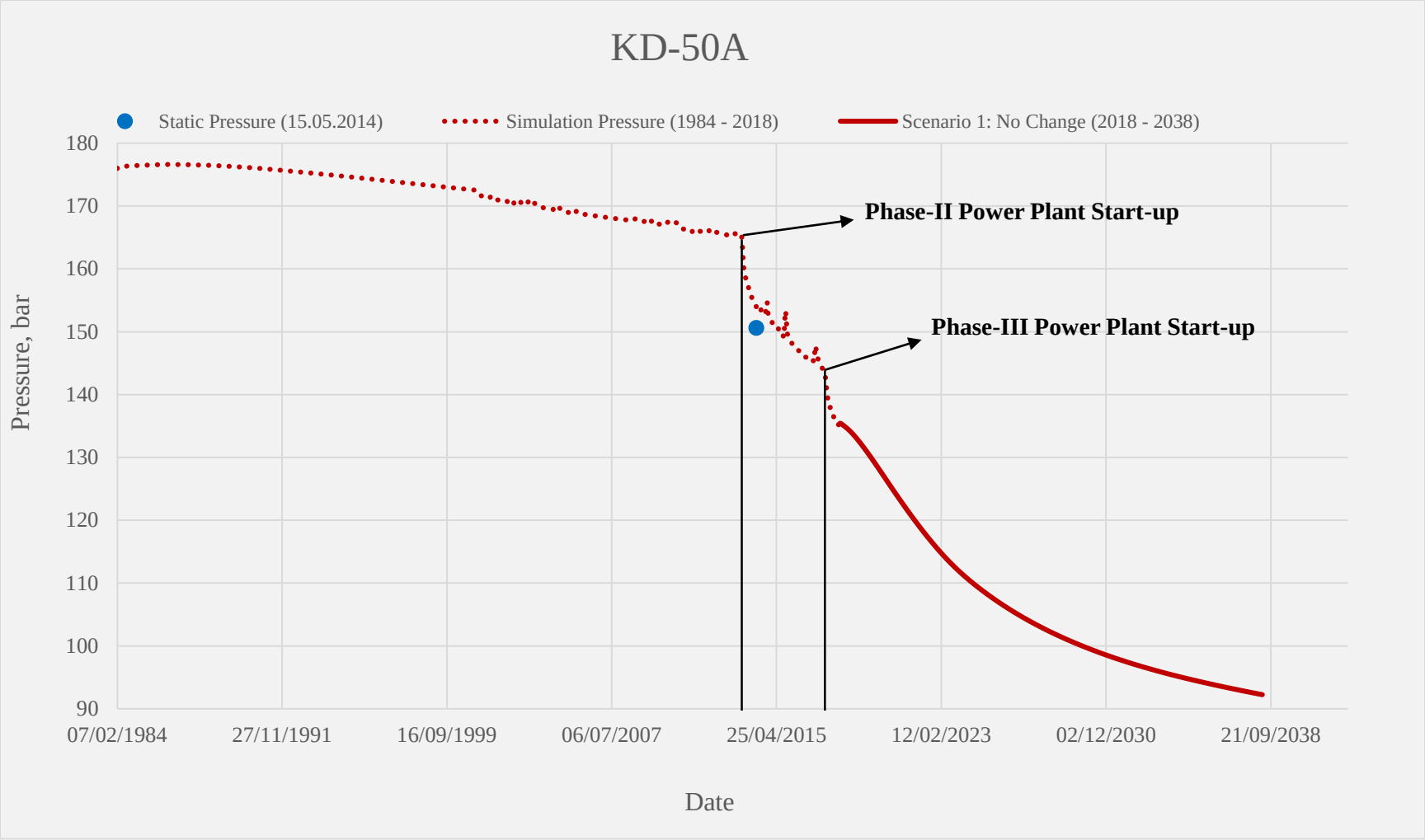

Figure 5.3 Pressure profile of KD-50A between 1984 – 2038 (Scenario 1 – Strategy 1)

In Kızıldere geothermal power plants, CO_2 is released into the atmosphere at the surface, and only trace amount of CO_2 remains in the reinjection fluid. Since carbon dioxide is not reinjected into the reservoir, the partial pressure of carbon dioxide reduces with the production. This further explains the rapid decline in the reservoir pressures of the Kızıldere geothermal field.

Decline in the dissolved CO_2 ratios can be seen for the production wells; KD-42, KD-47, and KD-50A. At the beginning of the scenario (May 2018), approximately 3wt% of the geothermal water was comprised of dissolved CO_2.

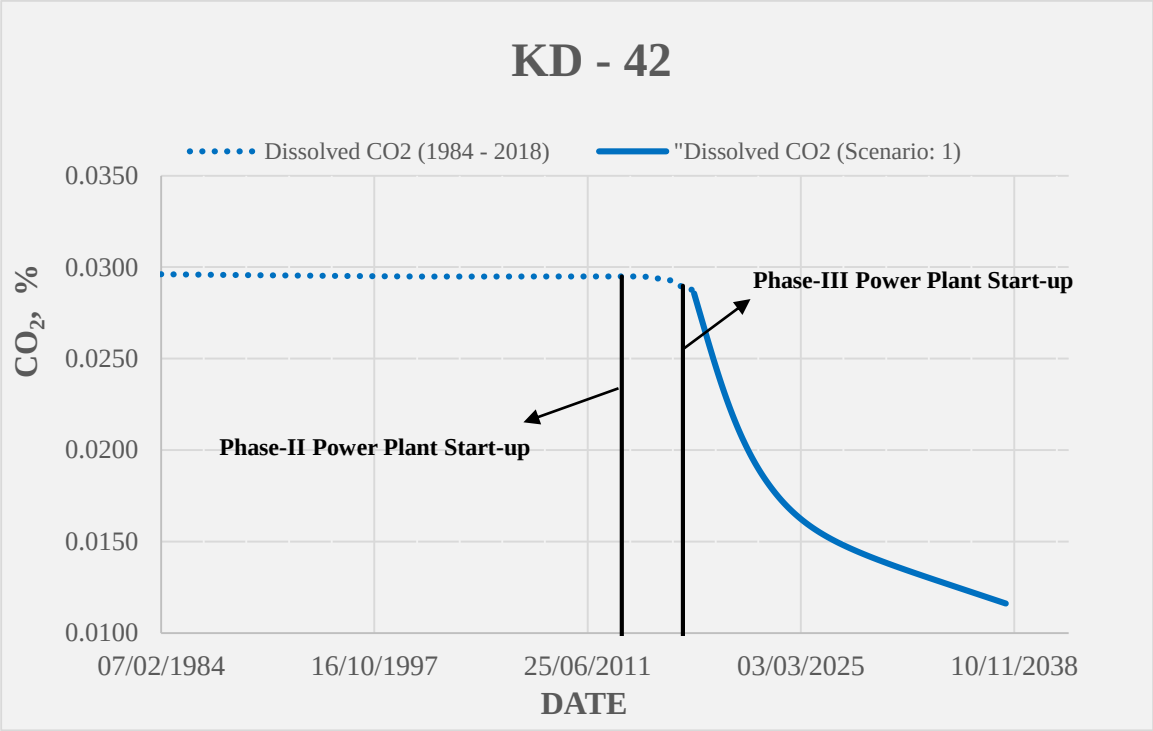

Figure 5.4 Dissolved CO_2 profile of KD-42 (Scenario 1 – Strategy 1)

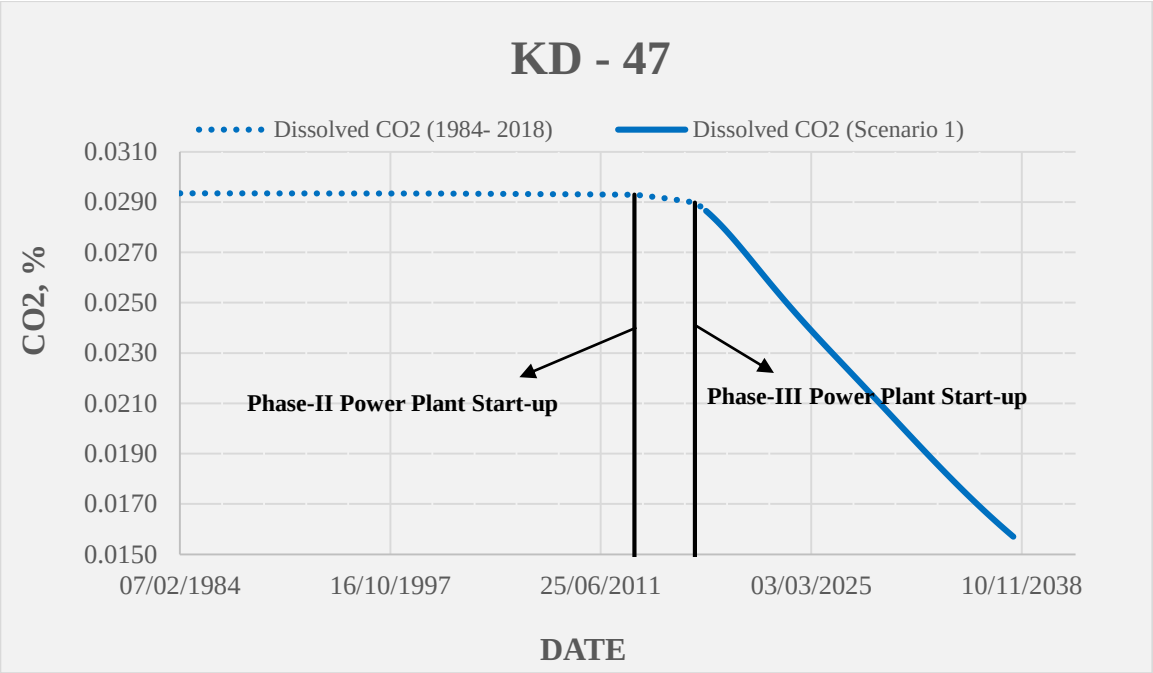

Figure 5.5 Dissolved CO_2 profile of KD-47 (Scenario 1 – Strategy 1)

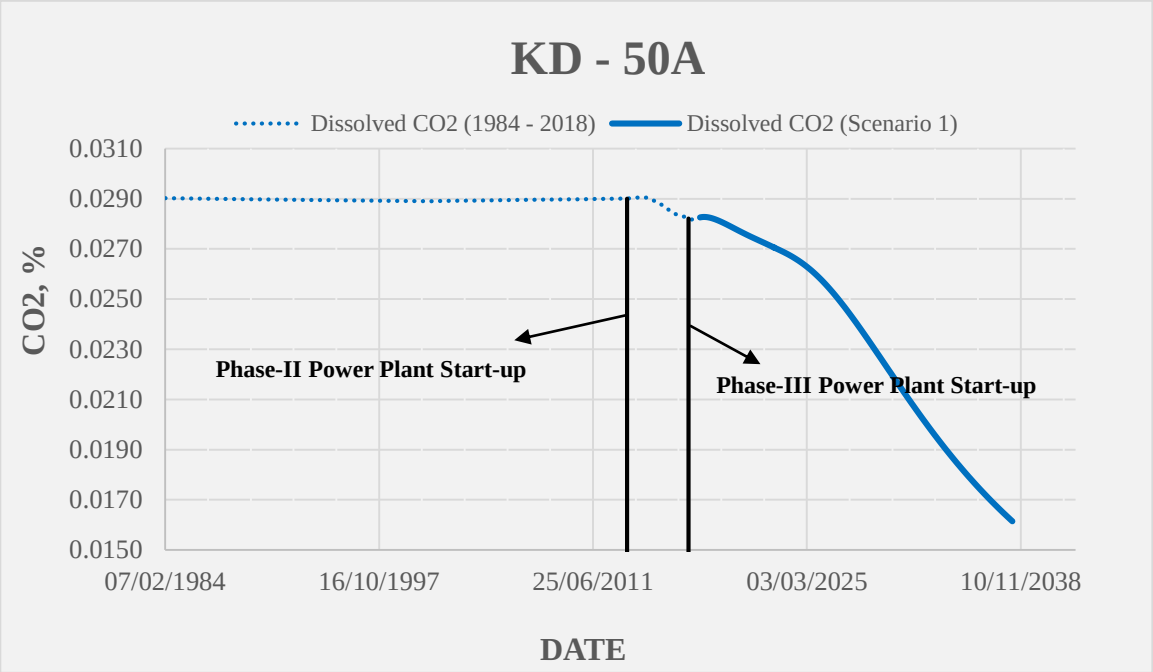

Figure 5.6 Dissolved CO_2 profile of KD-50A (Scenario 1 – Strategy 1)

Although the decrease in the CO_2 content of the geothermal fluid is significant in the vicinity of the reinjection wells at shallow depths, it is not significant in deeper sections.

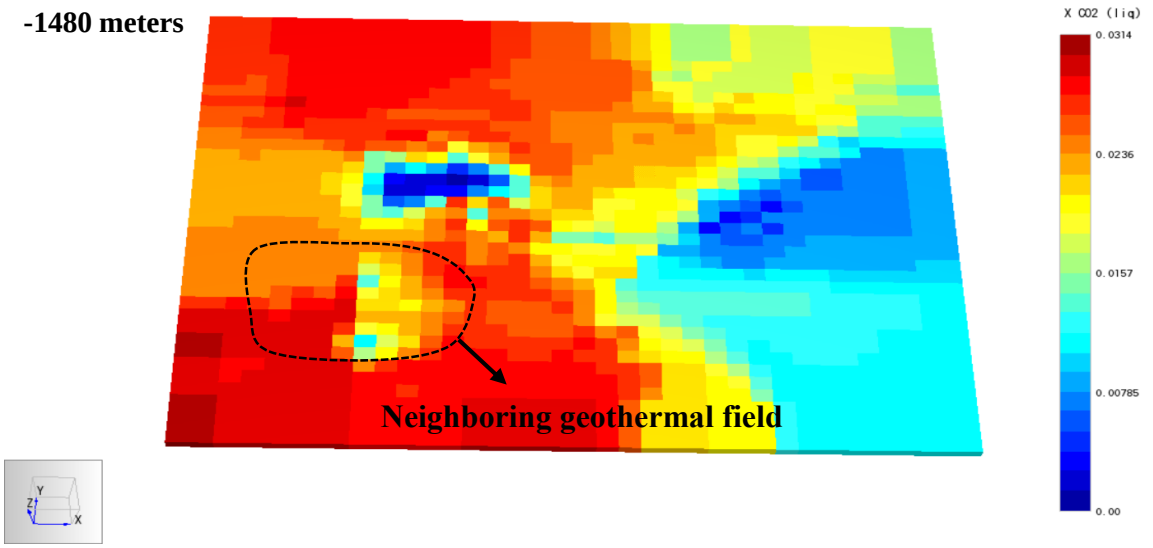

Figure 5.7 CO_2 distribution at 1480 meters at the end of the Scenario 1 – Strategy 1

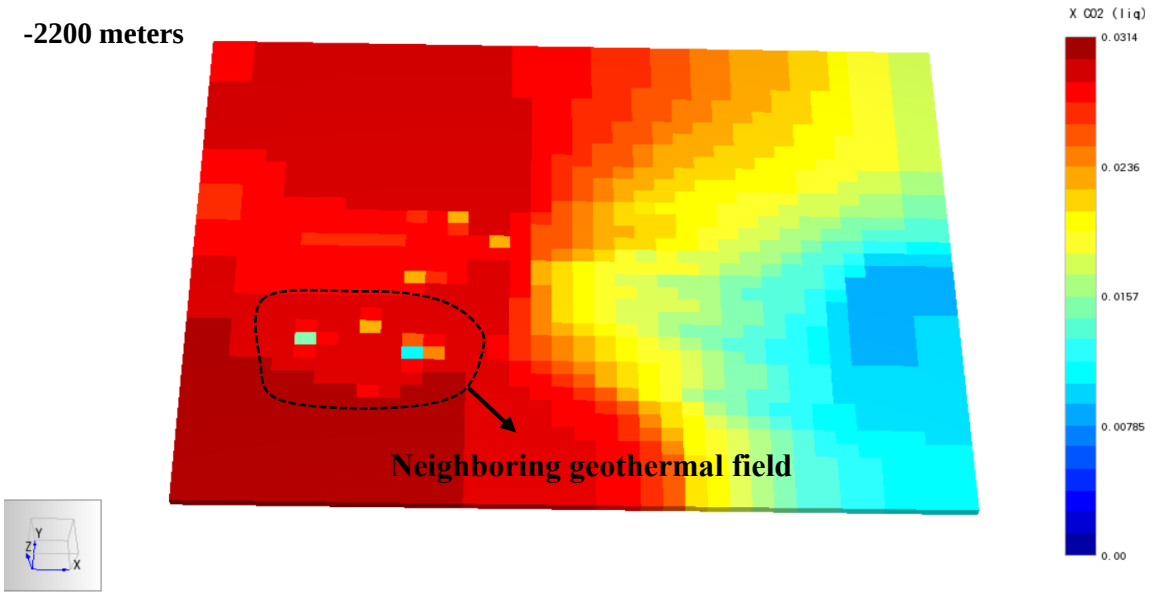

Figure 5.8 CO_2 distribution at 2200 meters at the end of the Scenario 1 – Strategy 1

Although the average injection temperature is around 100 °C in Kızıldere geothermal field (much lower than the reservoir temperature), the cooling effects have been found only limited in the no-change scenario. For most of the production wells, reservoir temperature did not reduce to critical levels during the 20 years of simulation. The highest decline has been observed in KD-42 with 14 °C reduction at the end of 20 years. For the rest of the wells, temperature decline has been found to be less than 8 °C, and even less than 1 °C for some wells. This situation points out that reinjected geothermal fluid does not penetrate into the production zone.

Temperature profiles of KD-42, KD-47, and KD-50A are given below.

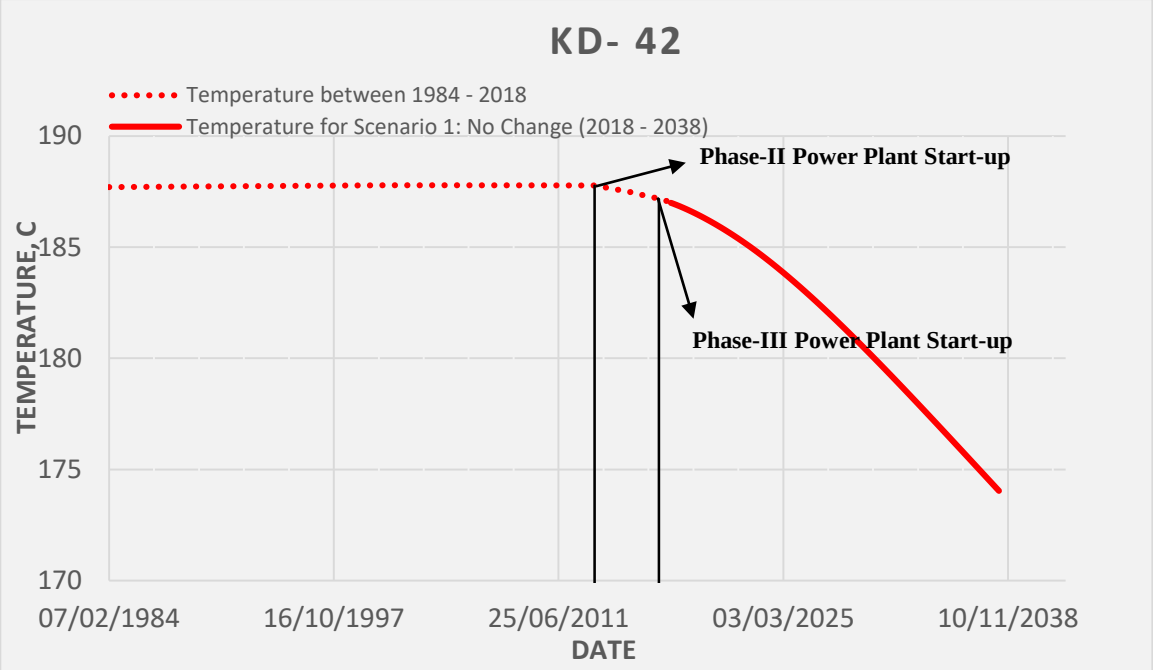

Figure 5.9 Temperature profile of KD-42 (Scenario 1 – Strategy 1)

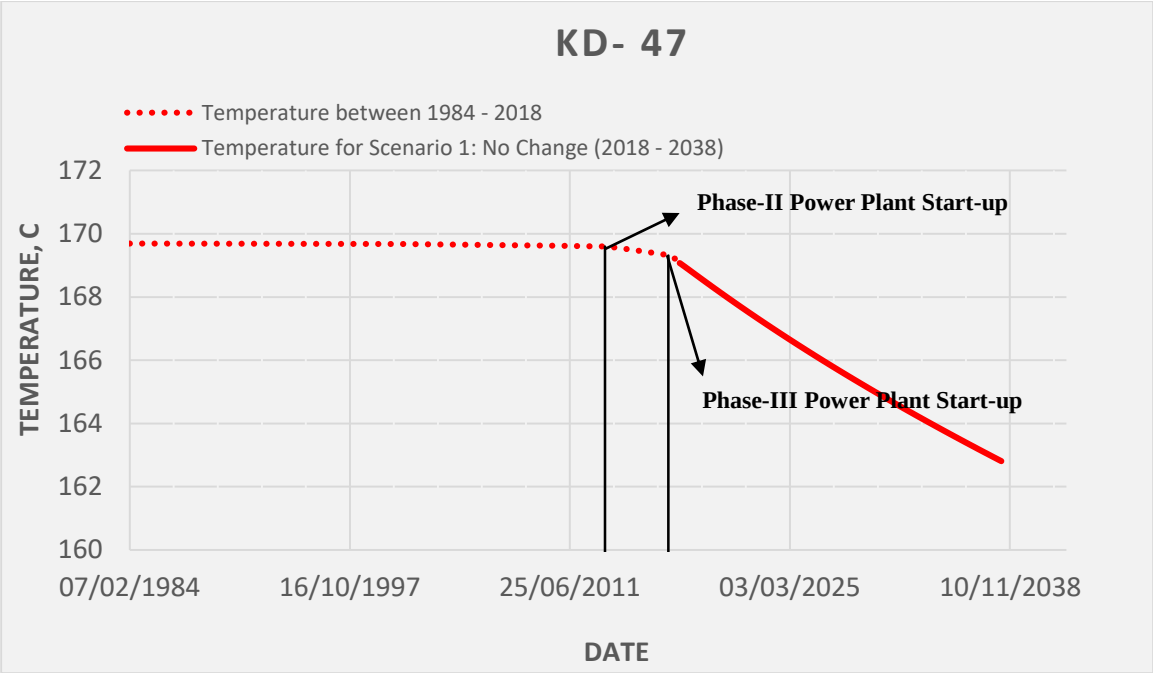

Figure 5.10 Temperature profile of KD-47 (Scenario 1 – Strategy 1)

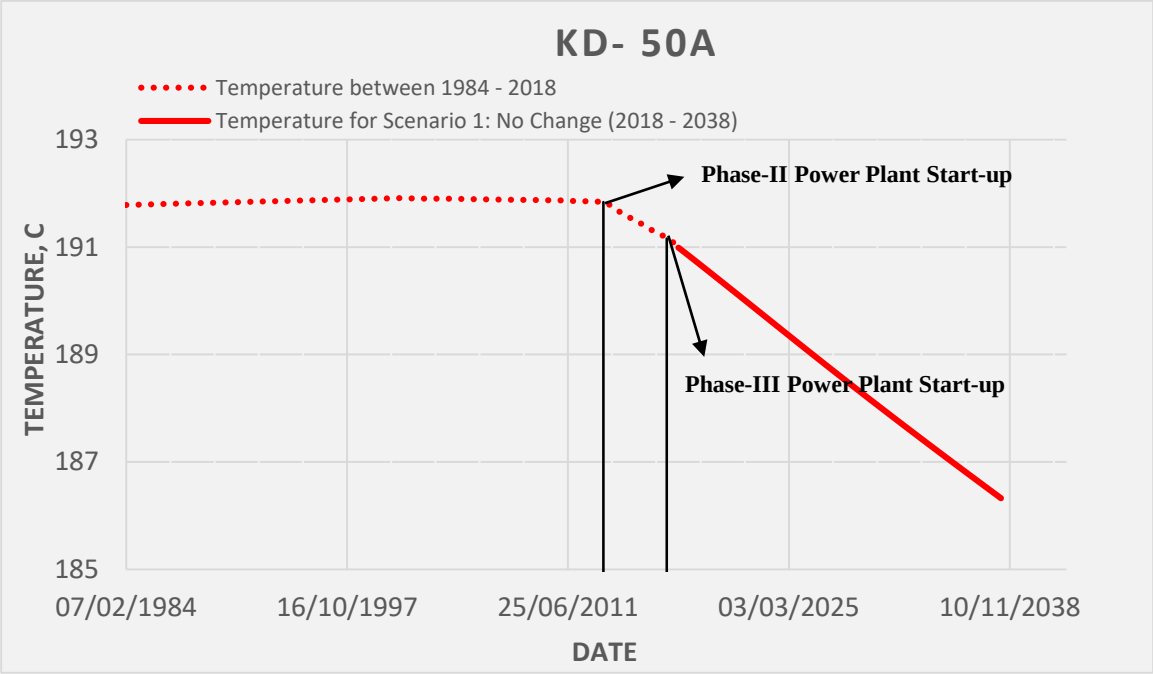

Figure 5.11 Temperature profile of KD-50A (Scenario 1 – Strategy 1)

The reservoir temperature distribution at 2200 meters and the temperature isosurfaces show that there is not a significant decrease in the temperatures compared to the natural state conditions in the production zone.

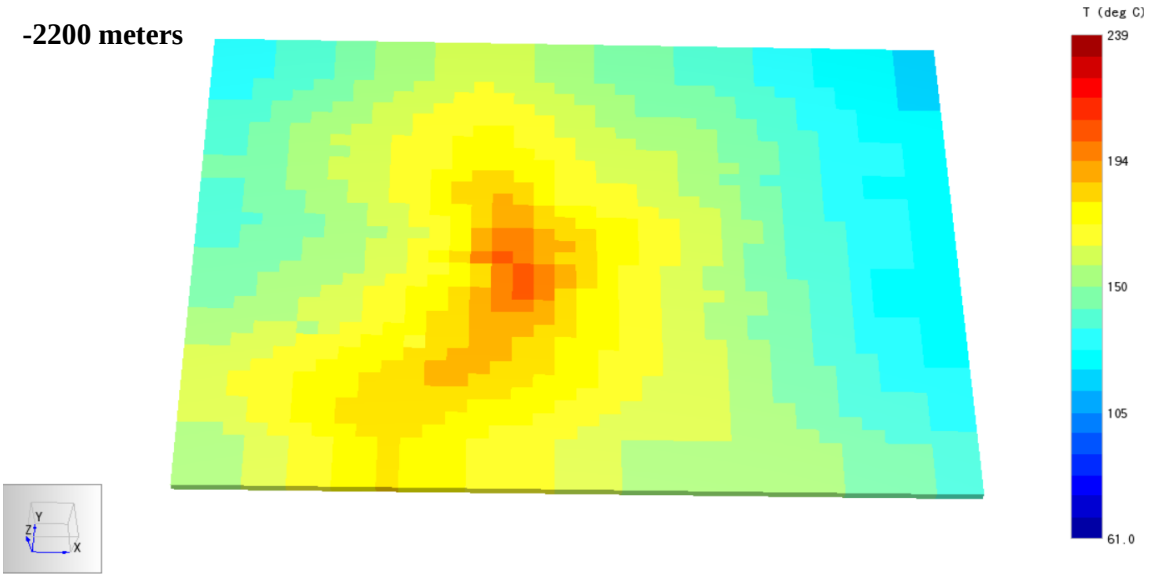

Figure 5.12 Temperature distribution at the end of the Scenario 1 – Strategy 1

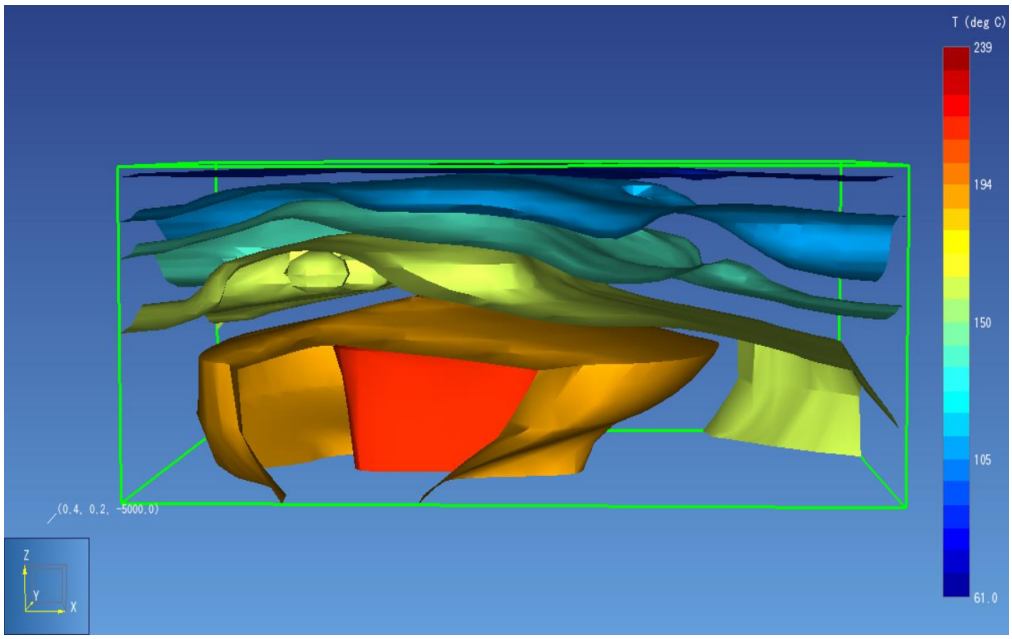

Figure 5.13 Temperature isosurfaces at the end of the Scenario 1 – Strategy 1

5.1.2 Scenario 2: Reinjecting what is produced

In the second scenario, production rates have been kept unchanged, and reinjection of the produced fluid have been simulated in two parts. In the first part, the produced CO_2 is assumed to continue to be released into the atmosphere and all of the produced water is reinjected back to the reservoir. Assuming a 3% dissolved CO_2 is present in the produced water, the reinjection rates are:

Part I: 6700 tph of water, no CO_2

Part II: 6700 tph of water, and 200 tph of CO_2

Since the current (May 2018) injection rate is around 5200 tph, an additional 1500 tph fluid has been added to the rates of 27 injection wells. In order to account for the injectivities of the wells and situation of the surface infrastructure, 1500 tph has been divided according to the injection shares of the wells. For example, KDE-11 accounts for approximately 10% of the total injection, so 150 tph is added to its injection rate in the second scenario. It is also correct for the CO_2 reinjection rates. The reduction in the pressure decline in both parts of the second can be seen clearly on all of the production wells. Comparison of the pressure declines in Scenario-1 and Scenario-2 has been shown on the "pressure vs. time" plots of the KD-42, KD-47, and KD-50A.

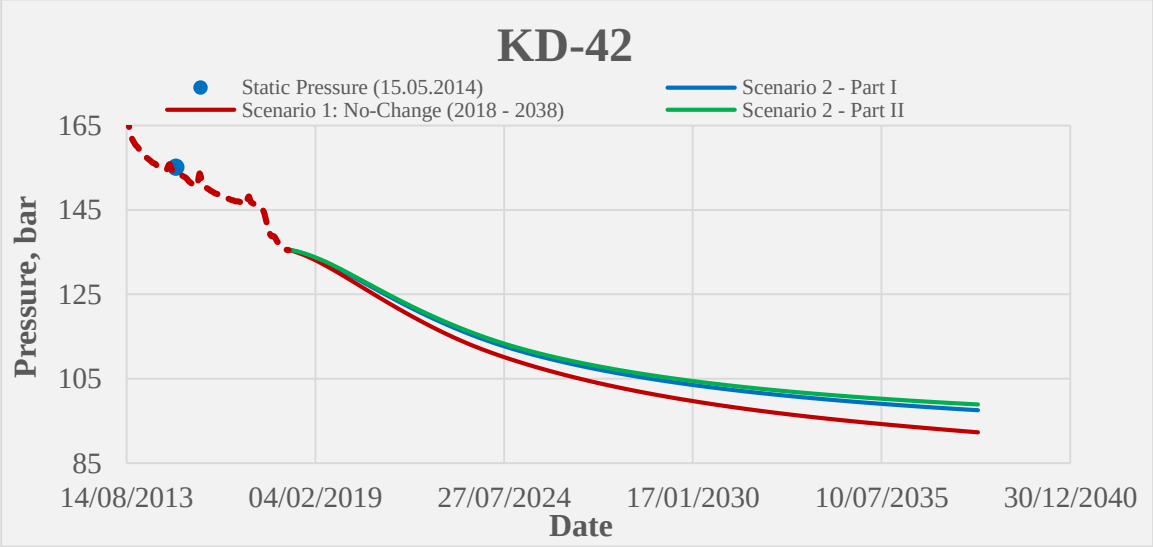

Figure 5.14 Pressure decline of KD-42 in Scenario 2 – Strategy 1

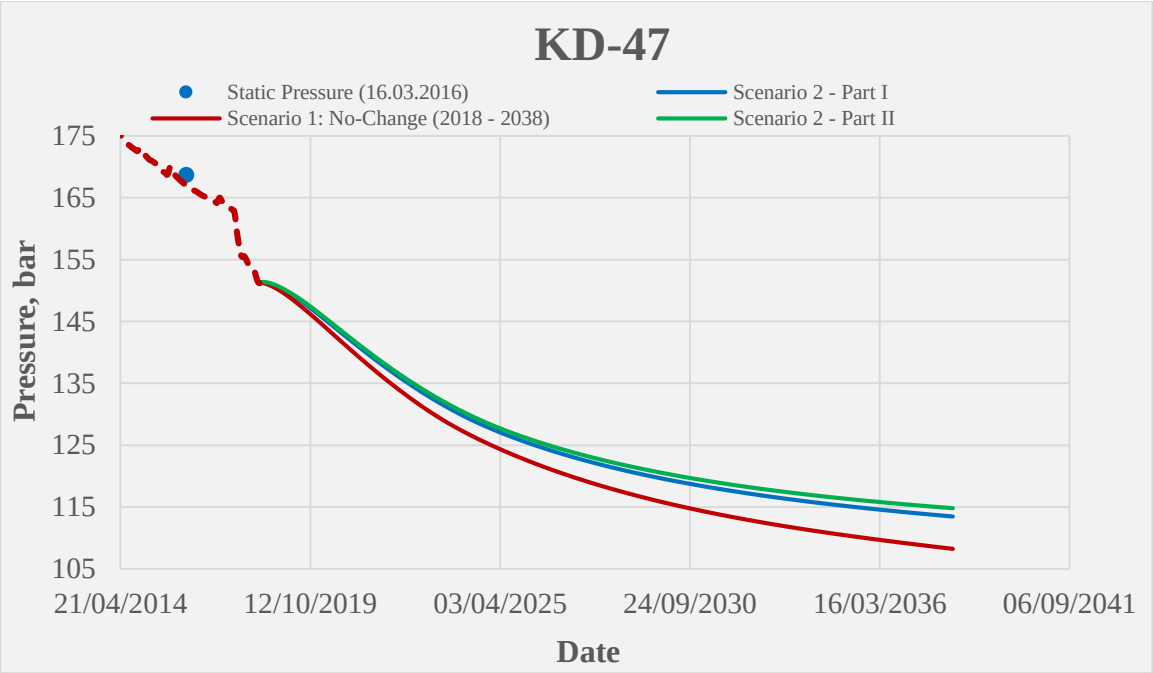

Figure 5.15 Pressure decline of KD-47 in Scenario 2 – Strategy 1

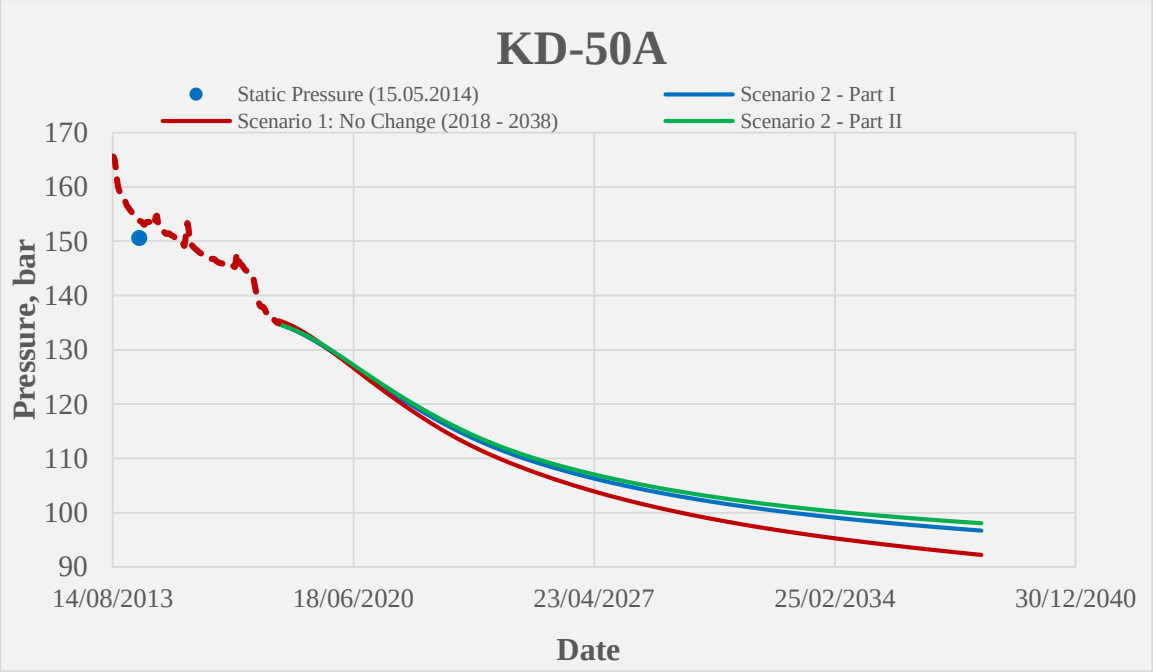

Figure 5.16 Pressure decline of KD-50A in Scenario 2 – Strategy 1

Reservoir pressures have been supported 5 – 7 bars at the end of the Part I of the Scenario-2, and this value is 1 – 2 bar higher in the Part II, as a result of the extra injection. Effects are relatively smaller in the near future (3 – 5 years) with 1 – 2 bars. Although the increase may seem small, the overall effects are considerable. For example, Kızıldere geothermal power plants are being operated with a minimum inlet pressure of around 9 bar, and considering the losses during the surface transportation, wellhead pressure of a production well should not be less than 10 bar. There are 12 wells with a well head pressure of less than 20 bars, and 5 of them are less than 15 bars. Considering the distances and elevation differences between the production wells and the power plants, some of these wells may reach critical pressure levels in the near future and productions may need to be reduced in order to keep the wellhead pressures higher. So, adding wellhead pressures 1 – 2 bars in the near future, and 6 – 8 bars in the long term would yield a considerable impact in terms of the reservoir management targets, and it may also increase the life span of the production wells. The following tables show the shifts in the time when 10% reservoir pressure decline occurs with respect to the first scenario.

Well	10% Pressure Reduction Date	Δt, days (S2 Part I - S1)	Well	10% Pressure Reduction Date	Δt, days (S2 Part I - S1)
KD-2A	27-05-2021	135	**KD-90A**	05-08-2022	180
KD-23B	25-08-2021	135	**KD-89**	05-08-2022	180
R-3A	09-09-2021	150	**KD-54A**	20-08-2022	195
KD-50A	09-10-2021	150	**KD-90B**	04-09-2022	180
KD-29	08-11-2021	150	**KD-43**	19-09-2022	180
KD-42	08-11-2021	150	**KD-25B**	04-10-2022	180
KD-23D	08-12-2021	150	**KD-58**	04-10-2022	180
KD-83	08-12-2021	150	**R-5**	19-10-2022	195
KD-55	22-01-2022	150	**KD-61A**	03-12-2022	195
KD-60	21-02-2022	150	**KD-61**	03-12-2022	195
KD-59	22-04-2022	165	**KD-62**	02-04-2023	210
KD-54	22-04-2022	165	**KD-58A**	17-04-2023	210
KD-63	07-05-2022	180	**KD-66A**	01-06-2023	210
KD-47	07-05-2022	165	**KD-62A**	30-08-2023	240
KD-49	22-05-2022	165	**KD-68B**	30-08-2023	240
KD-45	21-06-2022	165	**KD-68A**	29-09-2023	240
KD-64	21-07-2022	180	**KD-9A**	23-09-2027	1080

Table 5.4 Time shifts in Scenario 2 Part I compared to Scenario 1

Well	10% Pressure Reduction Date	Δt, days (S2 Part II - S1)	Well	10% Pressure Reduction Date	Δt, days (S2 Part II - S1)
KD-2A	26-06-2021	165	**KD-90A**	19-09-2022	225
KD-23B	09-10-2021	180	**KD-89**	19-09-2022	225
R-3A	09-10-2021	180	**KD-54A**	04-10-2022	240
KD-50A	08-11-2021	180	**KD-90B**	19-10-2022	225
KD-29	23-12-2021	195	**KD-25B**	18-11-2022	225
KD-42	23-12-2021	195	**KD-58**	18-11-2022	240
KD-23D	22-01-2022	195	**KD-43**	18-11-2022	240
KD-83	22-01-2022	195	**R-5**	18-12-2022	255
KD-55	08-03-2022	195	**KD-61A**	17-01-2023	240
KD-60	07-04-2022	195	**KD-61**	17-01-2023	240
KD-59	22-05-2022	195	**KD-62**	17-05-2023	255
KD-54	06-06-2022	210	**KD-58A**	16-06-2023	270
KD-63	21-06-2022	225	**KD-66A**	31-07-2023	270
KD-47	21-06-2022	210	**KD-62A**	29-10-2023	300
KD-49	06-07-2022	210	**KD-68B**	29-10-2023	300
KD-45	20-08-2022	225	**KD-68A**	28-11-2023	300
KD-64	04-09-2022	225	**KD-9A**	17-10-2028	1470

Table 5.5 Time shifts in Scenario 2 Part II compared to Scenario 1

As can be seen, the reduction in the pressure decline is smaller in the short term, and increases in time.

In the both parts of the second scenario, reservoir temperatures at the production depths were not affected significantly with the extra reinjection rates. The decrease at the intermediate sections was not also worth to mention. The following figures show the temperature distribution at -1480 meters and -2200 meters. Compared to the first scenario, differences have been found to be in the range of 0 – 2 °C at the end of the scenario.

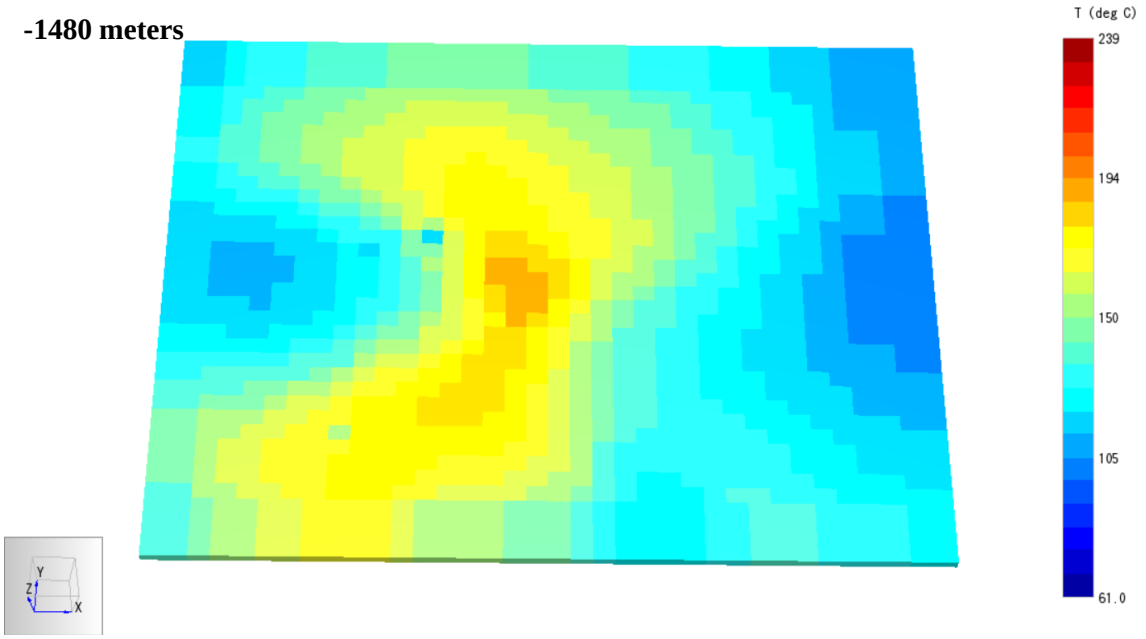

Figure 5.17 Temperature distribution at 1480 meters in Scenario 2 Part I – Strategy 1

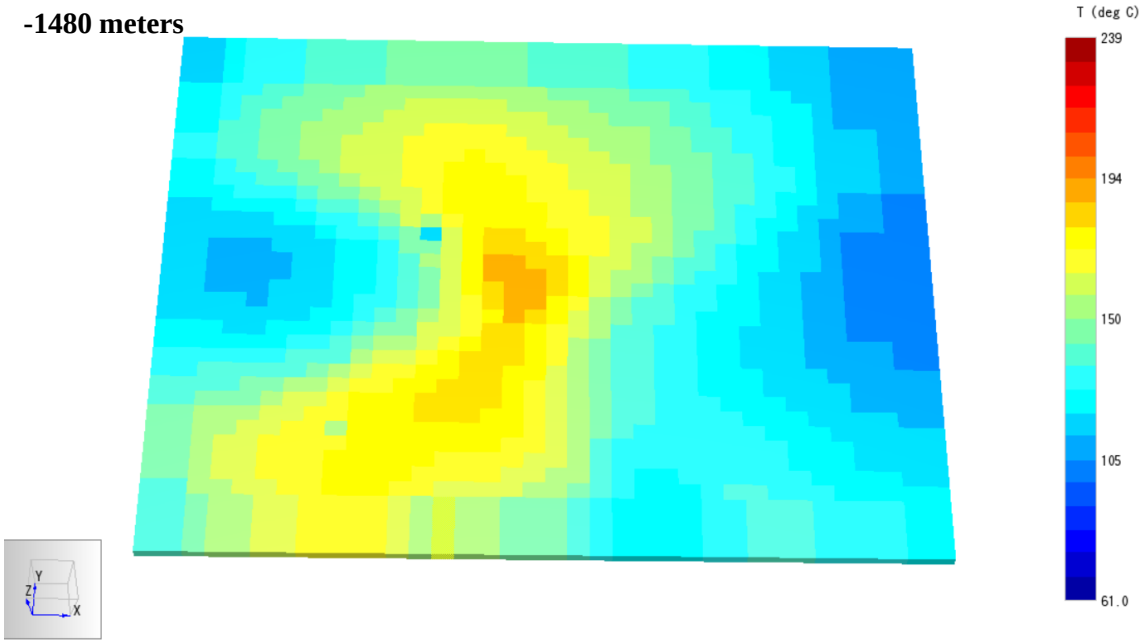

Figure 5.18 Temperature distribution at 1480 meters in Scenario 2 Part II – Strategy 1

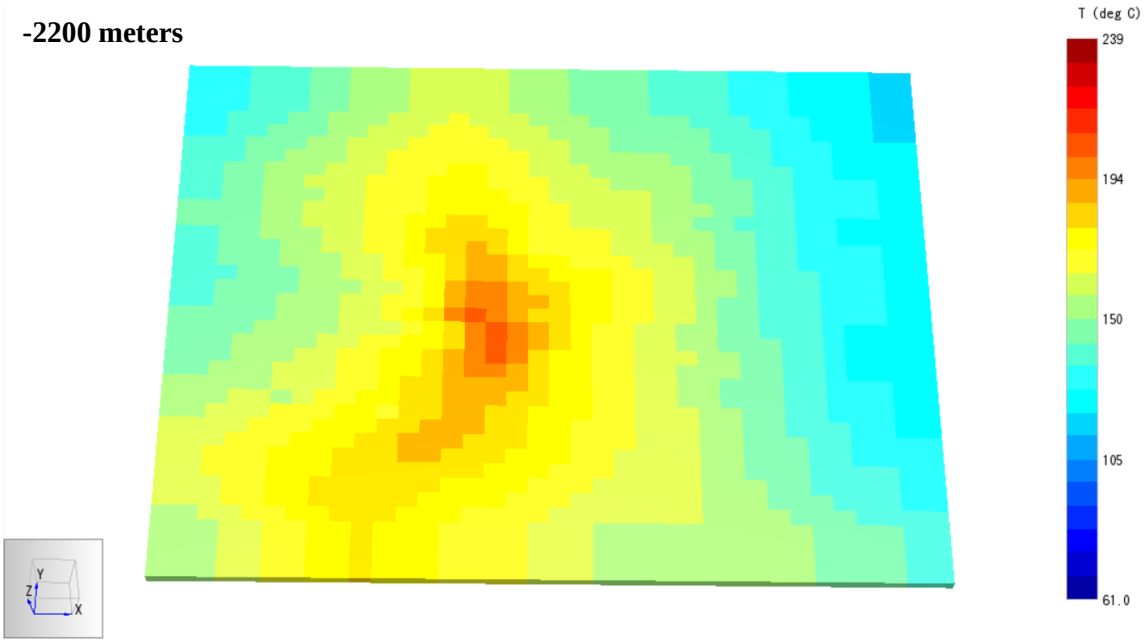

Figure 5.19 Temperature distribution at 2200 meters in Scenario 2 Part I – Strategy 1

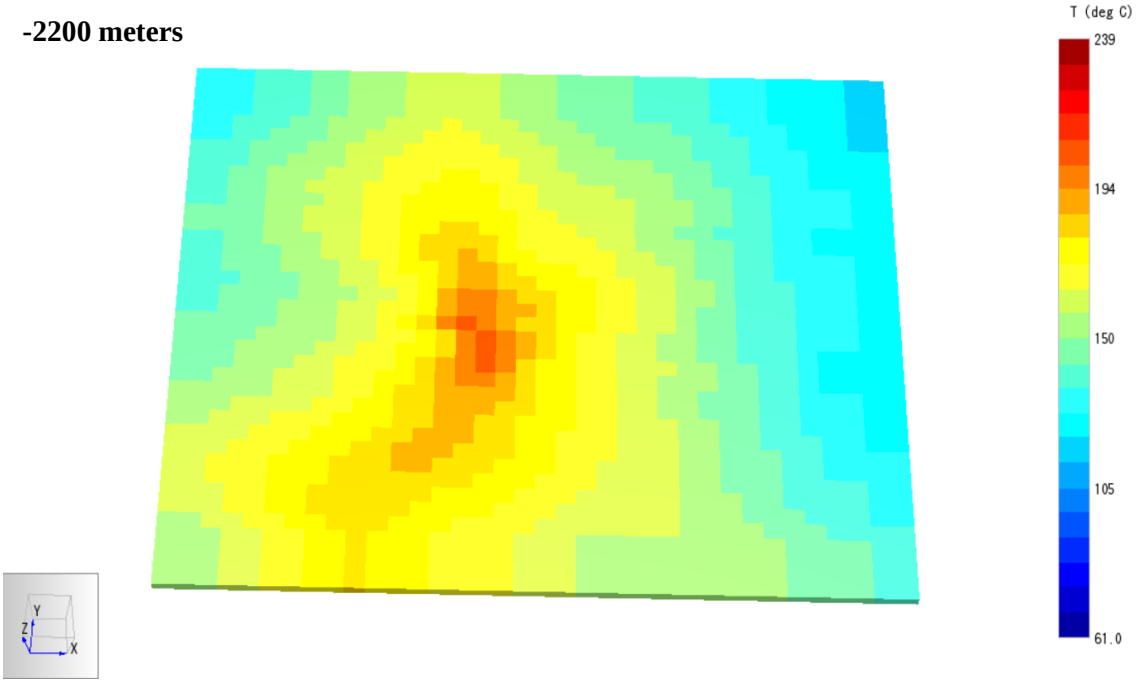

Figure 5.20 Temperature distribution at 2200 meters in Scenario 2 Part II – Strategy 1

On the other hand, temperature isosurfaces show that the temperature decline at the shallow depths and also at the western sections is significant, mostly due to the locations and completions depths of the reinjection wells. But the changes were almost the same in the both parts of the second scenario.

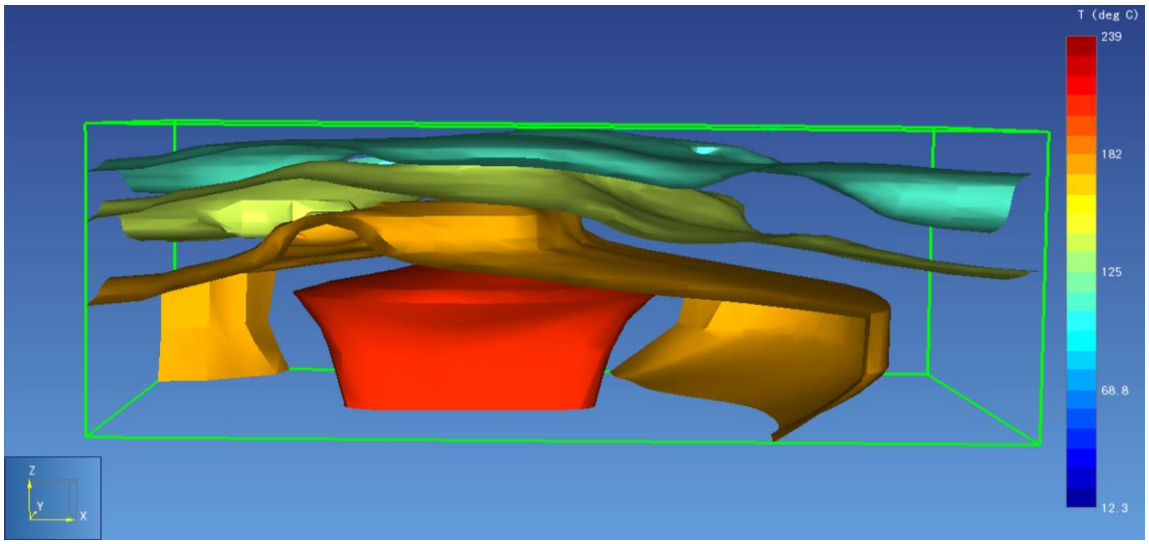

Figure 5.21 Temperature isosurfaces at the end of the Scenario 2 Part I – Strategy 1

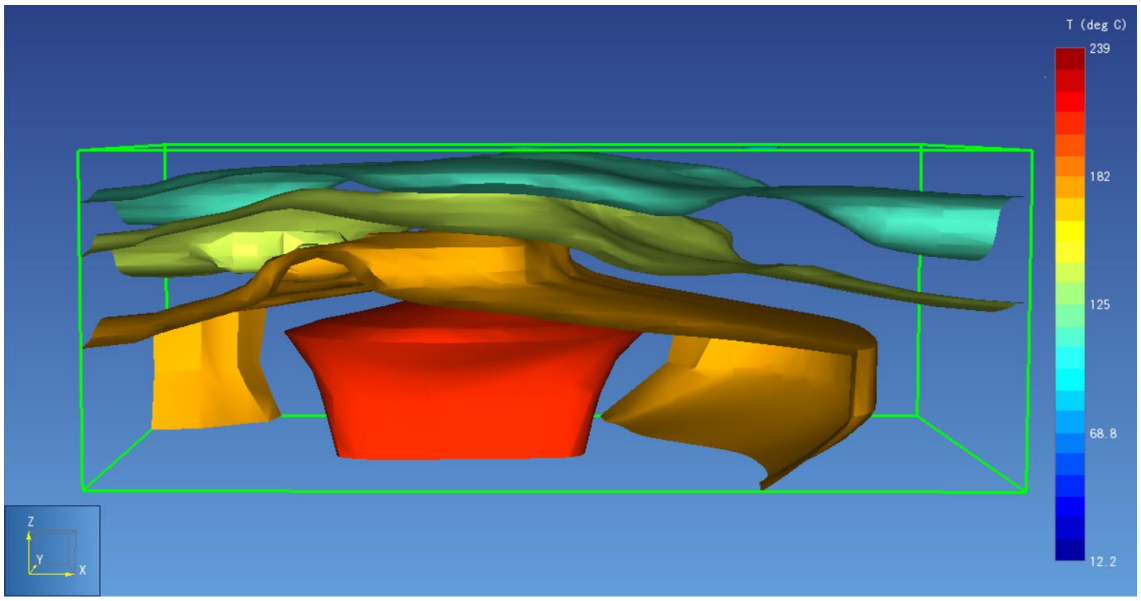

Figure 5.22 Temperature isosurfaces at the end of the Scenario 2 Part II – Strategy 1

Carbon dioxide content of the geothermal fluid at the production zone was not changed considerably by increasing the water reinjection rates (Part I). But in the CO_2 reinjection part (Part II), the decline in the CO_2 content of the produced fluid was found to be reduced, and the amounts are even increased in some wells. The wells which have deeper completion intervals were not affected significantly, but amount of the CO_2 in shallow sections and intermediate production zones affected by the reinjection of the produced CO_2. The significant reduction in the CO_2 decline at shallow depths can be clearly seen in the Figure 5.28. Also, the CO_2 decline due to the two deep reinjection wells, KD-44 and KD-46 was disappeared with the reinjection of the produced CO_2 in Scenario 2 part II (Figure 5.29).

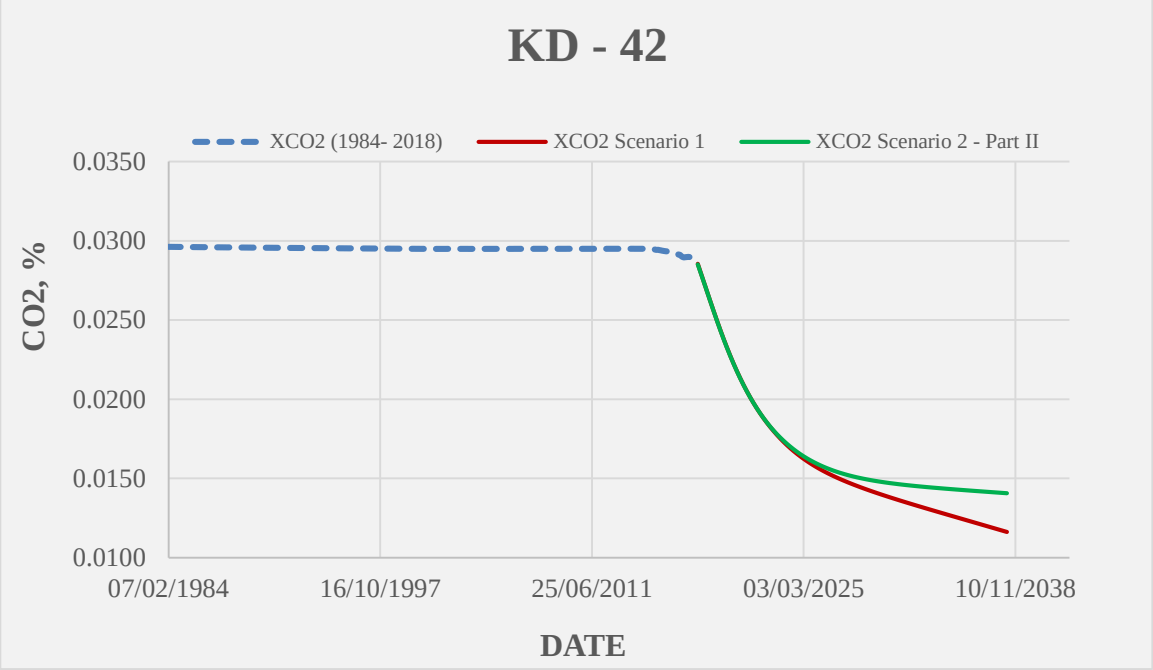

Figure 5.23 CO_2 profile of KD-42 in Scenario 2 Part II compared to Scenario 1

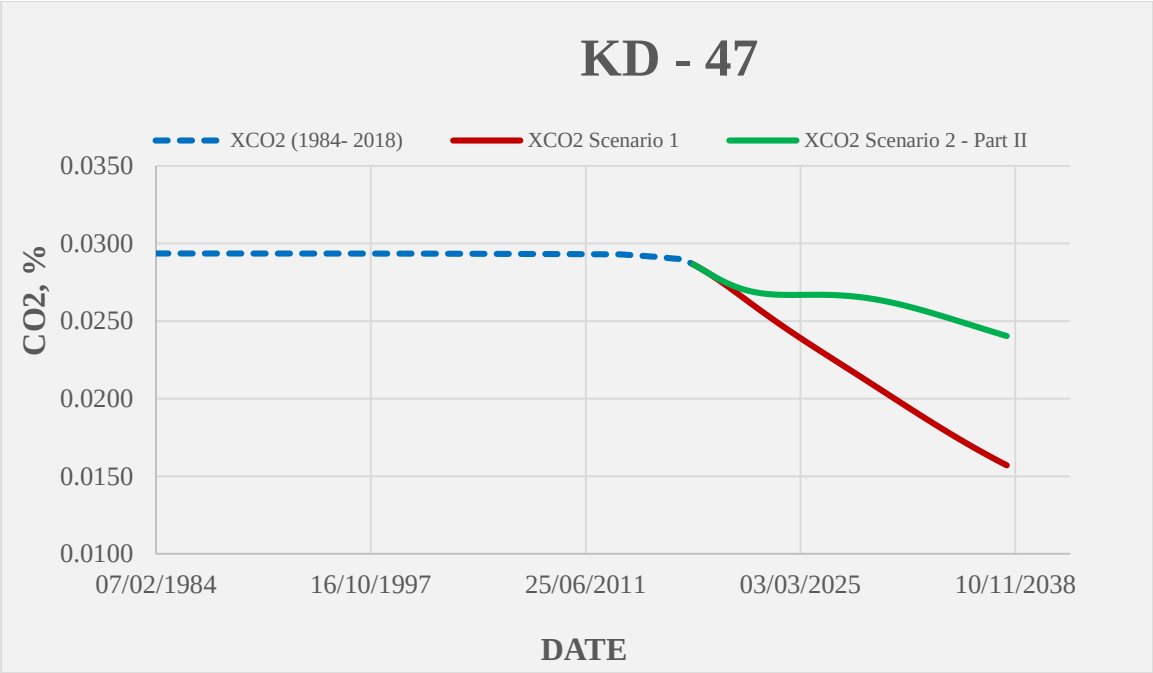

Figure 5.24 CO_2 profile of KD-47 in Scenario 2 Part II compared to Scenario 1

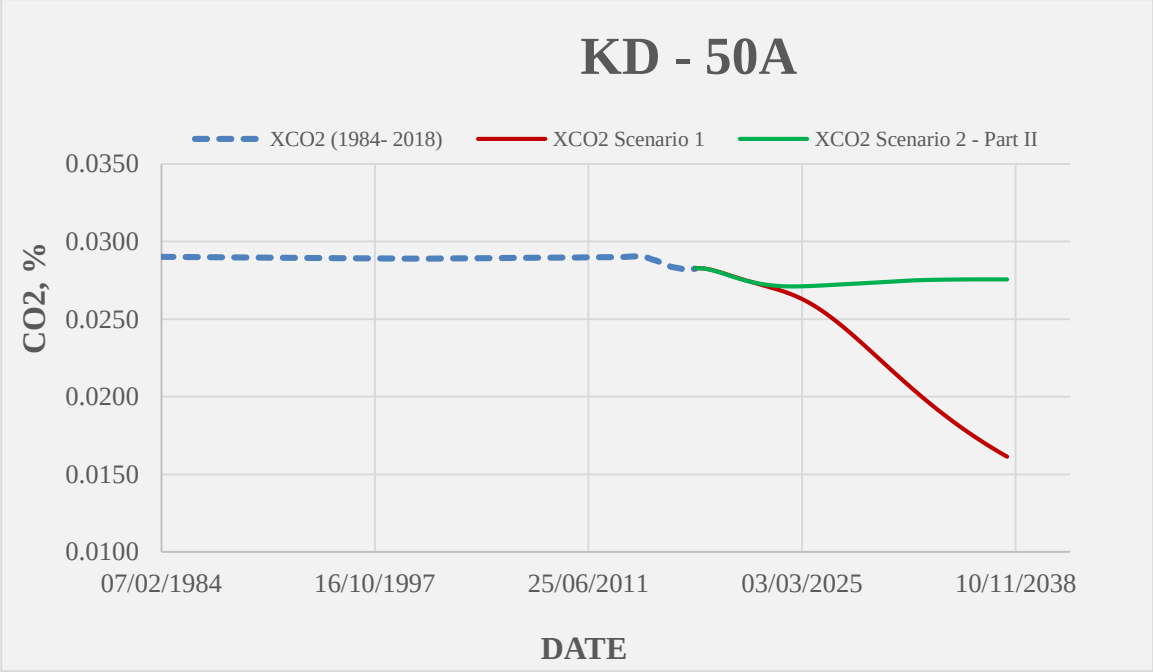

Figure 5.25 CO_2 profile of KD-50A in Scenario 2 Part II compared to Scenario 1

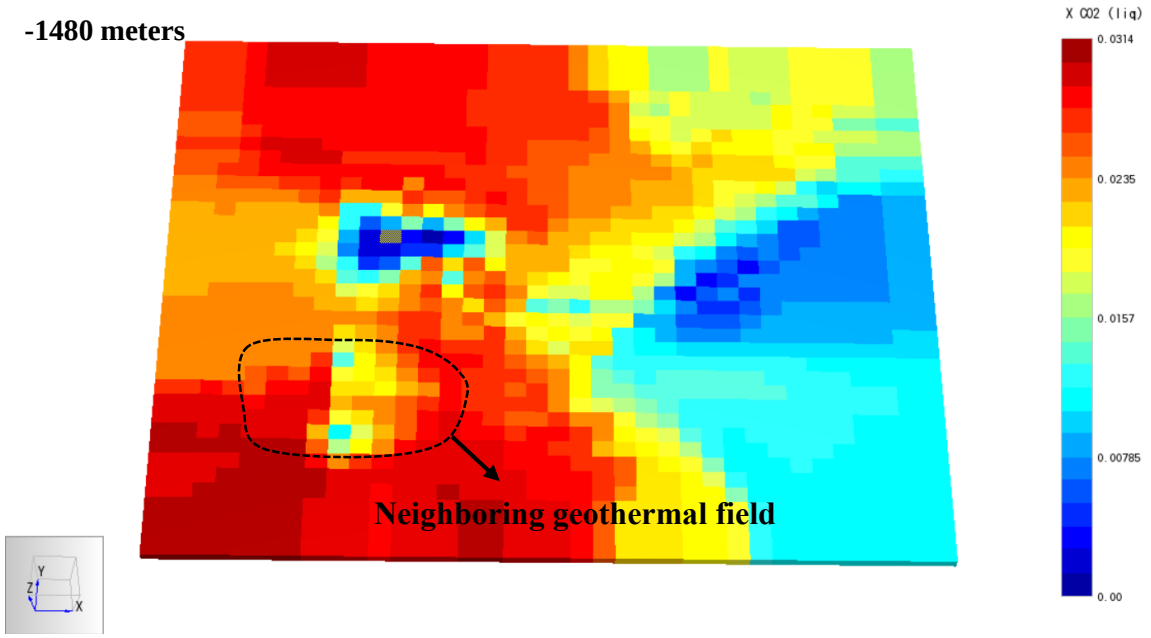

Figure 5.26 CO_2 distribution at 1480 meters (Scenario 2 Part I – Strategy 1)

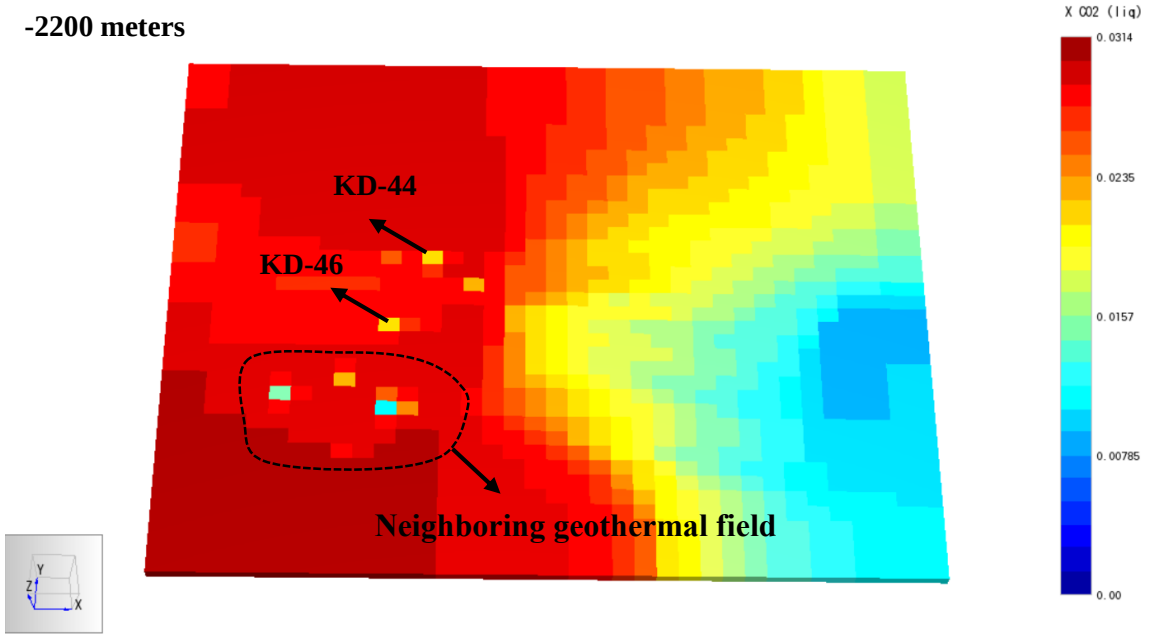

Figure 5.27 CO_2 distribution at 2200 meters (Scenario 2 Part I – Strategy 1)

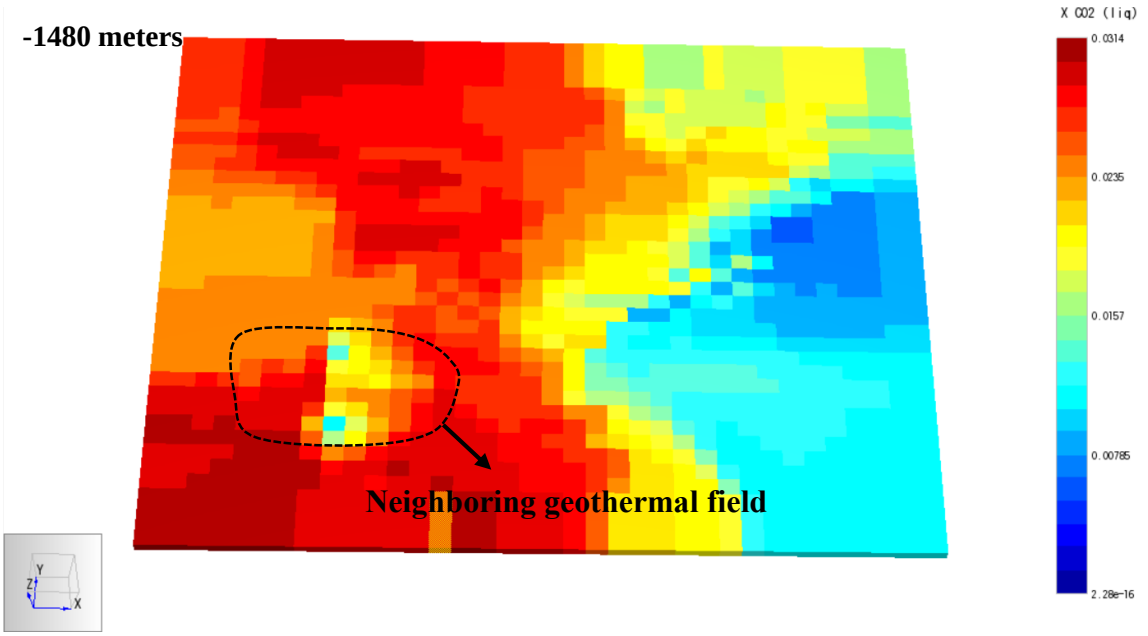

Figure 5.28 CO_2 distribution at 11480 meters (Scenario 2 Part II – Strategy 1)

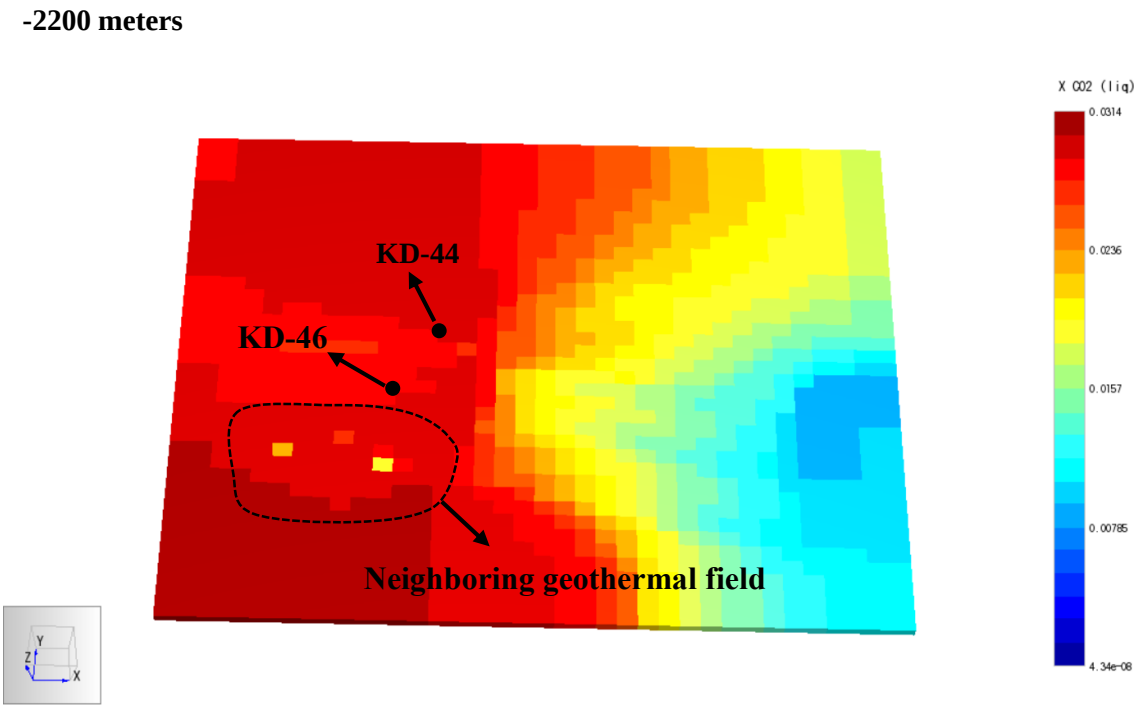

Figure 5.29 CO_2 distribution at 2200 meters (Scenario 2 Part II – Strategy 1)

5.1.3 Scenario 3: Carbon Dioxide Injection

Carbon dioxide content of the Kızıldere geothermal fluid is averagely 3wt%, which is dissolved in the water in the reservoir conditions and turns into gas phase in the wellbore and in the surface as the pressure is reduced. Approximately 200 tph of CO_2 is produced in the Kızıldere Geothermal Field as of May 2018, and currently there is no CO_2 reinjection operation in the field. Releasing the gaseous carbon dioxide into the atmosphere instead of reinjecting back to the reservoir causes a reduction in the reservoir pressures. In addition to the negative effects on the reservoir management, releasing the produced CO_2 into the atmosphere also contributes to the environmental concerns since CO_2 is one of the greenhouse gases. Geothermal energy is often attributed as a clean and sustainable source of energy, but the current CO_2 emission rates of the Kızıldere Geothermal Field is against the general opinion.

In the third scenario, greenhouse gas (CO_2) sink potential of the Kızıldere Geothermal Field was considered, and consequences of large amount of CO_2 injection were investigated in terms of the reservoir management point of view. It means that the changes in the reservoir pressures, flow rates, flowing enthalpies, and CO_2 content of the geothermal fluid were analyzed. Chemical reactions between the injected CO_2 and the formation rocks, as well as CO_2 sequestration mechanisms are beyond the scope of this scenario. It is also assumed that surface facilities and infrastructure are readily available on each injection well site for the large amount of CO_2 injection. The following injection scenarios were simulated on the model based on the current reinjection rates:

Part I: 10wt% of CO_2 was added to each well's injection rate. Considering the 5200 tph of total reinjection as of May 2018, 520 tph of CO_2 have been injected for 20 years, from 2018 to 2038.

Part II: 200 tph CO_2 (approximate total CO_2 production in the Kızıldere Geothermal Field as of May 2018) was reinjected in supercritical state through the deeper injection wells: KD-27A at the east (2300 meters bsl), KD-44 at the north-west (3200 meters bsl), and KD-46 at the west (2580 meters bsl). The current reinjection of these three wells (276 tph, total) was distributed among other injection wells.

The critical pressure and temperature values of CO_2 is 73.8 bar and 31.1 °C, respectively. Above the critical point, the liquid and gas phases cannot exist as separate phases, and CO_2 develops supercritical properties (sCO_2), where it has some characteristics of a gas and others of a liquid. For instance, sCO_2 expands to fill the space like a gas but with a density similar to that of a liquid, while the viscosities and diffusivities are closer to that of gases. A supercritical CO_2 can diffuse in a solid matrix faster than a liquid (Energy Institute, 2013). Since the reservoir conditions are higher than critical temperature and pressure values of CO_2 (reinjection is simulated starting from the sandface, not in the wellbore), CO_2 is assumed to be reinjected in supercritical state.

It should be noted that solubility of CO_2 in the water is quite complex and dependent on many variables including pressure, temperature, pH, and salinity. According to the Henry's Law, solubility of CO_2 is directly proportional to the partial pressure of the gas above the liquid. So, injecting more CO_2 into the reservoir also increase the amount of the dissolved CO_2 in the water. Henry's Law is;

$$P_{CO_2} = X_{CO_2} * K_h$$

where P_{CO2} is the partial pressure of carbon dioxide, X_{CO2} is the mole fraction of CO_2 in the liquid, and K_h is the Henry's constant (Pa^{-1}). K_h is strongly dependent on temperature. Based on the studies by Pistone et al. (2011) and Duan & Sun (2003), it can be said that CO_2 solubility in the reservoir conditions of Kızıldere Geothermal Field can be as high as around 7%. So, 10% (520 tph) carbon dioxide would be injected in two-phase, and would contain many operational challenges. This is also true for 200 tph of supercritical carbon dioxide injection through 3 wells, but the main focus of this study is to investigate the consequences of such implementations on the reservoir behavior by using the TOUGH2 simulation codes. The results are shown mainly by comparing the changes in the pressure and temperature profiles, and also the amount of the dissolved CO_2 in the reservoir conditions. The production wells KD-42, KD-47, and KD-50A are used for

exemplification. These well were selected, since KD-47 has the highest production rate, while KD-50A has the lowest. KD-42 is at the edge of the production and north-western injection wells. So, it was considered that these wells successfully reflect the results of different scenarios.

The following figures compares the pressure profiles of KD-42, KD-47, and KD-50A in the two parts of the Scenario 3, compared to the Scenario 1.

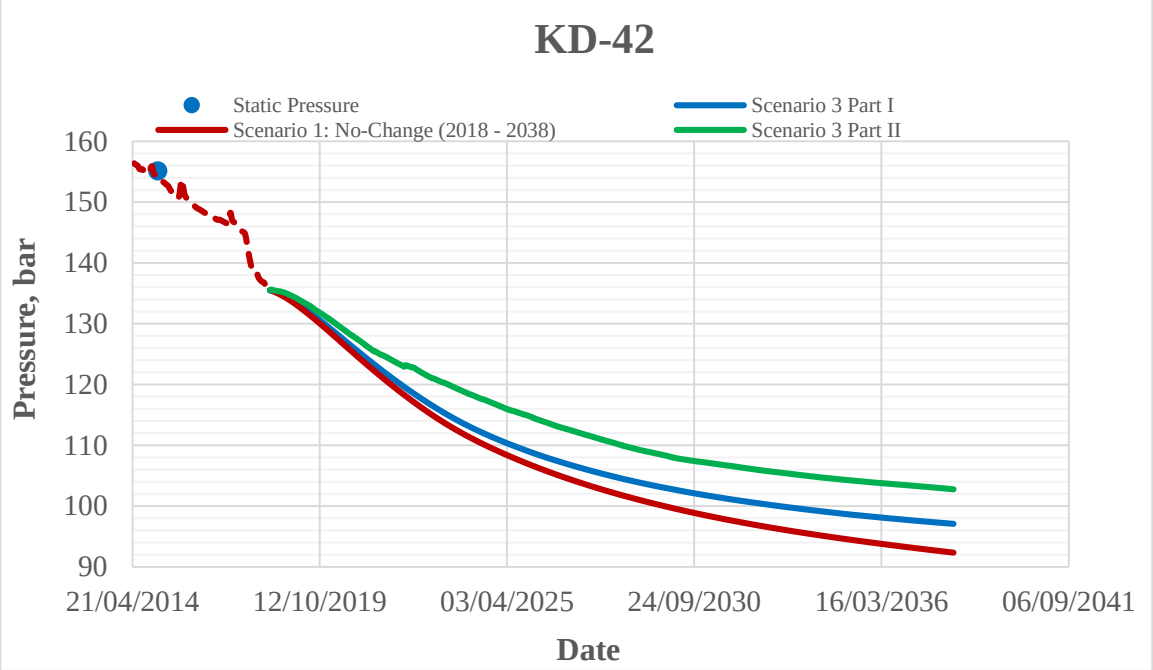

Figure 5.30 Pressure decline of KD-42 in Scenario 3 – Strategy 1

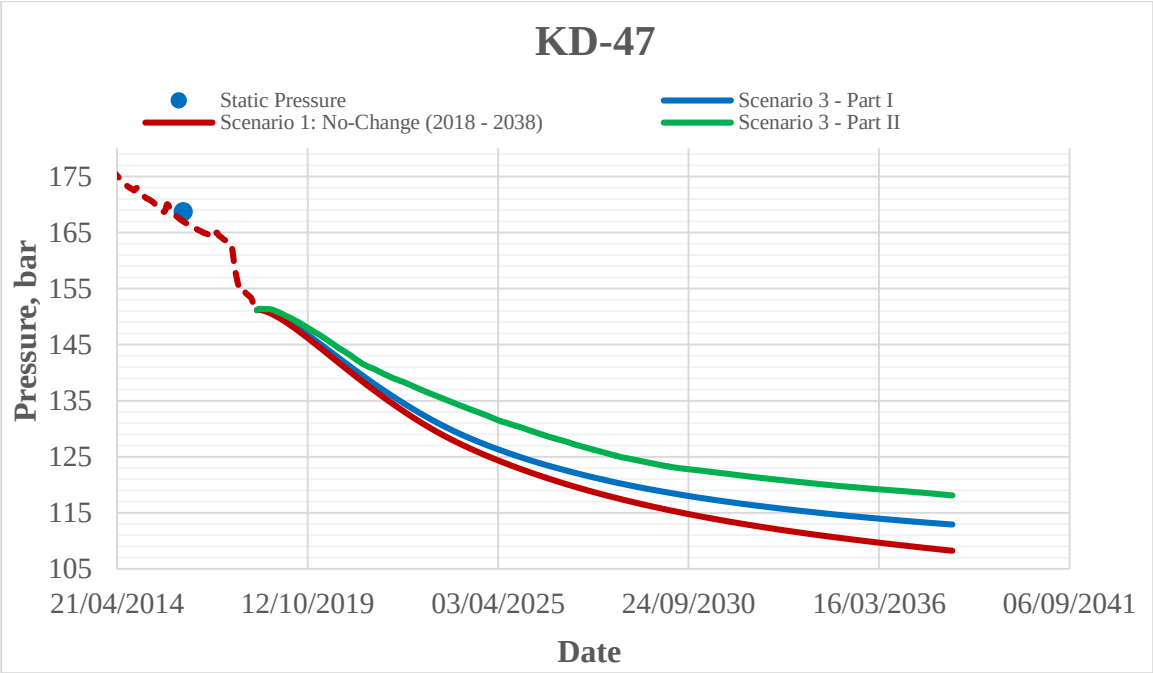

Figure 5.31 Pressure decline of KD-47 in Scenario 3 – Strategy 1

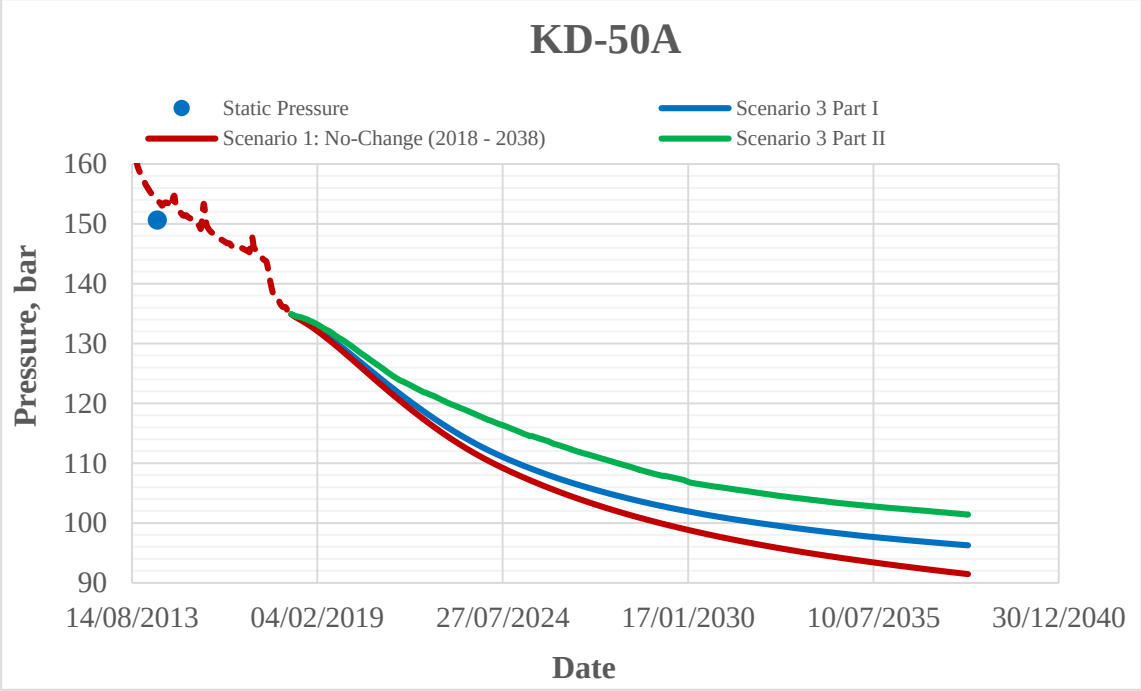

Figure 5.32 Pressure decline of KD-50A in Scenario 3 – Strategy 1

As a result of injection of high amount of CO_2 in the Scenario 3, the shifts in the 10% pressure decline occurring dates are shown in the following figures for the both parts.

Well	10% Pressure Reduction Date	Δt, days (S3 Part I - S1)	Well	10% Pressure Reduction Date	Δt, days (S3 Part I - S1)
KD-2A	31-03-2021	78.7	**KD-90A**	09-06-2022	123.7
KD-23B	14-07-2021	93.7	**KD-54A**	09-06-2022	123.7
R-3A	14-07-2021	93.7	**KD-89**	09-06-2022	123.7
KD-50A	13-08-2021	93.7	**KD-90B**	09-07-2022	123.7
KD-42	12-09-2021	93.7	**KD-43**	24-07-2022	123.7
KD-29	27-09-2021	108.7	**KD-25B**	08-08-2022	123.7
KD-23D	12-10-2021	93.7	**KD-58**	08-08-2022	123.7
KD-83	27-10-2021	108.7	**R-5**	23-08-2022	138.7
KD-55	26-11-2021	93.7	**KD-61A**	22-09-2022	123.7
KD-60	10-01-2022	108.7	**KD-61**	22-09-2022	123.7
KD-63	24-02-2022	108.7	**KD-62**	20-01-2023	138.7
KD-59	24-02-2022	108.7	**KD-58A**	04-02-2023	138.7
KD-54	24-02-2022	108.7	**KD-66A**	05-04-2023	153.7
KD-47	11-03-2022	108.7	**KD-62A**	04-06-2023	153.7
KD-49	26-03-2022	108.7	**KD-68B**	04-06-2023	153.7
KD-45	25-04-2022	108.7	**KD-68A**	04-07-2023	153.7
KD-64	10-05-2022	108.7	**KD-9A**	21-08-2026	682.5

Table 5.6 Time shifts in Scenario 3 Part I compared to Scenario 1

Well	10% Pressure Reduction Date	Δt, days (S3 Part II - S1)	Well	10% Pressure Reduction Date	Δt, days (S3 Part II - S1)
KD-2A	23-11-2021	315.2	**KD-89**	21-08-2023	561.8
KD-23B	23-03-2022	345.2	**KD-90B**	05-09-2023	546.8
R-3A	10-04-2022	363.9	**KD-64**	20-10-2023	636.8
KD-50A	15-06-2022	399.6	**KD-58**	04-12-2023	606.8
KD-29	01-09-2022	447.4	**R-5**	03-01-2024	636.8
KD-23D	01-09-2022	417.4	**KD-54A**	03-01-2024	696.8
KD-83	16-09-2022	432.4	**KD-25B**	18-01-2024	651.8
KD-42	16-10-2022	492.4	**KD-43**	18-01-2024	666.8
KD-55	31-10-2022	432.4	**KD-61A**	02-02-2024	621.8
KD-60	15-12-2022	447.4	**KD-61**	02-02-2024	621.8
KD-59	08-03-2023	485.8	**KD-62**	16-07-2024	681.8
KD-63	27-04-2023	535.5	**KD-58A**	12-10-2024	754.9
KD-49	23-05-2023	531.8	**KD-66A**	26-11-2024	754.9
KD-54	23-05-2023	561.8	**KD-62A**	11-05-2025	860.8
KD-47	07-06-2023	561.8	**KD-68B**	11-05-2025	860.8
KD-90A	06-08-2023	546.8	**KD-68A**	02-06-2025	852.9
KD-45	06-08-2023	576.8	**KD-9A**	23-07-2029	1749.1

Table 5.7 Time shifts in Scenario 3 Part II compared to Scenario 1

Similar to the previous scenarios, temperature changes are not significant in both parts of the Scenario 3 – Strategy 1. Although some local temperature drops are observed in the simulation, especially at shallow depths, the minimum and maximum values of the scale have been chosen to be the same as the previous temperature figures so that the distribution of the colors are analyzed much easily.

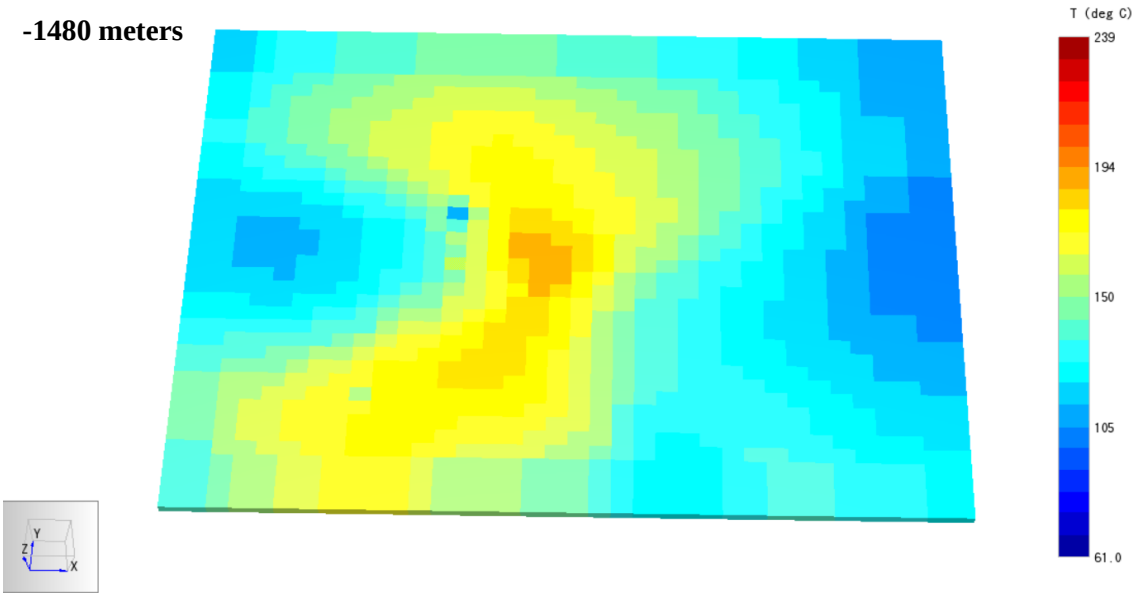

Figure 5.33 Temperature distribution at 1480 meters in Scenario 3 Part I – Strategy 1

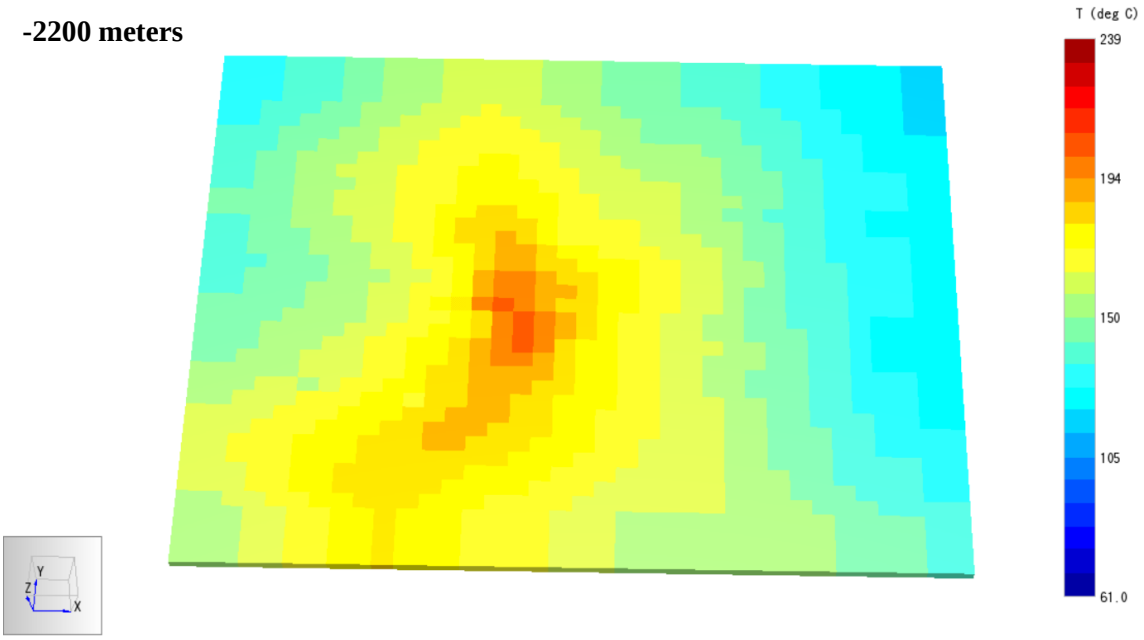

Figure 5.34 Temperature distribution at 2200 meters in Scenario 3 Part I – Strategy 1

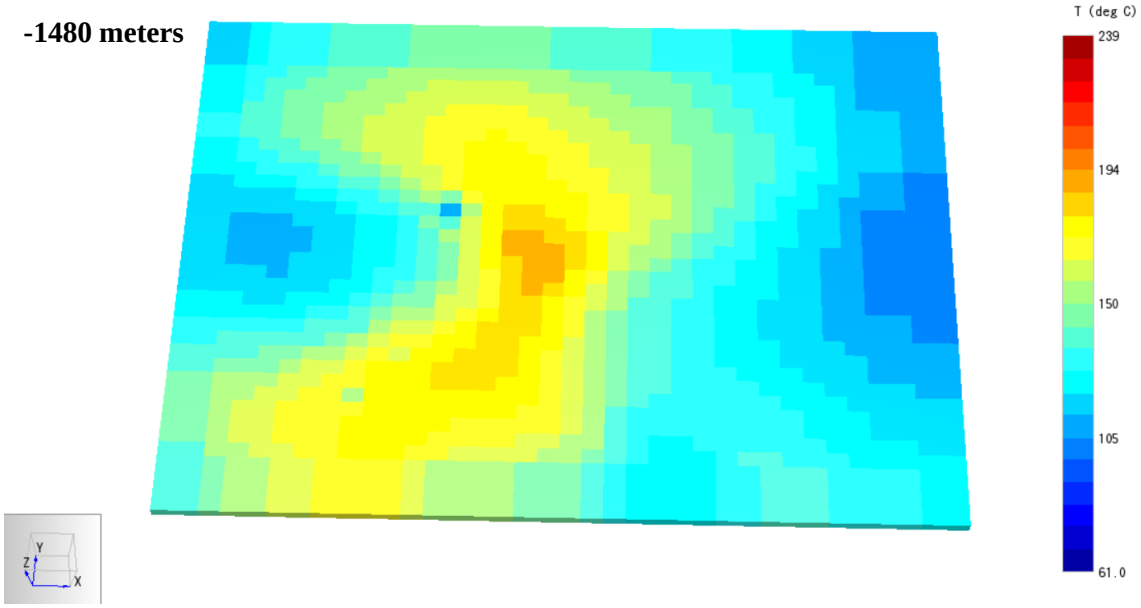

Figure 5.35 Temperature distribution at 1480 meters in Scenario 3 Part II – Strategy 1

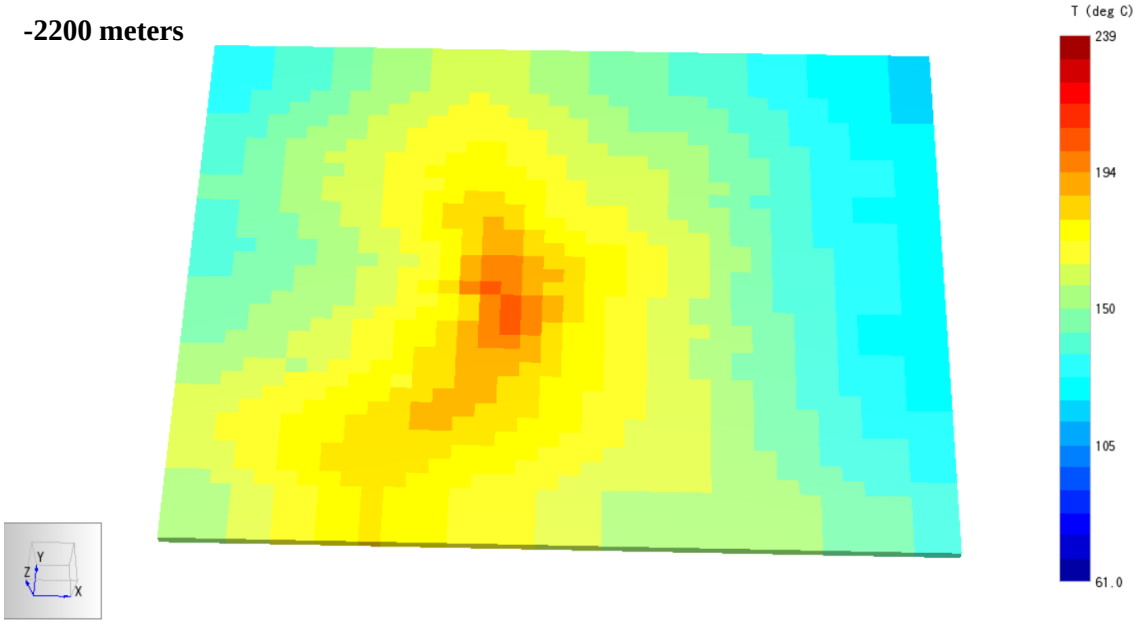

Figure 5.36 Temperature distribution at 2200 meters in Scenario 3 Part II – Strategy 1

Since high amount of carbon dioxide is injected in both parts of the Scenario 3, amount of the dissolved CO_2 in the production section increases significantly. As the amount of the CO_2 increases, gaseous CO_2 is observed in some parts of the field, especially at shallower sections. It is observed that the CO_2 amounts reach enormously high levels in the Part-II in the productions wells close to the reinjection wells, such as KD-42, due to the presence of high amount of gaseous CO_2.

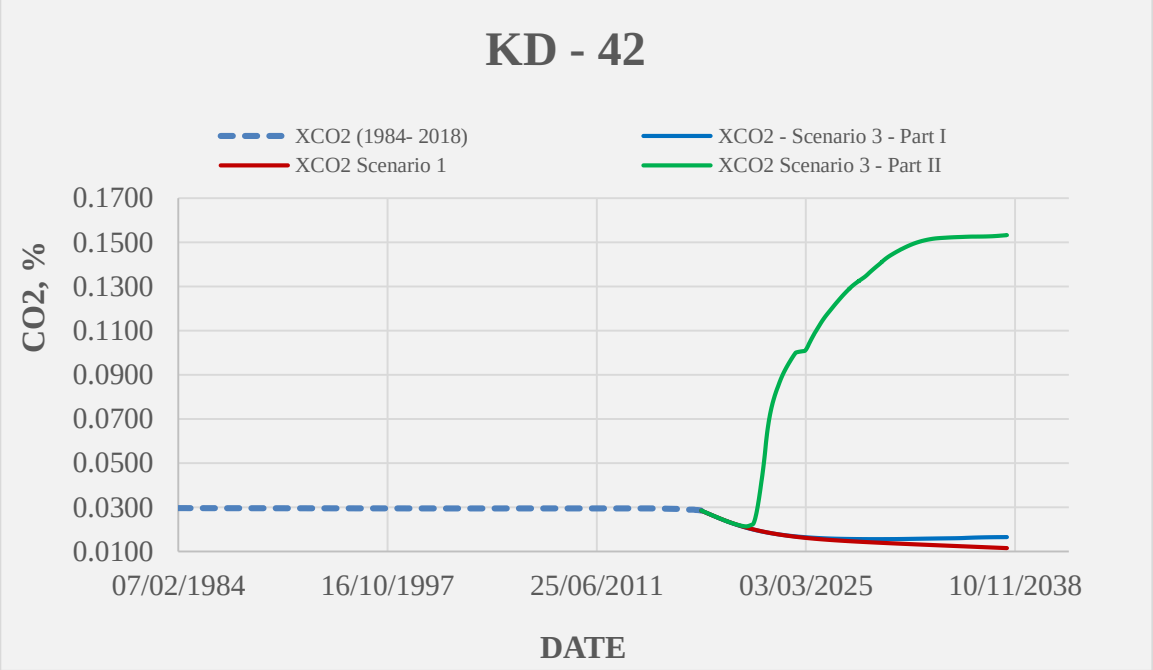

Figure 5.37 CO_2 profile of KD-42 in Scenario 3 compared to Scenario 1

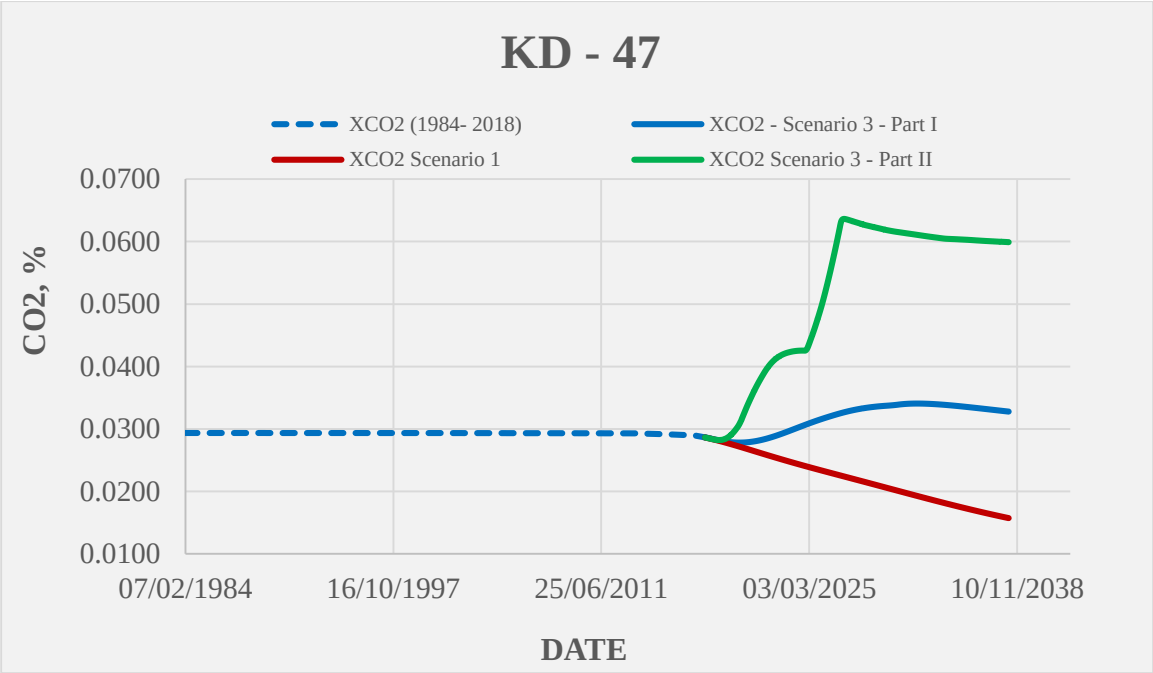

Figure 5.38 CO_2 profile of KD-47 in Scenario 3 compared to Scenario 1

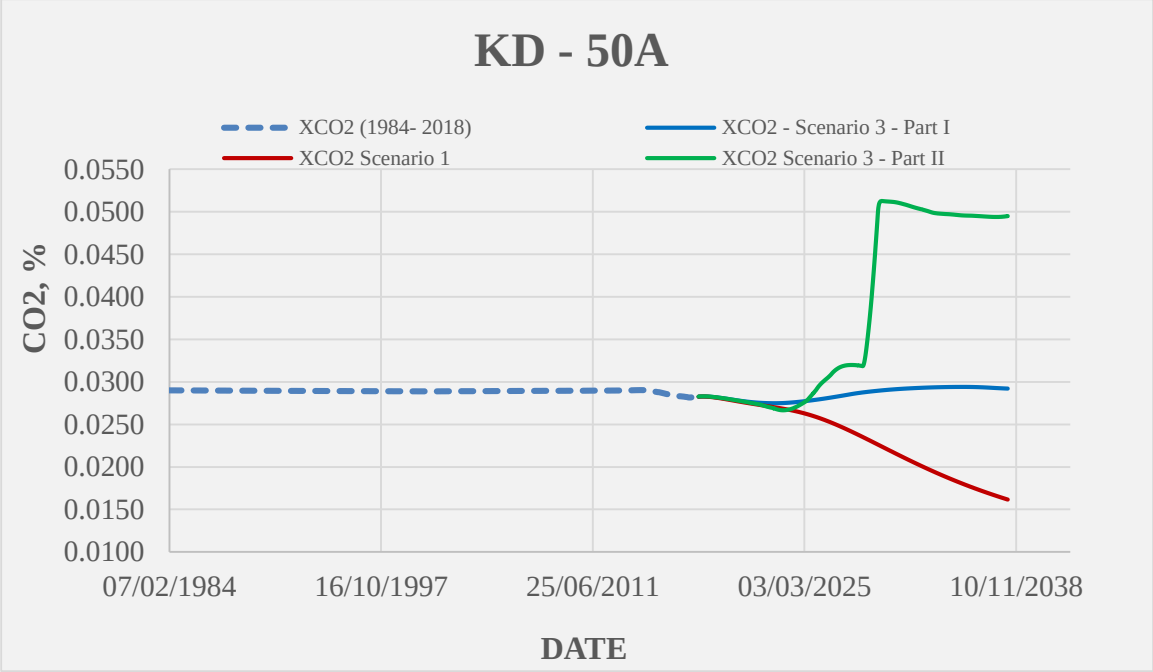

Figure 5.39 CO_2 profile of KD-50A in Scenario 3 compared to Scenario 1

In the 10% CO_2 injection scenario (Part I), the sharp increase in the CO_2 content around the shallower north-western reinjection wells (Figure 5.40) and three deeper reinjection wells, KD-27A, KD-44, and KD-46, (Figure 5.41) can be clearly seen. The effects can be better observed at much shallower sections and as high as 7.5% dissolved CO_2 is observed (Figure 5.42).

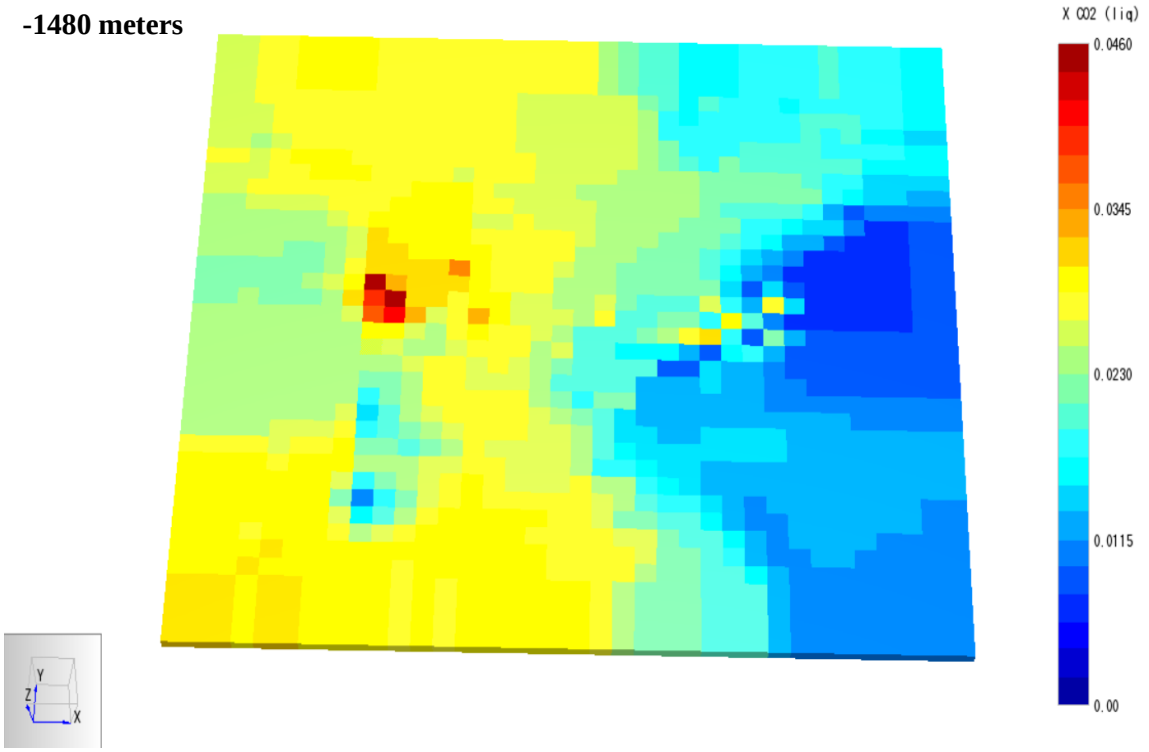

Figure 5.40 CO_2 distribution at 1480 meters (Scenario 3 Part I – Strategy 1)

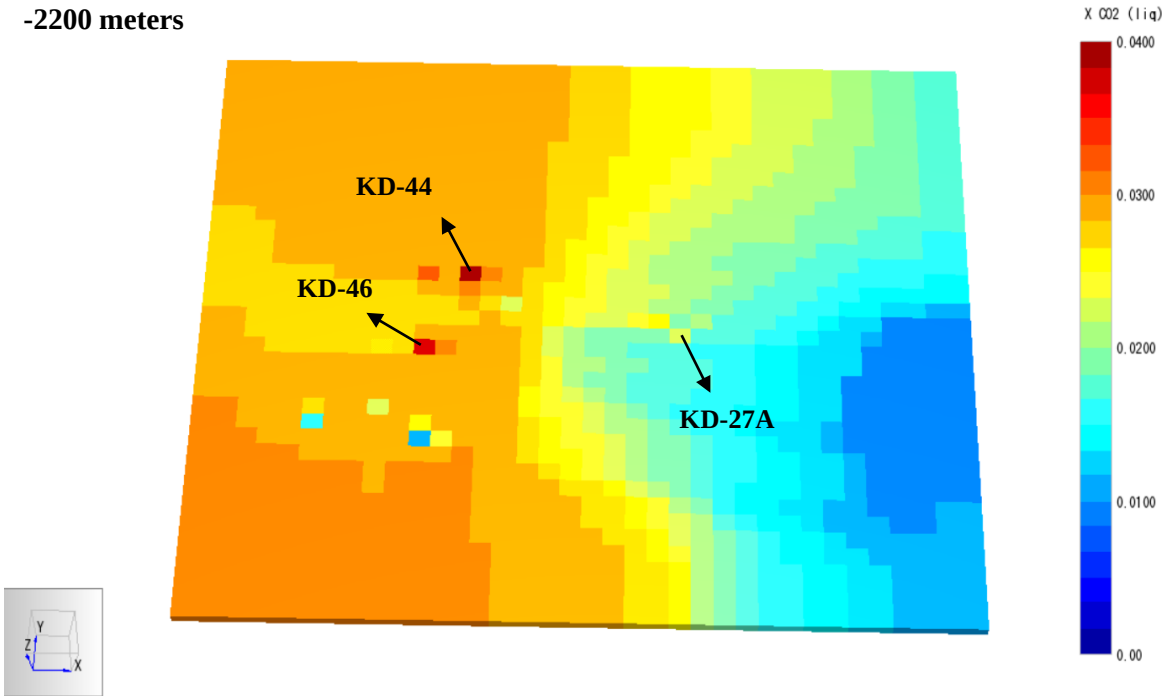

Figure 5.41 CO_2 distribution at 2200 meters (Scenario 3 Part I – Strategy 1)

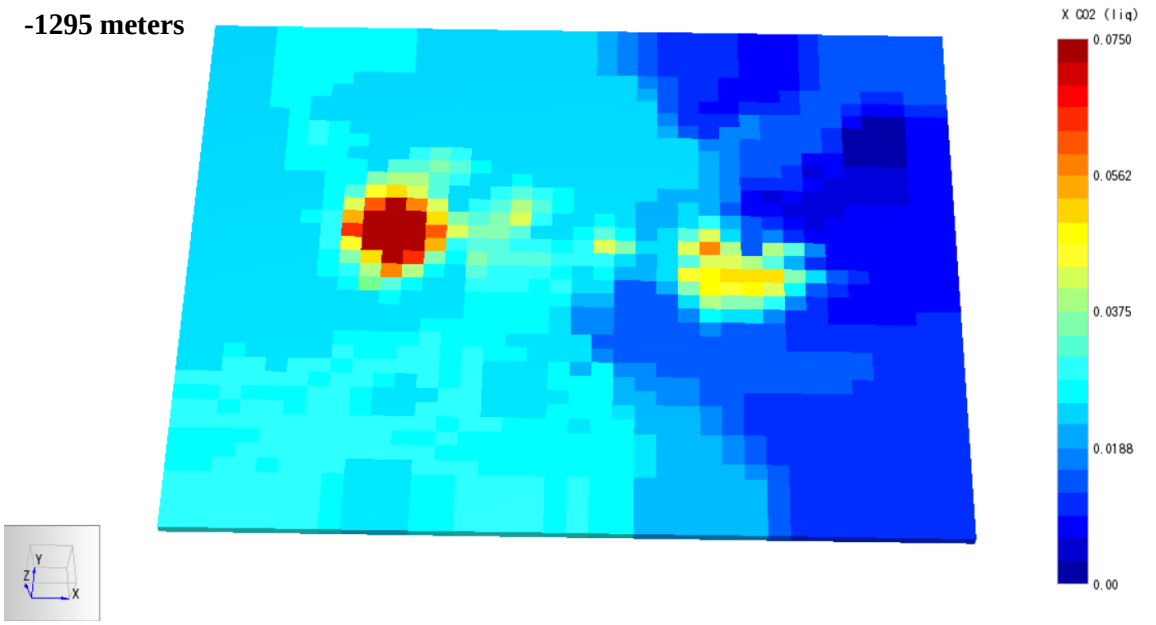

Figure 5.42 CO_2 distribution at 1295 meters (Scenario 3 Part I – Strategy 1)

In Scenario 3 Part II, the injected supercritical CO_2 from KD-27A and KD-44 tends to move towards each other in the shallow depths, because of the driving forces of the reinjected water from the eastern and north-western wells, and also the production wells which act like local sinks. The injected CO_2 from KD-46 moves to south-east direction where the production wells of the neighboring geothermal field are located. Since the other reinjection wells keep injecting geothermal brine, CO_2 dilution can be observed in the eastern and north-western areas. On the other hand, in deeper sections (Figure 5.44), only the vicinity of the KD-27A, KD-44, and KD-46 contains high amount of CO_2 due to the lack of driving forces of reinjection water.

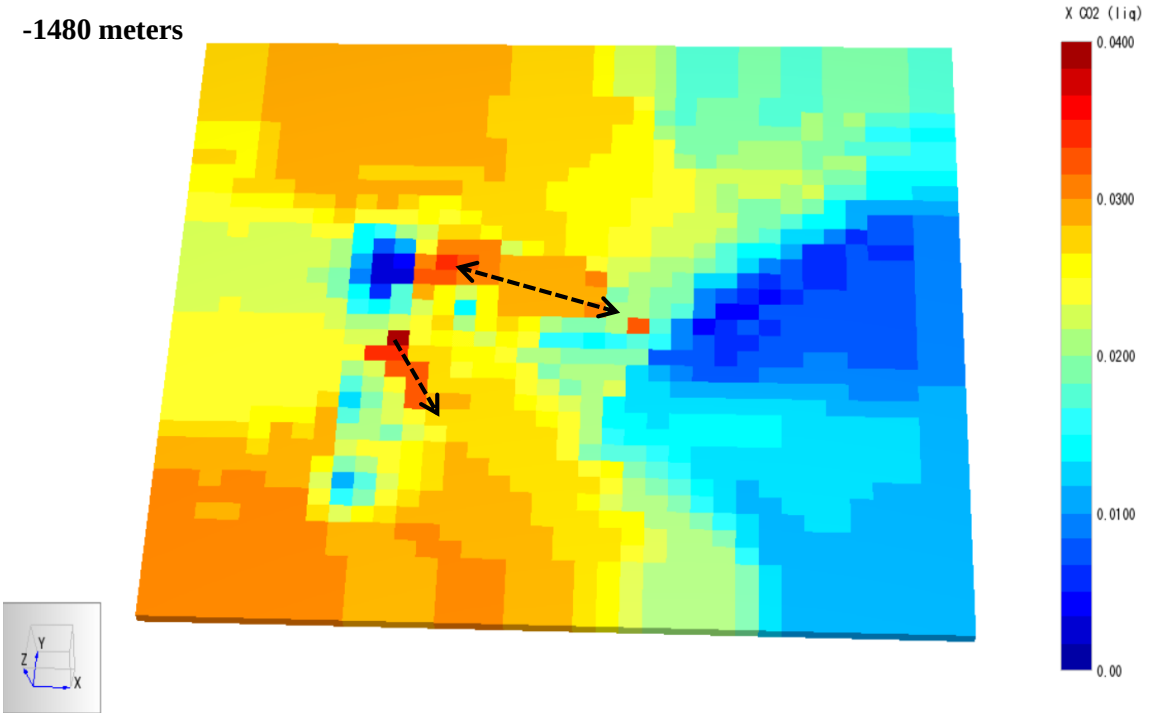

Figure 5.43 CO_2 distribution at 1480 meters (Scenario 3 Part II – Strategy 1)

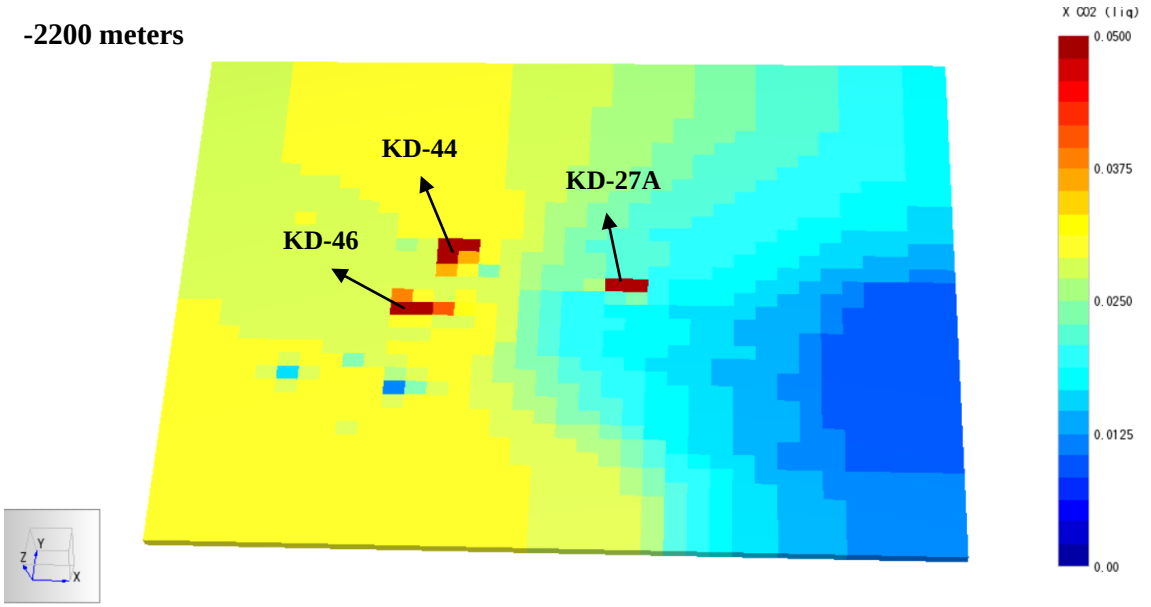

Figure 5.44 CO_2 distribution at 2200 meters (Scenario 3 Part II – Strategy 1)

In both parts of the Scenario 3, CO_2 turns into gaseous phase especially in shallow depths due to the high CO_2 concentrations and low pressures as a result of productions. Figures 5.45 and 5.46 shows the specific gravity distribution which reflects the existence of gaseous CO_2.

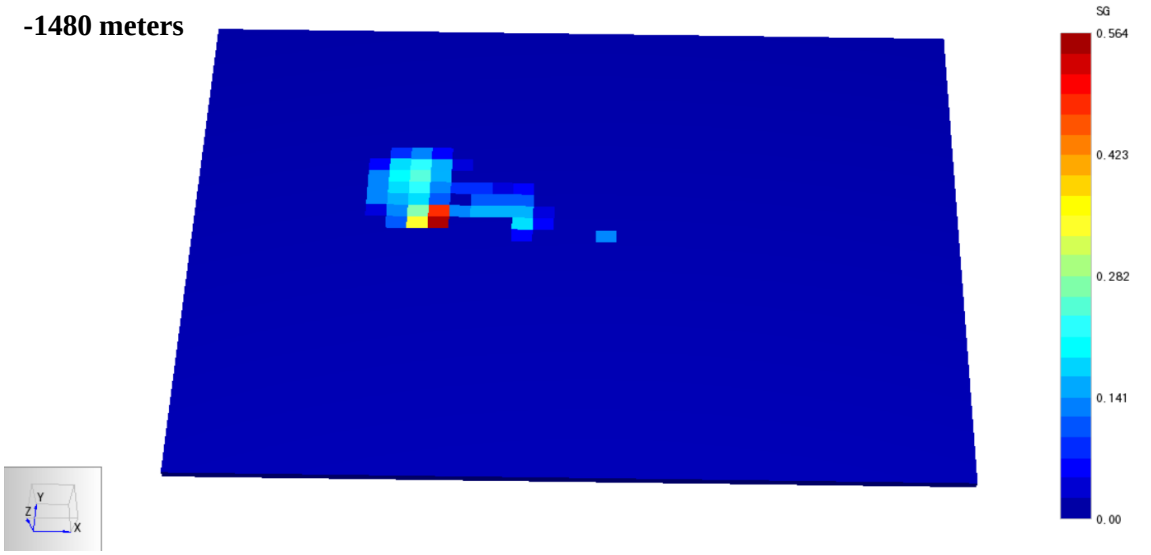

Figure 5.45 Gaseous CO_2 at 1480 meters (Scenario 3 Part I – Strategy 1)

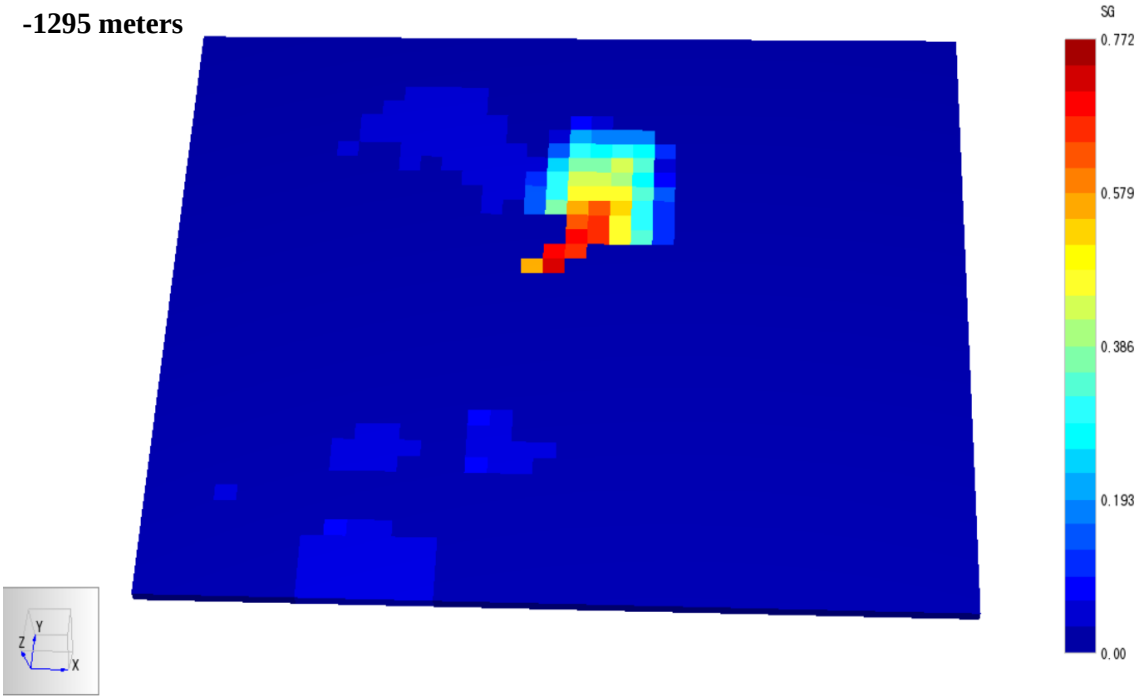

Figure 5.46 Gaseous CO_2 at 1295 meters (Scenario 3 Part II – Strategy 1)

5.2 STRATEGY 2: Keeping Wellhead Pressures Constant

As the production proceeds, reservoir pressure declines, and hence the wellhead pressures. But in Kızıldere geothermal power plants, the turbine inlet pressure should be at least 9 bara, which means that wellhead pressures should be kept above that level in exchange of the production rates. It is assumed in the Strategy 2 that any change in the wellhead pressures are instantly tolerated by adjusting the wellhead valves, so that changes in the production rates directly reflects the changes in the reservoir pressures. The previously mentioned 3 scenarios are repeated with the Strategy 2, and the results are given in the following sections.

5.2.1 Scenario 1: No-Change in the current reinjection rates

Current reinjection rates of 27 wells (Table 5.2) have been repeated for the next 20 years. Initial production rates (Table 5.1.) changes with respect to the changes in the reservoir pressures. The resultant total production rate is given in the following figure.

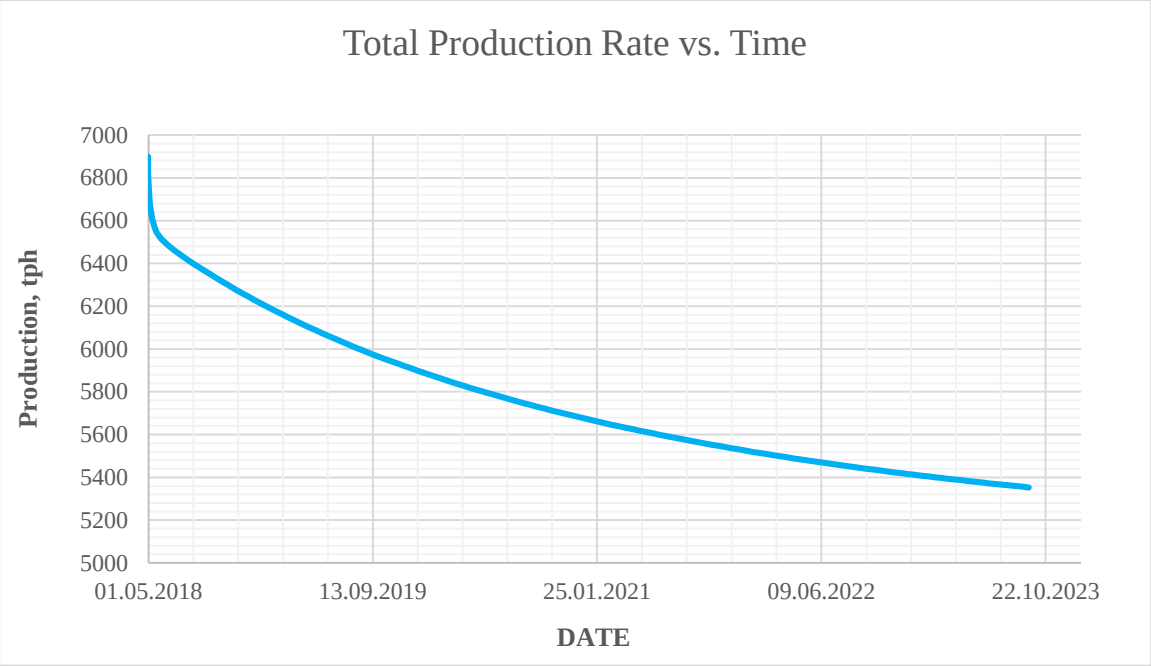

Figure 5.47 Plot of total production vs. time (Scenario 1 Strategy 2)

Since it is not logical to have higher reinjection rates than the production rates, simulation has been stopped when production rates decreased and became equal to the reinjection rates after the removal of the produced carbon dioxide. This situation occurred only 5 years after the beginning of the simulation.

It should be noted that the produced CO_2 is released into the atmosphere, and it is the case for the first scenario. The decline of the produced CO_2 amount is very identical to the total production decline.

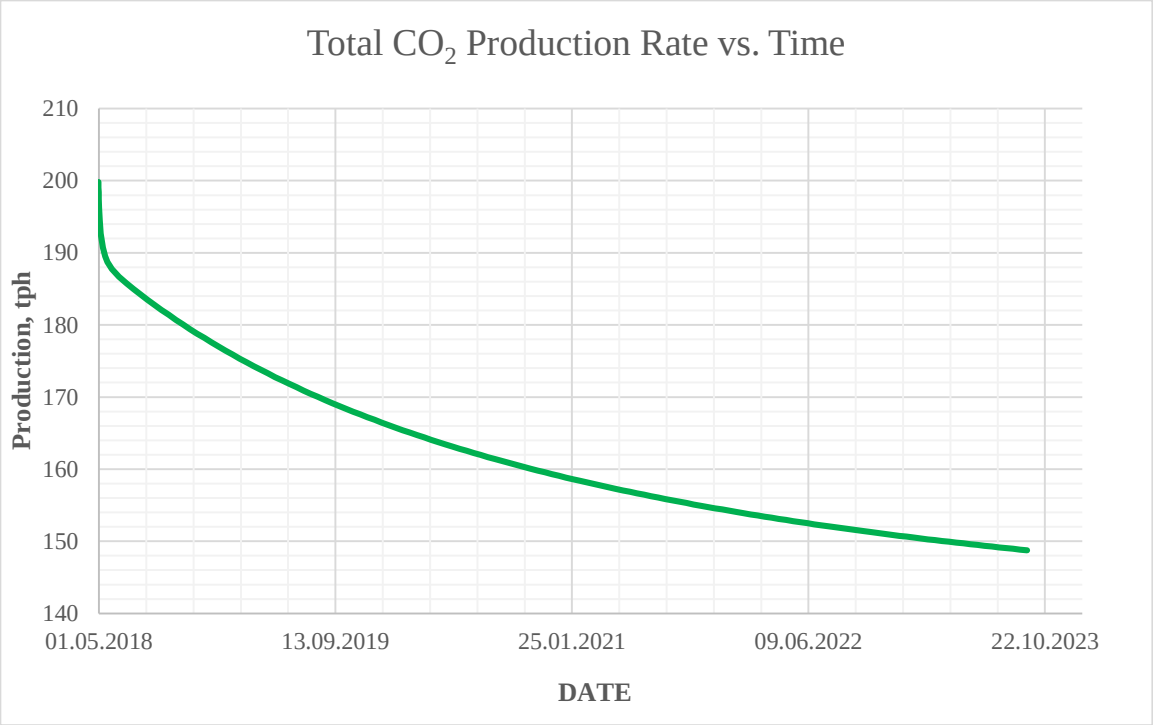

Figure 5.48 Plot of total CO_2 production vs. time (Scenario 1 Strategy 2)

Setting a critical level as 25% decline in the initial production rates (Table 5.1) of the production wells, some wells reach to the critical level long before than the other wells. Following table shows the dates when the critical production rates are reached for the 34 production wells. The rates of decline vary between 15 tph and 75 tph, depending on the initial production rate. The simulation was stopped when the total production rate decreased to the total reinjection rate, and it is observed that 12 wells reached their predetermined critical production levels before the end of the simulation at 2023.

Well	25% Production Rate Decline	Well	25% Production Rate Decline
KD-62	02.04.2020	**KD-60**	>2023
KD-68B	02.04.2020	**KD-47**	>2023
KD-61	17.04.2020	**KD-59**	>2023
KD-68A	28.11.2020	**KD-64**	>2023
KD-62A	11.02.2021	**KD-29**	>2023
KD-58A	23.11.2021	**KD-42**	>2023
KD-61A	23.11.2021	**KD-54**	>2023
KD-90B	22.05.2022	**KD-55**	>2023
KD-66A	04.09.2022	**KD-54A**	>2023
KD-89	04.09.2022	**KD-2A**	>2023
KD-25B	02.04.2023	**KD-9A**	>2023
R-5	30.08.2023	**KD-23B**	>2023
KD-58	>2023	**KD-23D**	>2023
KD-45	>2023	**R-3A**	>2023
KD-43	>2023	**KD-50A**	>2023
KD-90A	>2023	**KD-63**	>2023
KD-49	>2023	**KD-83**	>2023

Table 5.8 Dates of reaching 25% decline in the production rates

The pressure profiles, flowing enthalpy, and CO_2 production rates are shown for 3 representative wells: KD-42, KD-47, and KD-50A. KD-47 has the highest production rate, while KD-50A has the lowest. KD-42 is at the edge of the production and north-western injection wells. The effects of Phase-II and Phase-III production/injection operations are assumed to be better observed by these wells. The rapid pressure decline due to the less injection rates and releasing the produced CO_2 into the atmosphere can be seen clearly on the pressure vs. time plots.

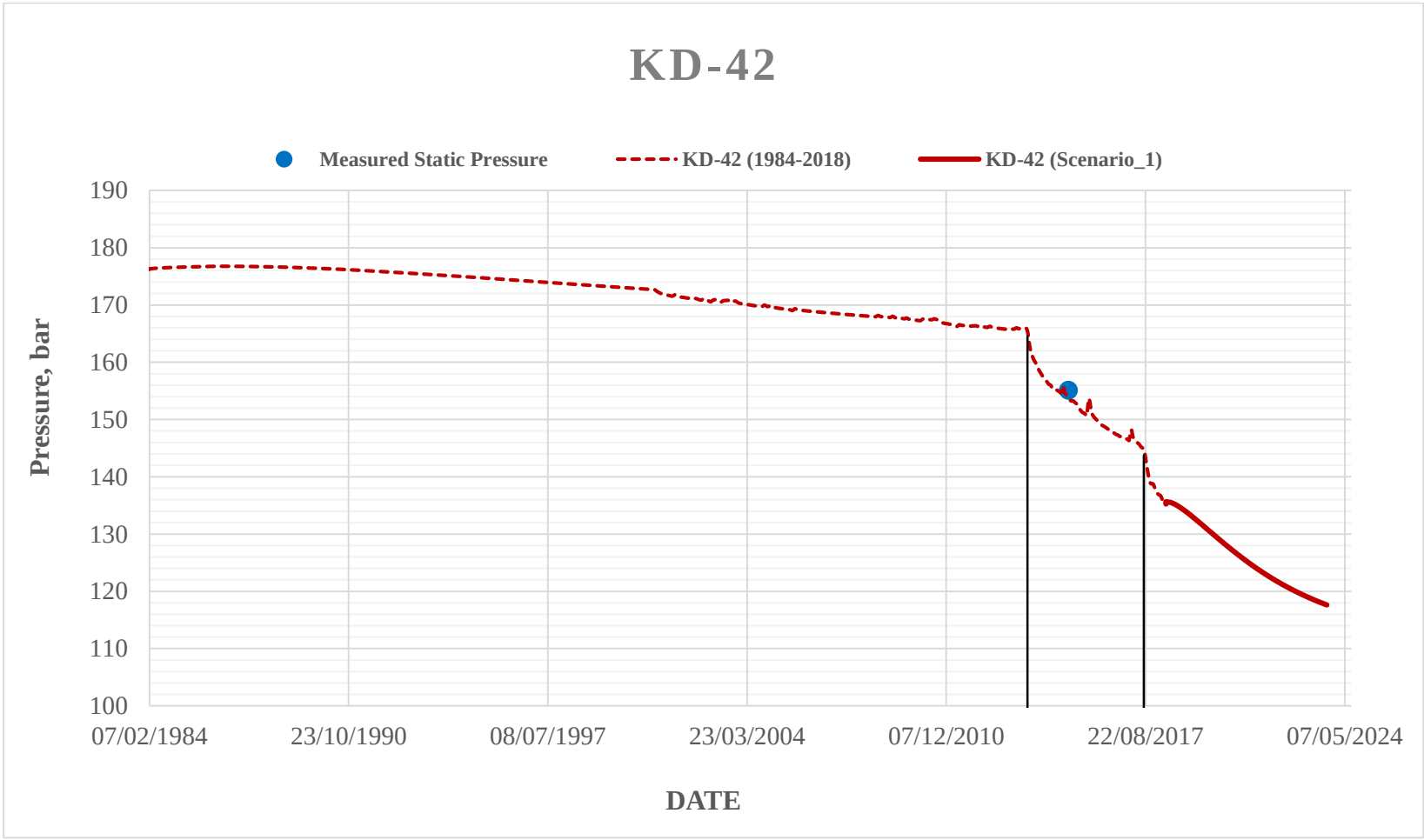

Figure 5.49 Pressure profile of KD-42 between 1984 – 2023 (Scenario 1 Strategy 2)

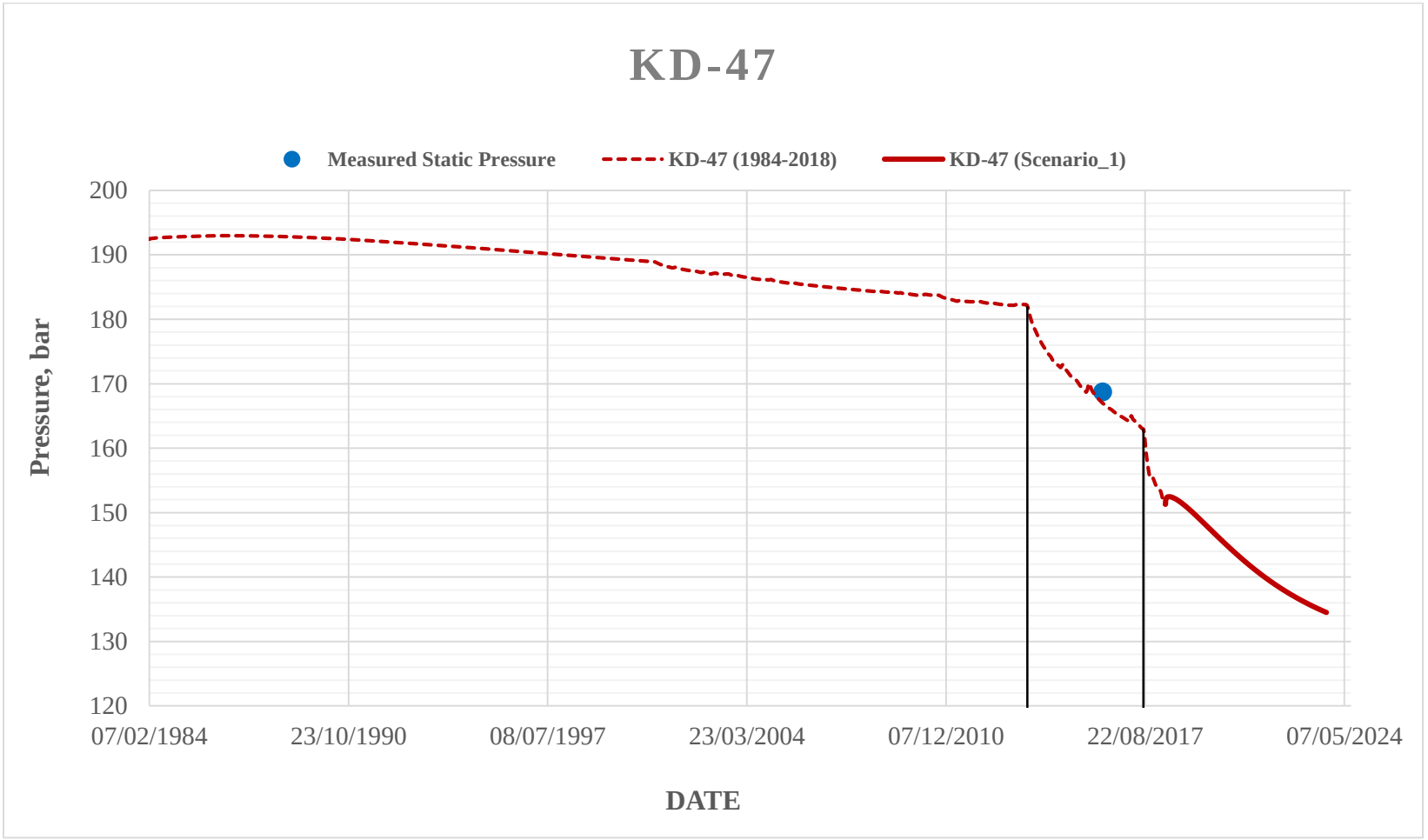

Figure 5.50 Pressure profile of KD-47 between 1984 – 2023 (Scenario 1 Strategy 2)

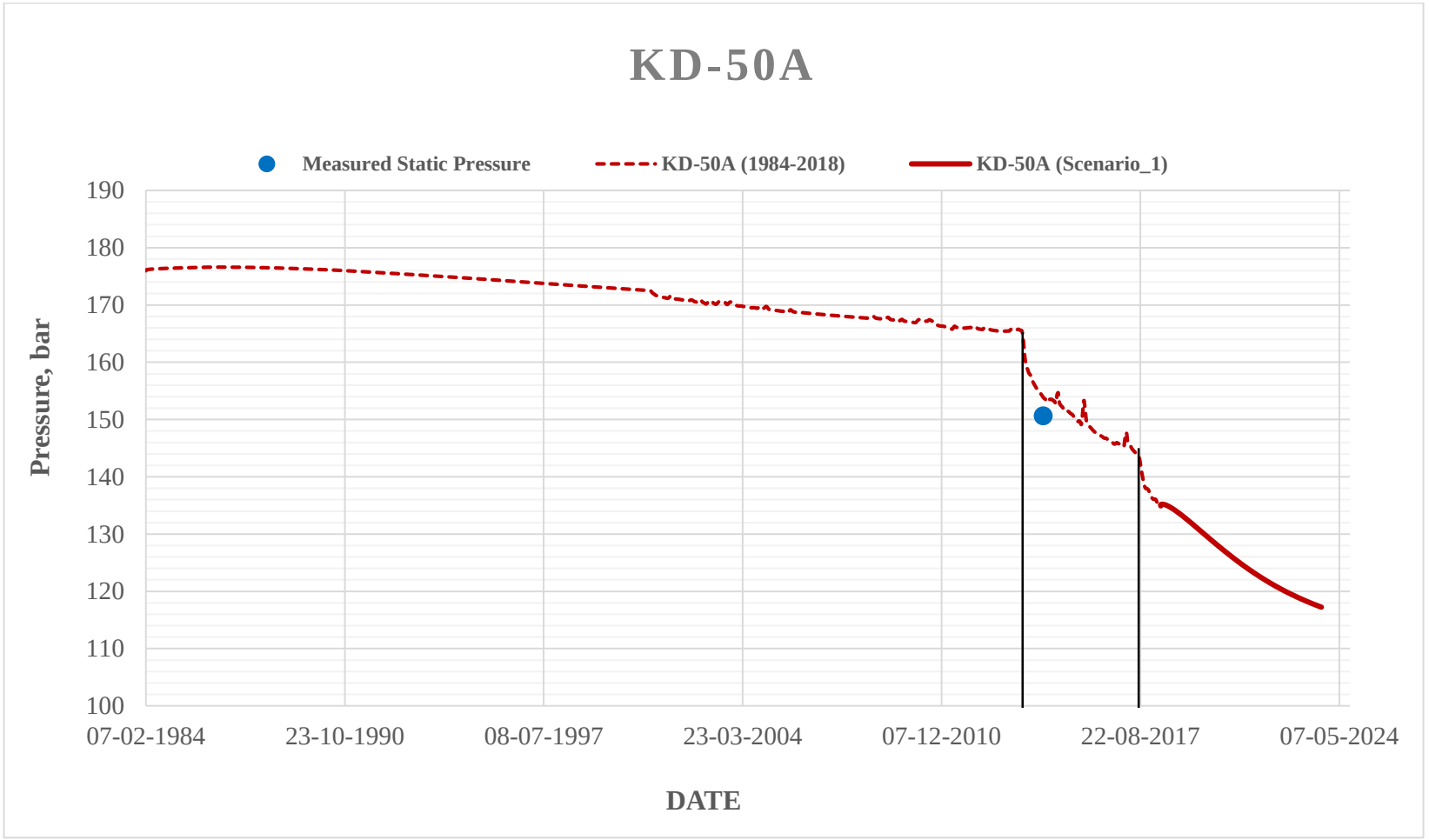

Figure 5.51 Pressure profile of KD-50A between 1984 – 2023 (Scenario 1 Strategy 2)

As mentioned previously, CO_2 is released into the atmosphere at the surface in Kızıldere geothermal power plants, and only trace amount of CO_2 remains in the reinjection fluid. Since carbon dioxide is not reinjected back into the reservoir, the partial pressure of carbon dioxide reduces with the production. This further explains the rapid decline in the reservoir pressures of the Kızıldere geothermal field.

Decline in the produced CO_2 can be seen in the production wells; KD-42, KD-47, and KD-50A. The major reason of the decline in the CO_2 production rates is actually the decline in the production rates.

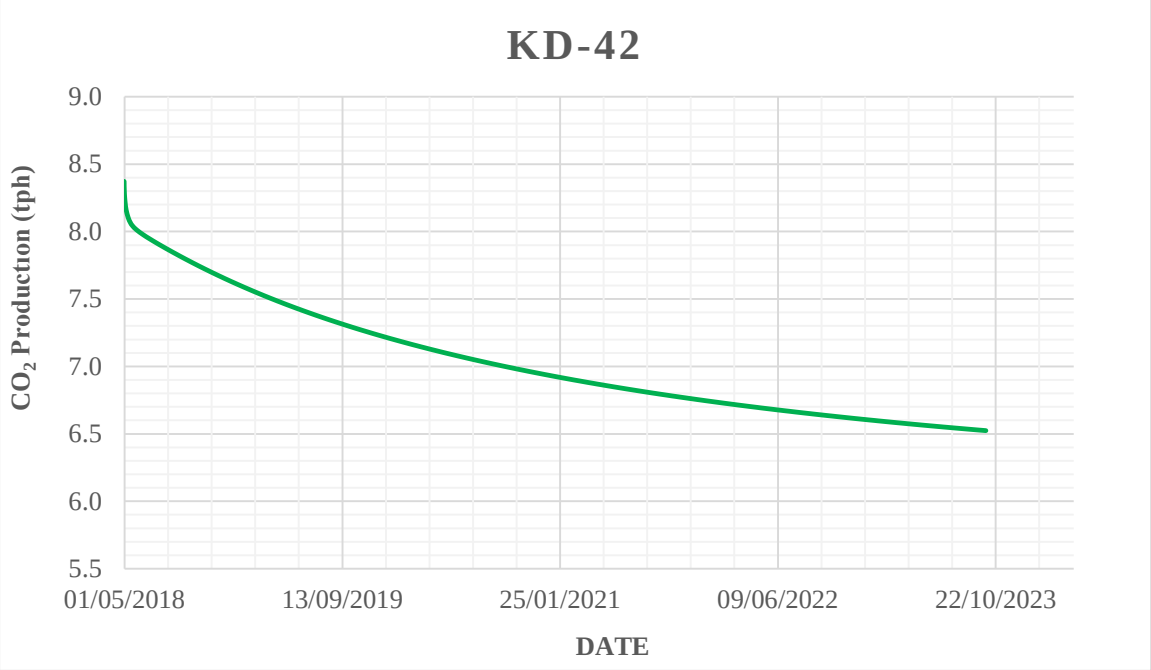

Figure 5.52 CO_2 production of KD-42 (Scenario 1 Strategy 2)

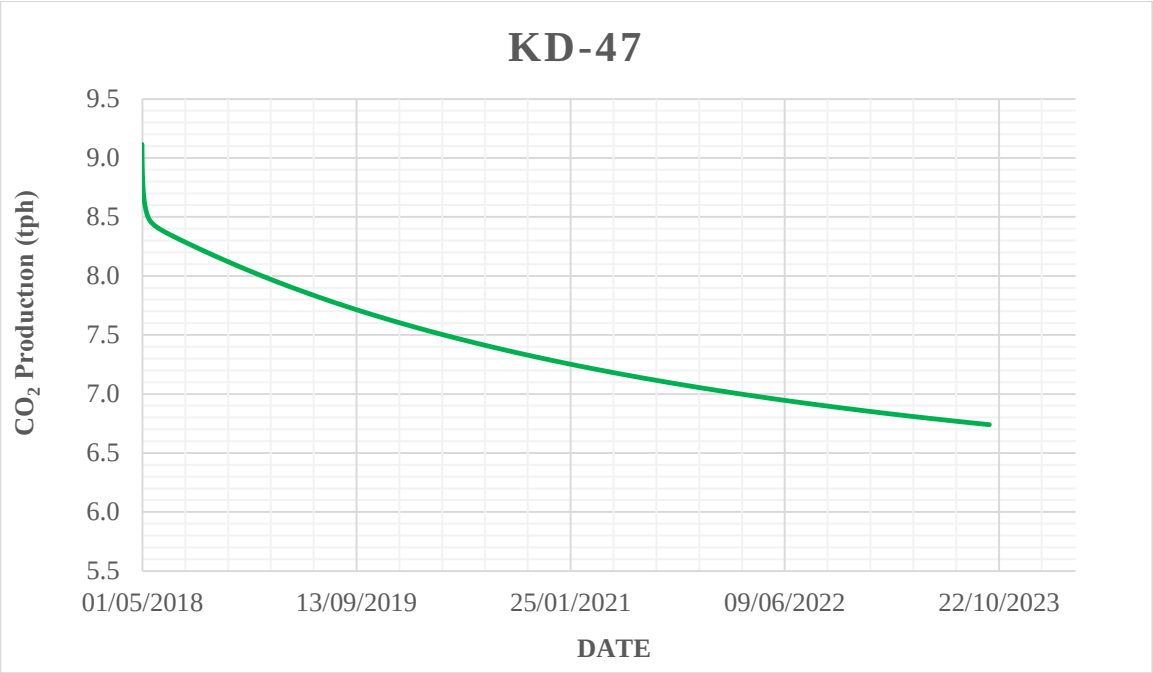

Figure 5.53 CO_2 production of KD-47 (Scenario 1 Strategy 2)

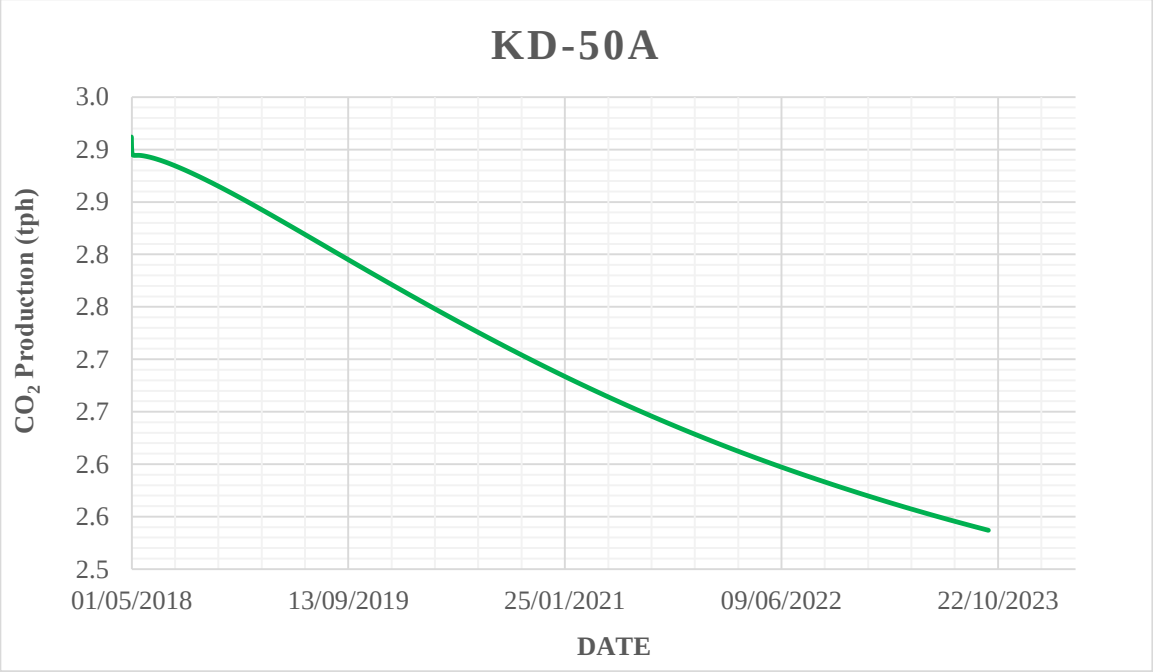

Figure 5.54 CO_2 production of KD-50A (Scenario 1 Strategy 2)

Compared to the natural state conditions, no significant decrease in the CO_2 ratios have been observed in the deeper sections. However, two deep reinjection wells, KD-44 and KD-46, decreased the CO_2 ratios at the vicinity of their wellbores, since there is no CO_2 present in the reinjection fluids. But the decrease is only limited, since the reinjection rates of these wells are relatively smaller, caused by high wellhead pressures during the reinjection operations in these deep wells.

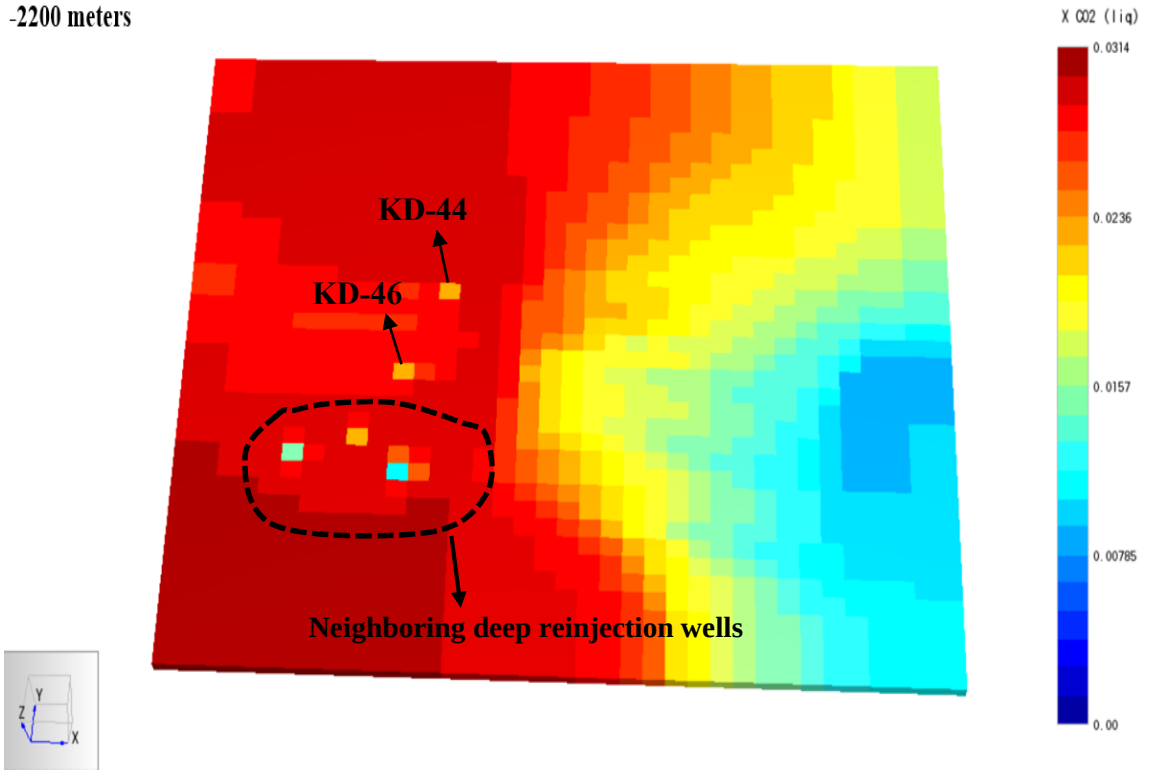

Figure 5.55 CO_2 distribution at 2200 meters in 2023 (Scenario 1 Strategy 2)

The CO_2 dilution caused by the reinjection operations can be better observed at the shallower sections of the field, since majority of the reinjection wells are completed at shallower depths. The Figures 5.10 and 5.11 show the CO_2 distribution in 2018 and 2023, respectively, at 1480 meters. The change in the dissolved CO_2 ratio is significant at shallow sections, especially at the north-western reinjection area.

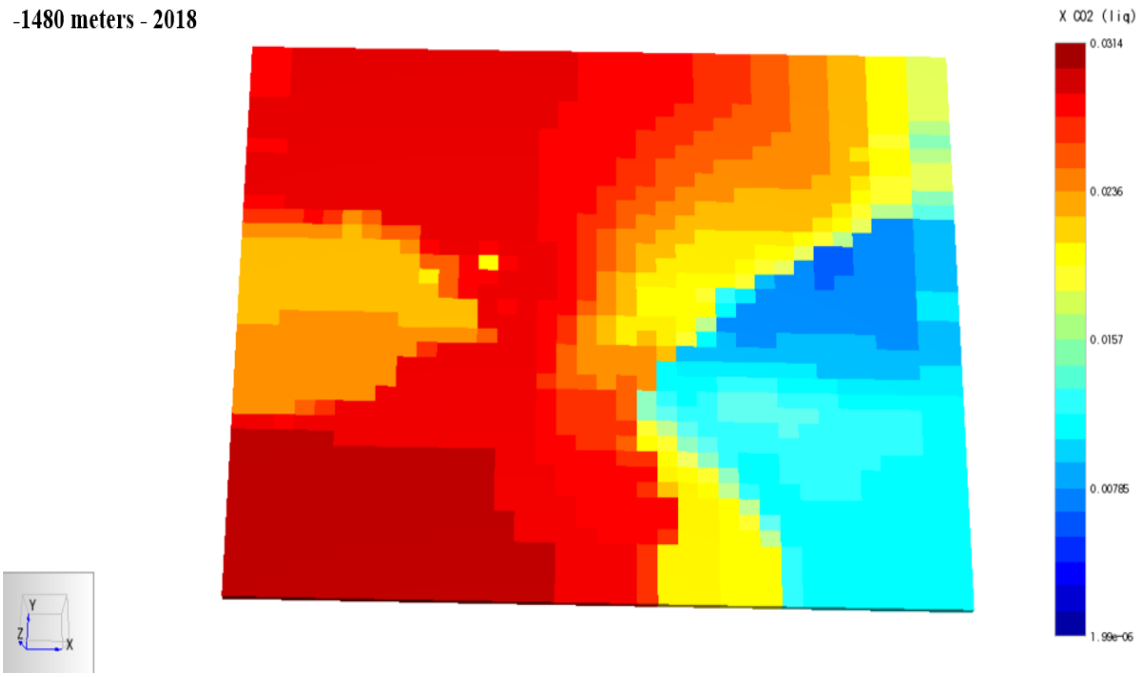

Figure 5.56 CO_2 distribution at 1480 meters in 2018 (Scenario 1 Strategy 2)

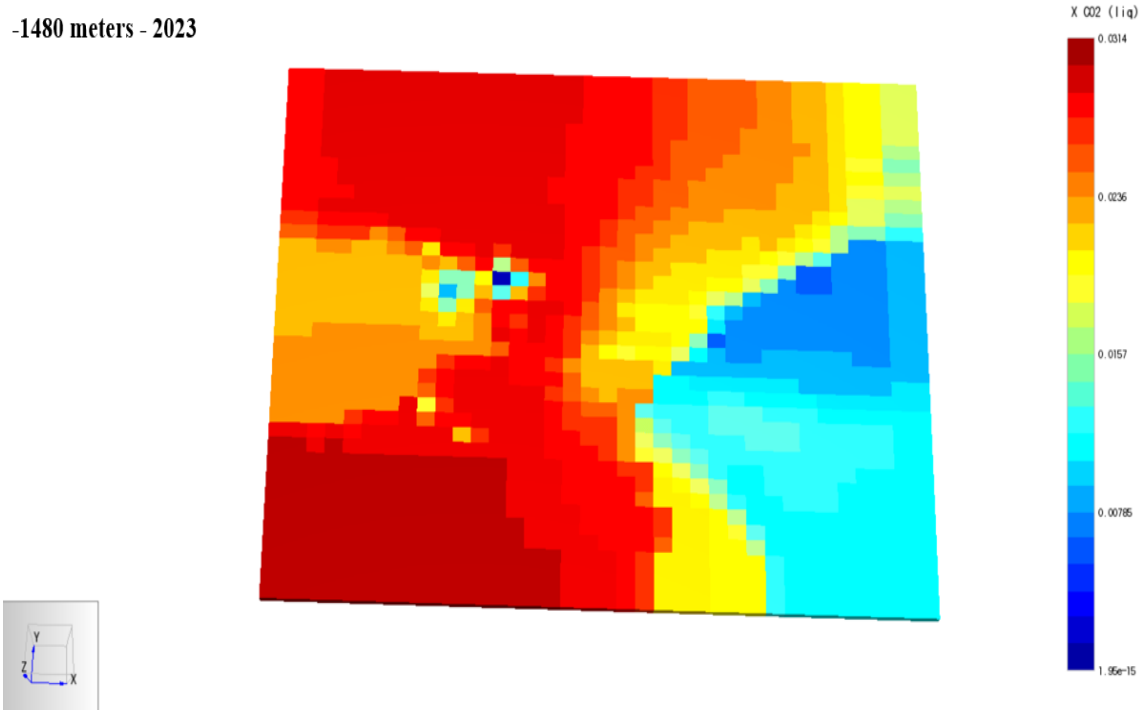

Figure 5.57 CO_2 distribution at 1480 meters in 2023 (Scenario 1 Strategy 2)

The cooling effects of the reinjection fluid are found to be insignificant in the Strategy 2 of the Scenario 1. For most of the production wells, the flowing enthalpy did not reduce significantly during the simulation. The highest decline has been observed in KD-47 with around 22 kj/kg reduction at the end of the simulation. For the rest of the wells the decline is less than that, and the average decline is 11 kj/kg. This situation points out that the reinjected geothermal fluid does not have cooling effects on the production zone.

Flowing enthalpies of KD-42, KD-47, and KD-50A are shown.

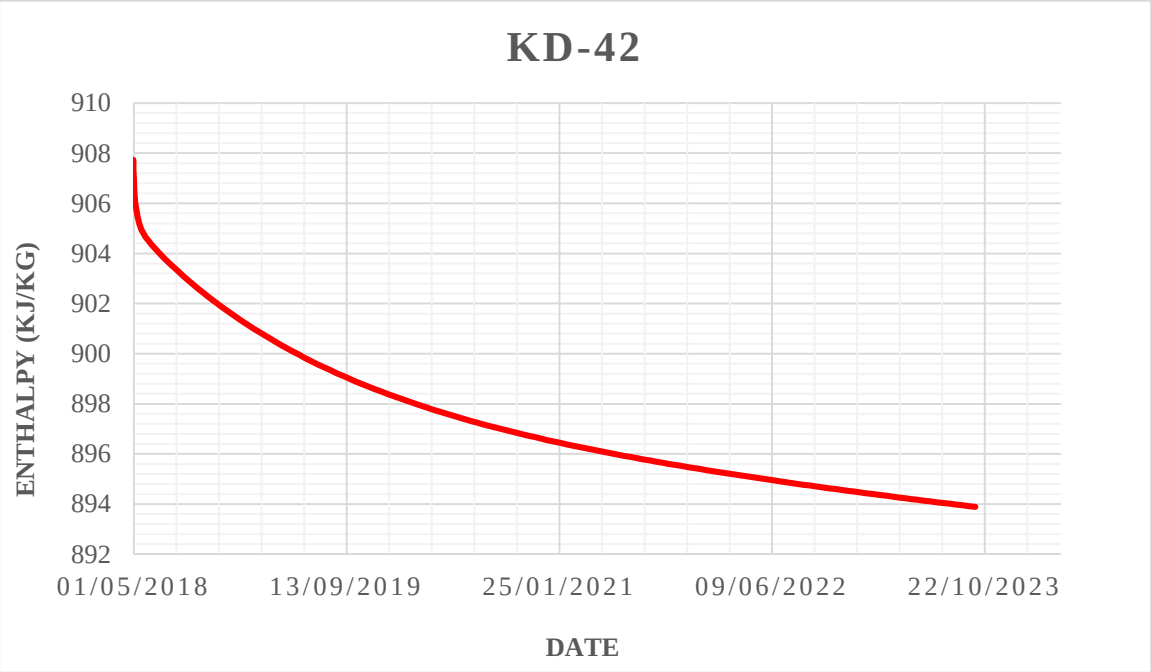

Figure 5.58 Flowing enthalpy profile of KD-42 (Scenario 1)

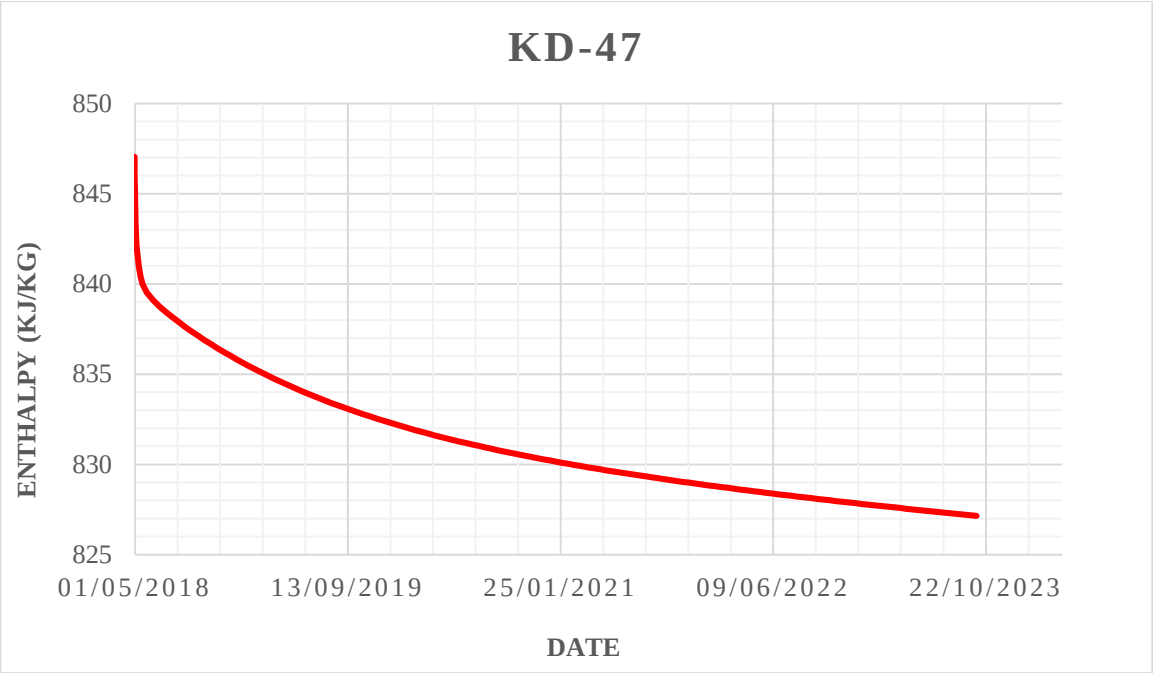

Figure 5.59 Flowing enthalpy profile of KD-47 (Scenario 1)

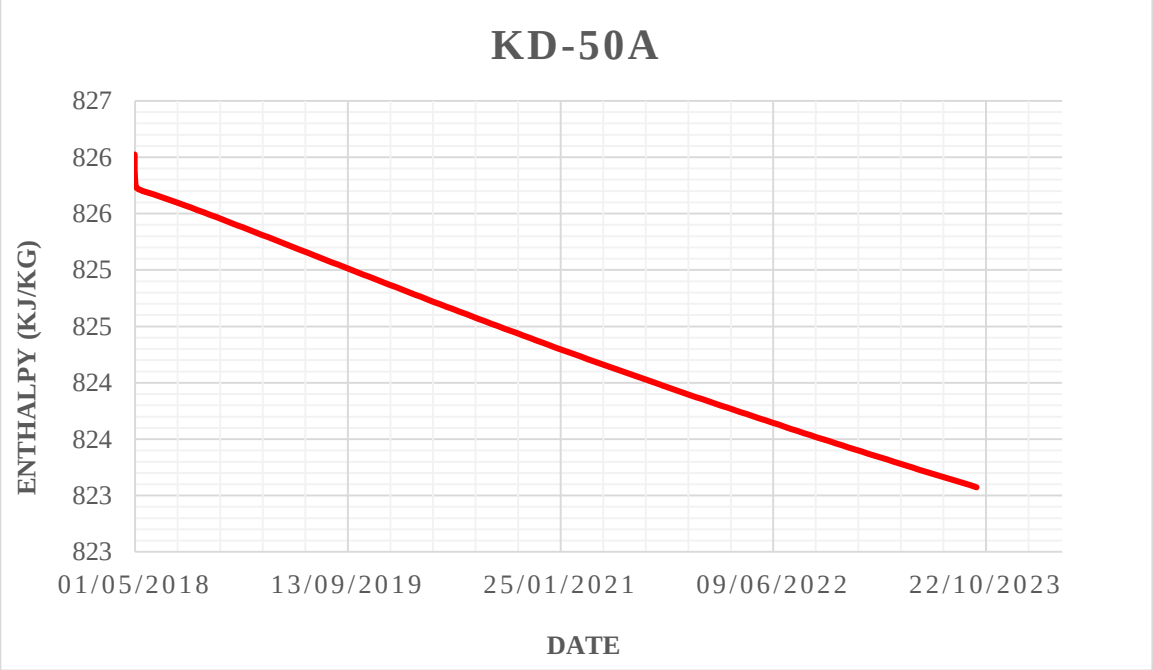

Figure 5.60 Flowing enthalpy profile of KD-50A (Scenario 1)

No considerable changes in the temperature distribution at the deep production sections and temperature isosurfaces can be investigated visually in the following figures.

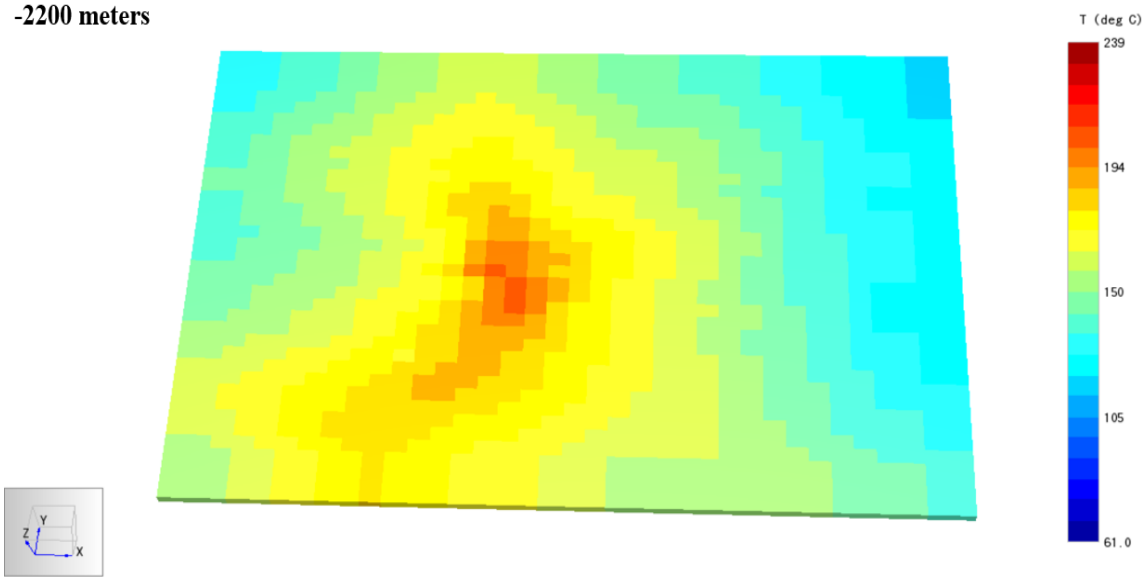

Figure 5.61 Temperature distribution at the end of the Scenario 1

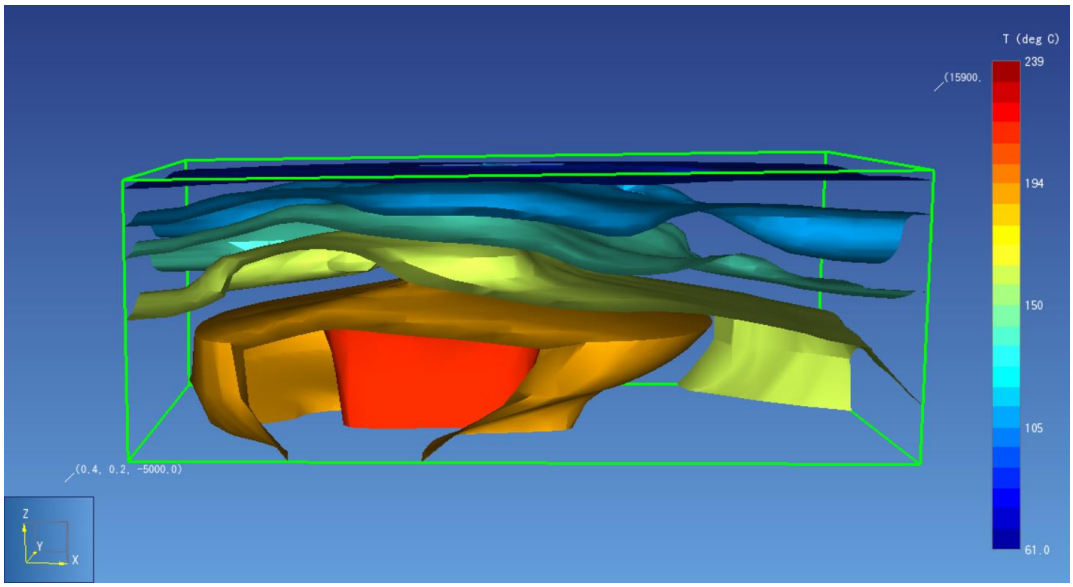

Figure 5.62 Temperature isosurfaces at the end of the Scenario 1

5.2.2 Scenario 2: Reinjecting what is produced

Instead of using constant reinjection rates as in the case of Scenario 2 – Strategy 1, reinjection rates are adjusted in a way that the decline in the production rates are taken into account. So, both parts of the Scenario 2 are repeated with the Strategy 2, and rest of the features kept as mentioned in the section 5.1.2.

The simulation was run for 20 years. In the first part produced CO_2 was released into the atmosphere and all of the produced water was reinjected through the reinjection wells. In the second part, all of the produced water and CO_2 was reinjected. For exemplification, the production well KD-47 is used. To make a healthier comparison with the Scenario 1, parameters are plotted until the end of 2023, where production and reinjection rates become equal in Scenario 1.

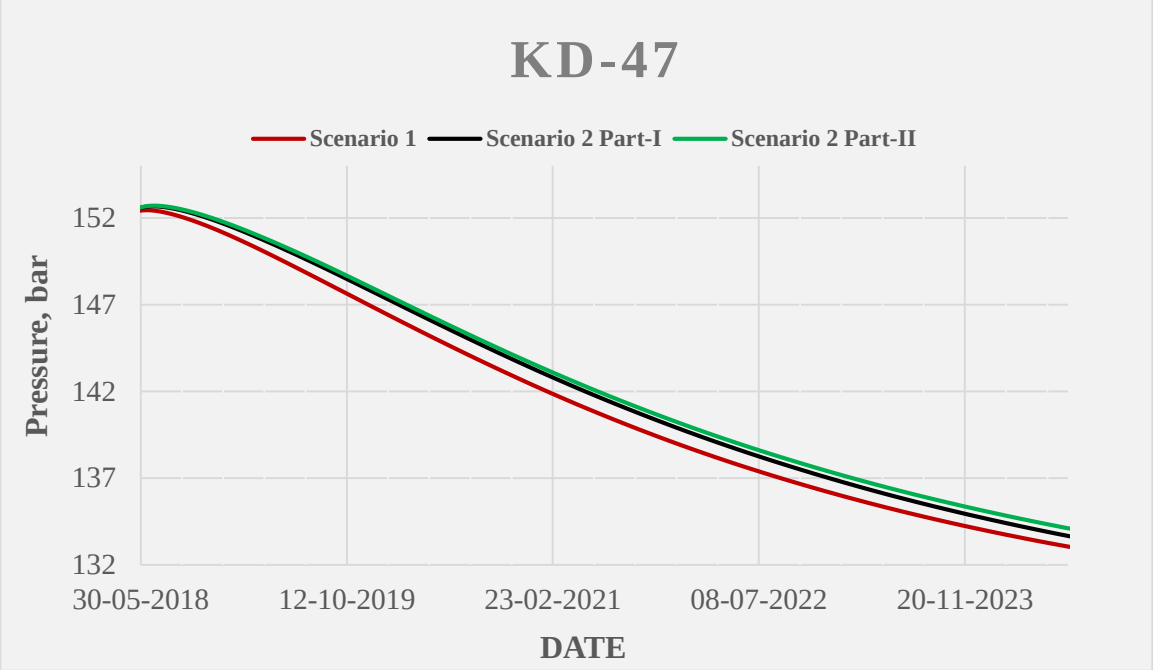

Figure 5.63 Comparison of Scenario 2 and Scenario 1 (Strategy 2)

At the end of the 20 years, total produced water amount increased moderately when carbon dioxide is included in the reinjection scenario. Considering the near future (until the end of 2023, run time of the Scenario 1), total produced water (after removal of carbon dioxide) amounts are shown in the table below. Also, two parts of the second scenario are compared for the next 20 years.

	Total Produced Water, tonnes		
Time Period	Scenario 1	Scenario 2 - Part I	Scenario 2 - Part II
2018 - 2023	263,700,000	266,180,000	268,000,000
2018 - 2038	-	903,100,000	905,610,000

Table 5.9 Total produced waters for the first and the second scenarios

Injecting all the produced water through the injection wells increases the total produced water (part I). Compared to the first scenario, where current reinjection rates are repeated until the production rates decrease and become equal to the reinjection rates (until the end of 2023), the total production is increased approximately 2.5 million tonnes of water. If the carbon dioxide is included in the reinjected fluid (part II), the increase becomes 4.3 million tonnes of water. Considering the current total production rate of the Kızıldere Geothermal Field, which is around 6700 tph after the removal of CO_2, the first part of the second scenario provides an extra 375 hours of energy production, while the second part provides 640 hours of extra energy production until the end of 2023.

Effects of the increased reinjection scenarios can also be investigated by comparing the dates when the wells reach their critical production rates (determined as 25% decline compared to the May 2018 rates). Recall that productions of 12 wells declined 25% before the end of the first scenario, where the current reinjection rates were repeated for the next years. The following table shows the shifts in the dates caused by the Part-I and Part-II of the second scenario.

Scenario 1		Scenario 2 Part I	Scenario 2 Part II
KD-68B	02.04.2020	**+12 days**	**+17 days**
KD-62	02.04.2020	**+27 days**	**+32 days**
KD-61	17.04.2020	**+27 days**	**+32 days**
KD-68A	28.11.2020	**+42 days**	**+47 days**
KD-62A	11.02.2021	**+27 days**	**+47 days**
KD-58A	23.11.2021	**+72 days**	**+92 days**
KD-61A	23.11.2021	**+72 days**	**+92 days**
KD-90B	22.05.2022	**+87 days**	**+107 days**
KD-66A	04.09.2022	**+87 days**	**+122 days**
KD-89	04.09.2022	**+87 days**	**+122 days**
KD-25B	02.04.2023	**+87 days**	**+122 days**
R-5	30.08.2023	**+87 days**	**+137 days**

Table 5.10 Shifts in the 25% production decline dates in the Scenario 2

Locations and completion depths of the injection wells prevents to have higher impacts with higher injection rates. The pressure support by the extra injection is only limited, which increases the production rates only moderately. This situation can also be seen by comparing the carbon dioxide productions in the Part-I and Part-II. The increase is not significant, and mainly due to the increase in the production rates. It means that the reinjected carbon dioxide does not flow into the production zone with a significant rate. Following table shows the carbon dioxide productions obtained from the scenarios.

	Total Produced CO_2, tonnes		
Time Period	**Scenario 1**	**Scenario 2 - Part I**	**Scenario 2 - Part II**
2018 - 2023	**7,630,000**	**7,645,000**	**7,745,000**
2018 - 2038	**-**	**25,660,000**	**26,000,000**

Table 5.11 Total produced CO_2 for the Scenario 1 and Scenario 2

Although there are significant temperature reductions in the shallower sections (main reinjection areas), flowing enthalpies show negligibly small changes in both parts of the Scenario 2 when compared to the Scenario 1 at the deep metamorphic production zones. This further explains the moderate impact of reinjecting all of the produced water and CO_2 on the production rates, flowing enthalpies, and CO_2 rates.

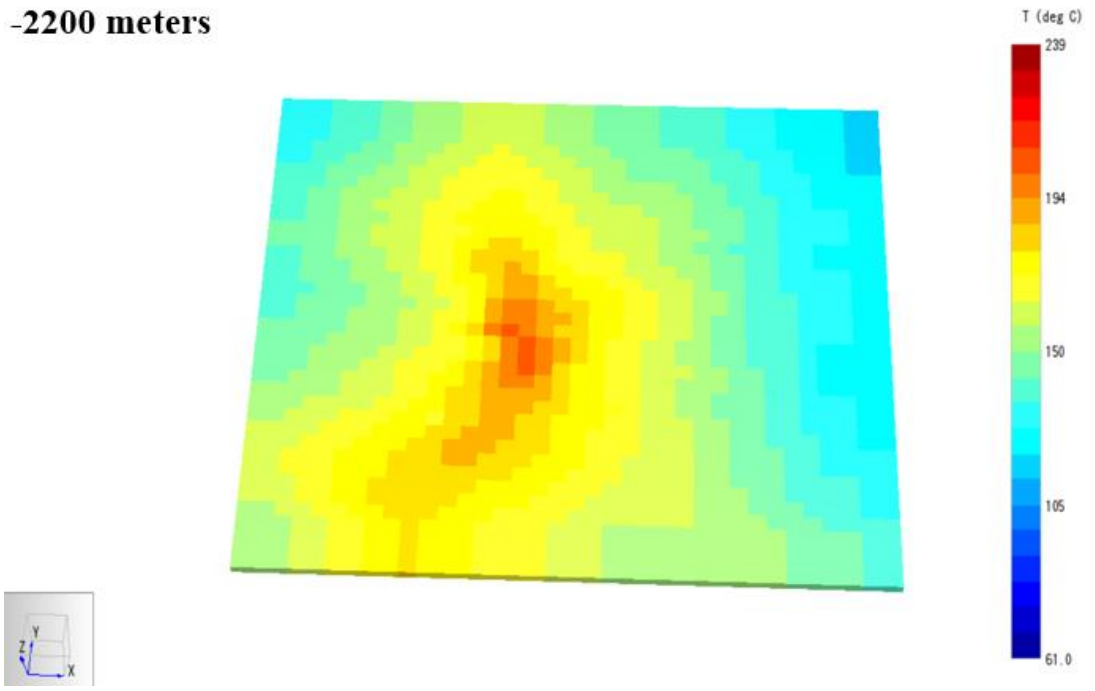

Figure 5.64 Temperature distribution at 2200 meters in 2038 (Part I)

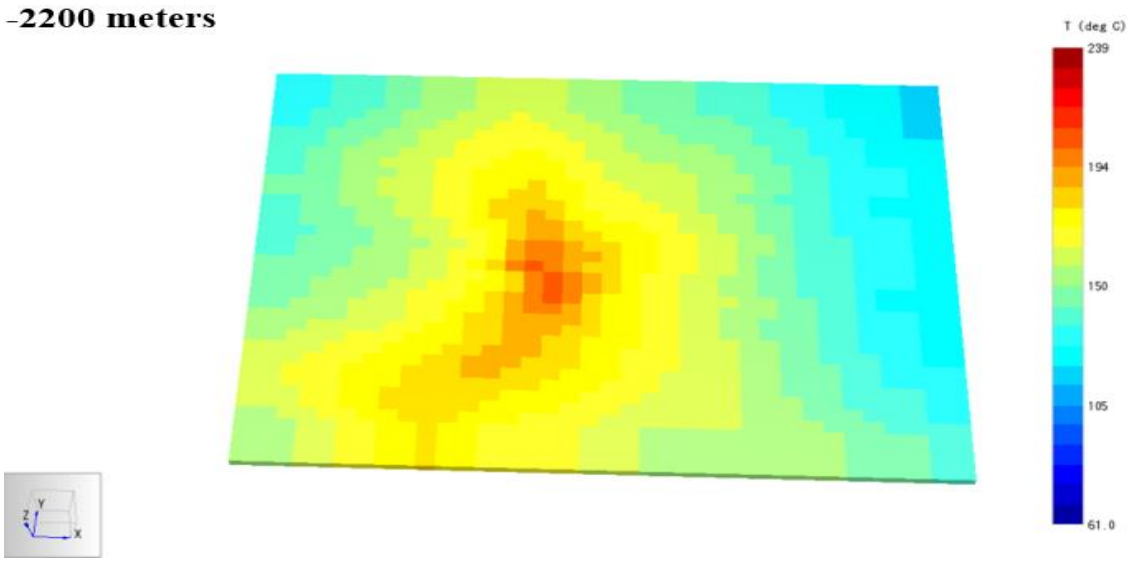

Figure 5.65 Temperature distribution at 2200 meters in 2038 (Part II)

The CO_2 distribution in the Part-I of the Scenario 2 is very identical to that of the Scenario 1. But in the Part II, where the produced CO_2 is assumed to be captured and reinjected, less CO_2 dilution is observed in the shallow depths. Dilution caused by the deep reinjection wells, KD-44 and KD-46, at the deeper sections are also disappeared in the Part II.

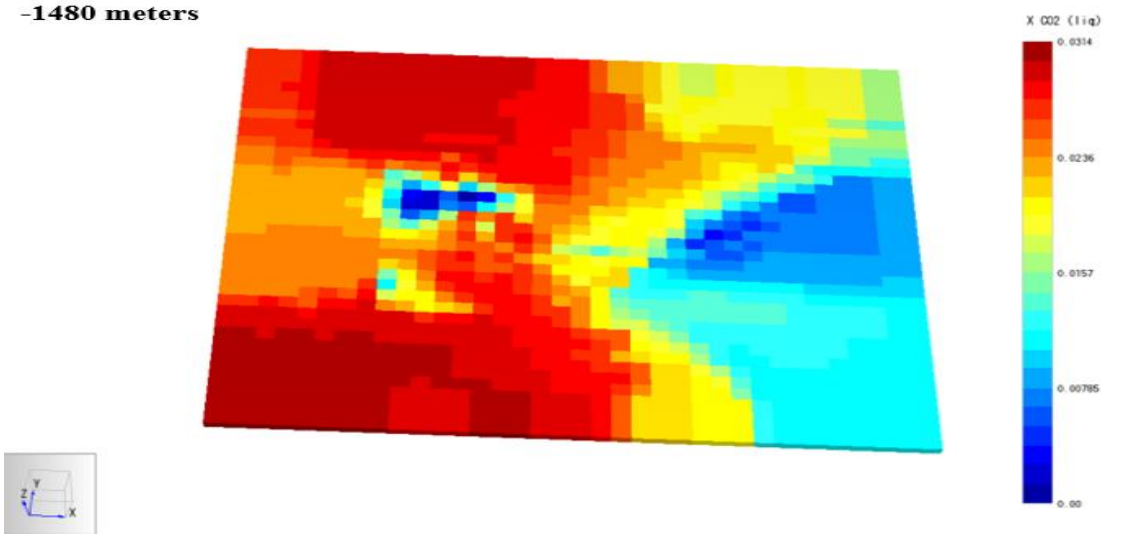

Figure 5.66 Scenario 2 Part I – CO_2 distribution at 1480 meters in 2038

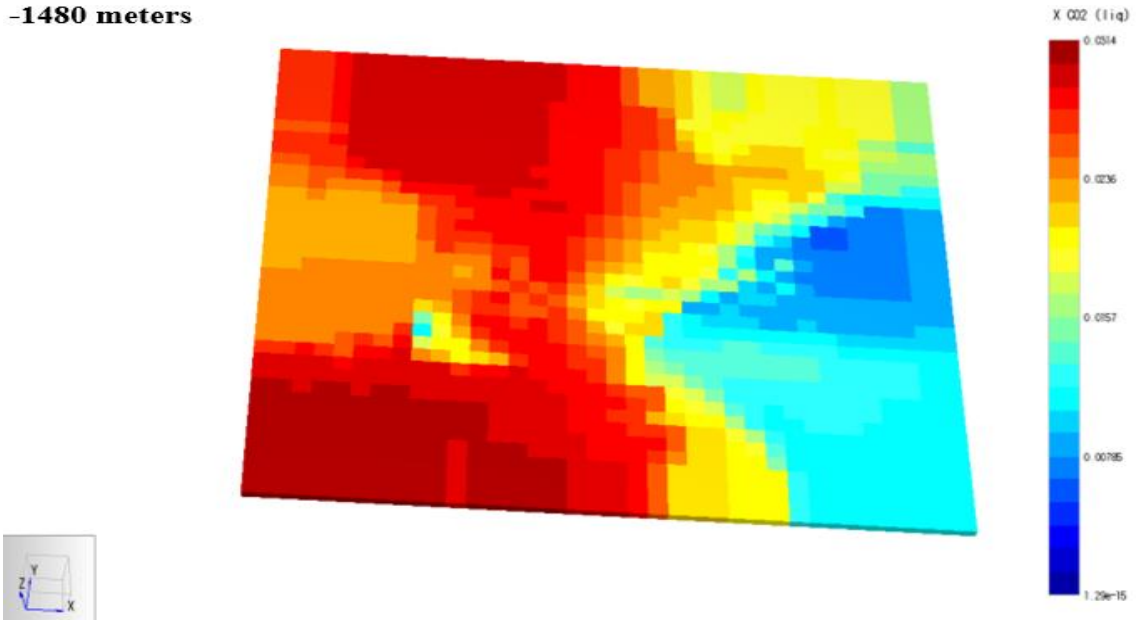

Figure 5.67 Scenario 2 Part II – CO_2 distribution at 1480 meters in 2038

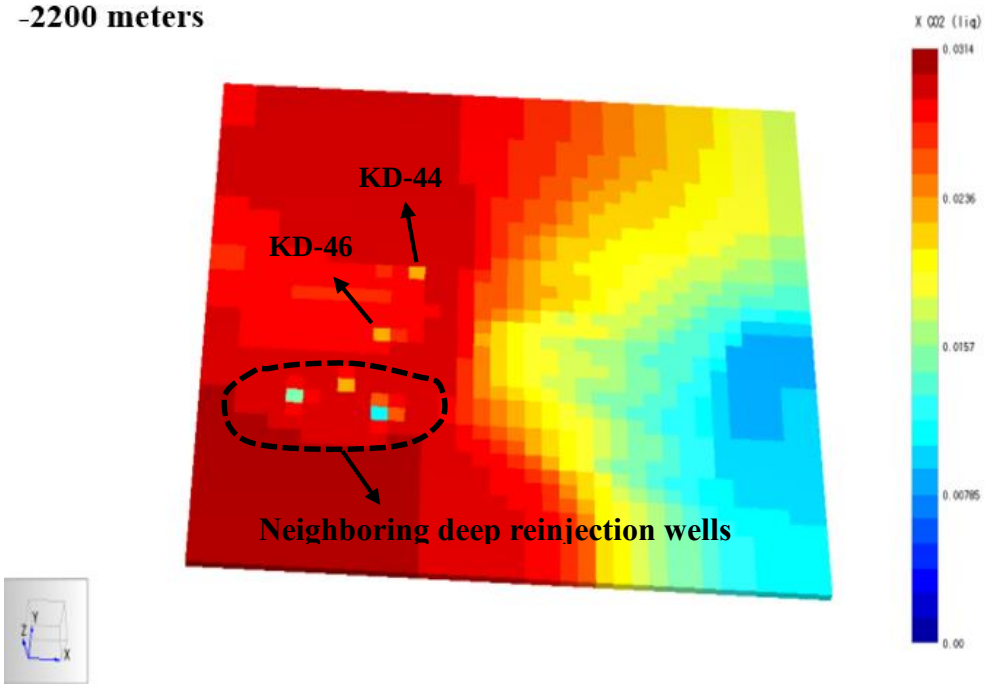

Figure 5.68 Scenario 2 Part I – CO_2 distribution at 2200 meters in 2038

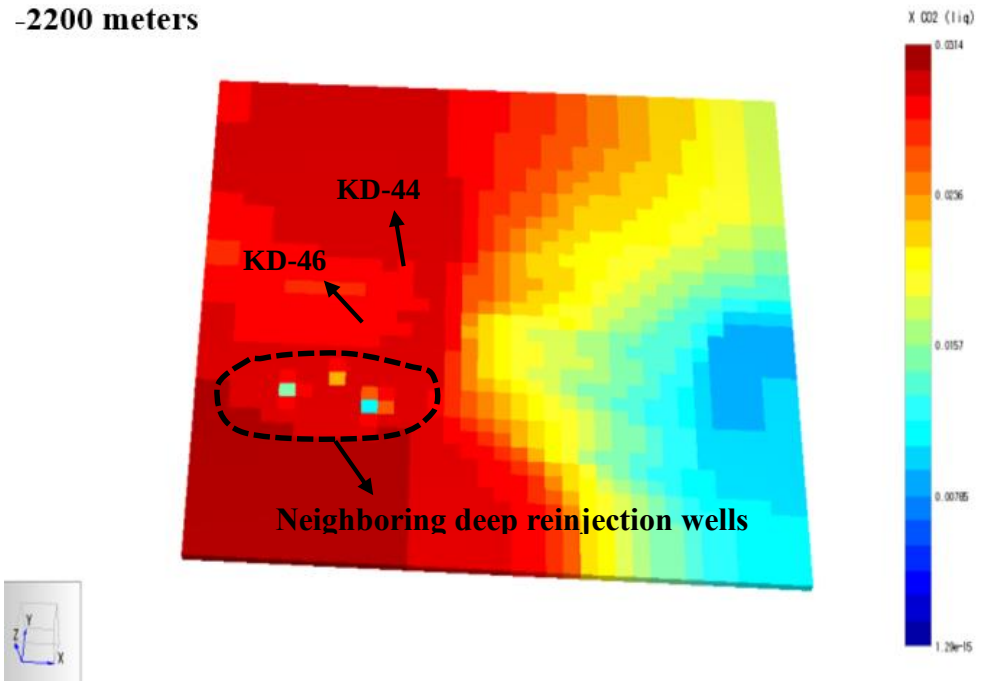

Figure 5.69 Scenario 2 Part II – CO_2 distribution at 2200 meters in 2038

5.2.3 Scenario 3: Carbon Dioxide Injection

In this section, the two parts of the Scenario 3 are repeated with the Strategy 2. The general features are the same as described in section 5.1.3. In both of the 10wt% CO_2 injection and 200 tph supercritical CO_2 injection scenarios, current water reinjection rates were kept constant. To make a healthy comparison, the Scenario 1 extended to the end of 2038 with a total reinjection rate of 5200 tph, although the production rate declines to below 5000 tph at the end of the simulation. The resultant effects of large amount of CO_2 injection are investigated by comparing the reservoir pressure decline, water and CO_2 production rates, and flowing enthalpies of the KD-47, the well with the highest production rate.

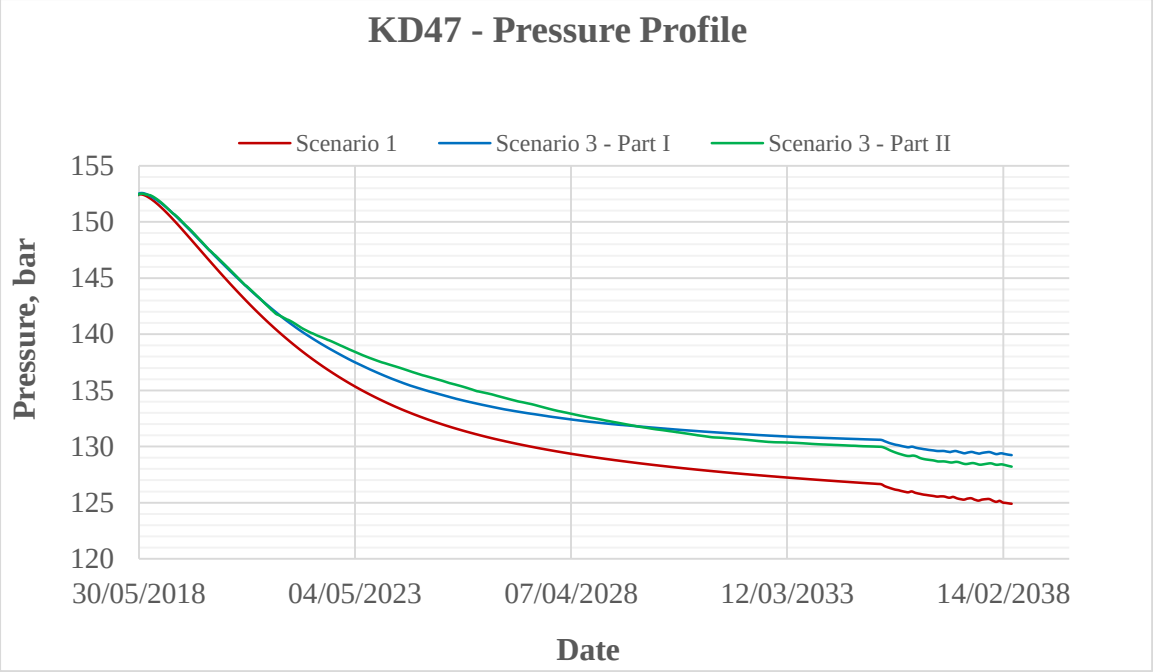

Figure 5.70 Pressure support due to extra CO_2 injections – Scenario 3

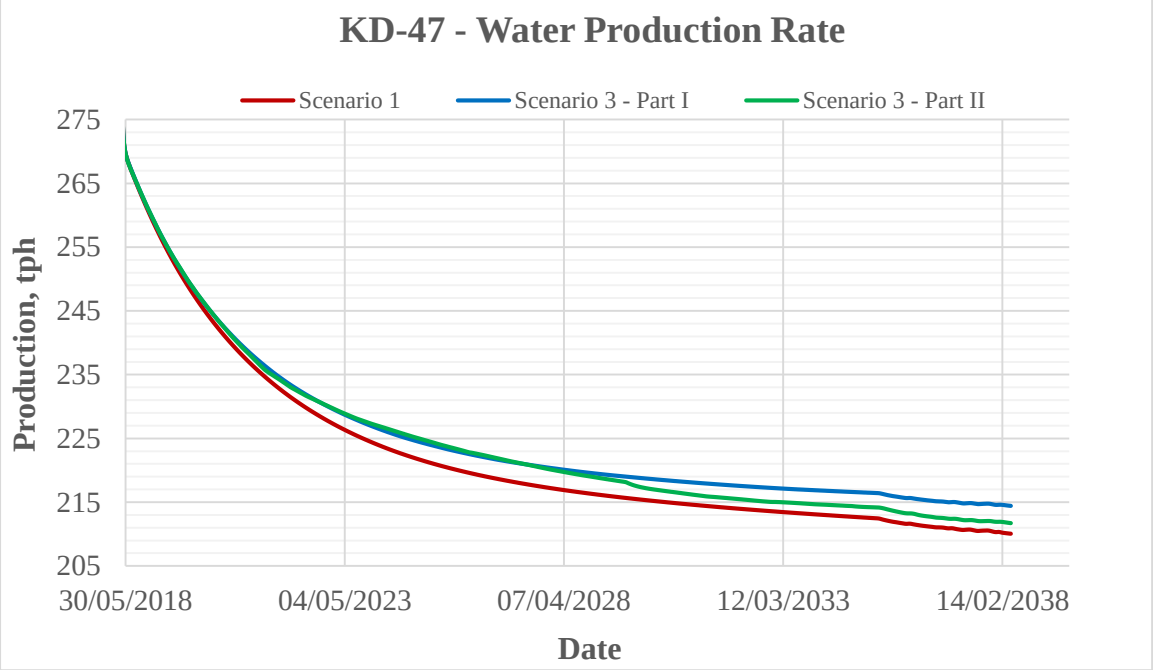

Figure 5.71 Water production rates of Scenario 1 and Scenario 3

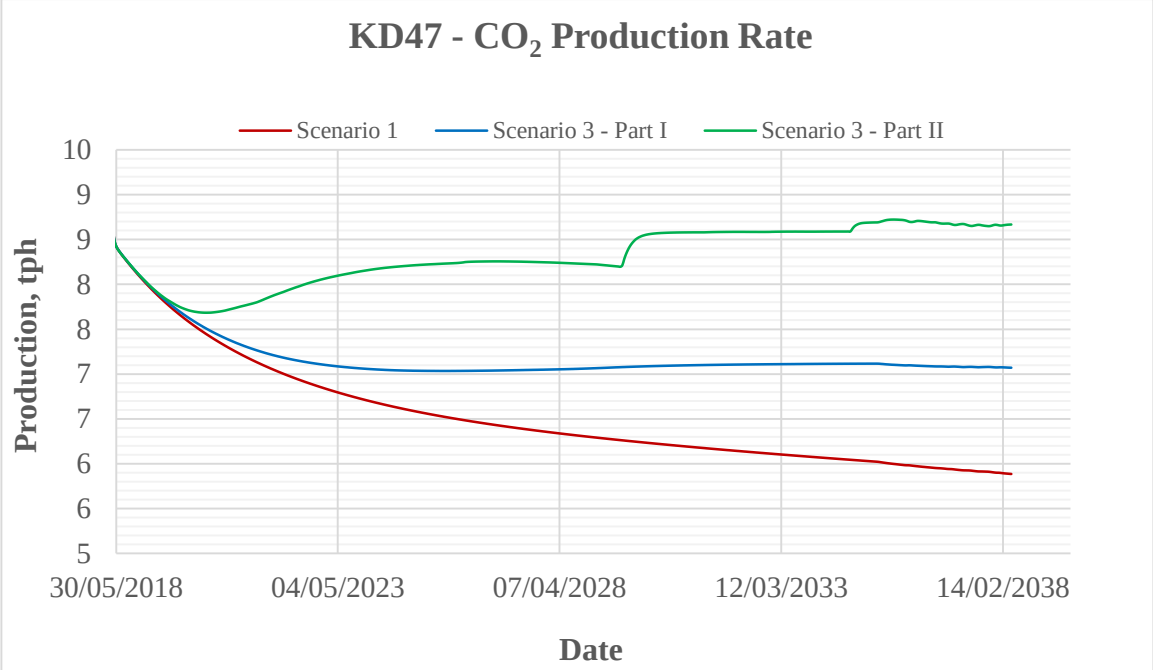

Figure 5.72 Increase in the CO_2 production due to large amount of CO_2 injection

The CO_2 distribution is affected significantly in the both parts of the 3rd Scenario. As expected, the changes are higher at the shallow sections and especially in the north-western region. In the 10% CO_2 injection scenario (Part-I), high CO_2 ratios are observed at the north-western injection zone. In the supercritical CO_2 injection scenario (Part-II), it is observed that the injected sCO_2 at the north-western region is swept away towards the eastern and south-eastern regions, while sCO_2 from KD-27A is swept towards the west by the reinjected water. The injected sCO_2 from KD-44 and KD-27A moves towards each other. Note that the scales are readjusted in order to clearly distinguish the colors.

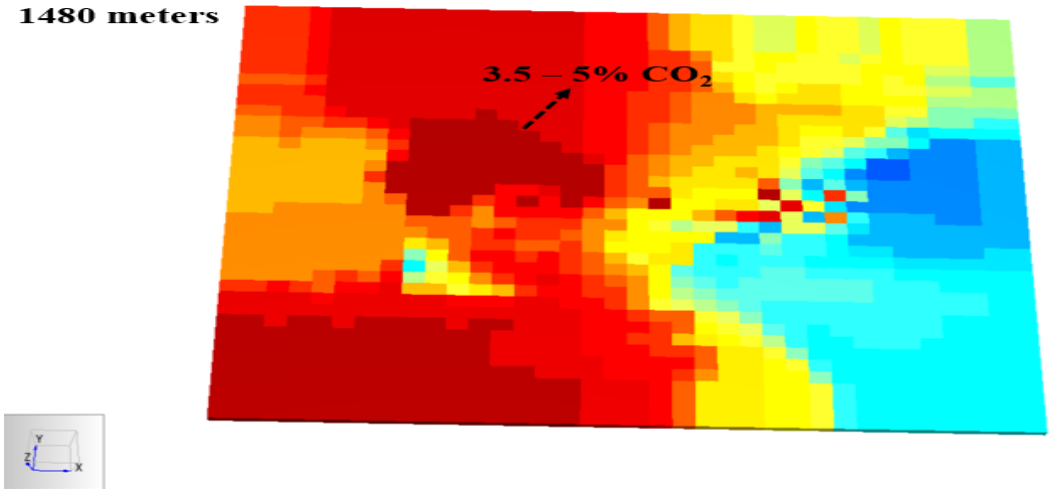

Figure 5.73 Scenario 3 Part I – CO_2 distribution at 1480 meters in 2038

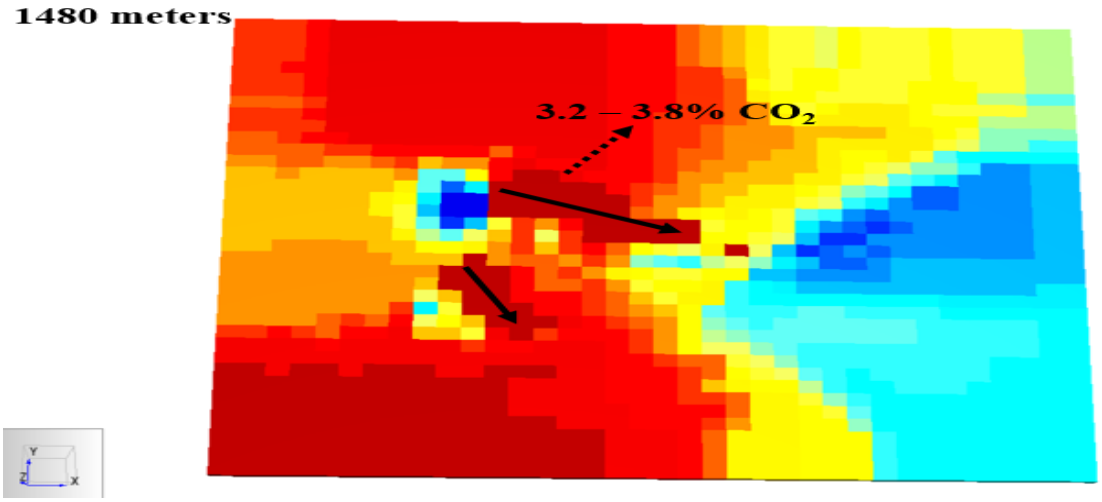

Figure 5.74 Scenario 3 Part II – CO_2 distribution at 1480 meters in 2038

On the other hand, at the deeper sections, as high as 9% CO_2 ratios were observed, mainly at the vicinity of the deep injection wells KD-27A, KD-44, and KD-46.

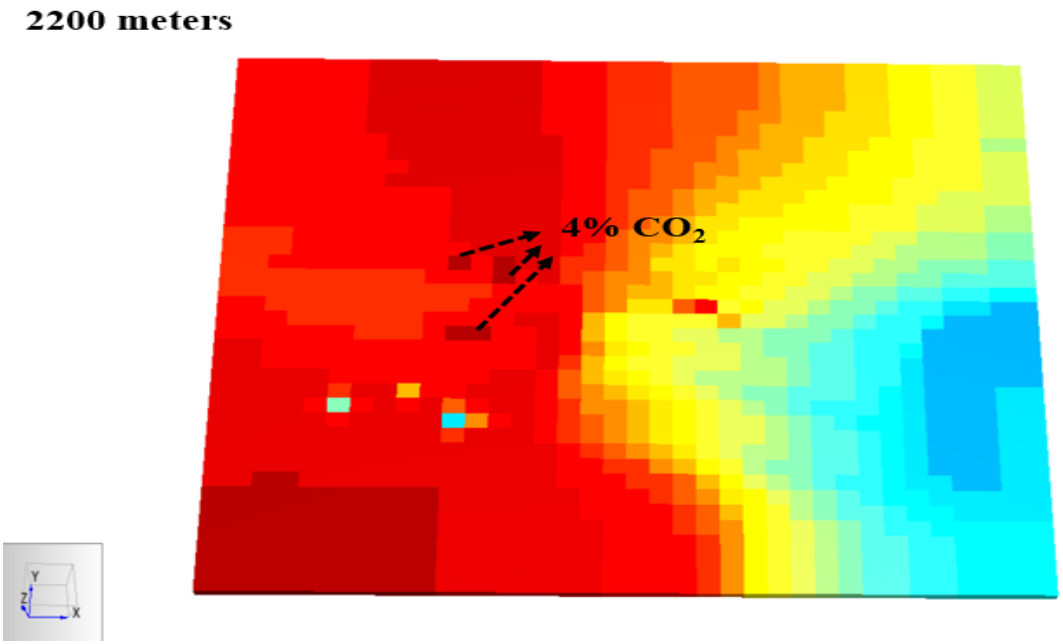

Figure 5.75 Scenario 3 Part I – CO_2 distribution at 2200 meters in 2038

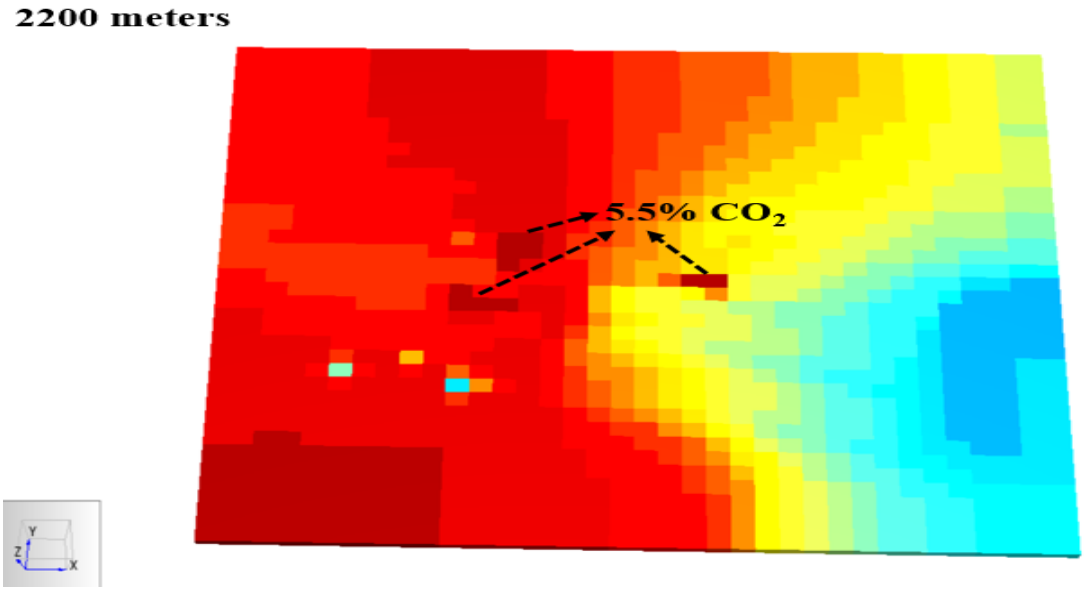

Figure 5.76 Scenario 3 Part II – CO_2 distribution at 2200 meters in 2038

The decline in the flowing enthalpy of KD-47 was recovered less than 10 kj/kg at the end of the both Part-1 and Part-II of the 3rd Scenario, compared to the 1st Scenario. The effects of large amount of CO_2 injection on the flowing enthalpies were found to be less significant in the production zone. In shallow sections, temperature reduction was relatively higher compared to Scenario 1, but not considerably significant.

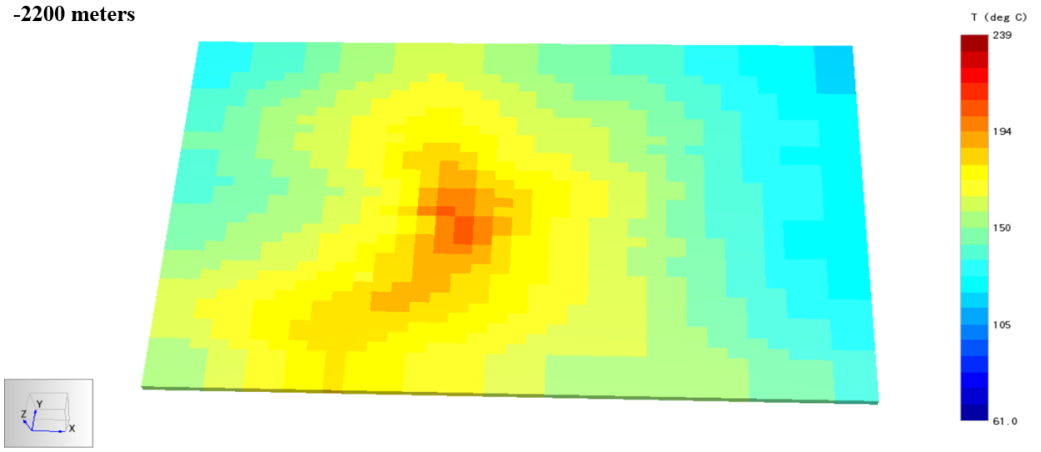

Figure 5.77 Scenario 3 Part I – Temperature distribution at 2200 meters in 2038

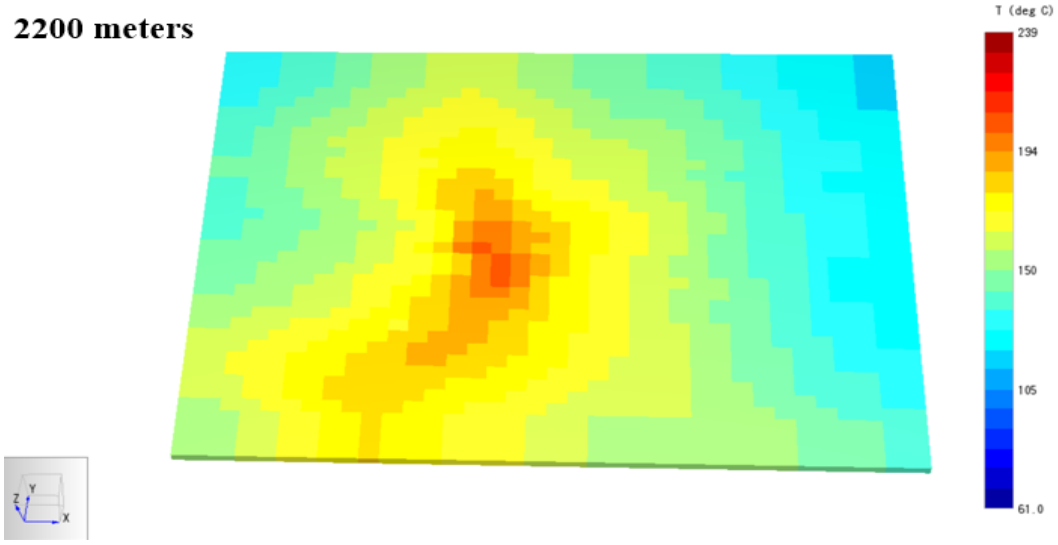

Figure 5.78 Scenario 3 Part II – Temperature distribution at 2200 meters in 2038

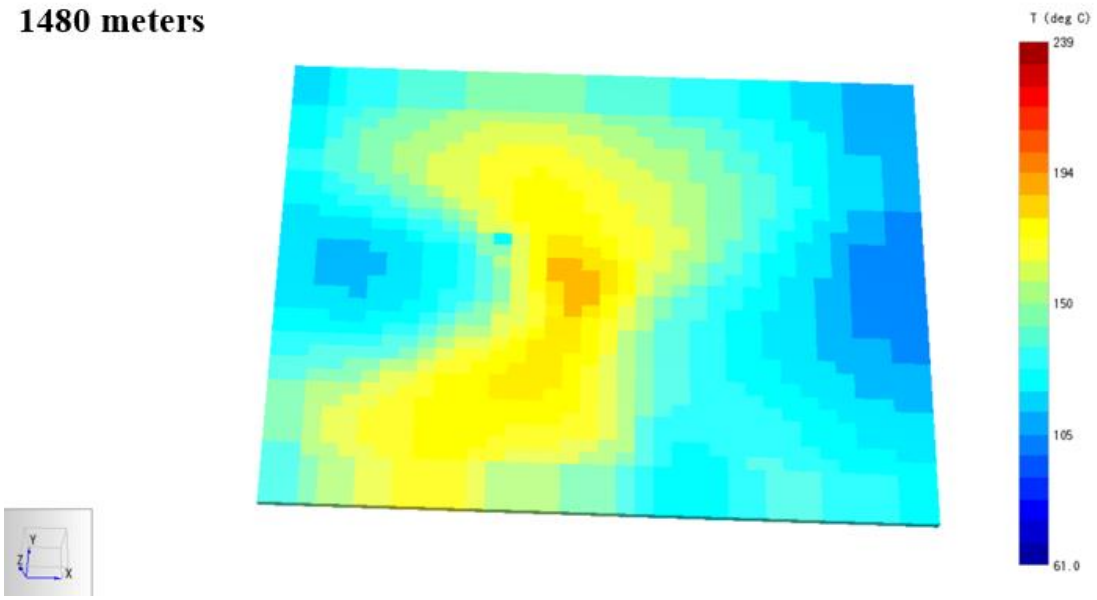

Figure 5.79 Scenario 3 Part I – Temperature distribution at 1480 meters in 2038

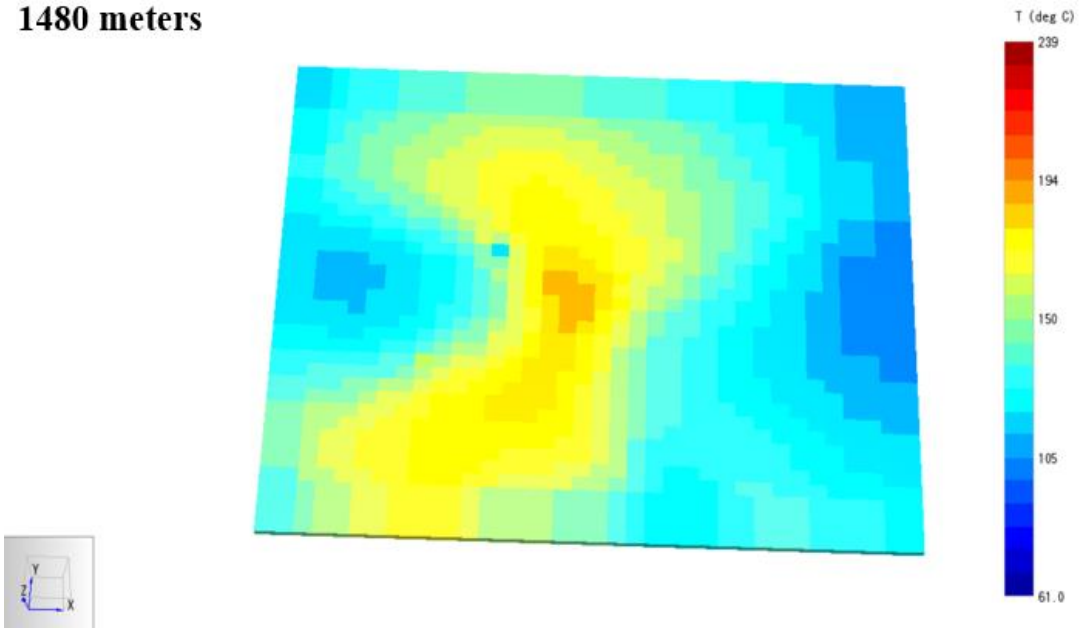

Figure 5.80 Scenario 3 Part II – Temperature distribution at 1480 meters in 2038

The total water and CO_2 productions at the end of the simulations are given in the following tables.

	Total Produced Water, tonnes		
Time Period	Scenario 1	Scenario 3 - Part I	Scenario 3 - Part II
2018 - 2038	902,325,000	915,000,000	904,205,000

Table 5.12 Total produced water at the end of the 1st and the 3rd scenarios

	Total Produced CO_2, tonnes		
Time Period	Scenario 1	Scenario 3 - Part I	Scenario 3 - Part II
2018 - 2038	25,645,000	27,330,000	39,710,000

Table 5.13 Total produced CO_2 at the end of the 1st and the 3rd scenarios

Both 10wt% (520 tph) CO_2 injection and 200 tph supercritical CO_2 injection increased the total water production. Compared to the extended version of the 1st scenario (from 2018 until 2038), the increase was around 1.9 million tonnes of water for the supercritical CO_2 injection scenario, whereas it was around 13 million tonnes for the 10wt% CO_2 injection scenario. Considering the current water production (6700 tonnes), it means an extra 283 hours and 1,900 hours of energy production, respectively.

The pressure support and production increase are more effective in the near-term, until the carbon dioxide production starts to dominate some wells, and reduce their water production. Short term effects can be clearly seen by checking the 25% production decline dates of the previously mentioned 12 wells.

Scenario 1		Scenario 3 Part I	Scenario 3 Part II
KD-68B	18.03.2020	**+35 days**	**+42 days**
KD-62	02.04.2020	**+28 days**	**+27 days**
KD-61	17.04.2020	**+28 days**	**+42 days**
KD-68A	28.11.2020	**+43 days**	**+56 days**
KD-62A	27.01.2021	**+58 days**	**+71 days**
KD-58A	23.11.2021	**+110 days**	**+111 days**
KD-61A	23.11.2021	**+118 days**	**+131 days**
KD-90B	22.04.2022	**+193 days**	**+210 days**
KD-89	21.07.2022	**+219 days**	**+165 days**
KD-66A	04.09.2022	**+189 days**	**+218 days**
KD-25B	01.02.2023	**+309 days**	**+83 days**
R-5	01.07.2023	**+369 days**	**+354 days**

Table 5.14 Shifts in the 25% production decline dates in the 3rd scenario

One of the most important effects of injecting high amount of CO_2 into a geothermal reservoir is that as the partial pressure of the CO_2 increases, boiling is promoted. In the 3rd scenario this situation observed clearly by means of increasing the produced gas ratio. As much as 85% gas ratios were observed especially in the production wells completed at shallower depths and closer to the injection wells, such as KD-2A, KD-9A, KD-25B, KD-42, KD-47, KD-54, and KD-64. As an example, increase in the produced gas ratio at the top of the completion depth of KD-42 is shown in the figure 5.31, for the 200 tph supercritical carbon dioxide injection scenario. At that depth, the CO_2 partial pressure increased from 70 bar to 100 bar at the end of the simulation, and as high as 6.7wt% dissolved CO_2 value was observed.

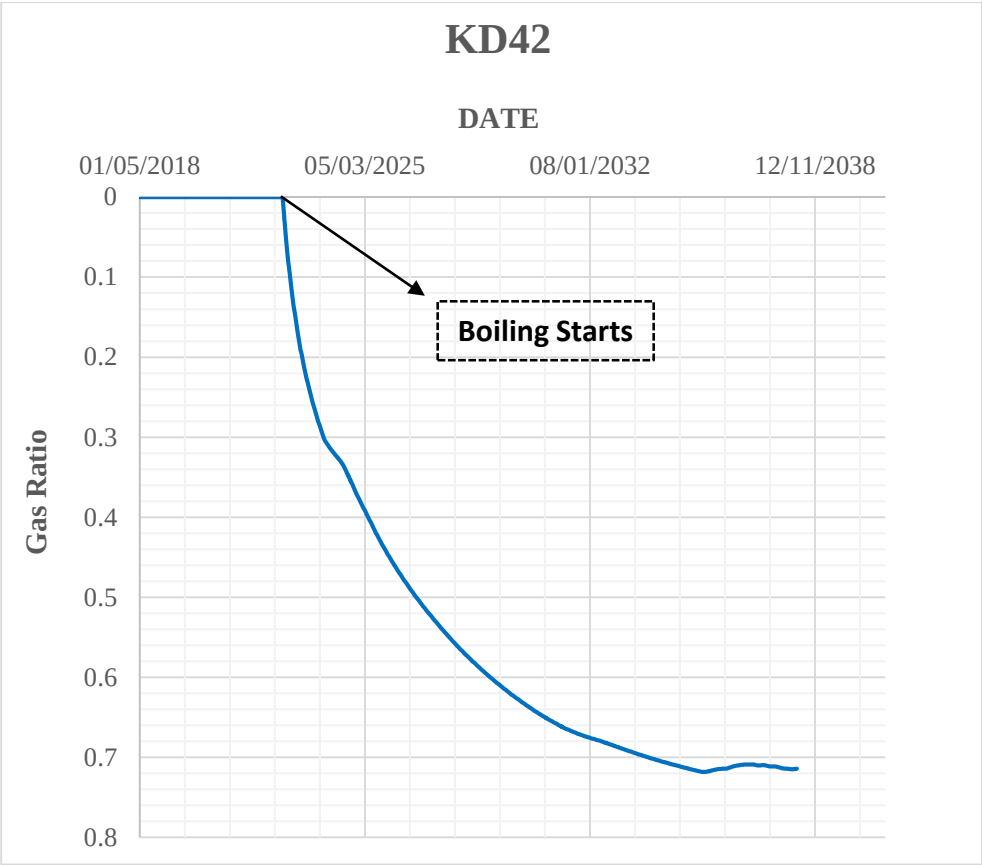

Figure 5.81 Increase in the produced gas ratio of KD-42

Boiling is found to take place mainly in shallow depths. The following figures illustrates the specific gravity distribution in -1480 meters, actually showing the places where gases came out due to the increase in the CO_2 ratios as a result of CO_2 injections. Although boiling is observed at deeper sections, especially at the vicinity of KD-27A, KD-44, and KD-46 in the supercritical CO2 injection scenario, their extent was only limited.

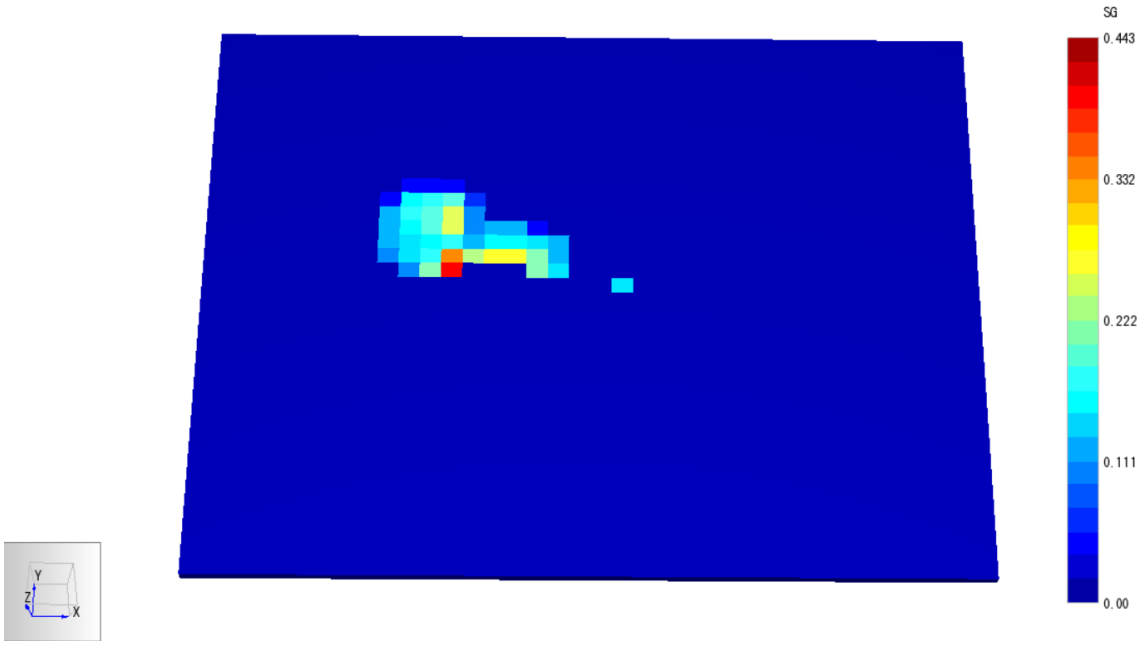

Figure 5.82 Scenario 3 Part I – Specific gravity distribution at 1480 meters in 2038

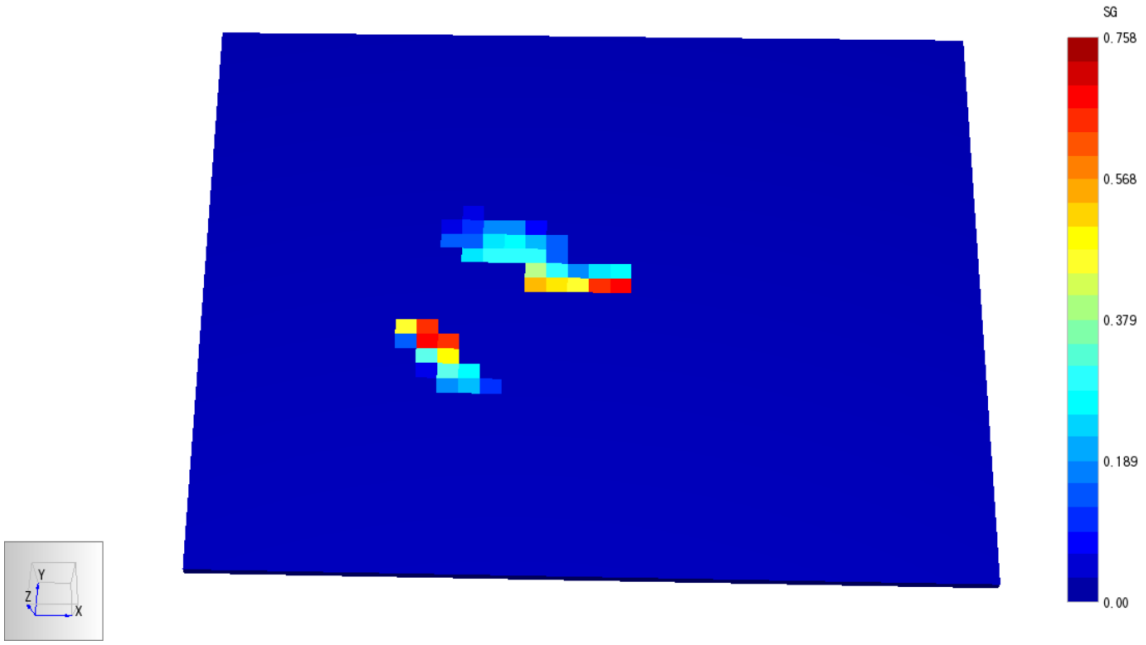

Figure 5.83 Scenario 3 Part II – Specific gravity distribution at 1480 meters in 2038

CHAPTER 6

DISCUSSION

- The first and the most important part of the modeling of the Kızıldere Geothermal Field was collecting and interpreting as much and as accurate data as possible. The conceptual model of the field was constructed based mainly on the data from seismic analysis, geophysical surveys (resistivity, magnetic, gravity), pressure transient analysis, and well logs. Instead of relying on a single source of data, all these sources were utilized collaboratively.

- Previous studies have shown that three formations have reservoir characteristics in Kızıldere Geothermal Field, which are from top to bottom; Sazak Formation, İğdecik Formation, and the deep metamorphics. Kolankaya Formation (on top of Sazak Fm.) and Kızılburun Formation (on top İğdecik Fm.), and impermeable unconformities on top of the deep metamorphic rocks are the caprocks of these reservoirs. Seismic and drilling studies have shown that İğdecik Formation and deep metamorphic rocks gets shallower at the northern – north western sections of the field. Currently, İğdecik Formation is targeted for reinjection purposes, while the deep metamorphics are the main production sections. There is no an active operation currently in the Sazak Formation.

- Kızıldere Geothermal Field is a liquid-dominated geothermal system. Convective forces are the dominant heat flux sources in the field. Geochemical studies have

shown the geothermal water of the Kızıldere Geothermal Field has a meteoric origin, mainly collected at the highs of the Buldan Horst and penetrates into the deeper sections through the flow conduits. Fluid is heated up at the deeper parts of the field, and rises towards upper sections through faults and fractures, as a result of buoyancy. According to geochemical interpretations, the geothermal fluid of the field shares the same common parent fluid, meaning that there is likely only one high temperature up-flow zone.

- Among others, fault characteristics, caprock thicknesses, and formation permeabilities were found to be the main geological and hydrogeological properties of the model. The NE-SW trending strike-slip Gebeler Fault and the fractures at the vicinity of this fault were found to be the most dominant features in the fluid circulation network of the model. Fault properties (shape, angle, depth) and caprock thicknesses were determined using mostly the well log and drilling data. Permeability values were determined quantitatively by using the pressure transient analysis, but mostly considered qualitatively since the investigation area of the PTAs were only limited; long measurements were restricted by high temperatures. All properties have been adjusted according to the simulation results throughout the course of the study. The caprock overlying the deep metamorphics were found to be very effective, resulting in a hotter reservoir (almost 40 °C) than the İğdecik Formation. The caprock permeabilities were assigned in the range of 0.5 – 5 mD, horizontally, and 0.05 – 0.5 mD, vertically.

- Petrasim interface and TOUGH2 simulation codes have been used to visualize the conceptual model, and carry out simulations on the model, respectively. The areal extent of the constructed model is around 200 km^2; 15.9 km in E-W direction, and 12.9 km in N-S direction. But, the main study area, where most of the wells are located, covers only half of that value. The reason to have a larger model is to include the potential effects of production/injection operations of neighboring geothermal power plants, and also to be able to include the possible future operations out of the current operation area into the model easily. The highest point

on the surface is 1,114 meters above the sea level, and the total depth is taken to be -5,000 meters below the sea level.

- During initial studies, the model was divided into 11,000 grid blocks, where the required computational power was lesser and simulation time was short. But since the distances between adjacent wells in Kızıldere geothermal field are around 500 meters, the grid size should be less than that to represent each well individually. As a result, grid sizes were downscaled and the model was divided into 24,000 grid blocks. The following table shows the dimensions and distributions of the grid blocks in x-y directions (x is in the E-W direction; y is in the N-S direction).

X, East to West		Y, North to South	
Number of Grids	**Grid Size, m**	**Number of Grids**	**Grid Size, m**
2	750	2	970
30	354.7	30	265
2	750	1	1000
1	2250	1	2000
Total: 15890m		**Total: 12890m**	

Table 6.1 Grid size distribution along the model area

- The upper layer of the model was set at -100 meters. The reason behind this is to set an upper reference depth below the sea level. In the z-direction, the model was divided into 18 layers where the first 16 layers (to the depth of -3000 meters) are relatively thinner and the bottom 2 layers are relatively thicker. Since most of the production wells reach out to the depth of -3000 meters, this section (-100 meters to -3000 meters) was divided into more and thinner layers to increase the resolution and to get more detailed information from the simulation.

- The outer boundary grids were kept relatively bigger compared to inner sections, since these cells are actually away from the main study area, and it is desired to minimize the interactions between outer boundary cells and the cells in the main

study area. Conversely, it desirable to have grid sizes as small as possible in the main study area (around the wells and faults), in order to be able to better represent the variations and heterogeneities, and also to make necessary changes more elaborately, according to the results of the simulation, throughout the study.

- The initial pressure/temperature values were assigned by using the static measurements conducted at the drilled wells. During the initial studies performed by Directorate of Mineral Research & Exploration, more than 20 shallow and intermediate-depth wells (Phase-I) were drilled in the Kızıldere Geothermal Field. It can be said that, the measured parameters (temperature, pressure, CO2, etc.) were reflecting the natural state conditions, since there was no any fluid removal from the system. But compared to the areal extent of the model, those wells were covering only a small area in the field, and these wells were not reaching deep metamorphic rocks. After the acquisition, Zorlu Energy drilled many wells for the Phase-II (2013) and Phase-III (2017) power plants, many of them were reaching as deep as 3500 meters (below the sea level). Although these new wells provide more information from a larger area, parameters obtained from these wells could not be used directly as the initial state conditions for our simulation, since the field was under exploitation, and perturbations caused by production and injection wells were affecting the pressure-temperature-CO2 distributions and natural flow pattern. However, information coming from the new wells, together with the previous wells, could be considered as a good starting point to obtain the natural state conditions (i.e. pre-production conditions, initial state conditions). So, initial pressure and temperature values were assigned by combining the data from initially and recently drilled wells, and they have been adjusted and modified throughout the study.

- The pressure/temperature values of the top layer were set as fixed state, meaning that these values stay constant throughout the simulation. By that way, the cooling effects of the rain waters entering to the system are simulated in the model. In addition to the fixed state top layer, a cold water source was placed into the shallower İğdecik Formation at the bottom of the Buldan Horst. A 13 km^2 hot

water source was placed at the bottom of the model. The water and CO_2 fluxes from this source are 27.5 kg/s and 1.1 kg/s (4wt%), respectively. The water and CO_2 enthalpies are 1000 kj/kg and 700 kj/kg, respectively. The conductive heat flux is 0.7 Joule/s/m^2 through an area of 9 km^2 inside the same source.

- Salinity and non-condensable gas (NCG) contents of geothermal fluids are important parameters, and their presence must be taken into account in a reservoir simulation. For Kızıldere geothermal fluids, especially the carbon dioxide (CO_2) content is of a great importance, since it has considerable effects on the reservoir parameters, and surface and subsurface operations. Although there is not a continuous CO_2 measurement well by well, studies showed that 1.5wt% dissolved CO_2 comprises the water produced from İğdecik Formation, and this value increases to 3 – 3.5wt% for the water coming from the deeper metamorphics. The carbonate rocks such as marble and limestone are the sources of the CO_2 found in the geothermal fluid of Kızıldere Geothermal Field. But in this simulation, CO_2 is introduced only from the bottom source and its distribution depends only on the natural flow pattern and caprock properties. So, satisfying the above-mentioned CO_2 levels in corresponding formations is also a good measure of the flow characteristics of the model.

- The production and injection wells are the inner sources and sinks. As of May 2018, there are 34 production wells (10 of Phase-II and 24 of Phase-III) with a total production rate of 6900 tonnes per hour, and 27 injection wells with a total reinjection rate of only 5200 tonnes per hour. 6 production wells of Phase-I power plant ceased operating at the beginning of 2018. Most of the production wells penetrate into deeper sections of the metamorphics, while majority of the reinjection wells were completed in the shallower İğdecik Formation. The reinjection wells are mainly located at the eastern and north-western regions of the field. Production wells have been drilled mostly along NE-SW direction, targeting the fractured sections around the strike-slip Gebeler Fault.

- After the construction of the model based on the above-mentioned field characteristics, and after assigning the initial and boundary conditions, it must be simulated for a long time, until the stabilization of the reservoir parameters is achieved. It is found in this study that 700,000 years were long enough for the model to reach the stabilized conditions, the natural state conditions.

- Based on the natural state model of the Kızıldere Geothermal Field, simulations can be carried out for future predictions. But firstly the model must be validated that it is a good representation of the Kızıldere Geothermal Field, before proceeding further.

- To validate the constructed model, the natural state model must be compared with the actual field data (pressure/temperature). But the main issue of making a healthy comparison is that majority of wells have been drilled only recently, long after the perturbations have been started in the field, thus the measured static pressure/temperature values are not representing the natural state condition of the actual field. In order to avoid making such erroneous comparisons, the natural state model have been tested with the actual field data at the measurement date while the field is under operation.

  The following four steps have been applied:

  1. Run the model for 700,000 years (until it reaches stabilized conditions).
  2. Insert the production/injection histories of the wells between 1984 and 2018.
  3. Compare the measured and simulation parameters at the measurement date.
  4. If the differences between the simulation and measured parameters are higher than a predetermined level, make necessary changes and adjustments and rerun the model. If the differences are small enough, this model is a good representation of the natural state conditions of the field.

- Calibrations and adjustments have been made according to the differences between the actual and the measured data. The most effortful studies have been made to determine the temperature profiles, both vertically and laterally. Mostly,

permeability and fault properties (especially the angle and extension) were calibrated, since convective heat flow is dominant in the Kızıldere geothermal field. The amount and enthalpy of the mass flux from the bottom heat source and the shallower cold water source were other important calibration parameters.

- The confidence interval for the validation of the natural state model was taken as 10%. It means that the model was calibrated until the pressure and temperature values obtained from the simulation are in the range of 10% (or less) of the actual pressure and temperature measurements. Results have shown that 10% error target was successfully satisfied. In addition to the static pressure and temperature matches, pressure profiles of 15 observation wells were also matched with a great accuracy.

- Pressure behavior of the observation well KD-23A is quite inconsistent, implying that human interventions might be effecting the measured pressure. But the simulation results are still in an acceptable range of error.

- Although shallow depths are not the main focus of this study, dynamic pressure profiles of two shallow observation wells, KD-7 and KD-9, are matched with a great consistency.

- Unstable profiles of two western-most observation wells, KDE-8 and KDE-12, may be due to the production/injection operations occurring in the neighboring geothermal field.

- The future predictions were made mainly on the effects of different reinjection operations. Lesser water reinjection rates than the production rates, and also releasing the produced CO_2 into the atmosphere are the current situation of the Kızıldere Geothermal Field, and they have negative effects both on the reservoir management targets and on the environment.

- The three main scenarios have been simulated under two different strategies. The three main scenarios are:

Scenario 1: No-change in the current situation

Scenario 2: Reinjecting what is produced

Part-I: Only water is reinjected, and CO_2 is released into the atmosphere,

Part-II: All of the produced CO_2 and water are reinjected

Scenario 3: Carbon Dioxide Injection

Part-I: 10% CO_2 injection with current reinjection rates

Part-II: Reinjecting the produced CO_2 in supercritical state

And the two strategies are:

1. Keeping the production rates as constant as possible in exchange for the wellhead pressures.
2. Keeping the wellhead pressures as constant as possible by arranging the production rates.

The first strategy is currently applied in the Kızıldere Geothermal Field.

- Both of these strategies have their own advantages and disadvantages. For example, in the first strategy, energy extraction is maximized in the short term, but the reduction of the reservoir pressures may reach the critical levels more quickly due to the high amount of withdrawal from the reservoir. On the other hand, the second strategy provides moderate extraction rates compared to the first strategy, but it provides a much more balanced reservoir management in terms of the pressures. So, instead of keeping production rates as high as possible, applying the second strategy would yield a better management of the field in the middle and the long term.

- The following figure compares the reservoir pressure profile of KD-47 in Scenario 1 under both Strategy 1 and Strategy 2.

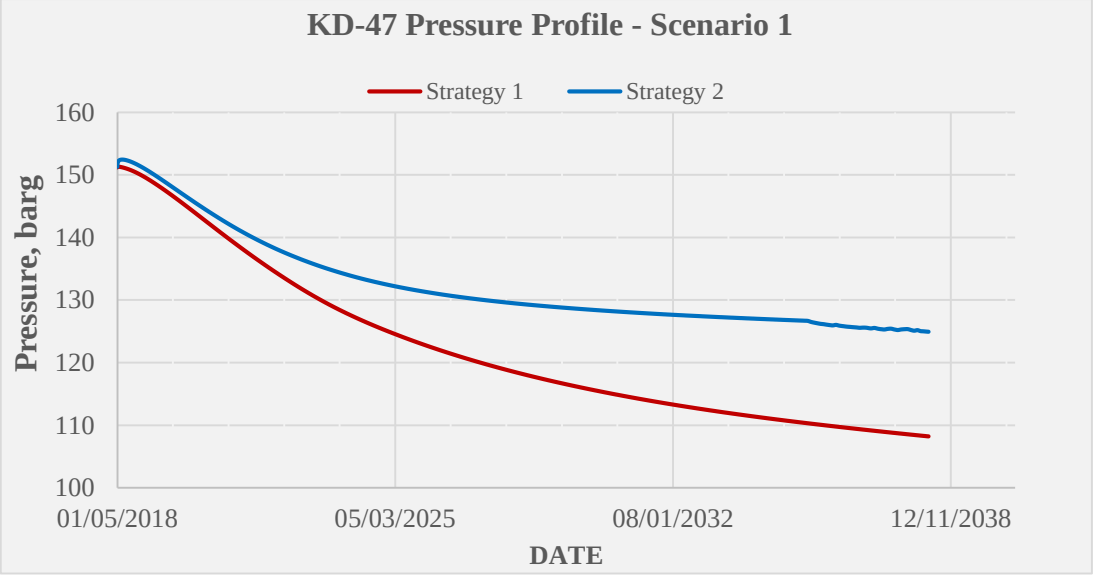

Figure 6.1 Pressure profile of KD-47 in Scenario 1, under Strategy 1 and Strategy 2

- The field has been operated by applying the Scenario 1 so far. When the simulation is converted to Strategy 2, sharp declines in the production rates are observed, implying that the current production rates are not suitable for the current reservoir pressures. So, it can be deduced that fluid withdrawal in the Kızıldere Geothermal Field is so fast and may cause sharp pressure declines in the short term.

- In all of the above mentioned scenarios, extra reinjection rates provided only a moderate, and even insignificant support to the reservoir pressures under the corresponding strategy. This situation can be explained by the locations and the completion depths of the reinjection wells. Most of the reinjection wells have been completed at shallower depths compared to the production wells, which means that the injected water could not be supporting the production zone due to lack of permeable flow connections between the deeper sections and the injection zone. Also, the reinjected geothermal water might be flowing into the western or eastern sections of the field, away from the production wells, since the injection wells have been located mostly in the eastern and north-western outer regions of the field.

❖ Among others, 5 shallow reinjection wells comprise the 45% of the total reinjection rate. These wells are mostly located away from the production wells. Figure 6.2 shows the locations of these wells, and the Table 6.2 shows the reinjection rates and the bottom depths of these wells.

Well	Reinjection, tph	Well Bottom, meter
KDE-20A	431	-224
KDE-20B	489	-798
KD-38C	506	-935
KDE-11	527	-903
KD-50	363	-365
	2316 tph (45%)	

Table 6.2 Rates and bottom depths of the 5 shallow reinjection wells

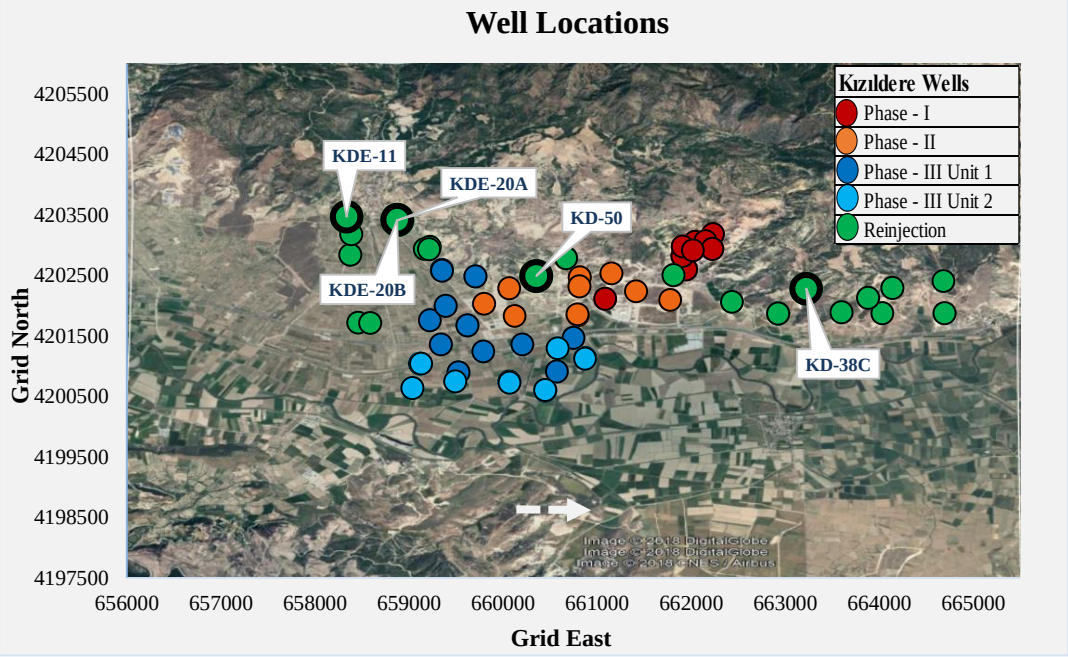

Figure 6.2 Locations of the 5 shallow wells comprising 45% of the total reinjection

- In both strategies, flowing enthalpies and reservoir temperatures are not an issue in any of the scenarios. This situation further explains the small impact of the current reinjection operations on the production zones.

- In Scenario 3, Kızıldere Geothermal Field is attributed as a greenhouse gas (GHG) sink. High amount of CO_2 injection scenarios were simulated. In the first part of the 3rd scenario, around 91.1 million tonnes of CO_2 were injected into the deeper parts of the Kızıldere Geothermal Field. This scenario shows that 91.1 million tonnes of CO_2 would be absorbed from the atmosphere and be a part of a geothermal power production cycle, which in turn provides more energy production. In the second part, only the produced CO_2 were reinjected in supercritical state through 3 wells. In this case, the amount of the injected CO_2 was 35 million tonnes. But since only the produced CO_2 is reinjected, no CO_2 transportation from other places is required.

- In the Strategy 1, CO_2 injection scenarios provide an extra support to the reservoir pressures, but this support is found to be only moderate. In Strategy 2, CO_2 injections increased the total production rates, but the ratio of the produced CO_2 is also increased. In both strategies, CO_2 levels increases with the extra CO_2 injection up to a point where CO_2 turns into gaseous phase. After some point CO_2 reaches critical saturation and starts to move into the production wells. This situation explains the high CO_2 production rates with the continuous CO_2 injections.

- One of the most important effects of injecting high amount of CO_2 into a geothermal reservoir is that as the partial pressure of the CO_2 increases, boiling is promoted. In the 3rd scenario this situation observed clearly by means of increasing the produced gas ratio. As much as 85% gas ratios were observed especially in the production wells completed at shallower depths and closer to the injection wells.

- High amount of CO_2 production would cause some troubles. As mentioned above, CO_2 promotes boiling and gas ratio increases in the reservoir, as well as in the

wellbore. Production of CO_2 gas pockets is expected. This is actually very undesired for pump-assisted production wells, but there is no any such well in the Kızıldere Geothermal Field, currently.

- Considering the short term effects, supercritical CO_2 injection provides more pressure support than the 10wt% CO_2 injection. When compared to the first scenario, supercritical CO_2 injection results in higher production rates in the short term, but in the long term, CO_2 production increases due to the penetration of injected supercritical carbon dioxide into the production wells, which reduces the water production. This is also true for the 10wt% CO_2 injection case, but reduction in the water rate is smaller.

- The amount of total water production of 3 three scenarios are shown in the Figure 6.3 Note that the first scenario extended to 2038 in order to make a healthy comparison, even though the reinjection rates become higher than the production rates after 2023. In all scenarios, it is assumed that surface facilities and infrastructure are readily available on each injection well site for the large amount of CO_2 and water injection operations.

- It should also be recalled that chemical reactions between the injected CO_2 and the formation rocks, as well as CO_2 sequestration mechanisms are beyond the scope of this study. Also, one of the most important issues during the production-injection-power generation operations, calcite scaling, and the effects of the CO_2 reinjection scenarios on the scaling problems are not the focus of this thesis.

- In all scenarios under both strategies, it can be clearly inferred that locations and shallower completion depths of the injection wells restricts the cooling effects of the injected fluid. No significant flowing enthalpy change have been observed in the scenarios. But this situation also restricts to have a higher impact on the reservoir pressures by higher injection rates. Some of the reinjection fluid might even be flowing away from the production zone.

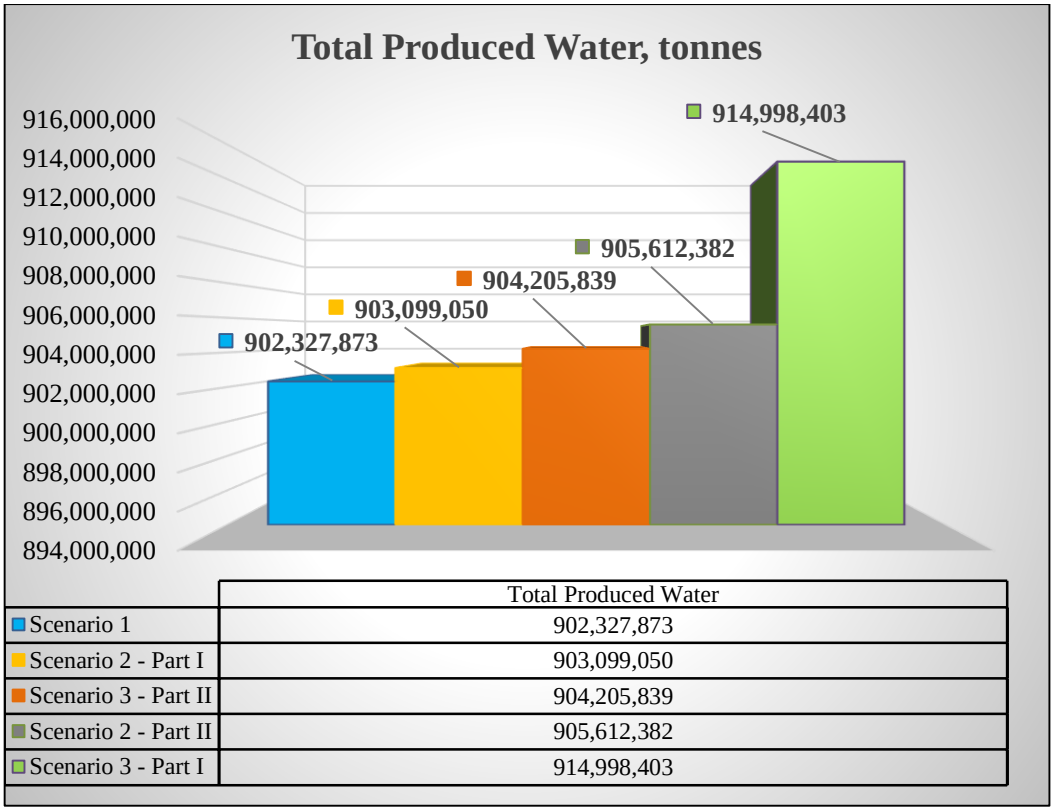

	Total Produced Water
Scenario 1	902,327,873
Scenario 2 - Part I	903,099,050
Scenario 3 - Part II	904,205,839
Scenario 2 - Part II	905,612,382
Scenario 3 - Part I	914,998,403

Figure 6.3 Total produced water as a result of different scenarios – Strategy 2

CHAPTER 7

CONCLUSION

Kızıldere Geothermal Field is one of the most important and large scale geothermal energy fields of the world. Understanding and assessing its characteristics are of a great importance. Currently, high amount of greenhouse gas production (especially CO_2) and the rapid decline in the reservoir pressure are the main issues in Kızıldere Geothermal Field. Since geothermal energy is often attributed as a clean and sustainable source of energy, this situation of the field must be studied and solutions must be developed. For that purpose, a numerical model of the field has been constructed by using the Petrasim interface, and numerical simulations have been carried out by using the TOUGH2 simulation codes. All possible information about the field were collected and utilized during the construction of the natural state model of the field. Eventually, the model was numerically simulated, and the results were tested by comparing the measured static pressure/temperature profiles, as well as observed pressure behavior of 15 observation wells. Consequently, the model was found to be very successful in reflecting the actual field behavior and validated as the natural state model of the Kızıldere Field. Then, by implementing the production and injection histories, the model was run until 2018. 3 different injection scenarios under two different strategies were simulated. The Strategy 1, where the production rates kept constant in exchange for the wellhead pressures, and the Strategy 2, where wellhead pressures kept constant by adjusting the production rates, are compared. It is that Strategy 1 provides higher energy extractions in the short term,

while the Strategy 2 provides more balanced reservoir pressure profiles considering the long term. It is also found in the scenarios under both strategies that reinjecting all of the produced water and the CO_2 supports the reservoir pressure, and reduces the decline in the production rates. Additionally, it is observed that supercritical CO_2 injection has more effects on the reservoir pressures than the 10% CO_2 injection part, although more CO_2 is injected in the 10% CO_2 injection part. This situation can be explained by the fact that supercritical CO_2 has both gas and liquid-like properties, and higher diffusivities are obtained in supercritical CO_2 injection scenario.

The current field development plan, where injection wells are located at the eastern, western, and northwestern outer edges of the main production zone and completed at relatively shallower depths, restricts to have higher impacts on the reservoir pressures by higher reinjection rates. But this development plan also helps to maintain the flowing enthalpies, which is another important parameter in geothermal energy generation operations.

All in all, different reinjection scenarios and their effects on the water and CO_2 production rates, reservoir pressure, and flowing enthalpies were examined in this study. It has found that the general sense of Kızıldere Geothermal Field of being environmentally unfriendly can be overcome by reinjecting the produced CO_2 and water, which also positively contributes to the reservoir management targets.

REFERENCES

Akin, S. (2017). Geothermal resource assessment of Alaşehir geothermal field. In *Proceedings: 42nd Workshop on Geothermal Reservoir Engineering, Stanford University, Stanford, California*. Retrieved from https://pangea.stanford.edu/ERE/pdf/IGAstandard/SGW/2017/Akin.pdf

Archie, G. E. (1942). The Electrical Resistivity Log as an Aid in Determining Some Reservoir Characteristics. *Transactions of the AIME, 146*(01), 54–62. https://doi.org/10.2118/942054-G

Artun, E. (2016). An Overview of Numerical Reservoir Simulation. In *Exploration and Production of Petroleum and Natural Gas and* (pp. 177–196). https://doi.org/10.1520/MNL7320140010

Axelsson, G. (2013a). Geothermal Well testing. In *"Short Course V on Conceptual Modelling of Geothermal Systems", organized by UNU-GTP and LaGeo, in Santa Tecla, El Salvador*. https://doi.org/10.1016/S0167-5648(09)70036-X

Axelsson, G. (2013b). Tracer tests in geothermal resource management. In *EPJ Web of Conferences* (Vol. 50, p. 02001). https://doi.org/10.1051/epjconf/20135002001

Axelsson, G., & Steingrimsson, B. (2012). Logging , Testing and Monitoring Geothermal Wells. *"Short Course on Geothermal Development and Geothermal Wells", Organized by UNU-GTP and LaGeo, in Santa Tecla, El Salvador*.

Bakar, H. A., & Zarrouk, S. J. (2016). Transient Pressure Well Test Analysis of Fractured Geothermal Wells. In *Proceedings 38th New Zealand Geothermal Workshop, Auckland, New Zealand*.

Barenblatt, G. E., I.P. Zheltov, & I.N. Kochina. (1960). Basic Concepts in the Theory of Seepage of Homogeneous Liquids in Fissured Rocks. *Journal of Applied*

Mathematics and Mechanics, *24*(5), 1286–130.

Bozkurt, E., & Oberhänsli, R. (2001). Menderes Massif (Western Turkey): Structural, metamorphic and magmatic evolution - A synthesis. *International Journal of Earth Sciences*, *89*(4), 679–708. https://doi.org/10.1007/s005310000173

BP. (2017). *BP Statistical Review of World Energy 2017* (Vol. 66th). Retrieved from http://www.bp.com/content/dam/bp/en/corporate/pdf/energy-economics/statistical-review-2017/bp-statistical-review-of-world-energy-2017-renewable-energy.pdf

Brown, D. (1995). The US hot dry rock program-20 years of experience in reservoir testing. *Proc. World Geothermal Congress*, 2607–2611. Retrieved from http://www.geothermal-energy.org/pdf/IGAstandard/WGC/1995/4-Brown.pdf

Brown, D. (2000). A Hot Dry Rock Geothermal Energy Concept Utilizing Supercritical Co2 Instead of Water. In *Twenty-Fifth Workshop on Geothermal Resevoir Engineering*. https://doi.org/10.1016/j.apenergy.2014.02.027

Bundschuh, J., & Suarez, M. (2010). *Introduction to the Numerical Modeling of Groundwater and Geothermal systems* (Vol. 2). London: CRC Press.

C. Chatenay and T. Jóhannesson. (2014). Industrial applications of geothermal resources. In *"Short Course VI on Utilization of Low- and Medium-Enthalpy Geothermal Resources and Financial Aspects of Utilization*.

Callos, V., Kaya, E., Zarrouk, S. J., Mannington, W., & Burnell, J. (2015). Injection of Co 2 Into Liquid Dominated Two-Phase Geothermal Reservoirs. *Proceedings 37th New Zealand Geothermal Workshop*, (November), 9.

Corrado, G., Lorenzo, S. De, Mongelli, F., Tramacere, A., & Zito, G. (1998). Surface heat flow density at the Phlegrean Fields caldera (Southern Italy). *Geothermics*, *27*(4), 469–484. https://doi.org/10.1016/S0375-6505(98)00023-6

Demirörer, M. (1969). *Kızıldere-Tekkehamam ve Karakova Jeotermal Gradyan Etüdleri*.

Directorate of Mineral Research & Exploration. (2017). Türkiye Jeotermal Enerji

Potansiyeli ve Arama Çalışmaları. Retrieved May 25, 2018, from http://www.mta.gov.tr/v3.0/arastirmalar/jeotermal-enerji-arastirmalari

Duan, Z., & Sun, R. (2003). An improved model calculating CO2 solubility in pure water and aqueous NaCl solutions from 273 to 533 K and from 0 to 2000 bar. *Chemical Geology*, *193*(3–4), 257–271. https://doi.org/10.1016/S0009-2541(02)00263-2

Edlefsen, N. E., & Anderson, B. C. (1943). Thermodynamics of Soil Moisture. *HILGARDIA*, *15*(2).

Edwards, A. (1972). *TRUMP: a computer program for transient and steady-state temperature distributions in multidimensional systems.* Retrieved from http://www.osti.gov/scitech/biblio/4524731

Energy Institute. (2013). *Hazard analysis for offshore carbon capture platforms and offshore pipelines*. *Hazard Analysis for Offshore Carbon Capture Platforms and Offshore Pipelines* (Vol. Research R). London.

Falta, R. W., Pruess, K., Finsterle, S., & Battistelli, A. (1995). *T2VOC User's Guide*.

Finsterle, S. (2007). *iTOUGH2 User's Guide*. *Earth Sciences Division Lawrence Berkeley National Laboratory*. https://doi.org/10.1111/j.1600-0447.2011.01711.x

Garg, S. K., Haizlip, J., Bloomfield, K. K., Kindap, A., Haklidir, F. S. T., & Guney, A. (2015). A Numerical Model of the Kizildere Geothermal Field, Turkey. In *World Geothermal Congress 2015* (p. 15).

Georgsson, L. S. (2009). Geophysical Methods Used in Geothermal Exploration. *"Short Course on Surface Exploration for Geothermal Resources", Organized by UNU-GTP and LaGeo, Ahuachapan and Santa Tecla, El Salvador*.

Gökgöz, A. (1998). *Geochemistry of the Kızıldere-Tekkehamam-Buldan-Pamukkale Geothermal Fields, Turkey*.

Grant, M. A., & Bixley, P. F. (2011). *Geothermal Reservoir Engineering* (2nd ed.). Elsevier.

Griggs, J. (2005). A REEVALUATION OF GEOPRESSURED- GEOTHERMAL AQUIFERS AS AN ENERGY SOURCE. In *PROCEEDINGS, Thirtieth Workshop on Geothermal Reservoir Engineering*. Stanford.

Jung, Y., Pau, G. S. H., Finsterle, S., & Pollyea, R. M. (2017). TOUGH3: A new efficient version of the TOUGH suite of multiphase flow and transport simulators. *Computers and Geosciences*, *108*(November), 2–7. https://doi.org/10.1016/j.cageo.2016.09.009

Karamanderesi, İ. (2013). Characteristics of Geothermal Reservoirs in Turkey. In *IGA Academy Report 0102-2013*.

Kleppe, J. (2018). *TPG4160 Reservoir Simulation: Review of Basic Steps in Derivation of Flow Equations*.

Kristján Saemundsson. (2015). Geothermal systems in global perspective. In *Short Course X on Exploration for Geothermal Resources*. Lake Bogoria and Lake Naivasha.

Lund, B., & Zoback, M. D. (1999). Orientation and magnitude of in situ stress to 6 . 5 km depth in the Baltic Shield. *International Journal of Rock Mechanics and Mining Sciences*, *36*, 169–190.

Lund, J. W. (2005). 100 Years of Geothermal Power Product. In *PROCEEDINGS, Thirtieth Workshop on Geothermal Reservoir Engineering Stanford University, Stanford, California* (pp. 1–10).

Manzella, A. (1973). *Geophysical Methods in Geothermal Exploration*. Pisa, Italy.

Mariita, N. O. (2011). Application of geophysical methods to geothermal energy exploration in Kenya. In *Short Course V on Exploration for Geothermal Resources, organized by UNU-GTP, GDC and KenGen, at Lake Bogoria and Lake Naivasha, Kenya, Oct* (pp. 1–8).

Massiot, C., Asmundsson, R., & Pezard, P. a. (2010). Achievements and Ongoing Progress of the European HiTI Project : High Temperature Instruments for Supercritical Geothermal Reservoir Characterization and Exploitation. In

Proceedings World Geothermal Congress, Bali, Indonesia.

Moog, G. (2013). *ADVANCED DISCRETIZATION METHODS FOR FLOW SIMULATION USING UNSTRUCTURED GRIDS A DISSERTATION SUBMITTED TO THE DEPARTMENT OF ENERGY RESOURCES ENGINEERING AND THE COMMITTEE ON GRADUATE STUDIES OF STANFORD UNIVERSITY IN PARTIAL FULFILLMENT OF THE REQUIREMENTS*. STANFORD UNIVERSITY. Retrieved from http://purl.stanford.edu/cq077bt3779

Moridis, G. J., Kowalsky, M. B., & Pruess, K. (2008). *TOUGH + HYDRATE v1 . 2 A CODE FOR THE SIMULATION OF SYSTEM B EHAVIOR IN H YDRATE-BEARING GEOLOGIC MEDIA*. Berkeley, California.

Moridis, G. J., & Pruess, K. (1998). T2SOLV: An enhanced package of solvers for the TOUGH2 family of reservoir simulation codes. *Geothermics*, *27*(4), 415–444. https://doi.org/10.1016/S0375-6505(98)00021-2

Narasimhan, T. N., & Witherspoon, P. A. (1976). An integrated finite difference method for analyzing fluid flow in porous media. *Water Resour. Res.*, *12*(1), 57–64. https://doi.org/10.1029/WR012i001p00057

O'Sullivan, M. J., Bodvarsson, G. S., Pruess, K., & Blakeley, M. R. (1985). *Fluid and Heat Flow In Gas-Rich Geothermal Reservoirs*. *Society of Petroleum Engineers Journal* (Vol. 25).

Özgüler, M. E., Turgay, M. İ., & Şahin, H. (1983). Geophysical Investigations in Denizli Geothermal Fields, Turkey. *Bulletin of the Mineral Research and Exploration*, *99*(99–100). Retrieved from http://dergipark.gov.tr/bulletinofmre/issue/3922/52219

Özkaya, M. (2007). *NUMERICAL MODELING OF KIZILDERE GEOTHERMAL FIELD*. Middle East Technical University.

Pistone, S., Stacey, R., & Horne, R. (2011). the Significance of Co 2 Solubility in Geothermal Reservoirs. *PROCEEDINGS, Thirty-Sixth Workshop on Geothermal Reservoir Engineering Stanford University, Stanford, California*.

Pruess, K. (1987). *TOUGH User's Guide*.

Pruess, K. (1991). *TOUGH2: A general-purpose numerical simulator for multiphase fluid and heat flow*. *Lawrence Berkeley Laboratory Report*. https://doi.org/10.2172/5212064

Pruess, K. (2002). *Mathematical Modeling of Fluid Flow and Heat Transfer in Geothermal Systems - an Introduction in Five Lectures*. *Report*.

Pruess, K. (2003). The TOUGH Codes—A Family of Simulation Tools for Multiphase Flow and Transport Processes in Permeable Media. *Vadose Zone Journal*, *3*(3), 738–746. https://doi.org/10.2136/vzj2004.0738

Pruess, K. (2005). *ECO2N: A TOUGH2 Fluid Property Module for Mixtures of Water, NaCl,and CO2*. https://doi.org/10.2172/877331

Pruess, K. (2011). *ECO2M : A TOUGH2 Fluid Property Module for Mixtures of Water , NaCl , and CO2 , Including Super- and Sub-Critical Conditions , and Phase Change Between Liquid and Gaseous CO2*. *Earth Sciences Division, Lawrence Berkeley National Laboratory*.

Pruess, K., & Narasimhan, T. N. (1982). On Fluid Reserves and the Production of Superheated Steam from Fractured, Vapor-Dominated Geothermal Reservoirs. *Journal of Geophysical Research*. https://doi.org/doi: 10.1029/JB087iB11p09329

Pruess, K., & Narasimhan, T. N. (1985). A Practical Method for Modeling Fluid and Heat Flow in Fractured Porous Media. *Society of Petroleum Engineers Journal*, *25*(01), 14–26. https://doi.org/10.2118/10509-PA

Pruess, K., Oldenburg, C., & Moridis, G. (1999). *TOUGH2 User's Guide, Version 2.0*.

REN21. (2016). *Renewables 2016 Global Status Report*. https://doi.org/ISBN 978-3-9818107-0-7

Rutagarama, U. (2012). *The Role of Well Testing in Geothermal Resource Assessment*. University of Iceland.

Santos, P. a, & Rivas, J. a. (2009). Gravity Surveys Contribution To Geothermal Exploration in El Salvador : the Cases of Berlín , Ahuachapán and San Vicente Areas. In *Short Course on Surface Exploration for Geothermal Resources*.

Serpen, U., & Uğur, Z. (1998). Reassessment of Geochemistry of the Kızıldere Geothermal Field. *Geothermal Resources Council Transactions, 22*. Retrieved from https://www.geothermal-library.org/index.php?mode=pubs&action=view&record=1015895

Şimşek, Ş. (1985a). Geothermal model of Denizli - Sarayköy - Buldan area. *Geothermics, 14*(2–3), 393–417.

Şimşek, Ş. (1985b). Present Status and Future Developments of the Denizli-Kizildere Geothermal Field of Turkey. In *International symposium on Geothermal Energy. International volume. pp.203-215 Hawaii.*

Şimşek, Ş. (2002). ORIGIN AND CHARACTERISTICS OF GEOTHERMAL ENERGY RESOURCE OF THE WIDER AEGEAN REGION. In *International Workshop on Possibilities of Geothermal Energy Development in the Aegean Islands Region, Proceedings, p.1-18 Milos Island, Greece.*

Şimşek, Ş., Parlaktuna, M., & Akin, S. (2009). *Data Gathering and Evaluation of Kızıldere Geothermal Field*.

Spichak, V., Menvielle, M., & Roussignol, M. (1999). Three-Dimensional Inversion of MT Fields Using Bayesian Statistics. *Three Dimensional Electromagnetics*. Retrieved from http://www.igemi.troitsk.ru/rus/Spichak_pdf/EM3D95-1.PDF

Steingrímsson, B. (2011). Geophysical Well Logging : Geological Wireline Logs and Fracture Imaging. In *"Short Course on Geothermal Drilling, Resource Development and Power Plants", organized by UNU-GTP and LaGeo, in Santa Tecla, El Salvador*.

Thunderhead Engineering. (2016). *Petrasim User Manual*. Retrieved from www.thunderheadeng.com

U.S. Department of Energy's Office of Energy Efficiency & Renewable Energy. (2016). Electricity Generation. Retrieved May 28, 2018, from https://www.energy.gov/eere/geothermal/electricity-generation

Warren, J., & Root, P. J. (1963). The behavior of naturally fractured reservoirs. *SPE Journal*, 245–255. https://doi.org/10.2118/426-PA

World Energy Council. (2016). *World Energy Resources: Geothermal 2016*. Retrieved from https://www.worldenergy.org/wp-content/uploads/2017/03/WEResources_Geothermal_2016.pdf

Wu, Y., & Pruess, K. (2005). A Physical Based Numerical Approach for Modeling Fracture-Matrix Interaction in Fractured Reservoirs. In *Proceedings World Geothermal Congress 2005, Antalya, Turkey*.

Xu, T., Spycher, N., Sonnenthal, E., Zheng, L., & Pruess, K. (2012). *TOUGHREACT User's Guide: A Simulation Program for Non-isothermal Multiphase Reactive Transport in Variably Saturated Geologic Media, version 2.0*. *Earth Sciences Division, Lawrence Berkeley National Laboratory University*. https://doi.org/10.2172/943451

Yeltekin, K. (2001). *Characterization and Modeling of Kızıldere Geothermal Field*. Middle East Technical University.

Zhang, K., Wu, Y., & Pruess, K. (2008). *User ' s Guide for TOUGH2-MP - A Massively Parallel Version of the User ' s Guide for TOUGH2-MP - A Massively Parallel Version of the TOUGH2 Code*.